UNIVERSIDADE DE LISBOA

Faculdade de Medicina

Delusions of space after stroke: clinical phenomenology and neural basis

Pedro Miguel Nascimento Alves

Orientadoras: Professora Doutora Maria Isabel Segurado Pavão Martins Catarino Petiz

Professora Doutora Ana Catarina Gaspar Fonseca

Tese especialmente elaborada para obtenção do grau de Doutor em Medicina, especialidade de Neurologia

2022

UNIVERSIDADE DE LISBOA

Faculdade de Medicina

Delusions of space after stroke: clinical phenomenology and neural basis

Pedro Miguel Nascimento Alves

Orientadoras: Professora Doutora Maria Isabel Segurado Pavão Martins Catarino Petiz

Professora Doutora Ana Catarina Gaspar Fonseca

Tese especialmente elaborada para obtenção do grau de Doutor em Medicina, especialidade de Neurologia

Júri:

Presidente: Doutora Helena Maria Ramos Marques Coelho Cortez Pinto,
Professora Catedrática e Presidente do Conselho Científico da Faculdade de Medicina da Universidade de Lisboa

Vogais: Doctor Paolo Bartolomeo,
Research Director do Institut du Cerveau, Sorbonne Université, Paris (France)

Doutor Albino Jorge Carvalho de Sousa Oliveira Maia,
Professor Auxiliar Convidado da Faculdade de Ciências Médicas da Universidade Nova de Lisboa

Doutora Patrícia Margarida Piedade Figueiredo,
Professora Associada do Instituto Superior Técnico da Universidade de Lisboa

Doutora Maria Isabel Segurado Pavão Martins Catarino Petiz,
Professora Associada com Agregação da Faculdade de Medicina da Universidade de Lisboa

Doutora Patrícia Martins Canhão,
Professora Auxiliar da Faculdade de Medicina da Universidade de Lisboa

Instituições Financiadoras:

Santa Casa da Misericórdia de Lisboa, Prémio João Lobo Antunes 2018

European Academy of Neurology, Research Fellowship grant 2018

Sociedade Portuguesa do AVC, Bolsa de Investigação em Doença Vascular Cerebral 2017

2022

A impressão desta tese foi aprovada pelo Conselho Científico da Faculdade de Medicina de Lisboa em reunião de 24/5/2022.

As opiniões expressas nesta publicação são da exclusiva responsabilidade do seu autor.

Acknowledgements

I am extremely grateful to my supervisors, Professor Isabel Pavão Martins and Professor Ana Catarina Fonseca. Professor Isabel Pavão Martins has inspired me since the first day I started working in Laboratório de Estudos de Linguagem, Centro de Estudos Egas Moniz. Her fascinating knowledge about cognitive and behavioural neurology, her bright scientific ideas, and her generosity to teach and provide scientific opportunities have been fundamental for me and for this work. Professor Ana Catarina Fonseca has also been profoundly influential in my career and for this thesis. Her invaluable advice since I started my residency in neurology, her exceptional expertise in stroke and in medical research and her constant support, availability and encouragement have been crucial.

I would like to extend my special thanks to Professor Michel Thiebaut de Schotten. Since my visiting research fellowship in his lab, his work and mentoring opened my passion for neuroimaging and connectome research. He generously taught me advanced tools of imaging analyses, and provided me with the privilege to maintain an exciting and fruitful collaboration.

I also express my gratitude to project's funders and to the institutions where it was developed. I thank my colleagues of Laboratório de Estudos de Linguagem, Centro de Estudos Egas Moniz and of the Department of Neurology, Hospital de Santa Maria for their support, collaboration and friendship. A particular acknowledgement to the Stroke Unit team and its director Dra. Teresa Pinho-e-Melo, where the patients were recruited. I also thank to my thesis committee members, Professor Patrícia Canhão, Professor Patrícia Figueiredo and Professor Jorge Almeida for their constructive feedback.

Finally, my deep gratitude to my family. This thesis is dedicated to them. I wish to thank Inês for her loving and unfailing support, patience and understanding, and for always being by my side. This work also belongs to her. I thank my parents, brother and grandparents, for their determinant role and wise guidance during all my life.

Abstract

Orientation in space is an important determinant of human behaviour. Spatial delusions are a disrupting form of spatial disorientation characterized by a firm conviction of place mislocation. Patients believe they are in a reduplicated, transformed or dislocated place and are rather insensitive to surrounding incongruences. Spatial delusions are frequent after right hemispheric lesions and in neurodegenerative diseases, but empirical evidence about their presentation and pathophysiology is lacking. Here, we aimed to comprehensively study stroke-associated spatial delusions' clinical features and neural basis.

The first study systematically reviewed the reported evidence about lesion-associated spatial delusions. Then, we performed a prospective screening for spatial delusions in right hemisphere acute stroke patients and were able to identify the largest sample of patients with spatial delusion, to our knowledge. The second study described spatial delusions' clinical and phenomenological features and analysed their neural correlations (n=60). Most places of mislocation were closer to the patient's home than to the hospital. The duration of the syndrome was short (median: 3 days, interquartile range: 1-7 days) and moderately correlated with structural disruption of left inferior temporal fibres (r=0.39). Each clinical subtype (i.e., place reduplication, transformation or dislocation) had characteristic response patterns, which were reported, and representative examples were provided. In the third study, we performed a case-control analysis of the structural and functional predictors of the syndrome (stroke patients with spatial delusions, n=64; stroke controls, n=233). Spatial delusions were most strongly predicted by the structural disconnection of two distinct streams, connecting right fronto-thalamic and right occipitotemporal structures. The multivariate model also included age, anosognosia and lesion sparing of right dorsal fronto-parietal regions as independent predictors. It was nested cross-validated with a support-vector machine analysis and a good discrimination accuracy was demonstrated (median area under the curve: 0.80, interquartile range: 0.75–0.85).

Cognitively, spatial delusions do not seem to be explained by deficits in single cognitive domains but by a dysfunctional combination of multidomain information. The brain's functional organization comprises multimodal integrative networks, namely the default mode network, and ventral and dorsal attention networks. The neuroimaging study of their anatomy has taken a predominantly corticocentric approach, but clinical,

electrophysiological and phylogenetic-derived data suggest that they have essential subcortical components. In the fourth study, we applied neuroimaging methods of functional alignment to healthy subjects' resting-state functional MRI and demonstrated that the default mode network comprises a subcortical network that matches the anatomical model of the limbic system. Using a similar methodology, the fifth study revealed that the ventral and dorsal attention networks include the pulvinar, the superior colliculi and group brainstem nuclei whose projections are spatially correlated with the acetylcholine nicotinic receptor and dopamine transporter systems.

The sixth study explored the relationship between spatial delusions and acute stroke treatment modalities. We performed a subanalysis of the ischemic stroke sample collected for the second and third studies and found an association between endovascular thrombectomy and occurrence of the syndrome (multivariate logistic regression model including age, clinical severity, vascular territory, inter-hospital transfer and endovenous thrombolysis as covariates; odds ratio: 2.46, 95% confidence interval: 1.18 to 5.16). We demonstrated that shared clusters of lesion and structural disconnection, overlapping right thalamo-orbitofrontal fibres and right anterior temporal areas, mediate the association. These regions are irrigated by proximal middle cerebral artery branches, which seem to be particularly prone to ischemia during clot manipulation and extraction.

In conclusion, our results provide a broader characterization of stroke-associated spatial delusions' clinical and phenomenological features, which may support their appropriate diagnosis. They also shed light on the functional and structural predictors of the syndrome and on the subcortical organization of multimodal integrative functional networks. They may contribute to a better understanding of delusional misidentifications and extend our knowledge about the neurobiology of spatial orientation disorders.

Keywords: spatial orientation, delusions, stroke, connectivity.

Resumo

A orientação no espaço é um importante determinante do comportamento humano. Os delírios espaciais são uma forma de desorientação espacial caracterizada pela firme convicção de estar num local diferente daquele em que realmente se está. Os doentes acreditam estar num local reduplicado, transformado ou deslocado e as sua convicção é resistente às incongruências circundantes. Os delírios de espaço são frequentes após lesões hemisféricas direitas e em doenças neurodegenerativas, mas a evidência empírica sobre a sua apresentação e fisiopatologia é escassa. Este trabalho teve como objectivo estudar as características clínicas e a base neuronal dos delírios espaciais associados ao acidente vascular cerebral.

No primeiro estudo, procedeu-se a uma revisão sistemática dos casos publicados de delírios de espaço após lesões focais. De seguida, realizámos uma avaliação prospectiva da presença de delírios espaciais em doentes com acidente vascular cerebral agudo do hemisfério direito, tendo sido possível identificar a maior amostra de doentes com delírios espaciais reportada até ao momento, do nosso conhecimento. O segundo estudo descreveu as características clínicas e fenomenológicas dos delírios espaciais e analisou as suas correlações neuronais (n=60). A maioria dos locais erradamente identificados localizavam-se mais próximo da casa do doente do que do hospital. A duração do síndrome foi breve (mediana: 3 dias, intervalo interquartil: 1-7 dias) e moderadamente correlacionada com a magnitude de lesão estrutural de fibras temporais inferiores esquerdas (r=0.39). Cada subtipo clínico (ou seja, reduplicação, transformação ou deslocação de local) apresentou padrões de resposta característicos, que foram descritos, e exemplos representativos foram reportados. No terceiro estudo, realizámos uma análise caso-controlo dos preditores estruturais e funcionais dos delírios de espaço (casos com acidente vascular cerebral e delírio espacial, n=64; controlos com acidente vascular cerebral, n=233). O maior preditor da ocorrência de delírios de espaço foi a desconexão estrutural de duas vias do hemisfério direito, conectando regiões fronto-talâmicas e occipitotemporais. O modelo multivariado incluiu também a idade, a anosognosia e a ausência de lesão em regiões fronto-parietais dorsais direitas como preditores independentes. Foi feita uma validação cruzada aninhada usando uma análise *support-vector machine* tendo-se demonstrado uma boa capacidade discriminativa (mediana da área sob a curva: 0.80, intervalo interquartil: 0.75-0.85).

Cognitivamente, os delírios espaciais não parecem ser explicados por défices em domínios cognitivos isolados, mas sim por uma combinação disfuncional da informação de

vários domínios. A organização funcional do cérebro compreende redes integradoras multimodais, nomeadamente a *default mode network*, e as *ventral and dorsal attention networks*. O estudo neuroimagiológico da sua anatomia tem tido uma abordagem predominantemente corticocêntrica, contudo dados clínicos, electrofisiológicos e filogenéticos sugerem que estas redes também possuem componentes subcorticais essenciais. No quarto estudo, aplicámos métodos neuroimagiológicos de alinhamento funcional do sinal de repouso de ressonância magnética funcional de indivíduos saudáveis e demonstrámos que a *default mode network* compreende uma rede subcortical condizente com o modelo anatómico do sistema límbico. Utilizando uma metodologia semelhante, o quinto estudo revelou que as *ventral and dorsal attention networks* incluem o pulvinar, o colículo superior e núcleos de tronco cerebral cujas projeções se correlacionam espacialmente com os sistemas de receptores nicotínicos da acetilcolina e de transportadores da dopamina.

O sexto estudo explorou a relação entre os delírios de espaço e as modalidades de tratamento do acidente vascular cerebral isquémico agudo. Realizámos uma subanálise da amostra de doentes com acidente vascular cerebral isquémico recolhida para o segundo e terceiro estudos e encontrámos uma associação entre a realização de trombectomia mecânica e os delírios espaciais (modelo de regressão logística multivariada incluindo as covariáveis idade, gravidade clínica, território vascular, transferência inter-hospitalar e trombólise endovenosa; odds ratio: 2.46, intervalo de confiança de 95%: 1.18 a 5.16). Demonstrámos que áreas partilhadas de lesão e desconexão estrutural, intersectando fibras tálamo-orbitofrontais direitas e regiões temporais anteriores direitas, medeiam esta associação. Estas regiões são irrigadas por ramos proximais da artéria cerebral média, ramos estes que são particularmente suscetíveis à isquemia durante a manipulação e extração do trombo.

Em conclusão, os resultados apresentado permitem uma caracterização mais ampla das características clínicas e fenomenológicas dos delírios espaciais associadas ao acidente vascular cerebral, o que pode facilitar o seu diagnóstico adequado. Evidenciam também novos modelos sobre os preditores funcionais e estruturais do síndrome e sobre a organização subcortical das redes funcionais integradoras multimodais. No seu conjunto podem contribuir para uma melhor compreensão das falsas identificações delirantes e para o progresso do conhecimentos sobre a neurobiologia dos distúrbios de orientação espacial.

Palavras-chave: orientação espacial, delírio, AVC, conectividade.

List of publications

The work of this thesis was published in the following articles and book chapters:

Articles

1) Alves PN, Silva DP, Fonseca AC, Martins IP (2021) Mapping delusions of space onto a structural disconnectome that decouples familiarity and place networks. Cortex 146:250–260. https://doi.org/10.1016/j.cortex.2021.11.008.
2) Alves PN, Fonseca AC, Pinho-e-Melo T, Martins IP (2022) Clinical features and neural correlates of stroke-associated spatial delusions. Eur J Neurol 30(1):125–133. https://doi.org/10.1111/ene.15557.
3) Alves PN, Fonseca AC, Silva DP, Andrade MR, Pinho-e-Melo T, Thiebaut de Schotten M, Martins IP (2021) Unravelling the neural basis of spatial delusions after stroke. Ann Neurol 89:1181–1194. https://doi.org/10.1002/ana.26079.
4) Alves PN, Foulon C, Karolis V, Bzdok S, Margulies DS, Volle E, Thiebaut de Schotten M (2019) An improved neuroanatomical model of the default-mode network reconciles previous neuroimaging and neuropathological findings. Commun Biol 2:370. https://doi.org/10.1038/s42003-019-0611-3.
5) Alves PN, Forkel JS, Corbetta M, Thiebaut de Schotten M (2022) The subcortical and neurochemical organisation of the ventral and dorsal attention networks. Commun Biol 5:1343. https://doi.org/10.1038/s42003-022-04281-0.
6) Alves PN, Fonseca AC, Pinho-e-Melo T, Martins IP. Novel patterns of stroke neural damage link endovascular thrombectomy to the occurrence of spatial delusions. *Submitted.*

Book chapters

1) Ferro JM, Alves PN, Martins IP. Memory loss. Caplan's Stroke Syndromes, 4th edition, Cambridge University Press. *In press*.

Grants and prizes

The work of this thesis received support and was acknowledge by the following grants and prizes:

Grants

1) Research grant "Prémio João Lobo Antunes", Santa Casa da Misericórdia de Lisboa, 2018.
2) Research grant of the Portuguese Society of Stroke, 2018.
3) Research Fellowship grant of the European Academy of Neurology, 2018.

Prizes

1) Runner-up prize of the European Academy of Neurology 2021 – Tournament clinical for neurologist in training. Congress of the European Academy of Neurology 2021.
2) 1st Experts prize of the XIV Annual CAML PhD Students' Scientific Meeting 2021.
3) Runner-up prize of the European Academy of Neurology 2018 – Tournament in basic neurosciences for neurologist in training. Congress of the European Academy of Neurology 2018.
4) Prize "Dr. Orlando Leitão", Portuguese Society of Neurology. Congress of the Portuguese Society of Neurology 2018.
5) Top 5 research proposal in the program Harvard Medical School Portugal - Clinical Scholars Research Training 2018.

Table of contents

List of abbreviations

ANTs	Advanced Normalization Tools
BOLD	Blood-oxygen-level-dependent
CT	Computed tomography
DAN	Dorsal attention network
DMN	Default mode network
FDR	False discovery rate
fMRI	Functional magnetic resonance imaging
FWE	Family-wise error
IQR	Interquartile range
MNI	Montreal Neurological Institute
MRI	Magnetic resonance imaging
NIHSS	National Institutes of Health stroke scale
PET	Positron emission tomography
TICI	Thrombolysis in cerebral infarction scale
VAN	Ventral attention network

I. Introduction

“Every act of perception, is to some degree an act of creation, and every act of memory is to some degree an act of imagination.”

— Oliver Sacks, *Musicophilia*

The house and the brain[*]

[*] Illustration created with WOMBO®

Knowing where we are is a core feature of human consciousness and an important determinant of human behaviour. Delusions of space, or reduplicative paramnesias, are a particular type of spatial disorientation characterized by a severe disturbance of space interpretation (Pick 1903). The analysis of a representative case of reduplicative paramnesia demonstrates the unique nature of these disorders.

Mr. AB was a 76 years-old patient, right-handed and former bus driver in Lisbon. He was admitted to the emergency department of 'Hospital de Santa Maria' with a severe right middle cerebral artery ischemic stroke. The neurological examination at admission showed left visuospatial neglect, anosognosia for hemiplegia, left homonymous hemianopsia, right-side eye deviation, left facial palsy, left hemiplegia and left pain anesthesia (NIHSS 20). The brain CT angiography revealed an occlusion of the proximal segment of the right middle cerebral artery (M1 segment) and the patient underwent endovascular thrombectomy. Complete arterial recanalization was achieved (TICI 3) and the patient had a notable clinical improvement. Figure 1 presents the cerebral digital subtraction angiography performed before and after thrombectomy and the brain MRI showing the infarcted brain regions.

Twenty-four hours after endovascular thrombectomy, Mr. AB presented left visuospatial neglect, mild left facial palsy, a slight drift of the left upper limb, and left pain hypoesthesia (NIHSS 5).

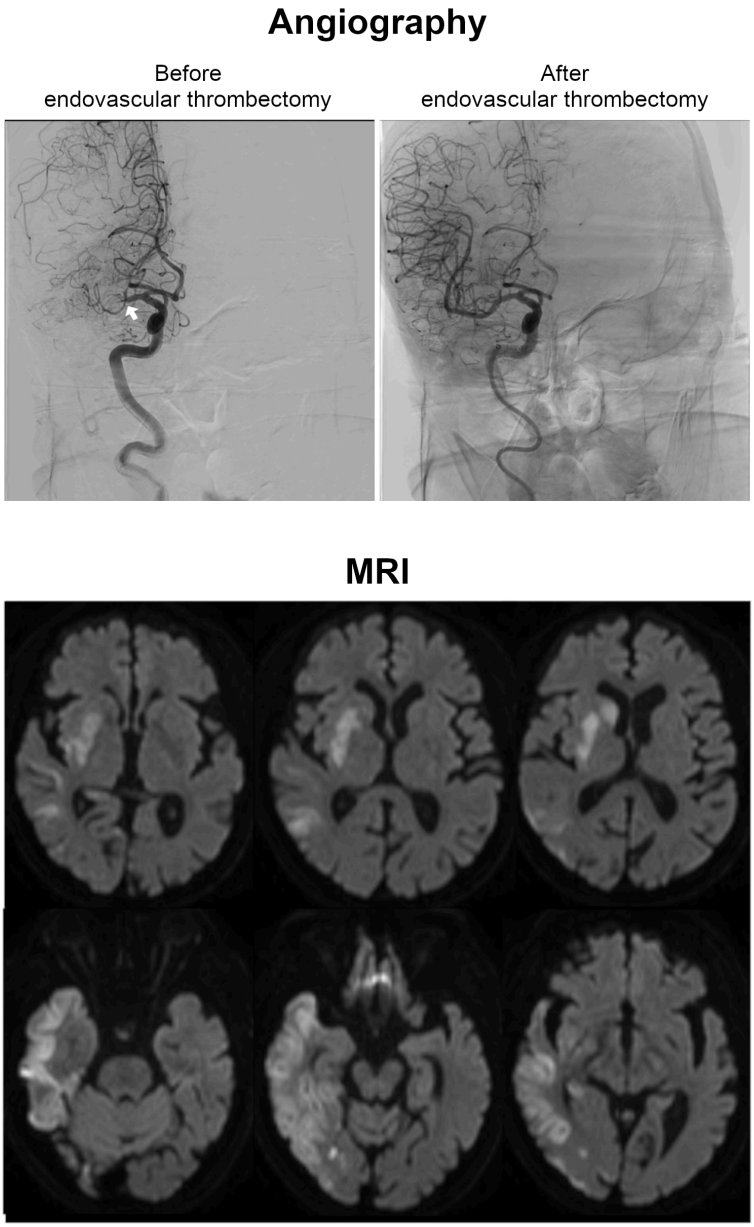

Figure 1. Stroke imaging of Mr. AB. Top: Angiography performed before (left) and after (right) endovascular thrombectomy. The white arrow highlights the arterial occlusion in the M1 segment of the right middle cerebral artery. Bottom: Diffusion-weighted MRI imaging performed 4 days after stroke. Hyperintensity indicates areas of brain infarct.

One week later, his hemi-attentional, motor and sensitive deficits had resolved entirely (NIHSS 0) and he was autonomous in the hospital ward. However, a remarkable disorientation in space persisted:

Question (Q): Do you know where you are?

Answer (A): I am at the hospital, at the 'Hospital de Santa Maria' (*correct answer*).

Q: Could you tell me our current location?
A: We are in Avenue 'Amália Rodrigues', in Odivelas (*a city inside Lisbon metropolitan area, 9km away from the correct location of 'Hospital de Santa Maria'*).

Q: Odivelas?! Where is 'Hospital de Santa Maria' located?
A: 'Hospital de Santa Maria' is located towards that side, in 'Cidade Universitária' (*correct answer*), but this building is in Odivelas.

Q: Is this hospital also called 'Hospital de Santa Maria'?! How many hospitals do you know with this name?
A: I knew only one. I had never realized that there was a hospital here. Now, with this one, there are two.

Q: Are you familiar with Odivelas? Is there a hospital in Avenue 'Amália Rodrigues'?
A: Yes, I know Odivelas very well. It is strange. I never realized there was a hospital here. It should have been built very recently.

Mr. AB was asked to look at the window. The video with the dialogue in front of the window is available at https://onlinelibrary.wiley.com/doi/abs/10.1002/ana.26079 or through the following QR code (Alves et al. 2021a):

Q: Could you tell me which building is that one?
A: That is Sporting's football stadium (*correct answer*).

Q: And there?

A: That is Lisbon Airport (*correct answer*).

Q: If you were in Odivelas, would you be able to see this stadium and the airport?

A: I thought it was not possible. Odivelas lays lower than the stadium. We must be in a high place in Odivelas.

Q: This is big trick your brain is playing you because of the stroke. You are in 'Hospital de Santa Maria' at 'Cidade Universitária'.

A: No. This is not 'Cidade Universitária'. It looks like it... the building, the view from the window... but it is not located at the right place.

Mr. AB was oriented in time. He could describe the correct route between 'Hospital de Santa Maria' and his home and between the place where he believed he was and his home (Figure 2).

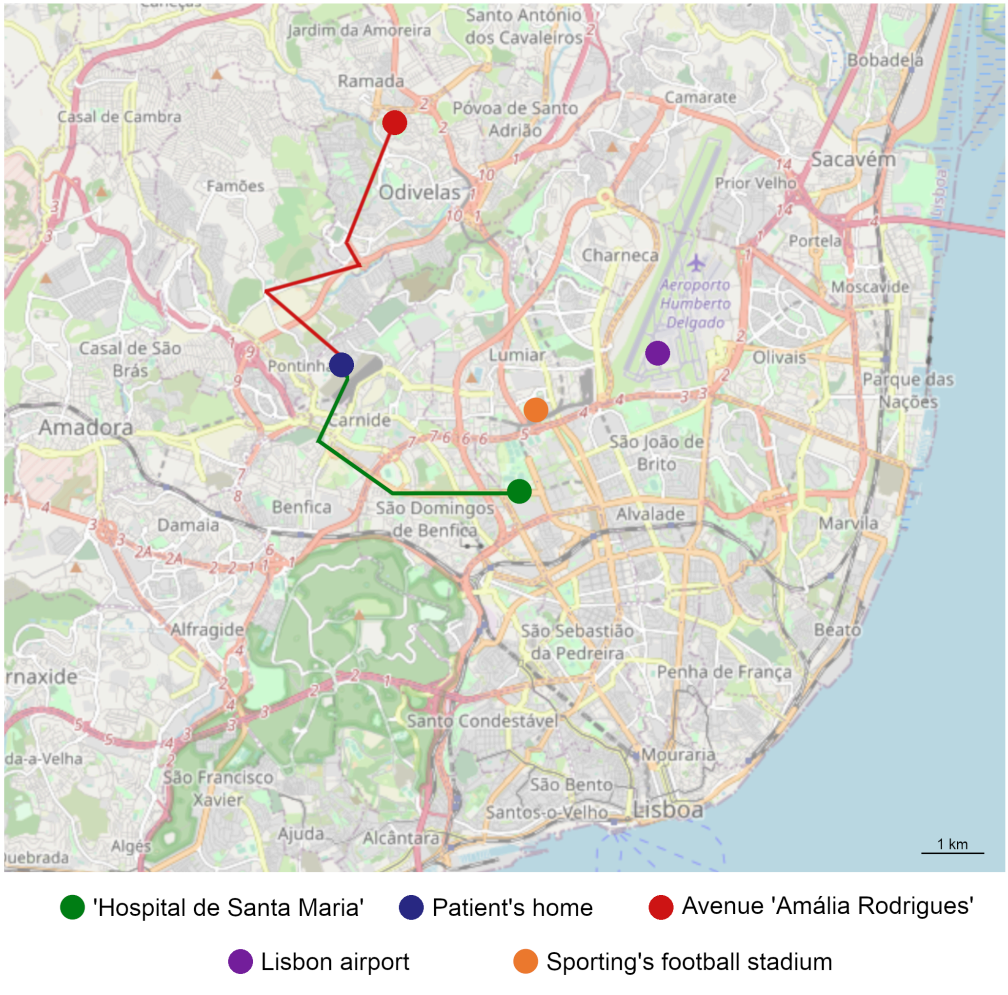

Figure 2. Map representing relevant places for Mr. AB spatial delusion. 'Hospital de Santa Maria' is where Mr. AB really was. Avenue 'Amália Rodrigues' is where he believed he was and where he located the replica of Hospital Santa Maria. Lisbon airport and Sporting's football stadium are the landmarks that Mr. AB correctly identified from the window's view. Red and green lines are the trajectories that Mr. AB mentally described correctly between "here" and his home and between 'Hospital de Santa Maria' and his home, respectively.

Immediately after discharge, his daughter took him to Avenue 'Amália Rodrigues' in Odivelas. Mr. AB asked to get into one building to ensure that there was not a hospital inside.

1. Spatial orientation

Spatial orientation can be defined as an incessant and dynamic process of perception, integration and interpretation of sensory stimuli from the outside world and our body (Gooddy and Reinhold 1952).

Space perception

Different perceptual afferences have complementary roles in spatial orientation (Lackner and Dizio 2005). A dual system processes visual stimuli, where a ventral (occipito-temporal) stream contributes to the recognition of environmental landmarks, and a dorsal (occipito-parietal) stream infers visuospatial relationships (Goodale et al. 1991; James et al. 2002). Vestibular inputs are fundamental for motion perception and real-time positioning in a 3-dimensional spatial frame (Brandt et al. 2005; Angelaki and Cullen 2008), while proprioceptive afferences contribute to continuous sensing of the body position in space (Berthoz et al. 1995; Simons and Wang 1998).

Space integration

Regarding sensory integration, Aguirre and D'Esposito proposed a taxonomic approach in which the deficits of spatial navigation were classified into four categories (Aguirre and D'Esposito 1999). Egocentric disorientation corresponded to the inability to represent the relative location of objects and spatial landmarks to self and was associated with lesions of the posterior parietal lobe. Heading or allocentric disorientation referred to the incapacity to establish the relative position between landmarks in a map-like representation and was found in lesions of the posterior cingulate or the right hippocampus and parahippocampal cortex (Bohbot et al. 1998). Landmark agnosia was characterized by a reduced ability to recognize salient environmental landmarks. It was associated with lesions of the right lingual gyrus. Finally, anterograde disorientation was defined by the inability to learn new environments or spatial routes. It was associated with lesions of the right parahippocampal cortex. Whereas the previous classes of topographic disorientation affected both familiar and novel spaces, patients with anterograde disorientation maintain a preserved orientation in familiar environments (Aguirre and D'Esposito 1999).

The incorporation of new cognitive, neurophysiological and neuroimaging data from human and animal research led to substantial improvements of this model. John O'Keefe and colleagues found a group of neurons in the rat hippocampus that changed their firing rate according to the animals' position in the environment (O'Keefe and Dostrovsky 1971; O'Keefe and Burgess 1996; Eichenbaum et al. 1999). These cells were called 'place cells'. In the rat entorhinal cortex, May-Britt Moser, Edvard Moser and collaborators discovered another cluster of cells whose pattern of activation geometrically mapped the space available to the animals. They were called 'grid cells' (Fyhn et al. 2004; Hafting et al. 2005; Moser et al. 2014). In addition, specific cellular activations were demonstrated for directional information. 'Head direction cells' increased their firing rates when the animals pointed their head in a particular direction (Taube et al. 1990). These types of cells had a broader distribution, being found in the rats' entorhinal cortex and across different structures of their Papez's circuit (Taube 2007). The existence of human brain homologous place, grid and head-direction cells was demonstrated later in functional MRI (fMRI) studies with healthy subjects and in single neuron electrophysiological recordings of neurological and neurosurgical patients implanted with intracranial depth electrodes (Ekstrom et al. 2003; Doeller et al. 2010; Jacobs et al. 2010), providing the cellular framework for the behavioural understanding of human spatial navigation.

Space interpretation

Ultimately, the spatial environment needs to be interpreted appropriately. The integrated spatial information is combined with previous spatial memories and continuous feedback input from external reality monitoring systems (Funahashi 2013; Eichenbaum 2017; Chen et al. 2018). Importantly, this process involves balancing between overt and covert mechanisms (Ellis and Young 1990; Ellis et al. 1997). Brain disease may selectively disrupt interpretation mechanisms, provoking a double dissociation between overt and covert deficits (Tranel et al. 1995). In overt recognition deficits (i.e., agnosia), patients cannot explicitly identify certain stimuli but have a preserved sense of familiarity (de Haan et al. 1991; Stumps et al. 2020). Conversely, patients with covert recognition deficits explicitly recognize the stimuli' physical features but cannot implicitly match them with proper identity and familiarity attributes. Their erroneous convictions may be strongly resistant to counterfactual evidence and lead to delusional misidentifications (Ellis and Young 1990; Coltheart et al. 2011).

2. Spatial delusions

Pioneer observations

Charles Bonnet is mainly known for describing the visual release hallucinations syndrome, however the fascinating neurological observations of this naturalist and philosophical writer of the eighteenth century are broader. He reported the clinical case of a 70 years-old female patient who had suffered a unilateral hemiparesis of sudden onset (presumably caused by a stroke) and started asking her maid to be dressed in a shroud and put in a coffin because she was dead (Moritz et al. 1788; Förstl and Beats 1992). Her family tried to convince her that she was alive, but their efforts were futile and even induced agitation and anger. After the resolution of her delusion of death, she started saying that she was not anymore in Copenhagen but in Norway. As an utmost attempt to persuade her, she was taken in a carriage around the city. When she arrived back home, she believed that she had just returned from Norway. This report corresponds to the first known description of delusions of death and delusions of space. Delusion of death became known as Cotard's syndrome, after Jules Cotard's manuscript in 1882 (Cotard 1882), and delusions of space as reduplicative paramnesias, after Arnold Pick's publication in 1903 (Pick 1903). Pick described a 67 years old woman admitted to a clinic due to the progressive onset of cognitive and behavioural changes. The clinic was located in Prague. During her stay, she started saying that she was not in the original clinic in Prague anymore, but in a 'suburb clinic' located in her birthplace, a replica of the original one (Pick 1903). As in the original Bonnet's description, the patient could not be convinced otherwise and constantly tried to find arguments against the counter-evidence that was being shown. For instance, she reported that she already knew the 'suburb clinic' doctors because they also worked in the original one in Prague.

Definition and clinical subtypes

Reduplicative paramnesia is defined as a spatial misidentification syndrome in which patients firmly believe that they are in a different place from the real one and their conviction does not change when are confronted with clear counterfactual evidence (Politis and Loane 2012; Bartolomeo et al. 2016). Three different subtypes of reduplicative paramnesia have been described: a) in place reduplication, patients believe that they are in a replica of the original place, as Pick described (Pick 1903); b) in chimeric assimilation

(Fisher 1982), patients are convinced that two places were combined or fused (e.g., the hospital is inside the patient's home); c) in confabulatory mislocation (Murai et al. 1997), patients localize themselves in a considerably different place from the real one (e.g., the conviction of being at home instead of being at the hospital). At the psychopathological level, these three subtypes have been positioned in opposite pathological familiarity poles (Devinsky 2009): place reduplication is thought to represent place hypofamiliarity, while chimeric assimilation and confabulatory mislocation express an excessive familiarity for places (Darby and Prasad 2016).

Pathophysiological models

At the behavioural level, spatial delusions seem to disrupt the matching between implicit memory and explicit spatial interpretation processes. Three main empiric models have been proposed in the literature to explain these phenomena. First, memory-related theories advocate that reduplicative paramnesia results from an abnormal integration of new visuospatial information with previous spatial memories, resulting in a pathological update of patients' mental representation of space (Staton et al. 1982). Second, implicit recognition models propose that delusion misidentification syndromes result from the abnormal unconscious assignment of familiarity and emotional values to spatial stimuli (Ellis and Young 1990). Despite maintaining intact explicit recognition mechanisms, they are overcome by the erroneous information provided by the covert recognition systems. Third, it was also proposed that there might be an inter-hemispheric unbalance, in which the right-hemispheric lesions impair self-monitoring and emotional valence attachment, while the left hemisphere release contributes to the emergence of false explanations (Devinsky 2009).

3. Macroscale brain changes in behavioural disorders

Historically, the analyses of macroscale brain changes associated with cognitive and behavioural disorders significantly contributed to the foundation of 'modern neuroscience' and to a better understanding of disease pathophysiology.

In the nineteenth century, Paul Broca reported a remarkable observation that revolutionized our knowledge about the neurobiology of language disorders. He studied two patients, *Monsieur* Leborgne and *Monsieur* Lelong, that lost the ability to produce speech. He observed that both had structural lesions in the left inferior frontal gyrus (Broca 1861; Dronkers et al. 2007). Associating a specific mental process with a localized brain region was the starting point of the cortical "localization" theories. A few years later, Carl Wernicke also used the focal lesion model to propose that the left superior temporal gyrus was the brain area responsible for language comprehension (Mesulam et al. 2015). Notably, he and other eminent neuroscientists, such as Theodor Meynert, contributed to the development of "connectionism", a complementary school of thought that highlighted the importance of anatomical connections between different regions for proper cognitive functioning (Catani and Thiebaut de Schotten 2012).

The mentioned observations were based on post-mortem assessments of brain anatomy. During the last decades, the methods used to explore the brain anatomical changes associated with behavioural disorders dramatically improved.

Structural imaging

The advent of brain CT and brain MRI allowed the *in vivo* delimitation of brain lesions. Later on, statistical methods were developed to analyze large groups of patients, such as voxel-based and cluster-based lesion-symptom mapping (Bates et al. 2003; Foulon et al. 2018). With this, the "localization" models of cognitive function were complemented and refined (Lerch et al. 2017).

Structural MRI also allowed the study of structural disconnection. Tractography consists of the indirect reconstruction of brain white matter tracts by analyzing anisotropic diffusion patterns of water molecules in the brain. The study of structural disconnection enlightened the pathophysiology of behavioral syndromes that were not sufficiently explained by a single lesion location, i.e., the disconnection syndromes (Catani and

Ffytche 2005; Catani and Thiebaut de Schotten 2008; Herbet and Duffau 2020; Thiebaut de Schotten et al. 2020).

Functional imaging

Furthermore, the analysis of the blood-oxygen-level-dependent (BOLD) signal in MRI permitted the indirect assessment of metabolically active brain areas during a particular cognitive task. This MRI modality was called functional MRI (fMRI).

Interestingly, the investigation of BOLD during rest revealed the existence of correlations between the low-frequency fluctuations (0.01– 0.1 Hz) of distant brain regions (Power et al. 2011). These synchronous fluctuations match the patterns of activation in task-based fMRI. The first demonstration was in the sensorimotor cortex when Biswal and colleagues realized that the map of fMRI activation during bilateral finger-tapping closely matched the low-frequency resting-state correlation maps seeded from the same region (Biswal et al. 1995). Later, the same effect was observed across different sensorial and cognitive tasks (Lowe et al. 2000; Cordes et al. 2001; Fox and Raichle 2007; Smith et al. 2009) and the correlation profiles were spatially consistent between subjects (Damoiseaux et al. 2006). The analysis of resting-state functional connectivity transition patterns led to the parcellation of the brain in major functional networks (Gordon et al. 2016; Eickhoff et al. 2018).

Resting-state functional networks

Functional networks can be organized according to their physiological roles: 1) the visual, the auditory and the sensorimotor networks are primary networks; 2) the language, the fronto-parietal and the executive-control networks are higher-order cognition networks; 2) the default mode, the ventral attention and the dorsal attention networks are multimodal integrative networks (Thomas Yeo et al. 2011; Sepulcre et al. 2012; Gordon et al. 2016; Margulies et al. 2016; Lopez-Larson et al. 2017; Jimenez-Marin et al. 2018). Aberrant patterns of network activation and deactivation have been associated with several neurological and psychiatric brain diseases, such as Alzheimer's disease, Parkinson's disease, epilepsy and schizophrenia (Menon 2011; Spetsieris et al. 2015), as well as with specific behavioural syndromes, namely visuospatial neglect (He et al. 2007a), anosognosia (Perrotin et al. 2015) and auditory hallucinations (Alderson-Day et al. 2016).

Phenomenologically, delusions of space do not seem to be explained by deficits in single cognitive domains but by a dysfunctional multidomain integration. Patients with reduplicative paramnesia can correctly identify and explicitly say the correct location of surrounding environmental landmarks, but still misinterpret their own spatial position (Benson et al. 1976). Furthermore, they understand the counter-arguments presented, and may even admit some oddness in their thoughts, but still do not update their spatial misbelieves (Kapur et al. 1988).

Multimodal integrative networks I: the default mode network

The default mode network was initially defined as a set of brain regions that were metabolically more active during resting wakefulness than when performing an externally oriented task (Shulman et al. 1997b; Raichle et al. 2001). It was viewed as the functional backbone of internally driven mental activities, such as mind-wandering, autobiographical memory, theory of mind and future thinking (Buckner and Carroll 2007). Currently, the actual role of the default mode network in brain physiology is still intensively discussed, but leading perspectives regard it as the central integrative system of high order functions, such as memory, emotion and abstract thinking (Vatansever et al. 2015; Smallwood et al. 2021). It is on the apex of functional cortical gradients, on the opposite side of primary networks, such as the somatosensory network (Margulies et al. 2016; Buckner and Margulies 2019). In addition, stepwise functional connectivity analysis places the default mode network at the top of the hierarchal organization, acting as a hub of brain activity (Sepulcre et al. 2012).

Anatomically, two core regions compose the default mode network: the posterior cingulate and anterior medial prefrontal cortex. The other network nodes are functionally organized in two subsystems: a) the dorsal medial prefrontal cortex subsystem, constituted by the dorsal medial prefrontal cortex, the temporal pole, the lateral temporal cortex and the temporoparietal junction; b) the medial temporal subsystem, comprised by the hippocampal formation, the parahippocampal cortex, the retrosplenial cortex, the posterior inferior parietal lobule and the ventral medial prefrontal cortex (Andrews-Hanna et al. 2010).

Multimodal integrative networks II: attention networks

The attentional processes integrate sensorial information with expectancies, prior knowledge and current objectives (Corbetta and Shulman 2002). Attention networks are segregated into two main systems: the ventral attention network and the dorsal attention network (Corbetta and Shulman 2002; Petersen and Posner 2012). The dorsal attention network acts as a top-down modulator and participates in goal-driven tasks. The ventral attention network is a stimulus-driven system that mediates reorientation to relevant or unexpected events.

Anatomically, the core regions of the dorsal attention network are the intraparietal sulcus, the superior parietal lobe and the frontal eye fields (Corbetta et al. 2000; Buschman and Miller 2007), whereas the temporo-parietal junction and the ventrolateral prefrontal cortex constitute the central regions of the ventral attention network (Downar et al. 2000).

4. Stroke

Stroke is the third most common cause of morbidity worldwide (Feigin et al. 2017). In Portugal, approximately 23.000 patients/year are discharged from hospitals with stroke diagnosis. It is estimated that more than 25 million people in the world have already had a stroke (Direcção Geral de Saúde 2014; Feigin et al. 2017).

Stroke and behaviour

Behavioural changes and cognitive impairment are very frequent after stroke. It is estimated that at least one cognitive deficit is present in almost 70% of patients during the first month after stroke (Rasquin et al. 2004) and in around 50% one year later (Barbay et al. 2018; Pendlebury and Rothwell 2019; Weaver et al. 2021). Cognitive deficits are a major contributor to stroke morbidity and the treatment of cognitive impairment was considered one of the most critical priorities of stroke research (Pollock et al. 2012).

Over decades, stroke-associated cognitive deficits have been conceptualized and their pathophysiology investigated (Caplan and van Gijn 2012). In language disorders, the subtypes of aphasia were defined (Geschwind 1971; Damasio 1992), reading and writing deficits were characterized (Benson 1977; Roeltgen and Lacey 2010) and category-specific naming impairments were reported (Hillis and Caramazza 1991; Martins and Farrajota 2007). Major elucidations were also made in other cognitive domains. For instance, neglect for personal, extra personal and representational spaces was described (Bisiach and Luzzatti 1978; Buxbaum et al. 2004), and its expression in different spatial references and sensory-motor forms was observed (Ferro et al. 1984; Andre et al. 2000; Corbetta and Shulman 2011; Heilman and Valenstein 2012). In the study of agnosias, the neuropsychological differentiation between apperceptive and associative deficits and their association with stroke-lesion patterns was reported (De Renzi et al. 1969; McCarthy and Warrington 1986). Advances of similar importance were made in other cognitive domains (Caplan and van Gijn 2012).

Acute stroke treatment

Acute stroke treatment evolved dramatically during the last three decades. Firstly, the clinical efficacy of endovenous thrombolysis in improving post-stroke disability was

shown (The NINDS rt-PA Stroke Study 1995). Alteplase and tenecteplase convert plasminogen to plasmin, a proteolytic enzyme that lyses fibrin and favours clot dissolution. More recently, endovascular thrombectomy has also been shown to reduce stroke-associated impairment. It consists of the mechanical removal of the occluding clot with an arterial catheter. Currently, endovenous thrombolysis and endovascular thrombectomy can be performed until 9 hours or 24 hours after symptoms onset, respectively, according to clinical and advanced imaging parameters (Badhiwala et al. 2015; Nogueira et al. 2018; Ma et al. 2019).

II. Open questions and aims

1. Clinical features and pathophysiology of spatial delusions

Open questions

Reduplicative paramnesia may be more frequent than classically thought. Murai and colleagues reported a prevalence of 17% in a cohort of patients admitted to a rehabilitation unit with either right-sided or bilateral lesions – mainly stroke and traumatic brain injuries (Murai et al. 1997). In neurodegenerative brain diseases, a prevalence of 20% was reported in Dementia with Lewy bodies (Nagahama et al. 2007, 2010). In the moderate stage of Alzheimer's disease, it might be as high as 30% (Perini et al. 2016). However, the available knowledge about reduplicative paramnesia is mostly based on case reports and small case series (Politis and Loane 2012) and broader empirical evidence is lacking. On the one hand, the neuroanatomical systems supporting the phenomenon of spatial delusions are generally undefined. Reduplicative paramnesia is mainly associated with right hemispheric injury, but the lesions' topography is heterogeneous (Politis and Loane 2012; Bartolomeo et al. 2016). Damage of right frontal, temporal and thalamic regions has been described (Leiguarda 1983; Hudson and Grace 2000; Pignat et al. 2013; Peckins et al. 2016) so that the dysfunction of a single brain region does not seem to be a satisfactory anatomical explanation. On the other hand, a comprehensive and systematic characterization of the clinical features of this syndrome, based on larger samples, is missing.

Narrowing the gap of unanswered questions about reduplicative paramnesia would be relevant. At the clinical level, spatial delusions can disturb patients' behaviour and their misdiagnosis as an acute confusional state (delirium) or psychomotor agitation might occur. Proper recognition of the syndrome might also be important to elucidate patients' relatives and reduce their distress when confronted with patients' beliefs. At the physiopathological level, delusions are a core manifestation of several brain diseases. However, the mechanisms underlying thought content incongruences and thematic specificities are still under large debate in the literature (Sacks and Hirsch 2008; Coltheart et al. 2011; Feeney et al. 2017). The association of reduplicative paramnesia with focal brain lesions constitutes a particular opportunity to better understand the pathophysiology of delusional and spatial interpretation disorders.

Aims

1. Describe the phenomenological features of spatial delusions in acute stroke.
2. Investigate the structural and functional basis of spatial delusion in acute stroke.

2. Anatomical models of multimodal integrative networks

Open questions

The neuroimaging exploration of the default mode and of the attention networks has taken a corticocentric approach. However, clinical, electrophysiological and phylogenetic data suggest that they also comprise subcortical components.

First, the default mode network topographically overlaps with the extended model of the limbic system (MacLean 1949, 1952). However, limbic subcortical structures, such as the anterior thalamic nuclei and the mammillary bodies, are not represented in the default mode network anatomical models (Papez 1937; Catani et al. 2013). Second, some paradigmatic attentional deficits arise from subcortical lesions, such as subcortical visuospatial neglect (Healton et al. 1982; Karnath et al. 2002; Lamar et al. 2011). Finally, phylogenetically distant animals, such as rats and pigeons, have markedly different cortical anatomies, but possess default mode network and exhibit human-like attention behaviours, respectively (Blough 1977; Sforazzini et al. 2014).

The main clusters of stroke lesions are subcortical (Corbetta et al. 2015). Understanding the subcortical anatomy of the default mode network and the ventral and dorsal attention networks would be important to better understand stroke-induced cognitive disturbances.

Aims

3. Investigate the subcortical anatomy of the default mode network.
4. Investigate the subcortical anatomy of the ventral and dorsal attention networks.

3. Spatial delusions and stroke treatment modalities

Open questions

Endovenous thrombolysis and endovascular thrombectomy may change the anatomy of stroke brain damage. These treatments reduce lesion volumes (Mair et al. 2018; Nogueira et al. 2018) and change their anatomical distribution. Successful recanalization of the middle cerebral artery after endovenous thrombolysis has been shown to result in predominantly peri-insular infarcts (Seitz et al. 2009). In endovascular thrombectomy, clot fragmentation and arterial ostia occlusion may occur during thrombus manipulation and extraction, leading to infarcts in initially spared arterial territories (Puntonet et al. 2019). The proximal branches of the middle cerebral arteries seem to be particularly prone to this phenomenon.

These new infarct configurations may modulate the behavioural consequences of stroke, by modifying the patterns of strategic lesions and connectivity disruptions. Previous studies demonstrated that endovenous thrombolysis alters the profile of post-stroke aphasia (Jacquin et al. 2014; Martins et al. 2017). The impact of intravenous thrombolysis and mechanical thrombectomy on the frequency and nature of other behavioural stroke syndromes, such as delusions of space, is largely unknown.

Aim

5. Analyse how acute stroke revascularization therapies may modulate the occurrence of spatial delusions.

III. Studies

In this chapter, we describe the studies that constitute this thesis. They are not presented by the chronological order of performance but in line with a scientific and clinical rationale. The sample sizes vary according to the periods of recruitment.

In study I, we performed a systematic review of focal brain lesion-associated spatial delusions reports and investigated their phenomenological and neuroimaging features.

In studies II and III, we analysed a prospectively collected sample of acute right hemisphere stroke patients screened for the occurrence of spatial delusions. Study II focused on describing the clinical and phenomenological features of spatial delusions and their neural correlates. In study III, we performed a case-control analysis of the structural and functional basis of the syndrome.

Given the putative relationship of the multimodal integrative networks with the pathophysiology of spatial delusions, studies IV and V investigated the anatomy of the default mode networks and the ventral and dorsal attention networks, particularly of their subcortical structures. These studies were based on the analysis of healthy subjects' MRI samples.

Finally, in study VI, we investigated the relationship between acute stroke treatment modalities and the occurrence of spatial delusions. This study derived from a subanalysis of the ischemic stroke patients included in studies II and III.

1. Spatial delusions after focal brain lesions: a systematic review

Part of this section was published in the following article:

- Alves PN, Silva DP, Fonseca AC, Martins IP (2021) Mapping delusions of space onto a structural disconnectome that decouples familiarity and place networks. Cortex 146:250–260. https://doi.org/10.1016/j.cortex.2021.11.008

Introduction

Observational studies have demonstrated that reduplicative paramnesia is a frequent manifestation of different brain disorders, either of degenerative or focal aetiology. In a cohort of patients with right hemispheric focal brain injuries (either right-side or bilateral) who were admitted to a rehabilitation centre (mostly stroke and traumatic brain injuries), Murai and colleagues reported a prevalence of 17% (Murai et al. 1997). In Dementia with Lewy bodies, the described prevalence is 20% (Nagahama et al. 2007), while in the moderate stages of Alzheimer's disease it might be as high as 30% (Perini et al. 2016). At the neuropsychological level, reduplicative paramnesia has been associated with neuropsychological deficits in executive functions and in non-verbal episodic memory tasks (Borghesani et al. 2019). However, the neuroanatomical basis of this syndrome remains elusive (Bartolomeo et al. 2016). On the one hand, delusions misidentifications have been associated with functional disturbances of familiarity and belief evaluation networks (Darby et al. 2017), but how this relationship is established at the structural level is uncertain. On the other hand, the neural basis of the content specificity for places that characterizes the delusional beliefs of reduplicative paramnesia is undetermined. The occurrence of delusions of space after focal brain lesions constitutes a particular opportunity to unveil the neuroanatomical circuits underlying their phenomenological and functional features.

Here, we performed a systematic review of lesion-associated spatial delusions. We aimed to analyse their clinical and phenomenological features, to study their topographic and connectivity patterns, and to investigate their spatial relationship with functionally related network maps.

Methods

Search strategy and selection criteria

To identify cases of reduplicative paramnesia associated with focal brain lesions, we performed a systematic review. Protocol development and result reports were done according to The Preferred Reporting Items for Systematic Reviews and Meta-Analyses (PRISMA) guidelines.

The search term 'reduplicative paramnesia' and the related search terms 'reduplicative phenomenon', 'chimeric assimilation', 'confabulatory mislocation', 'extravagant spatial localization', 'delusional misidentification', 'space confabulation', 'spatial confabulation'

and 'spatial delirium' were applied in the databases Pubmed, EMBASE, PsycInfo and Web of Science. First, the abstracts were screened. If there was not enough information in the abstract, the full text was consulted. The specific search formulas are available Table 1. The inclusion and exclusion criteria, and the data extracted are available in Table 2.

Table 1. Search formulas used in each database (from their inception until 30/1/2018).

Database	**Search formula**
Pubmed	(reduplicative paramnesia OR reduplicative phenome* OR chimeric assimilation OR confabulatory mislocation OR extravagant spatial locali* OR delusional misidentification OR space confabulation OR spatial confabulation OR spatial delusion)
EMBASE	reduplicative AND paramnesia OR (reduplicative AND phenome*) OR (chimeric AND assimilation) OR (confabulatory AND mislocation) OR (extravagant AND spatial AND locali*) OR (delusional AND misidentification) OR (space AND confabulation) OR (spatial AND confabulation) OR (spatial AND delusion)
PsycInfo	(reduplicative paramnesia OR reduplicative phenome* OR chimeric assimilation OR confabulatory mislocation OR extravagant spatial locali* OR delusional misidentification OR space confabulation OR spatial confabulation OR spatial delusion)
Web of Science	TOPIC:(reduplicative paramnesia) OR TOPIC: (reduplicative phenome*) OR TOPIC: (chimeric assimilation) OR TOPIC: (confabulatory mislocation) OR TOPIC: (extravagant spatial locali*) OR TOPIC: (delusional misidentification) OR TOPIC: (space confabulation) OR TOPIC: (spatial delusion) OR TOPIC: (spatial confabulation)

Lesion topography analysis

The reports with brain images available were selected. Each lesion was mapped onto a common brain atlas, the MNI152 1mm standard space. Two clinicians with experience in the analysis of brain images performed lesion tracing. The slices that best matched the published images in each article (either, axial, coronal or sagittal) were chosen by consensus between the two clinicians. Neuroanatomical landmarks were used as reference for slice selection (Boes et al. 2015). Then, both authors independently performed lesion tracing on the selected slices using FSLeyes (https://fsl.fmrib.ox.ac.uk/fsl/fslwiki/FSLeyes).

Inter-observer agreement was analysed by calculating the Dice similarity coefficient (Liew et al. 2018):

$$\mathrm{DC} = \frac{2|\mathrm{X} \cap \mathrm{Y}|}{|\mathrm{X}| + |\mathrm{Y}|}$$

where X and Y represent the voxels selected by each investigator, and DC represents the similarity coefficient that ranges from 0 (no overlap) to 1 (perfect overlap). The percentage of voxels for which the investigators disagreed was also calculated. Lesions were extended 2mm perpendicular to the planes they were registered. According to Boes and colleagues, this method allows a conservative balance between inflated and scarce lesion overlap when lesions are extracted from the literature (Boes et al. 2015).

Table 2. Inclusion and exclusion criteria, and data extracted.

Inclusion criteria	- Manuscripts reporting on reduplicative paramnesia. All types of observational studies were considered.
Exclusion criteria	- Spatial delusions secondary to a primary delusional disorder of psychiatric aetiology; - Studies about delusional misidentification syndromes in general, without a proper discrimination of delusional misidentification for places; - Reviews; - Inability to access the full version of the article.
Data extracted	- Study design; - Demographic features; - Aetiology; - Subtype of reduplicative paramnesia; - Place of mislocation; - Duration of reduplicative paramnesia; - Coexistence of other delusional misidentification syndromes; - Neuroimaging data.

For statistical analysis, two different control datasets were used. We used a database of 233 stroke lesions prospectively collected in our stroke unit. Patients were recruited from December 2016 to February 2020. Reduplicative paramnesia is a right-hemisphere syndrome (Bartolomeo et al. 2016). The database included ischemic stroke and intracerebral haemorrhage lesions with right hemisphere involvement (either right-sided or bilateral). Patients were systematically evaluated for reduplicative paramnesia and none of the included patients presented reduplicative paramnesia during the period of their

hospitalization (median length of hospitalization=7 days, interquartile range 5-11 days). Lesion delimitation was performed manually based on MRI (preferentially) or CT images in the native space. Then, the images were registered to the MNI152 space. For MRI, the sequence of reference for lesion delimitation was the diffusion-weighted imaging (de Haan and Karnath 2018). T1 images were linearly registered applying an affine transformation (12 degrees of freedom) using FSL's tool *flirt* (Jenkinson et al. 2012). Then, a non-linear registration was performed using FSL's tool *fnirt*. For CT images, a linear registration with an affine transformation was performed (de Haan and Karnath 2018). Finally, the deformation fields were applied to the lesion masks.

In addition, we used the open-source dataset ATLAS (Anatomical Tracings of Lesions After Stroke; Liew et al., 2018). ATLAS is a multicentre neuroimaging collection, derived from 11 cohorts worldwide, that includes 304 ischemic stroke lesions of different arterial territories. Lesions were manually delimited based on high resolution T1-weighted structural MRI, and 229 of them were normalized to the MNI152 space. No behavioural data is publicly available in this dataset.

For proper comparison of reduplicative paramnesia lesions extracted from the literature, we selected the slices from the stroke controls dataset where there were lesions in the reduplicative paramnesia group (Barahona-Corrêa et al. 2020). Then, they were matched for lesion volume and for hemispheric lateralization (either right, left or bilateral). Each reduplicative paramnesia lesion was matched with four control stroke lesions, two from our inward dataset and two from the ATLAS dataset.

Randomise is a FSL tool that computes nonparametric permutation inference on neuroimaging data (Winkler et al. 2014). To calculate brain areas significantly associated with reduplicative paramnesia, a permutation test comparing cases and stroke controls was performed using this tool (Winkler et al. 2014). Five thousand permutations were computed, applying a threshold-free cluster enhancement, and the statistical maps were family-wise error corrected.

To evaluate the generalization of our results, the sample was split in two groups: the exploratory sample and the validation sample. Splitting was performed randomly, controlling for lesion volume. First, we run randomise in the exploratory sample. If there were statistically significant differences between cases and stroke controls, we analysed if the results were replicable in the validation sample, i.e., if the regions that were found in the exploratory sample also presented statically significant differences in the validation sample.

Age is a proxy of brain reserve and is an important determinant of cognitive disturbances after focal brain lesions (Umarova et al. 2021). Therefore, we also performed a regression analysis, using FSL's tool *randomise*, in which we included patients' age as a covariate in the model (de Haan and Karnath 2018). In this analysis, we could not include the control stroke lesions from ATLAS dataset, because the information about the age of these patients is not publicly available. Since no information is available about the putative occurrence of reduplicative paramnesia in the ATLAS dataset, this sensitivity analysis also allowed a comparison with control stroke patients that were systematically assessed for the presence of the syndrome.

Structural connectivity

Disconnectome (http://www.bcblab.com; Foulon et al., 2018; Thiebaut de Schotten et al., 2014) is a tool that superimposes brain lesion maps onto tractography reconstructions obtained from a group of healthy controls and indirectly estimates which fibre tracts would be disrupted by a focal lesion. The output is a structural disconnection map representing the probability of each voxel being disconnected by a certain lesion. We derived disconnection maps from the 7 Tesla dataset of the Human Connectome Project (n=178; Vu et al., 2015). Tractographies were obtained using a whole-brain determinist approach, using the StarTrack software (https://mr-startrack.com), and applying a spherical deconvolution methodology, specifically a damped Richardson-Lucy algorithm. They were made available with BCBtoolkit (http://www.bcblab.com) and the full details of pre-processing are described in Karolis et al., 2019. Voxels were included in the disconnectome map if they were disconnected in more than 50% of tractographies (Foulon et al. 2018).

Randomise was used to perform the permutation test comparing the structural disconnection maps between cases and stroke controls, using the same settings and the same cross-validation approach detailed in the section about the lesion topography analysis. In addition, we performed a regression analysis including patients' age as a covariate in the model, as specified in the previous section. Since tumours may displace surrounding white matter tracts (Witwer et al. 2002) and bias the structural connectivity analysis, a supplemental analysis excluding tumoral lesions was also computed.

Classification performance of the lesion topography and of the structural disconnection maps

To evaluate the classification performance of the neuroimaging models, i.e. their accuracy to correctly identify cases of reduplicative paramnesia in an independent lesion sample, voxel-wise balanced accuracy maps were computed using lesion topography maps or structural disconnection maps as predictors. Logistic regression was the classification algorithm applied, and the output variable was the occurrence of reduplicative paramnesia. First, the models were trained (i.e. the logistic weights were estimated) in the exploratory sample. Then, the performance of the logistic model to correctly classify a neuroimaging input as corresponding or not to a case of reduplicative paramnesia (at a voxel level) was evaluated in the validation sample. Therefore, the classification performance was evaluated in a group of neuroimaging maps that did not contribute to the building of the model.

Our dataset was imbalanced, in a ratio of 1 case to 4 controls. Evaluation of classification performance in imbalanced datasets can be misleading, because most predictive techniques have a poor performance on the minority class (He and Garcia 2019). To address this issue, we used the Synthetic Minority Over-sampling Technique (SMOTE) algorithm to perform a synthetic over-sampling of the minority class in the exploratory sample, by linearly interpolating new minority instances between the 5 nearest neighbours, as recommended (Chawla et al. 2002; Luque et al. 2019). Balanced accuracy was chosen as the classification metric, to avoid the spuriously high accuracy estimations that may occur in the evaluation of imbalanced datasets (Chawla 2005). The analysis was performed using scikit-learn 0.24.1 package (Pedregosa et al. 2011).

Structural-functional coupling

Neurosynth (http://neurosynth.org/) is an automated and validated tool to extract large-scale neuroimaging data from the literature (Yarkoni et al. 2011). Based on text-mining and machine-learning techniques, it generates meta-analytic maps of functional studies whose abstract mention a certain term of interest.

Darby and colleagues (Darby et al. 2017) studied the relationship between the functional meta-analytic maps of familiarity and belief evaluation and the functional connectivity maps of 17 lesion-induced delusional misidentifications. They found an overlap between them, however it is unknown how this relationship is established at the structural level, i.e. if it is mediated directly by the lesions or by structural disconnection.

Here, we used Neurosynth to generate functional meta-analytic maps of similar terms, namely 'familiarity' and 'belief'. There are several forms of delusional misidentifications, which manifest for different kinds of stimuli. Reduplicative paramnesia is a delusional misidentification of space and places. Therefore, these two terms – 'space' and 'place' – were also included. Other monothematic delusional misidentification syndromes manifest for other kinds of stimuli (Devinsky 2009): Capgras and Fregoli syndromes for faces, somatoparaphrenia for parts of the body, most commonly limbs; and Cotard syndrome for interoceptive stimuli. To test the hypothesis that reduplicative paramnesia would be associated with 'place' or 'space'-related functional networks, but not with networks related to 'faces', 'limb', 'body' and 'interoceptive', these terms were included too.

Since reduplicative paramnesia was also associated with neuropsychological deficits in executive functions and in non-verbal episodic memory tasks (Borghesani et al. 2019), we performed a supplemental analysis including the Neurosynth terms 'executive functions' and 'memory task'.

The Neurosynth extracted maps are thresholded to correct for multiple comparisons, using a False Discovery Rate criterion of 0.01. This threshold is applied by default in Neurosynth (http://neurosynth.org/). No additional threshold was applied.

Then, we analysed the spatial correlation between the functional meta-analytic maps of the terms of interest and the lesion topography maps. In addition, we performed the same analysis with the structural disconnection maps. Since Neurosynth maps predominantly represent areas of cortical activation, while the tractography-derived masks mainly correspond to white matter regions, we projected the disconnectome maps to the cortical ribbon. First, we converted streamline tractographies into streamline density volumes, in which voxel values corresponded to the number of fibres crossing each voxel (Nozais et al. 2021). This step was performed using the MRtrix3 command *tckmap* (Tournier et al. 2019). Second, all individual streamline density volumes were aligned with each other by performing a diffeomorphic normalization (Nozais et al. 2021). This step was computed using the Advance Normalisation Tools' script *buildtemplateparallel.sh*, and defining cross-correlation as the similarity measure and greedy SyN as the transformation model (Avants et al. 2011). With this, we obtained an average template of the streamline density volumes. Third, we registered the average template to the MNI152 1mm standard space, using FSL's tool *flirt* (Jenkinson et al. 2012; Nozais et al. 2021), and applied the transformation warp to the individual disconnection maps. With this, we obtained disconnectome maps projected into grey matter. Then, we analysed the spatial correlation

between the functional meta-analytic maps of the terms of interest and the projected disconnectome maps.

Finally, we also analysed if the relative spatial overlap of the lesion topography and of the structural disconnection maps with the meta-analytic functional maps was significantly different, in the cases of reduplicative paramnesia. The Dice similarity coefficient was calculated and a paired comparison was performed.

Statistical analysis

Continuous variables were reported as mean (standard deviation) or median [interquartile range] and compared using two-tailed unpaired-t test or Mann-Whitney test, as appropriate. Categorical variables were reported as frequencies.

Alpha levels were set at 0.05 for statistical significance. In the neuroimaging analysis, a family-wise error rate approach was used to correct for multiple comparisons. For the comparison of other variables, a Bonferroni correction was applied.

The statistical approach to build and evaluate the classification performance of the neuroimaging models was presented previously, in the corresponding section.

Results

Our database search retrieved a total of 1949 references, 932 repeated references were removed and the free search resulted in 7 new references. The total number of analysed references was 1024. A total of 708 references were excluded after abstract screening and 166 after assessing the full text. Of the 57 articles included, most were case reports and case series. The flow diagram of study selection is displayed in Figure 3. The total number of patients with reduplicative paramnesia was 123. Of these, 67 were associated with focal brain lesions. Twenty-four cases had MRI or CT images available (MRI, n=10; CT, n=14). All images were reported separately, i.e., none corresponded to group-level analyses.

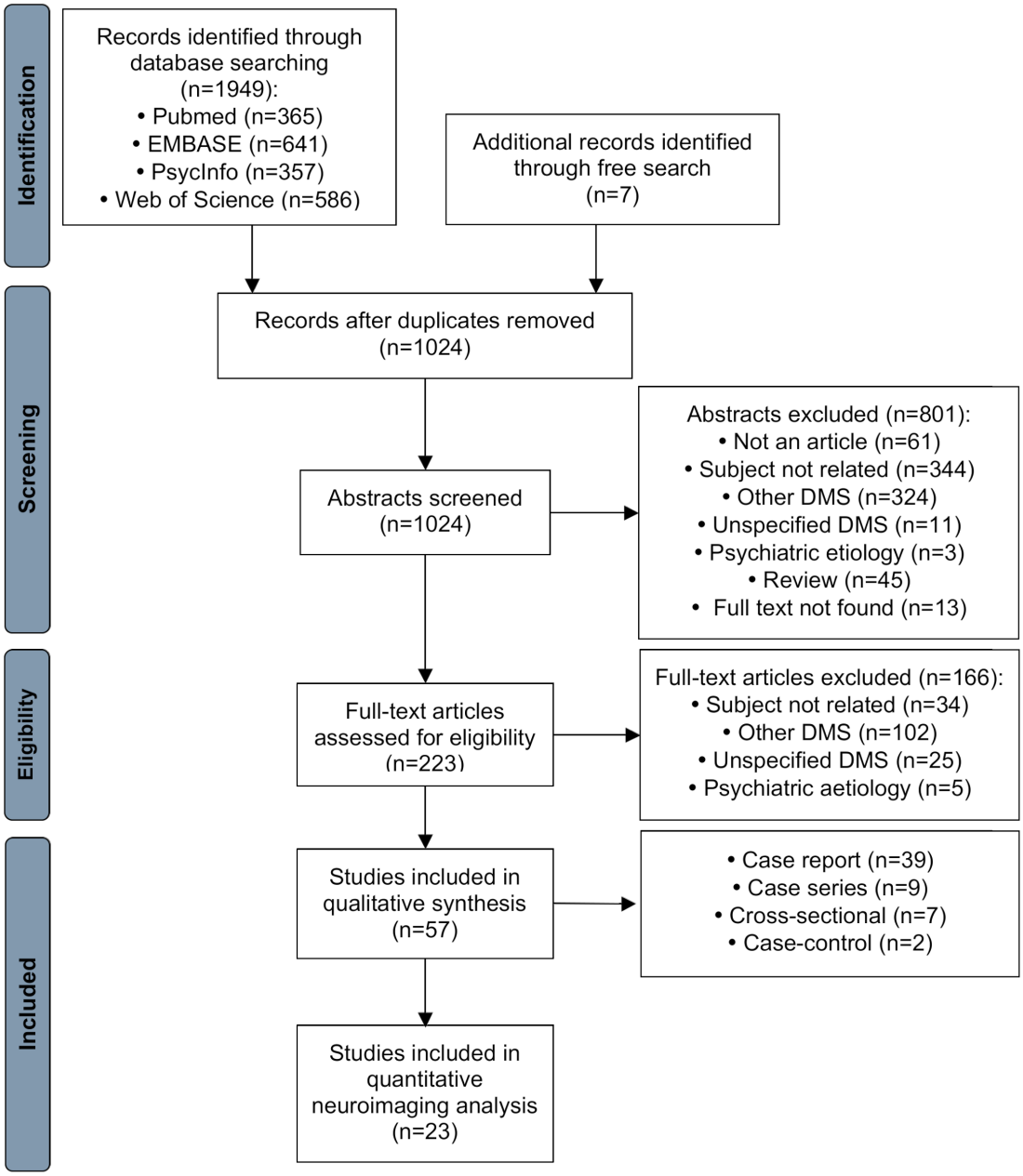

Figure 3. Flow diagram of study selection. DMS, Delusional Misidentification Syndromes. The numbers reported refer to the number of studies in each step of the flowchart.

Demographic and phenomenological characteristics

The median age of the 67 patients reported was 66 [53-72] years old and the median time duration of delusions of space was 60 [30-113] days (reported in 31 cases). The phenomenological features of the reported cases are presented in Table 3.

Table 3. Phenomenological characteristics of delusions of space

Subtype of reduplicative paramnesia (reported in 67)	Place reduplication	35 (52%)
	Chimeric assimilation	9 (13%)
	Confabulatory mislocation	9 (13%)
	Place reduplication and confabulatory mislocation	7 (10%)
	Reduplication and chimeric assimilation	3 (4%)
	Confabulatory mislocation and chimeric assimilation	4 (6%)
Content of delusions of space (reported in 67)	Reduplication of the hospital	31(46%)
	Reduplication of the patient's home	8 (20%)
	Combination of hospital and patient's home spaces	8 (12%)
	Mislocation of the hospital to a familiar place	2 (3%)
	Misidentification of home as another familiar place	2 (3%)
	Misidentification of the hospital as patient's home	2 (3%)
	Reduplication of other places	1 (1%)
	Combinations of other places	1 (1%)
	Other mislocations	2 (3%)
	Other misidentifications	1 (1%)
	Mixture of two of the previous delusional contents	9 (13%)
Association with other delusional misidentification syndromes (reported in 66)	Capgras syndrome	2 (3%)
	Reduplication of people	7 (11%)
	Fregoli syndrome	2 (3%)
	Reduplication of body parts	3 (5%)
	Intermetamorphosis	3 (5%)
	Cotard syndrome	2 (3%)
	Self-misidentification	1 (2%)
	Fregoli syndrome and reduplication of body parts	1 (2%)
	Unspecified misidentification of people	11 (17%)
	No association with other delusional misidentification syndromes	34 (52%)
Psychiatric history (reported in 49)	Previous suicide attempt (unspecified disease; no history of delusions)	1 (2%)
	No antecedents of major psychiatric disease	48 (98%)

The aetiologies of the lesions with brain images available (n=24) were: stroke, n=17; tumour, n=3; trauma, n=2; encephalitis, n=1; and subarachnoid haemorrhage with focal parenchymal lesions, n=1. A summarizing table, detailing the type of study, the number of patients assessed, the patients' age and schooling, the lesion aetiologies and locations, and the results of the neuropsychological assessment for each case is provided in Table 4.

Table 4. Summary of the study and clinical details of the included cases

Reference	Study type (patients included)	Age	Schooling	Aetiology	Lesion location	Neuropsychological assessment
Peckins et al., 2016	Case report (1)	88	NR	Ischemic stroke	Right thalamus	NR
Nishio and Mori, 2012	Case report (1)	69	University	Ischemic stroke	Right fronto-temporo-parietal and thalamus	MMSE score of 21. Left unilateral spatial neglect (Behavioural Inattention Test). Discrimination of pairs of unknown faces slightly below normal (Visual Perception Test for Agnosia).
Fisher, 1982	Case series (1 out of 2 described)	72	University	Ischemic stroke	Right parieto-occipital	NR
Budson et al., 2000	Case report (1)	45	NR	Ischemic stroke	Left occipito-temporal	Right-sided neglect (letter cancellation test). Deficits in visual-motor processing speed (Trail Making Test A and B), response inhibition (Stroop Test), visuospatial integration (Hooper Visual Organization Test and Ravens Colored Matrices) and visual memory (Wechsler Visual Memory - delayed)
Likitcharoen and Phanthumchind, 2004	Case report (1)	66	NR	Ischemic stroke	Right parieto-temporal	MMSE score of 26. Left tactile and visual neglect (clock-drawing). Deficits in working memory (Digit Span Backwards) and visuoconstructive abilities (copy of cube and intersecting pentagons). No deficits in person and time orientation, memory and language.

Hudson and Grace, 2000	Case report (1)	71	NR	Ischaemic stroke	Right temporal	Deficits in visual immediate memory (visual span), visual-motor processing speed (Trail Makin Test A and B), visual memory (Wechsler Visual Memory and Rey complex figure – memory), and semantic fluency. No deficits in attention and concentration, verbal intellectual skill and reasoning, verbal learning and memory, language, mental calculation, and oral and manual praxis.
Pignat et al., 2013	Case report (1)	53	NR	Traumatic brain injury	Right temporal and bilateral orbito-frontal	Deficits in time orientation, executive functions and memory - verbal anterograde (10 words CERAD test) and autobiographic modalities. No deficits in semantic memory, attention, language, motor praxia, and visuospatial perception.
Yamada et al., 2003	Case report (1)	73	NR	Brain tumour	Right fronto-temporal	MMSE score of 22. Deficits in cognitive abstraction and flexibility (Wisconsin Card Sorting test) and verbal memory (MMSE, delayed recall). No deficits in time orientation, working memory, visuoconstructive abilities and language.
Moser et al., 1998	Case report (1)	81	High school	Ischemic stroke and traumatic brain injury with parenchymal haemorrhage	Bilateral frontal	Deficits in verbal memory (Wechsler Logical memory), visual memory (Wechsler Visual memory) and executive functions (go/no-go task, trail making test, verbal fluency). No deficits in language and visuospatial perception.

Jocic and Staton, 1993	Case report (1)	67	High school	Ischemic stroke	Right fronto-temporo-parietal and basal ganglia (excluding thalamus)	Left visual neglect. Deficits in sustained attention, short-term memory, visual memory (Wechsler Visual Memory), verbal memory (California Verbal Learning Test), executive functions (verbal abstract reasoning and Trail Making Test B), and visual and visuospatial perception (Benton Visual Form Discrimination and Judgement of Line Orientation). No deficits in person and time orientation, language, and discrimination and matching unfamiliar of faces (Benton Facial Recognition test).
Lee et al., 2011	Case report (1)	69	NR	Ischemic stroke	Right fronto-insular	MMSE of 28. Deficits in non-verbal reasoning (WAIS-III matrix reasoning), verbal reasoning (WAIS-III similarities index), cognitive abstraction and flexibility (Wisconsin Card Sorting Test), visuocosntructive abilities (Rey-Osterrieth complex figure – copy, WAIS III object assembly and picture completion) and visual memory (Wechsler Visual Memory – delayed). No deficits in verbal memory.
Bez and Nurmedov, 2007	Case report (1)	71	NR	Brain tumour	Genu of corpus callosum	NR
Nighoghossian et al., 1992	Case report (1)	85	NR	Ischaemic stroke	Bilateral frontal and right lenticular	Deficit in non-verbal reasoning and visuopspatial abilities (Kohs block design test, Hooper Visual Organization Test), and visual memory (Whiteley and Signoret test). No deficit in time orientation and verbal memory.

Murai et al., 1997	Cross-sectional (2)	52	NR	Haemorrhagic stroke	Right frontal and striatum	Deficits in verbal memory (Miyake Retention test), visual memory (Rey-Osterrieth complex figure – recall) and cognitive abstraction and flexibility (Wisconsin Card Sorting Test). No deficit in time orientation.
		52	NR	Traumatic brain injury	Bilateral frontal	Deficits in verbal memory (Miyake Retention test) and cognitive abstraction and flexibility (Wisconsin Card Sorting Test). No deficits in time orientation and visual memory (Rey-Osterrieth complex figure – recall).
Kapur et al., 1988	Case report (1)	71	NR	Haemorrhagic stroke	Right frontal	Left visuospatial neglect. Deficits in verbal reasoning (similarities), non-verbal reasoning (picture arrangement and block design), verbal fluency, cognitive abstraction and flexibility (modified Wisconsin Card Sorting Test), verbal memory (word-list learning task) and visual memory (Rey-Osterrieth complex figure, faces recognition memory test).
Sellal et al., 1996	Case report (1)	64	High school	Viral encephalitis	Bilateral frontal and right temporal	Deficits in orientation in time, short-term visual memory (Corsi Block-Tapping test and Wilson's spatial memory test), cognitive abstraction and flexibility (Wisconsin Card Sorting Test), visual episodic memory (Rey complex figure – recall, Warrington Facial Recognition test) and famous face recognition, visuoconstructive abilities (tridimensional representation). No deficit in short-term verbal memory and episodic verbal memory.

Osmon, 1996	Case report (1)	45	NR	Subarachnoid haemorrhage with focal parenchymal lesion	Right parietal and left frontal	Deficit in time orientation, visual motor processing speed (Trail Makin Test A and B), cognitive abstraction and flexibility (Milwaukee Card Sorting Test), visual memory (Visual Memory Test), verbal memory (seven word memory list, Buschke Selective Reminding), visuoconstructive abilities (Rey-Osterrieth complex figure – copy), visuospatial perception (Judgement of Line Orientation), visual perception of faces (Facial Recognition).
Vighetto et al., 1980	Case report (1)	72	NR	Ischaemic stroke	Right parieto-temporal	Deficits in visuoconstructive abilities and right-left orientation.
Ovelacg et al., 1988	Case report (1)	61	NR	Ischaemic stroke	Right fronto-temporal	Deficits in visual memory (Benton Visual Retention test) and visuoconstructive abilities (Rey-Osterrieth complex figure – copy). No deficits in verbal memory.
Leiguarda, 1983	Case report (1)	74	NR	Haemorrhagic stroke	Right thalamus	Left visuospatial neglect. Deficits in verbal memory. No deficits in person and time orientation.
Vighetto et al., 1985	Case series (1)	77	NR	Brain tumour	Right temporo-parietal	NR
Aimard et al., 1981	Case report (1)	72	NR	Ischemic stroke	Right fronto-parieto-temporal	Deficits in visuoconstructive abilities. No deficits in time orientation, visuospatial attention (line crossing), right-left orientation and face recognition.

Cambier et al., 1980	Case report (1)	77	NR	Haemorrhagic stroke	Right thalamus	NR

MMSE, Mini-Mental State Examination; NR, Not reported; WAIS, Wechsler Adult Intelligence Scale.

Lesion topography

Individual lesions are represented in Figure 4.

Patient 1 (Peckins et al., 2016)

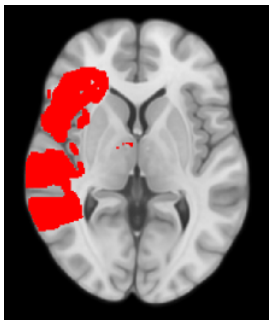

Patient 2 (Nishio and Mori, 2012)

Patient 3 (Fisher, 1982)

Patient 4 (Budson et al., 2000)

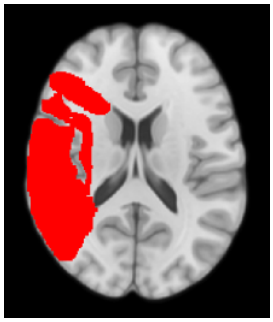

Patient 5 (Likitcharoen and Phanthumchinda, 2004)

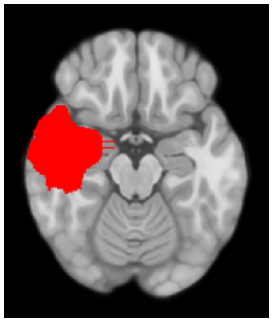

Patient 6 (Hudson and Grace, 2000)

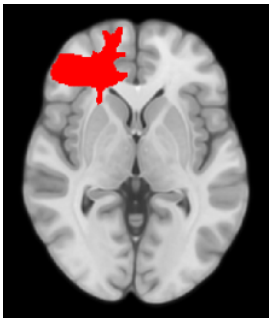

Patient 7 (Pignat et al., 2013)

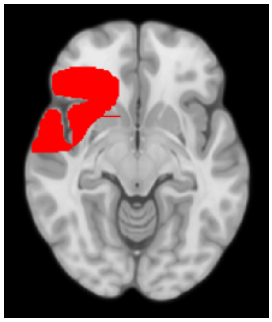

Patient 8 (Yamada et al., 2003)

Patient 9 (Jocic and Staton, 1993)

Patient 10 (Lee et al., 2011)

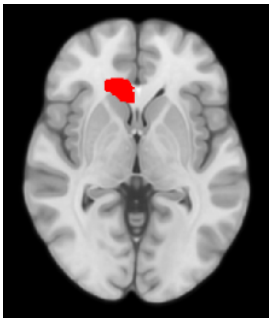

Patient 11 (Bez and Nurmedov, 2007)

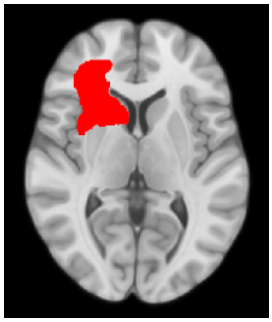

Patient 12 (Murai et al., 1997)

Continues in the next page

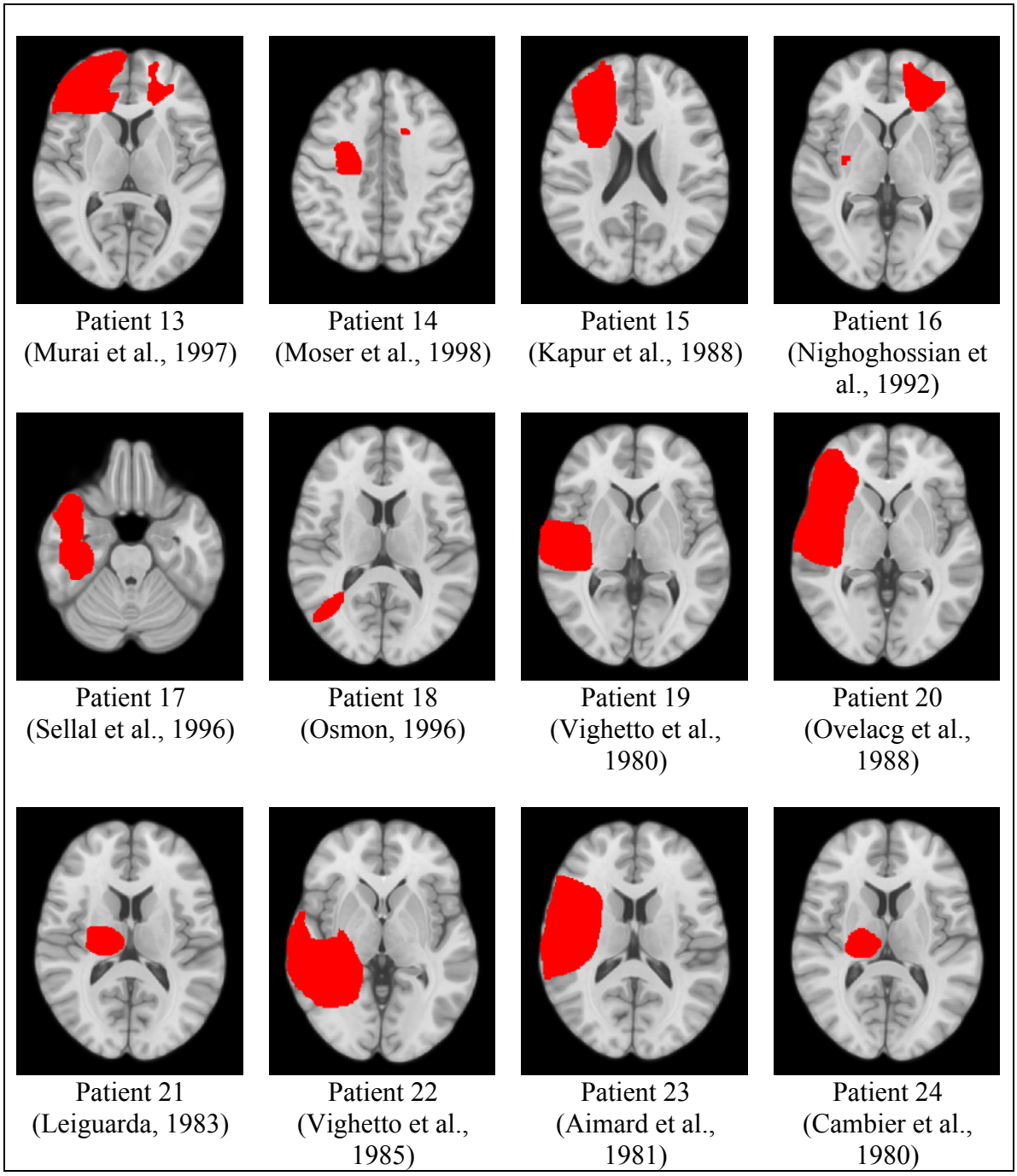

Figure 4. Lesions associated with spatial delusions. The 24 cases used in neuroimaging analysis are presented with the corresponding reference below. A single slice is presented per patient. Only the voxels that both authors agreed that were lesioned are presented.

The Dice similarity coefficient for lesion delimitation was 0.79 [0.77-0.84] (median [interquartile range]). The percentage of voxels for which the raters disagreed was 18% [12 – 27%] (median [interquartile range]). Almost all lesions were right sided or bilateral, except one (ischemic stroke) that was located in the left temporo-parieto-occipital junction

(Budson et al. 2000). This patient presented clinical evidence of right hemisphere dominance, namely right side neglect and impaired visual memory with preserved verbal memory.

The maximum value of overlap at a voxel-level was 3/24, in the right ventrolateral prefrontal, right temporal lateral and right insular regions (Figure 5A).

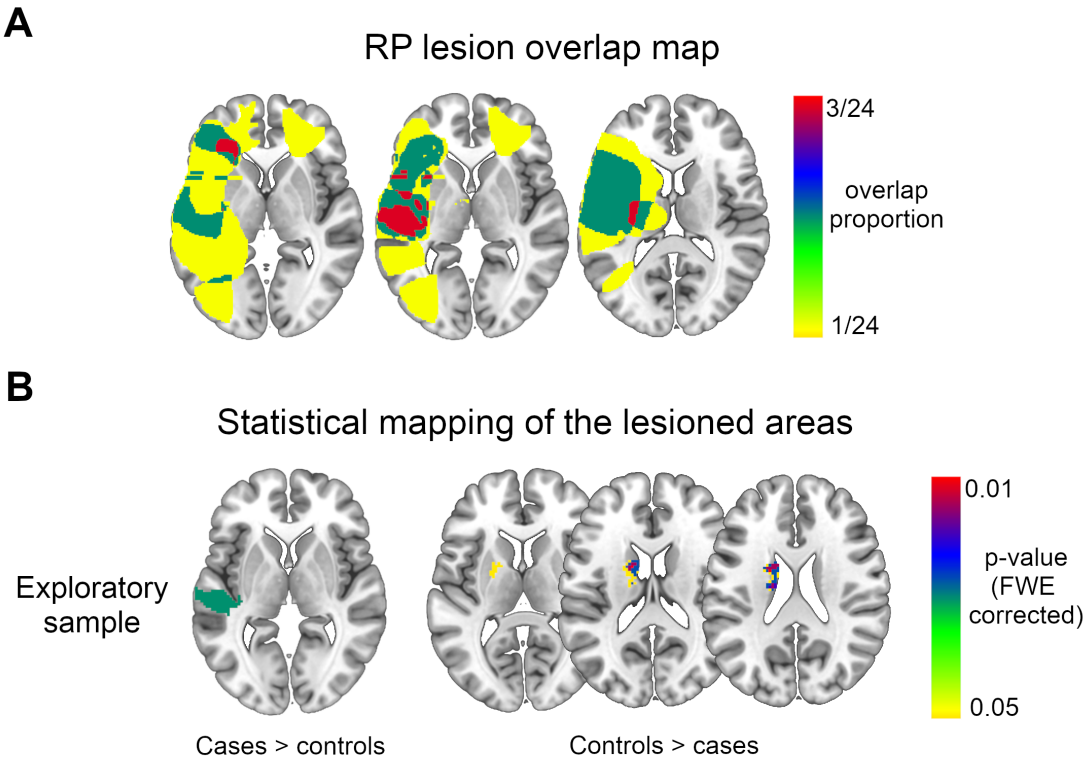

Figure 5. Lesion topography analysis. A - Lesion overlap maps of cases of reduplicative paramnesia. B - Statistical brain maps of the voxels more often lesioned in cases than in stroke controls (left) and more often lesioned in stroke controls than in cases (right), in the exploratory sample. The validation sample is not represented because no statistical significant differences were found. FWE, Family-wise error rate; RP, reduplicative paramnesia.

The permutation analysis of the exploratory sample revealed that: a) a region of the right lateral temporal lobe was more frequently lesioned in cases than in stroke controls; b) a region of the right dorsal striatum was more frequently lesioned in stroke controls than in cases (Figure 5B). However, these findings were not replicated in the validation sample and no statistically significant differences were found in the regression analysis including age as a covariate.

Structural disconnectome

In the structural connectivity analysis, the permutation test of the exploratory sample revealed that reduplicative paramnesia was significantly associated with higher probabilities of disconnection of: a) a right ventral temporo-occipital region; b) a right ventrolateral prefrontal region (Figure 6A, top row).

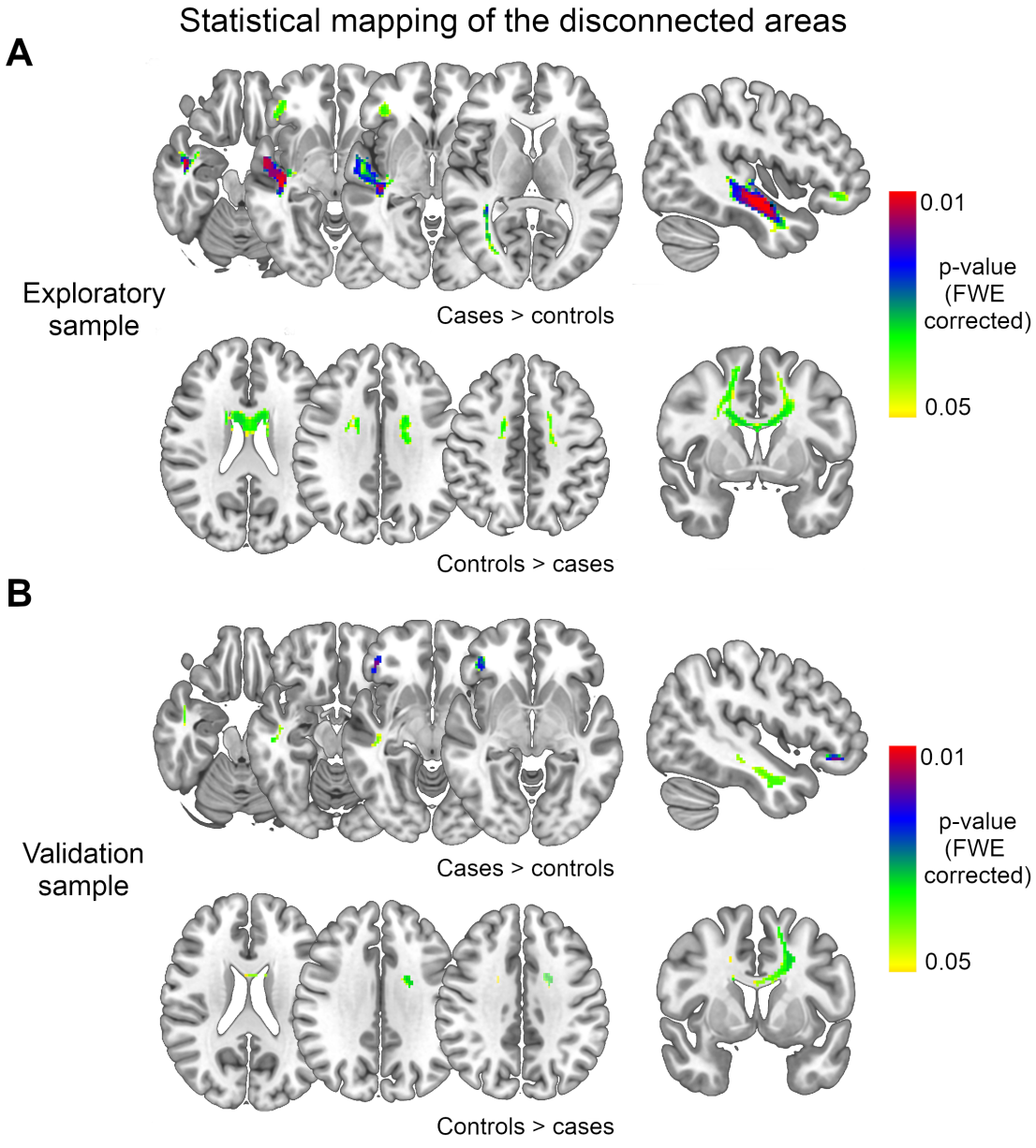

Figure 6. Structural disconnection analysis. A - Statistical brain maps of voxels with significantly higher probabilities of disconnection in cases than in stroke controls (top row) and with significantly higher probabilities of disconnection in stroke controls than in cases

(bottom row). B - Statistical brain maps of the replication analysis performed in the validation sample. FWE, Family-wise error rate.

A similar statistically significant disconnection map was obtained in the regression analysis including age as a covariate (Figure 7).

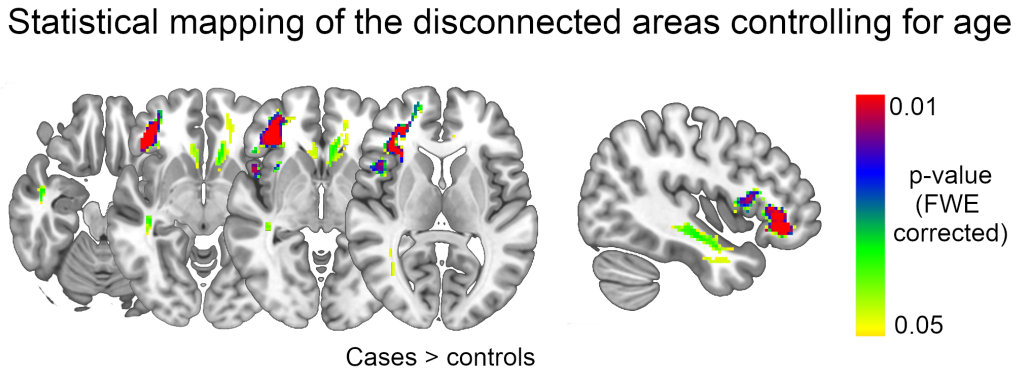

Figure 7. Structural disconnection analysis including age as a covariate in the regression analysis. Statistical brain maps of voxels with significantly higher probabilities of disconnection in cases than in stroke controls. No voxels had higher probabilities of disconnection in stroke controls than in cases. In this analysis, the control stroke lesions from ATLAS dataset could not be included, because the information about the age of these patients is not publicly available. FWE, Family-wise error rate.

Conversely, reduplicative paramnesia was significantly associated with lower probabilities of disconnection of dorsal inter-hemispheric pathways (Figure 6A, bottom row). These results were replicated in the validation sample (Figure 6B), but not when age was included as a covariate in the regression analysis.

The results of the sensitivity analysis excluding tumoral lesions were similar (Figure 8).

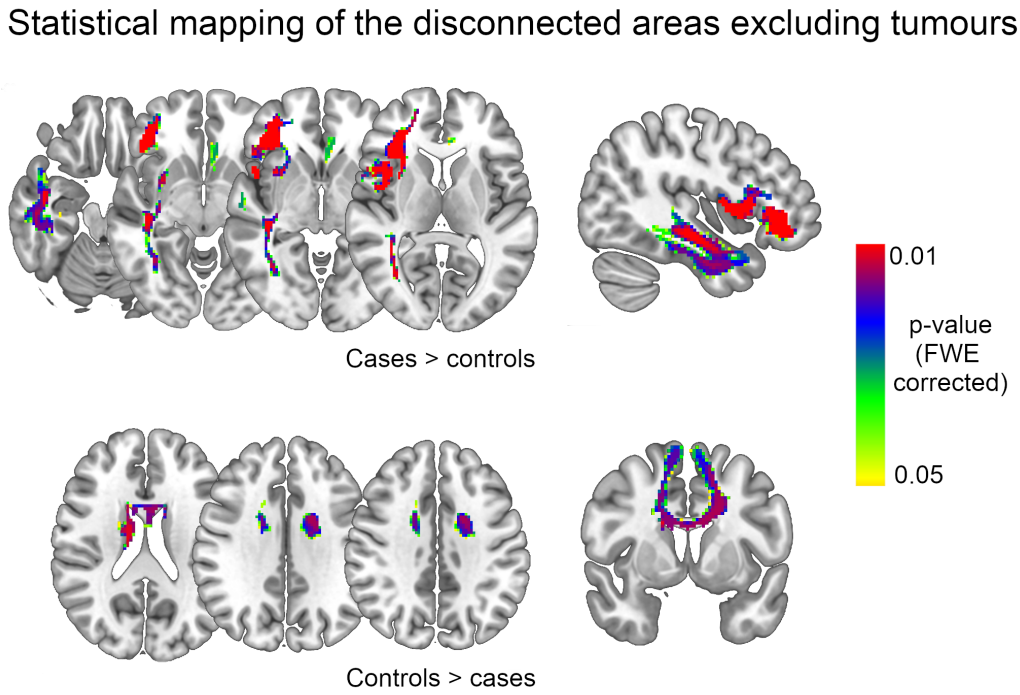

Figure 8. Structural disconnection analysis excluding tumoral lesions. Statistical brain maps of voxels with significantly higher probabilities of disconnection in cases than in stroke controls (top row) and with significantly higher probabilities of disconnection in stroke controls than in cases (bottom row). FWE, Family-wise error rate.

Classification performance of the lesion topography and of the structural disconnection maps

The structural disconnectome model demonstrated a maximum balanced accuracy value in the validation sample of 0.78 (Figure 9A). The voxels with higher balanced accuracy were located in two clusters: a) a right temporal cluster with an overall balanced accuracy of 0.77, a sensitivity of 0.75 and a specificity of 0.79; b) a right ventrolateral prefrontal cluster, with an overall balanced accuracy of 0.75, a sensitivity of 0.67 and a specificity of 0.83 (Figure 9B).

The lesion topography model revealed lower capacity to predict delusions of space with a maximum balanced accuracy value of 0.69.

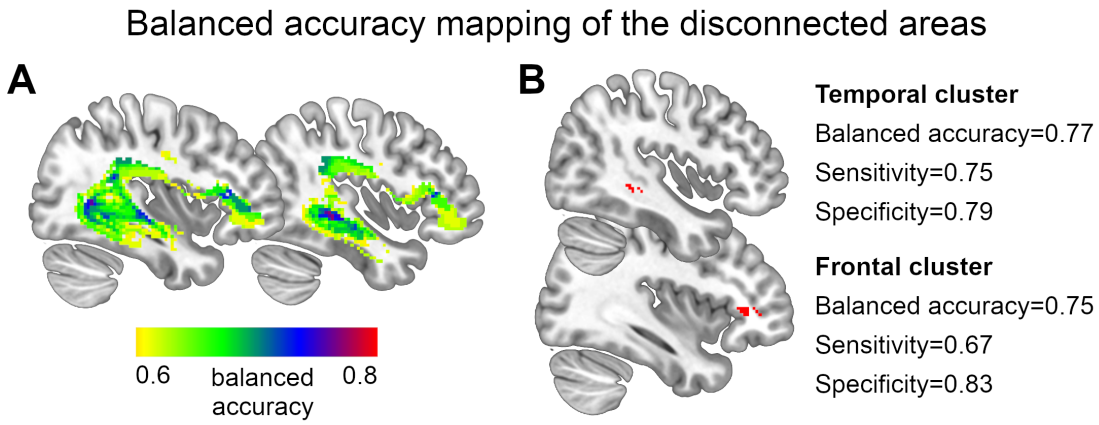

Figure 9. Balanced accuracy mapping of the structural disconnectome model. A - Voxel-wise representation of the balanced accuracy scores. B - Balanced accuracy score, sensitivity and specificity of the right temporal and of the right ventrolateral prefrontal clusters.

Structural-functional coupling

The meta-analytic functional maps are provided in Figure 10.

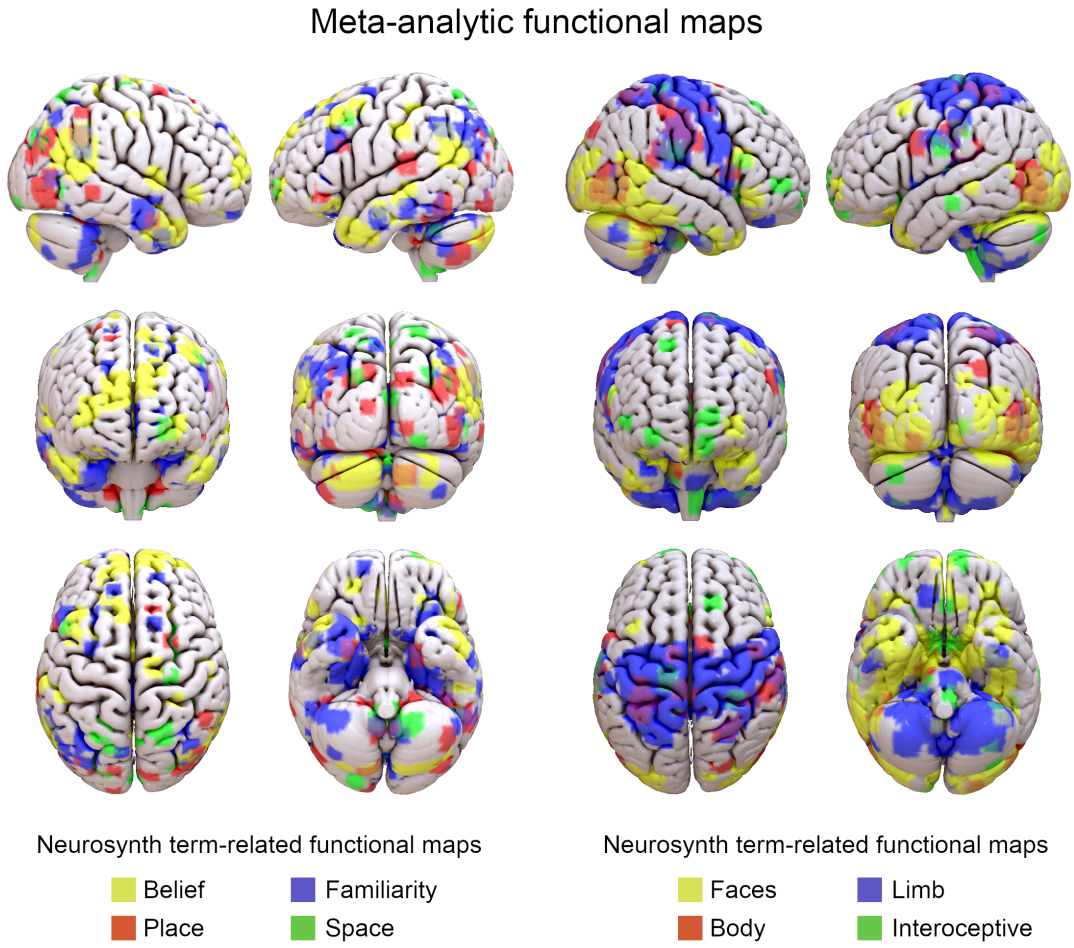

Figure 10. Brain surface representation of the functional meta-analysis results, for the different terms of interest.

The number of studies from which the meta-analytic maps derived from were: belief, n=83; familiarity, n=188; place, n=189; space, n=303; faces, n=864; limb, n=127; body, n=552; interoceptive, n=81.

The lesions associated with spatial delusions had significantly higher spatial overlap with the belief-related functional network than stroke controls (Figure 11A). There was no significant difference for familiarity, place and space-related functional networks.

Regarding structural disconnection, the disconnectome maps associated with delusions of space had significantly higher spatial overlap with the familiarity-related and with the place-related functional networks than stroke controls (Figure 11A).

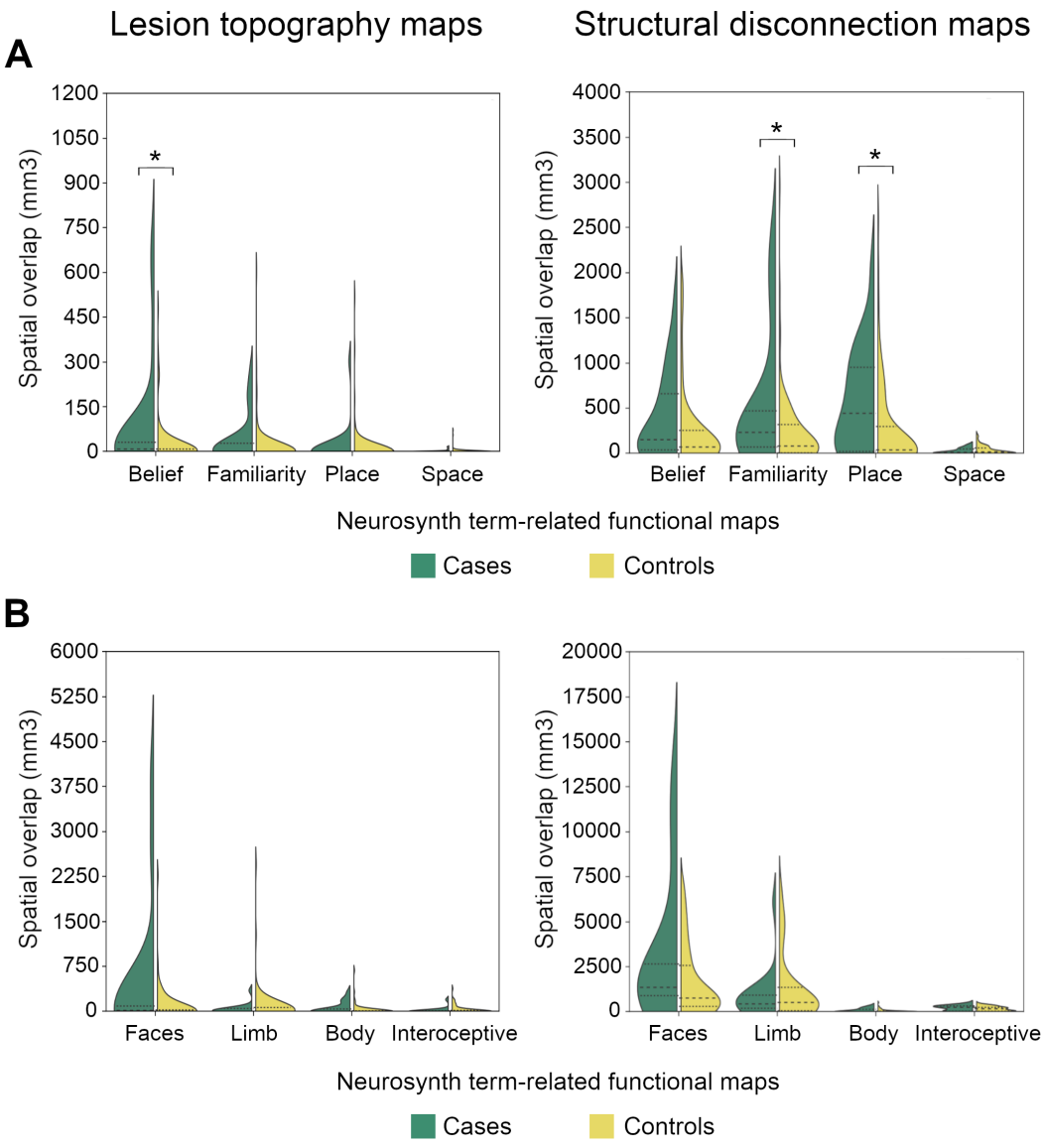

Figure 11. Spatial overlap between the meta-analytic functional maps and the lesion topography maps (left) and the projected structural disconnection maps (right). A - Comparison regarding spatial delusions-related terms. B - Comparison regarding the control terms that would be the content-related equivalents for other monothematic delusional misidentifications. Data is presented in violin plots. The dashed lines represent quartiles and the asterisks represent statistically significant differences between cases and stroke controls (Bonferroni-corrected p-value<0.0125).

For the control terms, that would be the content-related equivalents for other monothematic delusional misidentifications, there was no significant difference of spatial overlap regarding lesion topography or structural disconnection (Figure 11B). No significant difference was also found for the 'executive functions' and 'memory task'-related functional maps.

Comparing the relative spatial overlap (Dice similarity coefficient) with the meta-analytic functional maps, the structural disconnection maps had a higher coefficient of overlap with the familiarity and with the place-related functional networks than the lesion topography maps (Figure 12). No significant difference was found for the belief and for the space-related functional maps.

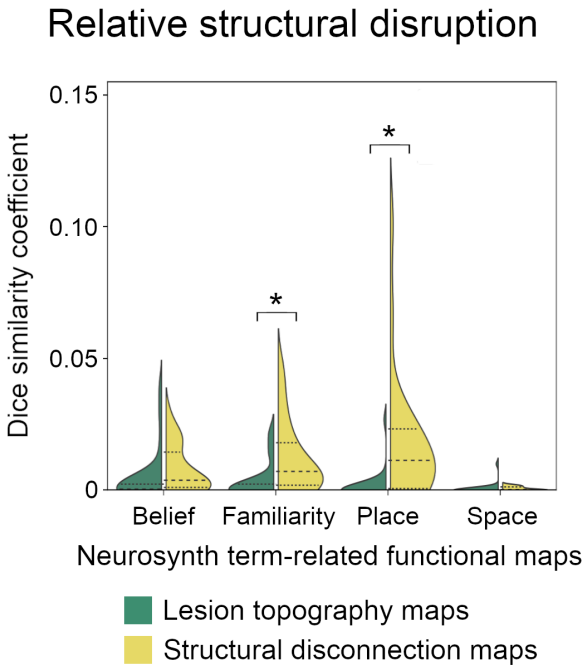

Figure 12. Comparison of the relative spatial overlap (Dice similarity coefficient) of the meta-analytic functional maps between the lesion topography and the projected structural

disconnection maps in the cases of reduplicative paramnesia. The dashed lines represent quartiles and the asterisks represent statistically significant differences (Bonferroni-corrected p-value<0.0125).

Discussion

In this work, we systematically reviewed cases reported in literature of lesion-associated reduplicative paramnesias. First, we presented their clinical and phenomenological features Second, we found that they are associated with structural disconnection of right temporal and right ventrolateral prefrontal areas. This pattern of disconnection was replicated in an independent validation sample. Third, we showed that structural disconnectomes provide the anatomical framework to explain associated functional changes. Specifically, we demonstrated the existence of a spatial relationship between the structural disconnectome maps of reduplicative paramnesias and the familiarity and place-related functional networks.

Reduplicative paramnesia is a right hemisphere syndrome (Feinberg 2013; Bartolomeo et al. 2016), however a sole lesion location or the lesion location per se may not be a satisfactory neuroanatomical explanation for this type of spatial disorientation (Griffis et al. 2019; Thiebaut de Schotten et al. 2020). Our results provide evidence to support that reduplicative paramnesia is a disconnection syndrome.

Darby and colleagues (Darby et al. 2017) previously showed the association between delusional misidentification syndromes and functional disconnection of the right ventrolateral prefrontal cortex and of the left retrosplenial cortex (Darby et al. 2017). Here, we showed that the right ventrolateral prefrontal region is also structurally disconnected, which provides evidence for the existence of structure-function coupling in this region and reinforces its pathophysiological relevance (Baum et al. 2020). The two-hit model of delusional belief states that two factors contribute to the emergence of delusional misidentifications (Coltheart et al. 2011). The first is an abnormal covert (i.e. implicit) recognition of the misidentified stimuli (Ellis and Young 1990). The second is an impairment of the belief and familiarity evaluation processes (Coltheart et al. 2011). Evidence suggests that the neural basis of the second factor is the dysfunction of the right lateral prefrontal cortex (Coltheart 2010) and our results support it. The ventrolateral prefrontal cortex is activated during the presentation of unexpected perceptual events and during implicit false belief processing (Sharp et al. 2010; Kandylaki et al. 2015). We also

replicated the previous finding that delusional misidentification lesions were spatially correlated with belief-related networks (Darby et al. 2017). In addition, the right ventrolateral prefrontal cortex has an important role in reality monitoring (Badre and Wagner 2004). Its damage or disconnection has been associated with anosognosia for hemiplegia (Berti et al. 2005; Prigatano 2010; Pacella et al. 2019), a disorder characterized by the patients' failure to acknowledge limb paralysis, even after being clearly confronted with the deficit. Our results fits this evidence, since both disorders share a disturbance in reality awareness and belief update (Vocat et al. 2013; Fotopoulou 2014).

The right ventrolateral prefrontal cortex is also a core area to emotional regulation, and seems to be particularly important when personal significance factors are involved in belief reasoning (Hartwright et al. 2012) and to explicit decisions on the relative familiarity of stimuli (Petrides et al. 2002). It establishes bi-directional connections with ventral limbic structures (Petrides 2005) and with limbic nuclei of the thalamus through the anterior thalamic radiations (Rojkova et al. 2016), and integrates the default mode network, a fundamental network for transmodal processing of limbic information (Alves et al. 2019). Ellis and Young proposed that a defective attribution of appropriate emotional valences to stimuli was involved in the pathogenesis of delusional misidentification syndromes (Young et al. 1994; Devinsky 2009). Darby and colleagues (Darby et al. 2017) established a functional association between delusional misidentifications and familiarity networks. We demonstrated that this association is neuroanatomically mediated by structural disconnection.

The delusional content of reduplicative paramnesia is very specific for places, distinguishing it from other monothematic delusional misidentifications. Still according to the two-hit model, all delusional misidentification syndromes would have a first factor that determines the content of delusional belief (Coltheart et al. 2011). Here, we provide the first group-level evidence showing that there is a spatial correlation between reduplicative paramnesia and place-related functional networks. Ventral occipito-temporal pathways are fundamental for orientation in allocentric spatial references (Ekstrom et al. 2014) and to the emotional recognition of visual cues (Herbet and Duffau 2020). We propose that the disconnection of this pathway may impair a proper update and integration of visual information in allocentric, place-related networks.

Other authors have hypothesized that delusional misidentifications results from unbalanced activity of the two hemispheres, with right hemisphere hypofunction and left hemisphere overactivity (Young et al. 1994; Devinsky 2009). We found that dorsal fronto-

parietal inter-hemispheric connections were more frequently spared in cases of reduplicative paramnesia, when compared with stroke controls. This might mediate dysfunctional interhemispheric communication, but this finding was not replicated when age was included in the model. Further studies are needed.

As limitations of our study, the meta-analytic functional maps do not reflect the complex associations and the dynamic interactions of brain systems. The lesion mapping analysis was also constrained by the available images in the cases reports. Although we replicated 2D lesion tracing methodologies that have been applied to study cognitive and behavioural syndromes about which the available neuroanatomical evidence is scarce (Boes et al. 2015; Cohen et al. 2019; Darby et al. 2019), the lesion masks may not represent the full 3D geometry of the original lesions. In addition, we cannot guarantee that the control stroke patients did not develop reduplicative paramnesia after the period of systematic assessment. These bias may increase the risk of false negative results (Cohen et al. 2019). It is also known that the years of education, as well as co-occurring cognitive deficits, may correlate with the cognitive syndrome of interest (de Haan and Karnath 2018; Borghesani et al. 2019; Umarova et al. 2021). However, the absence of information about the years of schooling, the heterogeneity of the reported neuropsychological evaluations and the number of cases available precluded the inclusion of these covariates in the neuroimaging model.

In conclusion, our work suggests that delusions of space may be associated with structural disconnection of right ventrolateral prefrontal and right temporal regions and that these structural connectivity changes might mediate functional interactions with familiarity and place-related networks.

2. Phenomenological features of stroke-associated spatial delusions

Part of this section is included in the following manuscript:

- Alves PN, Fonseca AC, Pinho-e-Melo T, Martins IP (2022) Clinical features and neural correlates of stroke-associated spatial delusions. Eur J Neurol 30(1):125–133. https://doi.org/10.1111/ene.15557.

And in the following book chapter (in press):

- Ferro JM, Alves PN, Martins IP. Memory loss. Caplan's Stroke Syndromes, 4th edition, Cambridge University Press. *In press.*

Introduction

Different forms of spatial delusions have been described (Politis and Loane 2012) representing different poles of pathological familiarity (Devinsky 2009). Place reduplication typifies hypofamiliarity for places and corresponds to the original description made by Pick, i.e. the patients are convinced that they are in a replica of the original place (Pick 1903). Chimeric assimilation is characterized by the fusion or combination of two different places (e.g. the hospital is inside patients' home). In confabulatory mislocation, patients believe that they are in a place that is substantially different from the real one (e.g. believing to be at home instead of being at the hospital). Both embody place hyperfamiliarity (Darby and Prasad 2016).

At the structural and functional levels, we demonstrated that spatial delusions are associated with a dual pattern of structural disconnection involving right frontal and temporal circuits, which prompts structural-functional decoupling of belief, familiarity and place-associated functional networks (Alves et al. 2021b). At the clinical level, the striking incongruence between the patients' conviction and the surrounding environment may markedly disturb patients' behaviour (Moser et al. 1998; Borghesani et al. 2019). Although traditionally seen as an infrequent syndrome, evidence suggests that spatial delusions can be a frequent manifestation of right hemisphere lesions (Murai et al. 1997). So far, the available knowledge about the clinical features of spatial delusions is mostly based in cases reports and small case series (Politis and Loane 2012; Borghesani et al. 2019). Misdiagnosis of spatial delusions as delirium or psychomotor agitation may lead to erroneous approaches in terms of pharmacological treatment, behavioural interventions, and support of family members and caregivers.

Here, we systematically studied the largest published sample of patients with spatial delusions after right hemisphere acute stroke to shed light on their clinical presentation and pathophysiology. First, we aimed to characterize the clinical phenotype of spatial delusions and their subtypes. Second, we studied the neural correlations of these clinical features. Specifically, we hypothesized that there was a correlation between the duration of the reduplicative paramnesia and the magnitude of structural disruption of belief-associated functional networks and that the disturbances of familiarity-associated networks would predict the subtype of reduplicative paramnesia.

Methods

Study sample

We performed a prospective, cumulative, case-control study from December 2016 to June 2021 in a stroke unit of a tertiary university hospital in Lisbon, Portugal. Five hundred and four patients admitted within the acute phase (72 hours or less) of right hemisphere stroke (ischemic or haemorrhagic) were screened for the presence of spatial delusions. The exclusion criteria were: acute confusional state (delirium), according to the criteria defined in the Diagnostic and Statistical Manual of Mental Disorders – fifth edition; decreased level of consciousness; subarachnoid haemorrhage; epileptic seizures during admission; aphasia or severe dysarthria precluding evaluation; severe visual deficit, precluding confrontation with counter-evidence stimuli; history of dementia, i.e. a cognitive decline that interfered with the instrumental activities of daily living, as stated in the criteria of major neurocognitive disorder of the Diagnostic and Statistical Manual of Mental Disorders – fifth edition; absence of a stroke lesion in brain imaging, or unavailable brain images.

Screening was performed in the first 72 hours of admission and then at regular intervals of 48 hours until the patients' discharge, using the systematic approach detailed in the following section. The patients that presented the syndrome and whose phenomenological presentation was fully registered were selected for this study.

The study was approved by the Joint Ethics Committee of the Lisbon Academic Medical Centre.

Screening and phenotypic characterization of reduplicative paramnesia

To screen for reduplicative paramnesia, patients were asked if they knew where they were, specifically the type of building (hospital), the city (Lisbon) and the city district they were in. If the patients did not know or gave a wrong answer, their correct location was explained, namely that they were in a hospital, which was called "Hospital de Santa Maria" and was located in Lisbon, more specifically in "Campo Grande/Cidade Universitária" (city district). When the patients disagreed, counter-evidence was systemically shown to convince them otherwise. The questions and confrontations were tailored to the subtype of reduplicative paramnesia. When the patients believed they were in a place other than a hospital (i.e. confabulatory mislocation) they were asked: question 1) why health care professionals would be in the referred place; question 2) why medical equipment (oxygen masks, infusion tubes, vital signs monitor) would be there; question 3)

why the patients' clothes and bed sheets were labelled "Hospital de Santa Maria"; question 4) why other patients would be in the referred place; question 5) in which home division they would be (in the case they believed they were at home/living house); question 6) why it would be possible to see from the window distinct landmarks, such as Alvalade Stadium (the stadium of a leading football club in Portugal), the Lisbon airport or the Lisbon University (for those whose clinical condition allowed to stand and show the window view).

For patients presenting chimeric assimilation, besides the questions referred above, they were asked: question 7) if they had noticed or heard about any construction work in the referred place; question 8) why a hospital would be constructed inside that place.

For patients presenting with place reduplication, questions 3 and 6 were posed. In addition they were asked: question 9) why "Lisbon" would be written next to the Hospital logo; question 10) how many "Hospital de Santa Maria" they think there were.

The diagnosis of reduplicative paramnesia was made when the patients maintained the belief of mislocation after being exposed to the referred counter-evidences.

Clinical characterization

Demographic and stroke clinical data were collected, namely, age, type of stroke (ischemic or haemorrhagic), NIHSS at admission and at discharge, and length of admission.

Regarding reduplicative paramnesia, we also registered: a) the duration of the phenomenon; b) the day it was diagnosed; c) if there was an observation prior to spatial delusion onset in which the patient was oriented in space; d) if the patient called "Hospital de Santa Maria" to the misidentified place; e) if the patients knew the location of the (original) "Hospital de Santa Maria" (to consider the answer correct, for patients living in Lisbon, the city and the city district were required; for patients living outside, saying Lisbon was enough); f) if the patient knew his own home address; g) if the patient was able to mentally describe routes between relevant places (specifically, between home, "Hospital de Santa Maria" and the place they believed they were); h) if the patient was oriented in time (namely, year and month).

The geodesic distances (based on latitude and longitude coordinates) between the misidentified place, the patients' home and "Hospital de Santa Maria" were calculated and

the relative distance of the misidentified place to the patients home and to "Hospital Santa Maria" was determined:

$$r\Delta = \frac{\Delta place\_hospital}{\Delta place_{hospital} + \Delta place_{home}}$$

where $r\Delta$ means the relative distance, $\Delta place\_hospital$ the distance between the misidentified place and the "Hospital de Santa Maria" and $\Delta place\_home$ the distance between the misidentified place and patients' home (values closer to one represent mislocation closer to the hospital; values closer to zero represent mislocation closer to patient's home). For illustration purposes, we used the geographical maps from OpenStreetMaps (https://www.openstreetmap.org).

Neuroimaging correlations

Stroke lesions were defined based on brain MRI (preferentially) or CT images performed 24 to 72 hours of stroke onset. Delimitation was manually performed on axial slices with a thickness of 3mm. Researchers were blind to patients' clinical features at the time of lesion delimitation. Lesions were normalized to a common space, the MNI152 (Jenkinson et al. 2012). MRI images were acquired in a Philips Achieva 3.0 Tesla or Philips Intera 1.5 Tesla scanner. The diffusion-weighted imaging was the sequence of reference for delimitation (de Haan and Karnath 2018). T1 images were registered to the MNI152 space using linear and nonlinear transformations (Jenkinson et al. 2012). CT images were acquired in a Philips Brilliance 64-channel scanner. Their registration was made to the CT-derived MNI152 template using a linear transformation (Rorden et al. 2012). Finally, the registration deformation fields were applied to the lesion masks.

To compute the structural disconnection pattern of each lesion, we used a tract-wise approach (Thiebaut de Schotten et al. 2011a). Using the tool *Disconnectome* from the software package BCBtoolkit (http://toolkit.bcblab.com), each lesion was overlapped with a group of 178 healthy subjects' tractography from the Human Connectome Project 7 Tesla dataset (Vu et al. 2015). Tractographies were obtained using a whole-brain deterministic approach, in StarTrack software (https://mr-startrack.com), applying a spherical deconvolution methodology, specifically a damped Richardson-Lucy algorithm. They were made available with BCBtoolkit (http://www.bcblab.com). The full details of pre-processing are described in Karolis et al (2019). A voxel-wise probability of disconnection

was calculated (Foulon et al. 2018). The voxels were included in the disconnectome map if they were disconnected in more than 50% of healthy subjects' tractographies (Foulon et al. 2018).

It has been demonstrated that delusional misidentifications are associated in structural-functional decoupling of belief and familiarity-associated functional networks (Darby et al. 2017; Alves et al. 2021b). Neurosynth is a validated brain-mapping platform that performs large-scale automated extraction of meta-analytic functional maps of terms of interest (Yarkoni et al. 2011). We used Neurosynth to extract the meta-analytic maps of the terms 'belief', 'familiar' and 'unfamiliar'. Neurosynth maps are corrected for multiple comparisons applying a False Discovery Rate of 0.01. No additional threshold was applied. Then, we computed the volumetric spatial overlap of these meta-analytic maps with the individual stroke lesion and with the structural disconnectome maps.

The Spearman's correlation between the duration of spatial delusions and the structural disruption (either lesion or structural disconnection) of belief-associated networks was calculated. Lesion volume is an important confounder in the establishment of lesion-behaviour associations (Sperber and Karnath 2017; DeMarco and Turkeltaub 2018). A regression analysis was computed to investigate if the putative correlations were independent of lesion volume. In addition, we computed a voxel-wise beta-coefficient map using the linear regression function of scikit-learn (Pedregosa et al. 2011), to analyse which voxels' lesion or disconnection best predicted the duration of the phenomenon. DSI Studio (http://dsi-studio.labsolver.org) and SurfIce (https://www.nitrc.org/projects/surfice/) were used to create tract and surface map illustrations.

To evaluate the classification performance of cases based on the structural disruption of familiarity-associated networks, we performed an unsupervised machine learning partition using a k-means clustering algorithm, from scikit-learn (Pedregosa et al. 2011). The number of clusters to form was defined as three (the number of clinical subtypes of reduplicative paramnesia). The variables included in the model were the structural disruption (either lesion or structural disconnection) of 'familiar' specific regions and the structural disruption of 'unfamiliar' specific regions. Then, we calculated the Rand index to determine the similarity between the familiarity-derived clustering and the clinical subtype classification (one meaning perfect agreement and zero no agreement). An alternative analysis was computed in which we defined the number of clusters to form as two, considering confabulatory mislocation and chimeric assimilation as a unique category of hyperfamiliarity syndromes and place reduplication as a hypofamiliarity syndrome

(Darby and Prasad 2016). For patients presenting more than one subtype of reduplicative paramnesia, the first presentation was considered. Graphical representations were created with matplotlib 3.4.2 (https://matplotlib.org).

Statistical analysis

Categorical variables were presented as frequencies and continuous variables as mean±standard deviation or as median[interquartile range (IQR)], according to their distribution. For patients who changed the place of mislocation during their presentation, the Wilcoxon signed-rank test was calculated to determine if the distance to the hospital between the first and the second places of mislocation was statistically different (paired analysis). The Spearman's correlation and the k-means clustering algorithm were applied, as explained above. For the multivariate analysis, a linear regression was computed. When the residuals of the model were not normally distributed (assumption of linear regression), a quantile regression was performed.

Alpha levels were set at 0.05 for statistical significance. The software packages scipy.stats 1.7.1, Stata14® and scikit-learn 0.24.1 (Pedregosa et al. 2011) were used to perform the statistical analysis.

Results

Clinical and demographic features

Sixty patients with spatial delusions were identified and fully characterized (the flowchart of patients' inclusion is available in the Figure 13).

Fifty-seven had an ischemic stroke (95%) and three a haemorrhagic stroke (5%). The median age of patients was 81 years old [IQR 73-85 years old, range 55-93 years old] and the female/male ratio was 31/29. The median NIHSS was 14 [IQR 12-18] at admission and 8 [IQR 3-12] at discharge. The median admission time was 8 days [IQR 6-12, range 2-46]. The arterial territories of ischemia and haemorrhage are reported in Table 5.

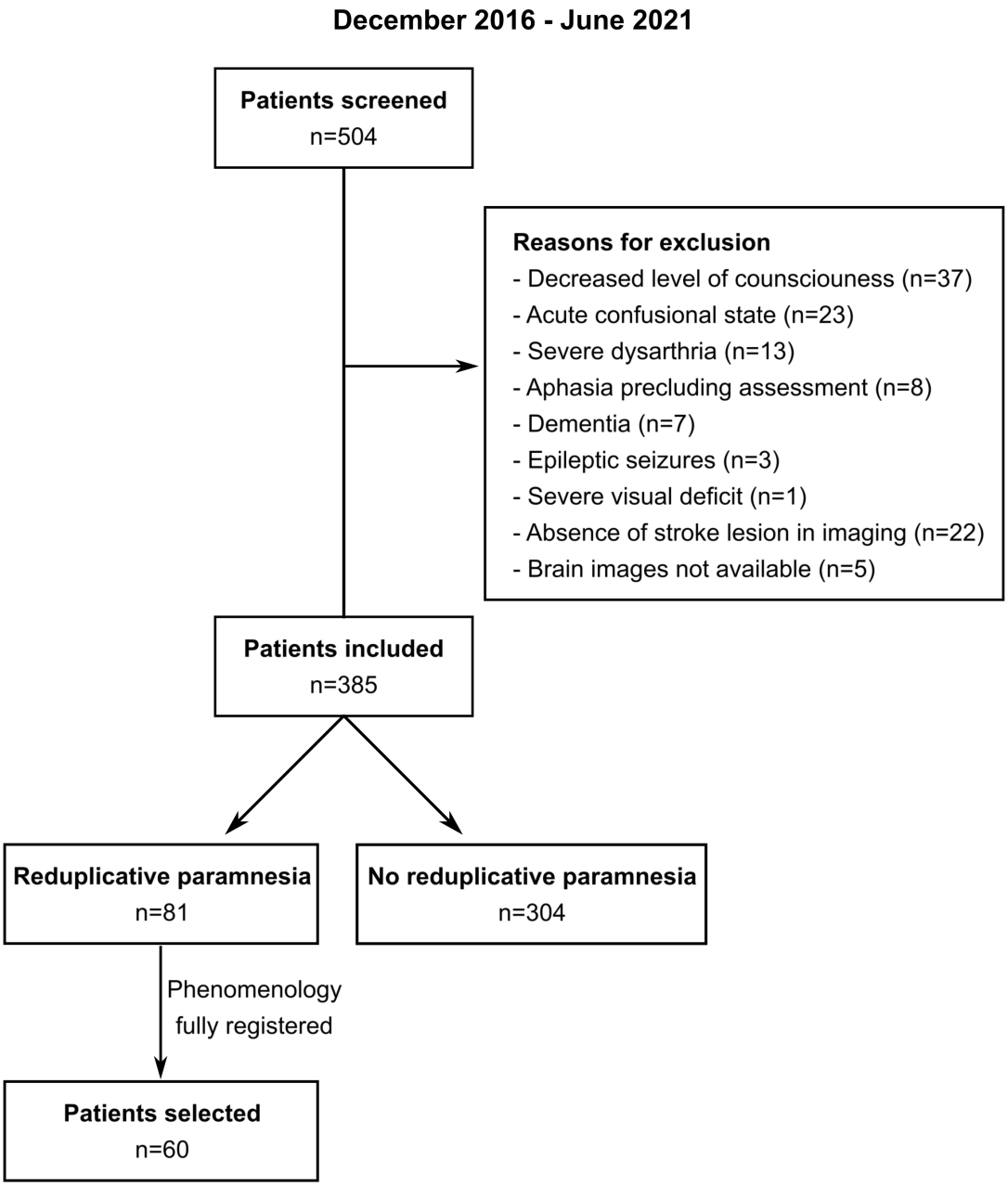

Figure 13. Flowchart of patients' inclusion.

The median time of diagnosis of reduplicative paramnesia was 1 day after stroke (IQR 1-3 days, range 0-7 days). Nineteen patients (32%) had at least one observation in which they were oriented in space before the manifestation of reduplicative paramnesia. Twenty-eight patients (47%) spontaneously referred that they had previously been in the (original) "Hospital Santa Maria" before being brought to the place they believed they were.

Table 5. Territories of ischemia and hemorrhage*

Ischemic strokes	
Right middle cerebral artery	43 (75%)
Right middle cerebral artery and right anterior cerebral artery	5 (9%)
Right middle cerebral artery and right posterior cerebral artery	4 (7%)
Right posterior cerebral artery (including thalamic branches) and basilar artery	2 (4%)
Right posterior cerebral artery	1 (2%)
Right and left middle cerebral arteries	1 (2%)
Right and left middle cerebral arteries and right posterior inferior cerebellar artery	1 (2%)
Haemorrhagic strokes	
Right lenticulo-capsular	2 (67%)
Right thalamo-capsular	1 (33%)

The right column represents the number of cases and the corresponding percentage. *Seven patients (12%) had history of a previous ischemic stroke and one (2%) of a previous hemorrhagic stroke.

Subtypes of reduplicative paramnesia and places of mislocation

Confabulatory mislocation was the most frequent presentation subtype (n=36, 60%), followed by place reduplication (n=16, 27%) and chimeric assimilation (n=8, 13%). The majority of patients maintained the same subtype during the period of spatial delusion (n=48, 80%).

The geographical positions of mislocation and their absolute and relative distances to the patients' home and to "Hospital de Santa Maria" are presented in Figure 14. Most places of mislocation were closer to the patients' home than to the hospital (n=56, 93%). The presentation subtypes of the four patients (7%) with an inverse pattern were: place reduplication (n=2), confabulatory mislocation (n=1) and chimeric assimilation (n=1).

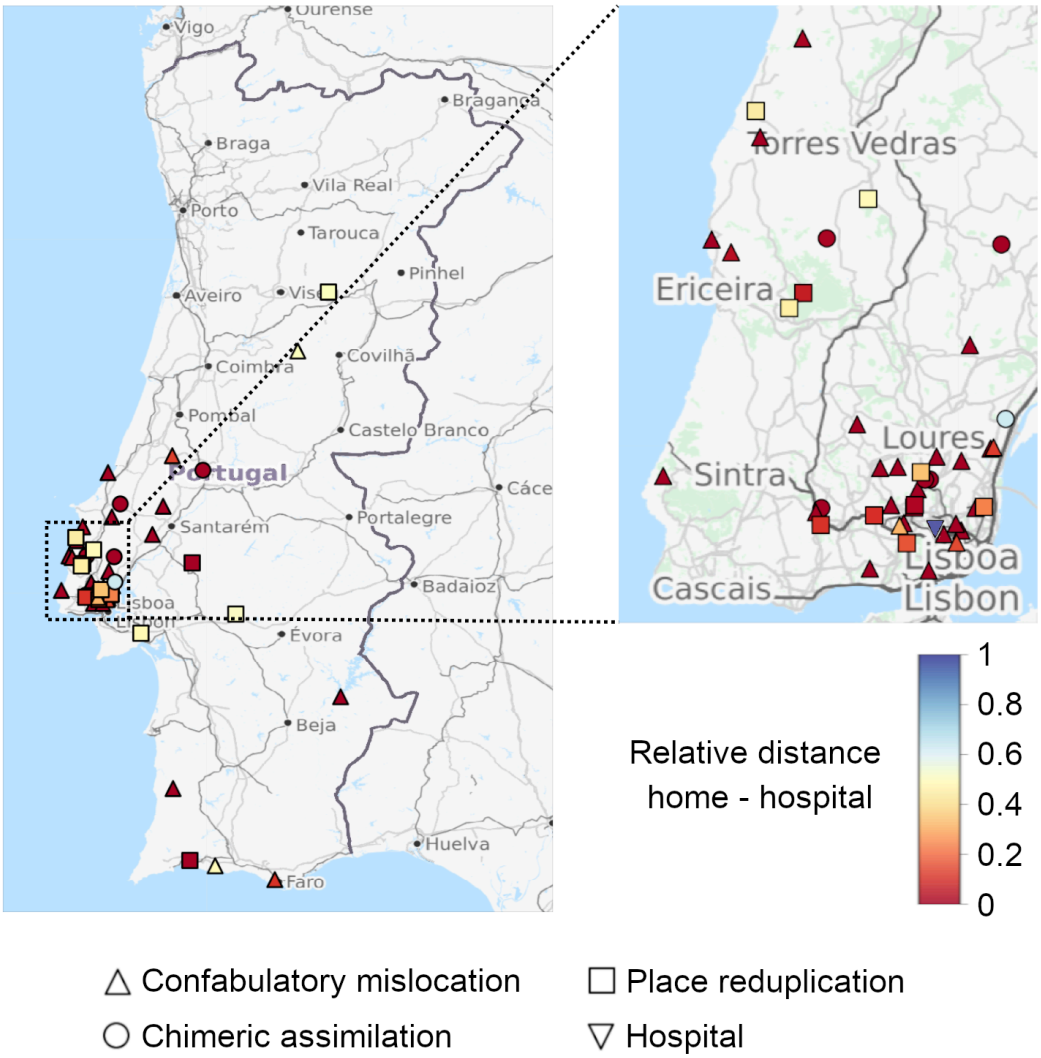

Figure 14. Geographical location of the mislocation places. The markers symbolize the different subtypes of reduplicative paramnesia and the actual location of "Hospital de Santa Maria". The colour gradient represents the relative position of the mislocation place to the patient's home and to the hospital (values closer to one represent mislocation closer to the hospital; values closer to zero represent mislocation closer to patient's home). In patients that presented more than one place of mislocation, only the first is shown. The geographical maps were obtained from OpenStreetMaps (https://www.openstreetmap.org).

Patients with confabulatory mislocation most frequently believed that they were at home (n=27, 75%), followed by believing they were in their relatives' home or holidays home (n=4, 11%) or in another hospital or clinic (n=2, 6%). The remaining were mislocated in extravagant places: in an ambulance (n=1, 3%), in a former bus garage (n=1, 3%) and in a social security office (n=1, 3%). Of these, 14 patients (39%) changed the

place of delusional mislocation during their presentation: five patients (14%) changed to a chimeric assimilation subtype, five patients (14%) to a place reduplication subtype and four patients (11%) changed the place of confabulatory mislocation.

All patients with place reduplication were convinced they were in a branch of "Hospital de Santa Maria" (n=9, 56%) or in a replica of the hospital (n=7, 44%), located in another place. During the period of spatial delusion, three of these patients (19%) changed the localization of the reduplicated building and one (6%) changed to a confabulatory mislocation form.

Regarding the patients presenting chimeric assimilation, three (38%) believed their home had been transformed into a hospital, three (38%) that the relative's home where they were had been transformed into a hospital and two (25%) that the hospital was inside their home. One patient (13%) changed his delusional belief to a place reduplication form.

Overall, 19 patients changed the place of mislocation during the period of reduplicative paramnesia (32%). The second place of mislocation was closer to the hospital in the majority of patients (n=11, 58%; distance difference: median 28.86 km, range 0.39-201.26 km) and farther in four patients (21%; distance difference: 0.08 km, range 0.01-2.03 km). The difference was statistically significant ($p<0.01$). The remaining four patients changed the misidentification belief, but the geographical position of the misidentified place remained the same (21%).

Name of the misidentified place

Eighteen patients (30%) called "Hospital de Santa Maria" to the place that was misidentified (two of them to the second place of mislocation). In these cases, the presence of reduplicative paramnesia was uncovered when the patients were asked about their location (i.e. the city or town they were). The majority (n=15) referred that the name was that one because they were in a replica or in a branch of the original hospital (i.e. place reduplication). The remaining three patients believed that there was a hospital ward inside their homes (i.e. chimeric assimilation), which was also called "Hospital de Santa Maria".

Duration of spatial delusions and disruption of belief-associated network

The median duration of reduplicative paramnesia was 3 days (IQR 1-7 days, range 1-29 days; Figure 15A). In 23 cases, the patients were discharged still presenting reduplicative paramnesia.

The duration of reduplicative paramnesia was moderately correlated with the volume of structural disconnection overlapping the belief-associated functional network (Spearman's correlation=0.39; p=0.02; Figure 15B), and this association was independent of lesion volume (beta coefficient = 3.18; 95% confidence interval [0.12, 6.24]; p=0.04). The disconnected fibres with the highest beta-coefficient values were located in left inferior temporal regions (Figure 15C). It was also moderately correlated with the volume of stroke lesion overlapping the belief-associated functional network (Spearman's correlation=0.41; p=0.01), but the association was not independent of lesion volume (beta coefficient = 0.54; 95% confidence interval [-1.20, 2.28]; p = 0.53). The lesion and the structural disconnection overlap maps are available in Figure 16. The belief-associated meta-analytic functional map, which derived from 83 studies, is available in Figure 17.

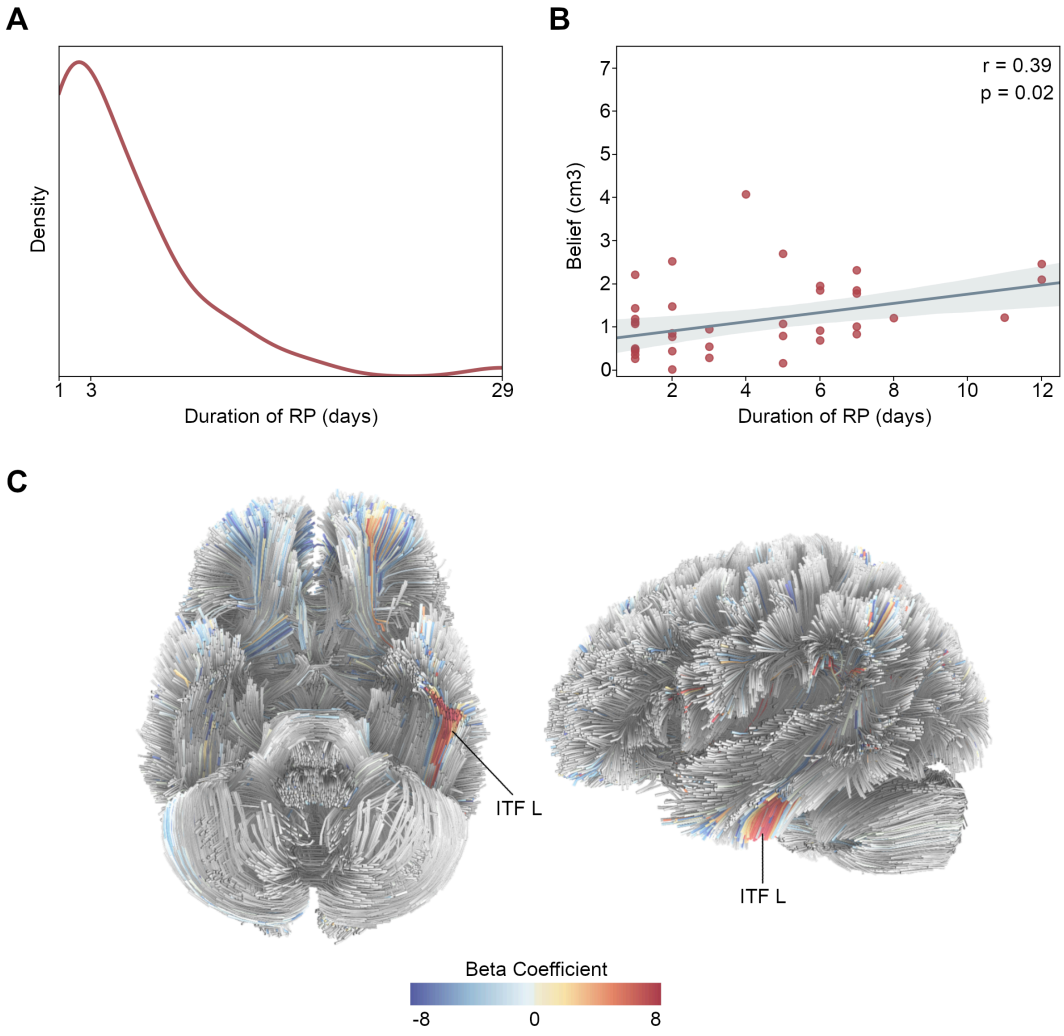

Figure 15. Duration of reduplicative duration. Density distribution of the duration of reduplicative paramnesia (A). Relationship between the duration of reduplicative

paramnesia and the structural disconnection of the belief network, expressed in the volume of overlap (B) and in a voxel-wise beta-coefficient tract representation (C). 'r' denotes the Spearman correlation value and 'p' the p-value. The blue line represents the robust regression line between the two variables and the blue shadows the 95% confidence interval. The colormap represents the beta-coefficient values. ITF, inferior temporal fibers; L, left; RP, reduplicative paramnesia. DSI Studio (http://dsi-studio.labsolver.org) was used to create tract map representations.

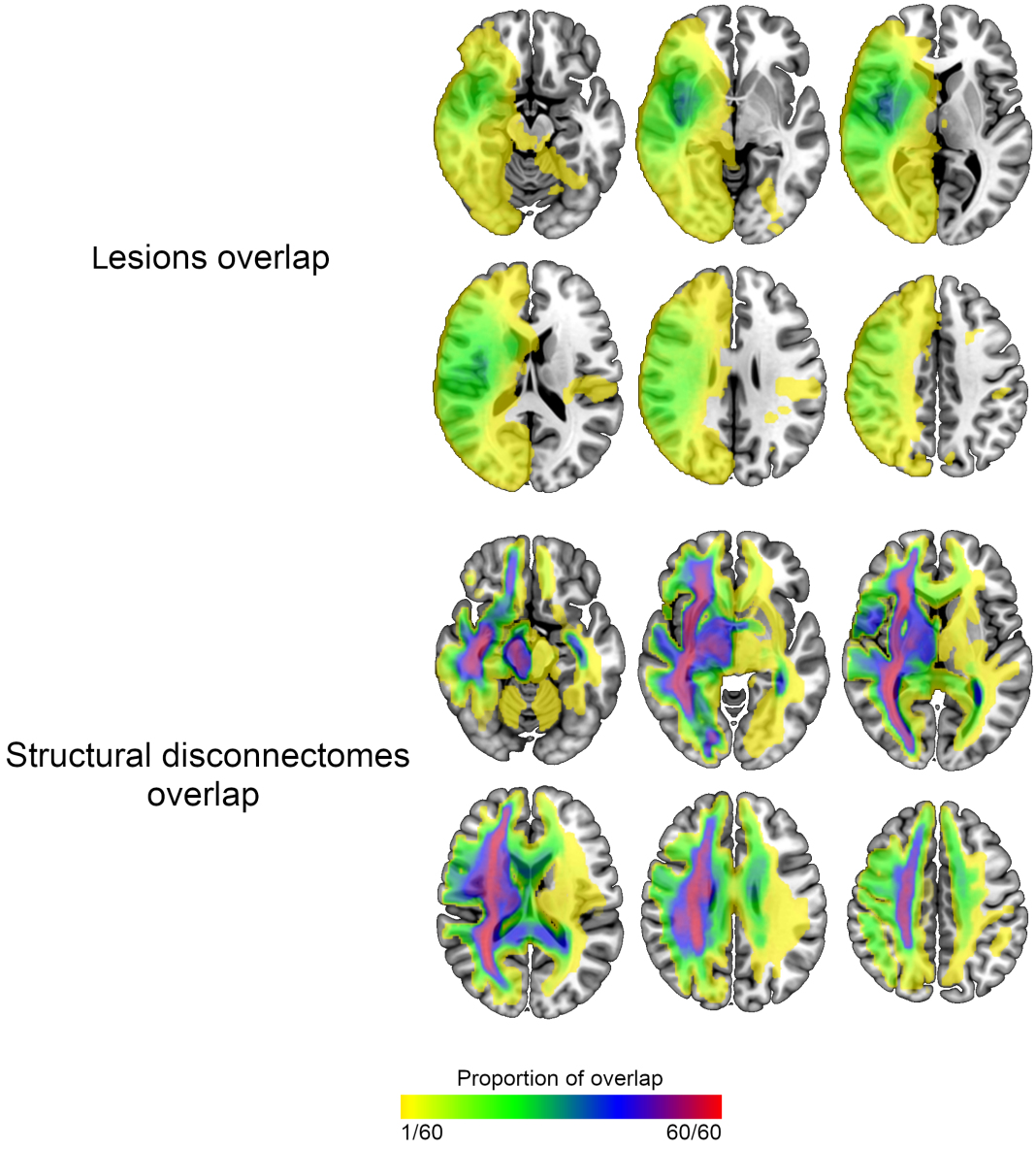

Figure 16. Lesion (top rows) and structural disconnectome (bottom rows) overlap maps of cases of reduplicative paramnesia. The colourmap represents the proportion of overlap.

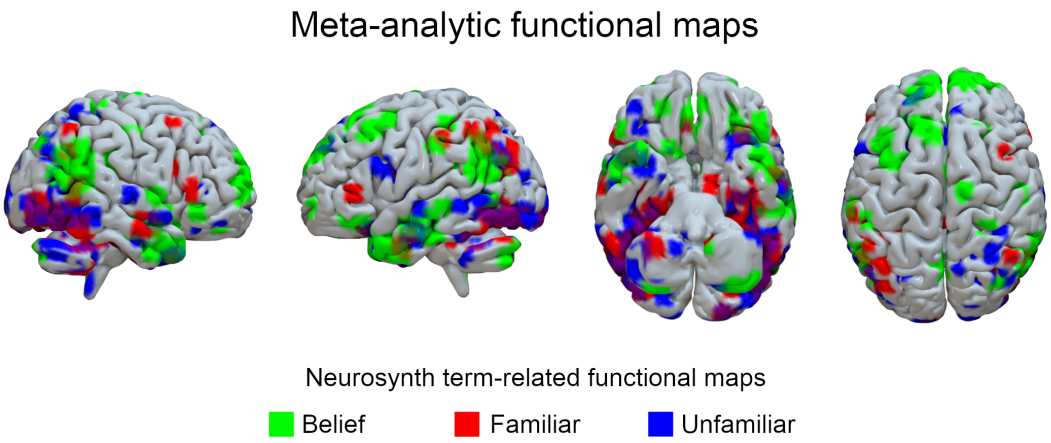

Figure 17. Surface representation of the Neurosynth meta-analytic functional maps for the terms 'belief', 'familiar' and 'unfamiliar'.

Semantic knowledge about the location of places and of spatial routes

All patients were able to say their own address and the majority knew the location of the (original) 'Hospital de Santa Maria' (n=52, 87%).

Twenty-eight patients (47%) were able to correctly describe the route between two or more points of interest in space (home – 'Hospital de Santa Maria', place of mislocation – home, place of mislocation – 'Hospital de Santa Maria').

Orientation in time

Most patients correctly knew the current year (n=48, 80%) and month (n=49, 82%).

Clustering based on familiarity-associated functional networks

The k-means clustering results based on the volume of lesion and volume of structural disconnection overlapping familiar and unfamiliar-associated functional networks are presented in Figure 18.

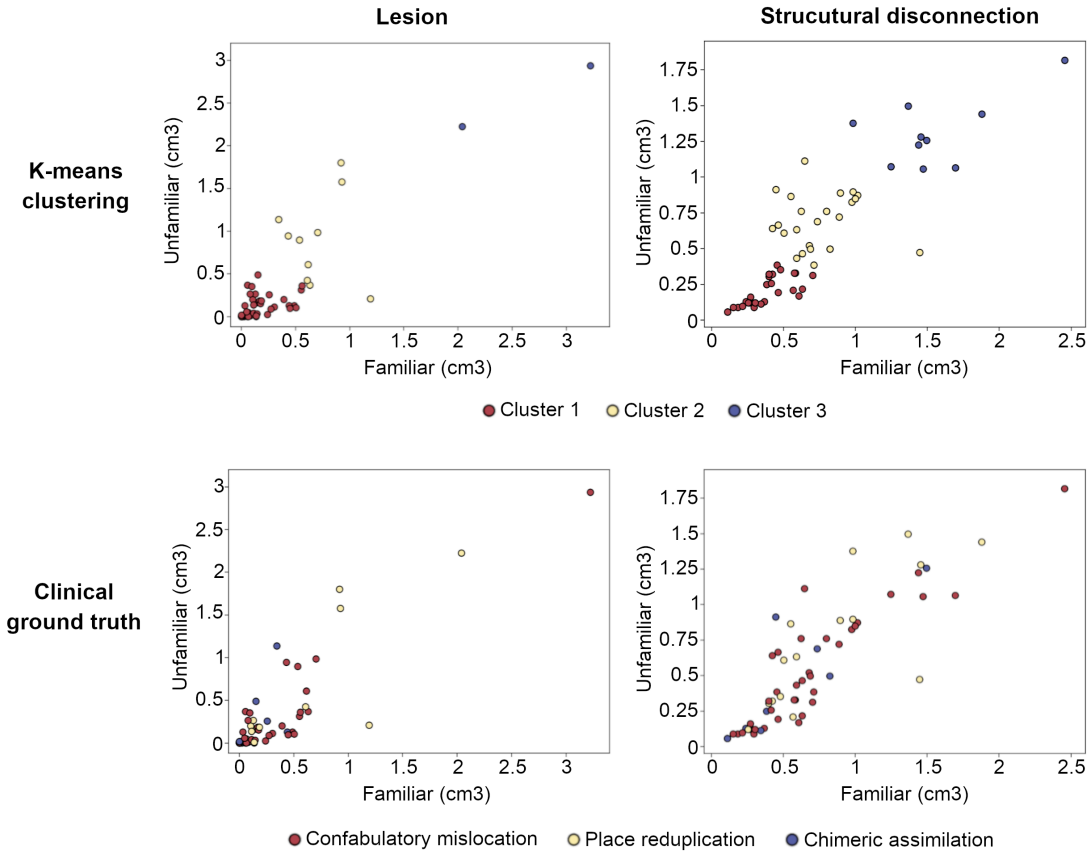

Figure 18. Reduplicative paramnesia subtypes and familiarity-associated functional networks. Clustering of reduplicative paramnesia cases based on the volume of lesion (top left) and of structural disconnection (top right) overlapping familiar and unfamiliar-associated functional networks, compared with the ground truth classification based on clinical presentation (bottom).

The familiar and unfamiliar-associated meta-analytic functional maps, which derived from 275 and 183 studies respectively, are available in the Figure 17.

The Rand index, expressing the similarity between the k-means clustering categorization and the clinical classification, was 0.47 for lesion maps and 0.51 for structural disconnection maps (poor similarity). The classification similarity remained low when the number of clusters was reduced to two (grouping confabulatory mislocation and chimeric assimilation in a unique category): Rand index of 0.64 for lesion maps and of 0.56 for structural disconnection maps.

Specific phenomenology of confabulatory mislocation

Representative descriptions of patients with confabulatory mislocation are presented in Table 6.

Table 6. Representative descriptions of patients with confabulatory mislocation

Why are health care professionals here?
"You are the doctor from 'Hospital de Santa Maria'. You came here to take care of me. I was there before. How did you know the address of my home? Did you find it well?"
"You are here to take care of me. The doctors and the nurses have been here, at my home, day and night. I don't have money to pay everything."
Why is medical equipment here?
"The equipment came in the ambulance. This looks like a hospital, but it's not. It's my home."
"Usually, this equipment exists in the hospitals. It is similar to the one I had in 'Hospital de Santa Maria'. The hospital should have put it here. Nowadays, technology can be anywhere. This building is my home, but a lot of things should have been brought from 'Hospital de Santa Maria'."
Why does it say 'Hospital de Santa Maria' in your bed sheets and hospital clothes?
"The coats may belong to 'Hospital de Santa Maria', but that doesn't mean that we are in 'Hospital de Santa Maria'. I can have a card with a certain name, but still don't be there."
"These clothes should have come in the ambulance. When the ambulance was called, the clothes should have been put inside."
Why are other patients in this room?
"These patients should have come with me in the ambulance, with the permission of the doctors and the nurses. It would be rude to send them away of my home."
"I don't know why these patients are at my home. I don't know them. The hospital might be full and they were brought here."
What do you think about this window view? The building, the stadium…
"I had never noticed that I could see Sporting's stadium from home. But if I were in 'Hospital de Santa Maria', I would see Benfica's stadium as well."
"I am seeing the stadium. This is a big confusion to my head, but I know I am at home. This is my home."

When asked about the presence of health care professionals in the misidentified place, most patients referred that they were there to help or assist them (n=22, 59%), followed by manifestations of surprise (n=5, 14%). When confronted with the presence of medical

equipment, the most common argument was that it had been brought from the hospital or by the health care professionals (n=11, 30%), followed by manifestations of surprise (n=10, 27%). When faced with the presence of the logo and the name of "Hospital de Santa Maria" in their bed sheets and hospital clothes, they most frequently stated that the clothes should belong to the "Hospital de Santa Maria" (n=18, 49%), followed by reaffirmations that they were not in "Hospital de Santa Maria" (n=6, 16%). Concerning the presence of other patients in the room, the patients most frequently did not present a justification (n=14, 38%). The most frequently presented argument was that they had come from the hospital or were sent by the hospital as well (n=9, 24%), and two of them added that the reason for that was that the hospital was full. It was possible to show the window view to 12 patients (32%). The most frequent reactions were justifying the unexpected view with changes in the neighbourhood or in the point of view (n=4, 33%) and of surprise (n=4, 33%).

For those who believed they were at home, in their relatives' home or in their holydays home (n=31, 84%), the most frequent house division of mislocation was the bedroom (n=16, 52%), followed by the living room (n=5, 16%).

Specific phenomenology of place reduplication

Representative descriptions of patients with place reduplication are presented in Table 7.

When faced with the presence of the logo and the name of "Hospital de Santa Maria" in their bed sheets and hospital clothes, most patients said that it was happening because the building was a branch of the main hospital (n=12, 55%), followed by saying that the replica had the same name of the original hospital (n=5, 23%). When confronted with the reference to "Lisbon" next to the logo, the most frequent answer was that the clothes should belong "Hospital de Santa Maria" in Lisbon. When asked about how many "Hospital de Santa Maria" they knew, most patients said that before they knew only one, but at that time they realized there should be two (n=10, 45%), followed by referring that there is only one and that the building where they were was a branch of the main one (n=9, 41%). It was possible to show the window view to 18 patients (82%). The most frequent reaction was of denial (n=6, 33%), i.e. despite recognizing that the window view was suggestive of being in the original "Hospital de Santa Maria", they refused they could be there. The second most common justification was that they were in a particular privileged

position that allowed them to see landmarks which would not usually be seen from the location they referred they were (n=4, 22%), namely that they were in very high positions.

Table 7. Representative descriptions of patients with place reduplication

Why does it say 'Hospital de Santa Maria' in your bed sheets and hospital clothes?
"This shall be a duplication of the service provided by 'Hospital de Santa Maria'. The name is the same, but it covers other geographical areas."
"You are the doctor from 'Hospital de Santa Maria'. But this is not 'Hospital de Santa Maria'. This is a dependency of 'Hospital de Santa Maria'. When there are many patients, they send some patients to here."
Why does it say 'Lisbon' next to the hospital logo?
"I hadn't read it. They made a mistake. They should have put the name of this town."
"I know I am in *(town X)*. The clothes might belong to the 'Hospital de Santa Maria' of Lisbon."
How many 'Hospital de Santa Maria' do you think there are?
"There is only one 'Hospital de Santa Maria'. I don't know why there is this one here too. You should ask the health minister why this is also called 'Hospital de Santa Maria'."
"There is only one. The original one. This is a dependency, not the main one. They might have built this one for the periods when the main one is completely full. 'Hospital de Santa Maria' is much bigger than this one."
What do you think about this window view? The building, the stadium…
"These buildings are not typical of this district. I had never seen them. The architecture has some similarities with the original 'Hospital de Santa Maria'. I am going to put my glasses, so that you don't say I am confused or disoriented. I might have loss some cognitive abilities after the stroke, but my spatial orientation is intact. The proof that it is possible to see Sporting's stadium from this district is that I am seeing it."
"I didn't know that we could see the Sporting's stadium, the airport and the University from here. We must be in a very high spot to have this window view."

Specific phenomenology of chimeric assimilation

Representative descriptions of patients with chimeric assimilation are presented in Table 8.

Table 8. Representative descriptions of patients with chimeric assimilation

Why does it say 'Hospital de Santa Maria' in your bed sheets and hospital clothes?
"The clothes should belong to 'Hospital de Santa Maria'. First I went to *(hospital X)*. Then, I was transferred to "Hospital de Santa Maria". After that, I was brought here, to my son's home. Now his home belongs to 'Hospital de Santa Maria'."
"That's because 'Hospital de Santa Maria' is here and my home is here too. Please open the door because my maid should be arriving. The house is mine. The hospital is not mine."
Why are other patients in this room?
"The hospital sent them to here as well. They may stay as long as they want. As the doctors came to my home, the patients also came. I am not paying these expenses."
"I don't know these patients. I don't know what they are doing here. They should have been brought here when I was sleeping. Probably, there weren't enough beds at the hospital and they were sent to here."
Have you noticed or heard about any construction work?
"It's strange how they have made it so quickly. They transformed my home into a hospital. In the future, I might make some profit from this."
"The construction was not ordered by me. I didn't pay it. It may have been my husband while I was at 'Hospital de Santa Maria'. My home is very different now. There is some furniture that is missing and I hadn't that basin there."
Why would a hospital be build inside your home (or in your relatives' home)?
"Maybe the hospital was full and they used this space. The other patients were brought here too. You are asking me all these questions to see if my thought is fine, but I assure you that it is."
"People from *(town X)* really needed a hospital here. Now they have it."
What do you think about this window view? The building, the stadium…
"The building looks like 'Hospital de Santa Maria'. It could easily trick you. But this is my home."
"My building is very similar to "Hospital de Santa Maria". It should have been designed by the same architect. Everything with public funds, maybe…"

When faced with the presence of the logo and the name "Hospital de Santa Maria" in their bed sheets and hospital clothes, most patients said that they should belong to "Hospital de Santa Maria" (n=7, 54%), followed by stating that it was because "Hospital de Santa Maria" was inside their home (n=2, 15%). Concerning the presence of other patients in the room, the most frequent explanation was that they had been sent by "Hospital de Santa Maria" (n=4, 31%), followed by stating that they came because the hospital was full (n=2, 15%). When asked if they had noticed or heard about any

construction work, none had a positive answer, but most regarded it as a positive occurrence (n=3, 23%), followed by saying that it should have been allowed or arranged by a relative (n=2, 15%). When questioned about the reason to build a hospital inside their homes or their relatives' home, the most frequent answer was that the hospital was full (n=4, 31%), followed by saying that the region they were convinced they were needed a hospital (n=2, 15%). It was possible to show the window view to six patients (46%). The most frequent reaction was of denial (n=3, 50%), followed by justifying the unexpected view with changes in the neighbourhood (n=2, 33%).

Regarding the division of the home or of their relatives' home that they believed they were, the most frequent was the bedroom (n=5, 38%), followed by the living room (n=3, 23%) and the kitchen (n=2, 15%).

Discussion

In this work, we analysed the clinical phenomenology and neural correlates of stroke-associated spatial delusions. First, we characterized the location of misidentified places and described the general phenotypic features of the syndrome. We demonstrated that the duration of spatial delusions is moderately correlated with the structural decoupling of belief-associated functional networks. Second, we reported associated clinical features, such as the patients' knowledge about the location of the misidentified places and their orientation in time. Third, we showed that case clustering based on structural disruption of familiar/unfamiliar-associated functional regions poorly matches the clinical classification. Finally, we described the most common patterns of patients' response according to spatial delusion subtypes and provided representative examples to facilitate recognition and diagnosis.

The large majority of patients localized the misidentified place closer to their homes than to the hospital. Limbic models of delusional misidentifications advocate that misidentified stimuli tend to be emotionally relevant for patients (Ellis and Young 1990), and an association between spatial delusions and structural disconnection of limbic structures was demonstrated (Alves et al. 2021a). Curiously, in those that changed the place of mislocation during the presentation, the second place was significantly closer to the hospital than the first, which putatively indicates that the update of spatial references until a correct allocentric localization might be a progressive process.

Belief, as a neural process, can be defined as the integration of perceived information with internal representations of personal significance and emotional value (Seitz 2021).

Distinct neural systems in the prefrontal cortex and in the limbic system mediate the states of assent, dissent and uncertainty (Harris et al. 2008; Sacks and Hirsch 2008). Deregulations of belief processes seem to be a cardinal condition for delusional misidentifications (Pacella et al. 2019; Seitz 2021). As our phenomenological analysis showed, patients recognize that the surrounding environment looks like "Hospital de Santa Maria" but still, they don't believe they are there. For the first time, we showed that the magnitude of structural disconnection of belief-associated functional networks is correlated with the duration of reduplicative paramnesia. Interhemispheric unbalance models propose that delusional misidentifications result from right hemisphere damage and left hemisphere unleashing (Devinsky 2009). While previous evidence show that the emergence of spatial delusions is predicted by disconnection of right temporal regions (Alves et al. 2021a, b), here we showed that it is the disconnection of left temporal regions that best predicts the duration of the syndrome. This result may provide a structural-functional support to the role of left hemisphere dysfunction in the pathophysiology of reduplicative paramnesia.

The erroneous beliefs and the disturbed mechanisms of implicit memory and recognition overwhelm the patient's semantic knowledge about the spatial localizations of misidentified places (Ellis and Young 1990; Ellis et al. 1997; Coltheart et al. 2011). In our sample, all patients were able to say their own address and the large majority knew the location of (the original) "Hospital de Santa Maria". Egocentric systems also seem to be preserved. Although we were not able to systematically assess real spatial navigation, nearly half of the patients were able to mentally describe routs correctly. This evidence is in line with neuroanatomical studies showing that reduplicative paramnesia is associated with disruption of ventral (allocentric-related) pathways (Budson et al. 2000; Alves et al. 2021a; Evensmoen et al. 2021), while dorsal (egocentric-related) regions are more frequently spared (Kravitz et al. 2011; Alves et al. 2021a). The spatial-specificity of the syndrome is also evident in the fact that the large majority of patients were oriented in time.

The strong emotional valence associated with reduplicative paramnesia, evident in the pioneer and in subsequent descriptions (Pick 1903; Benson et al. 1976; Murai et al. 1997), manifests at opposite poles of pathological familiarity (Devinsky 2009). However, the clustering classification based on structural disruption of familiar/unfamiliar-associated functional networks had a poor capacity to predict clinical subtype classification. Finer functional interactions between familiarity-associated brain regions not detected by our

model, as well as psychological factors (Ovelacg et al. 1988), might be crucial to determine this phenomenological divergence.

Knowledge about the phenomenological features of the syndrome is important to make an appropriate diagnosis and to avoid misinterpretations of patients' general cognitive status. Nearly one third of the patients called "Hospital de Santa Maria" to the misidentified place, which may contribute to the underdiagnosis of the syndrome. Simple questions, such as asking in which town/district patients are, might be crucial for the diagnosis and should be performed during neurological examination, specially in patients with right hemisphere lesions. In addition, in at least one-third of the patients, the syndrome was not hyperacute, i.e. the patients were at least one day oriented in space before the emergence of reduplicative paramnesia, and nearly half spontaneously said that they had previously been in the (original) "Hospital de Santa Maria" before being brought to the place they were at that moment. The physiopathological reason for this delayed onset remains to be clarified.

As limitation of our study, we were not able to conduct a prospective follow-up of patients after their hospital discharge. In addition, the study was performed in a tertiary stroke unit and may not be representative of the entire stroke population. Finally, our sample did not include patients with aphasia and severe dysarthria.

In conclusion, our work reports a systematic description of the peculiar clinical features of stroke-associated spatial delusions, which may boost the awareness and the proper diagnosis of the syndrome. It also provides novel evidence about the neural correlates of the syndrome.

3. Neural basis of stroke-associated spatial delusions

Part of this section was published in the following article:

- Alves PN, Fonseca AC, Silva DP, Andrade MR, Pinho-e-Melo T, Thiebaut de Schotten M, Martins IP (2021) Unravelling the neural basis of spatial delusions after stroke. Ann Neurol 89:1181–1194. https://doi.org/10.1002/ana.26079.

Introduction

Interpretation of space is a continuous process that allows us to explicitly know where we are (Gooddy and Reinhold 1952). Perceived sensorial information from the environment is integrated in spatial orientation networks that mediate the recognition of known spatial landmarks and navigation with regard to allocentric and egocentric references (Aguirre and D'Esposito 1999). While comprehensive cognitive models have been proposed for spatial representation (Burgess 2014), the anatomical systems supporting spatial interpretation remain poorly documented.

The intriguing nature of reduplicative paramnesia has fostered the development of different models to explain its pathophysiology. Memory-related theories have proposed an abnormal integration of new visual information with past memories, leading to a defective update of patients' spatial representations (Staton et al. 1982). Ellis and Young emphasized that patients with delusional misidentification have a deficit in the attribution of appropriate emotional valences to visual stimuli (Ellis and Young 1990). They demonstrated that the expected autonomic responses are not generated in these patients when confronted with familiar stimuli (Ellis et al. 1997). In addition, it has been proposed that reduplicative paramnesia and other delusional misidentification syndromes result from a combination of right hemisphere injury and left hemisphere overactivity (Devinsky 2009). Different neuroanatomical hypotheses have emerged from these cognitive models; however, solid empirical evidence is lacking (Politis and Loane 2012).

Here, we explored the anatomy of lesions leading to reduplicative paramnesia in a large dataset of patients to shed light on the brain mechanisms supporting the interpretation of space.

Methods

Study design and patient selection

We performed a prospective, cumulative, case-control study that included patients from the stroke unit of a tertiary university hospital in Lisbon, Portugal. Recruitment lasted from December 2016 to February 2020. Reduplicative paramnesia is a right-hemisphere stroke syndrome (Bartolomeo et al. 2016). We consecutively included adult patients with right hemisphere stroke who were admitted in the acute phase (72 hours or less) of stroke. Patients with either ischaemic or haemorrhagic strokes were considered. The exclusion criteria were as follows: acute confusional state, according to the criteria defined in the

fifth edition of the Diagnostic and Statistical Manual of Mental Disorders; decreased level of consciousness, either somnolence, stupor or coma; subarachnoid haemorrhage; epileptic seizures during admission, either symptomatic or in patients with a previous diagnosis of epilepsy; aphasia or severe dysarthria, precluding screening for reduplicative paramnesia; severe visual deficit, precluding confrontation with counter-evidence stimuli; previous history of dementia, defined as a cognitive decline that interfered with the instrumental activities of daily living (according to the clinical history provided by the patient's relatives and/or to the patient's medical records in the national electronic health platform), as referred in the criteria of major neurocognitive disorder in the fifth edition of the Diagnostic and Statistical Manual of Mental Disorders; absence of a stroke lesion in brain imaging or unavailable brain images.

A prior history of stroke was not an exclusion criterion, because there are reports hypothesizing that prior brain lesions may contribute to the occurrence of reduplicative paramnesia (Moser et al. 1998).

This study was approved by the Joint Ethics Committee of the Lisbon Academic Medical Centre.

Clinical screening

Patients were screened for reduplicative paramnesia within the first 72 hours of admission and then at regular intervals of 48 hours. Spatial orientation was evaluated through a structured interview asking patients if they knew where they were, namely, the kind of building (hospital), the city (Lisbon) and the city district they were in. The patients who did not know or who gave a wrong answer were given the correct location. If patients disagreed with the given answer, they were then confronted with clear evidence proving otherwise. Whenever they thought they were in a place other than a medical facility, they were shown and asked to identify medical equipment (vital signs monitor, venous infusion tubes, oxygen masks), other patients in the same room or medical staff (physicians, nurses, physiotherapist). Whenever they believed they were in another hospital or in another place/city, they were shown either a) the hospital logotype in the medical coats and bed sheets and asked to read the corresponding inscription, which included the hospital and the city names, or/and b) the view from a window and asked to identify unique nearby landmarks, such as Lisbon airport and the stadium of an emblematic Portuguese football team. The patients who maintained a false conviction of spatial mislocation after being

effectively exposed to these counterfactual stimuli (either confabulatory mislocation, place reduplication or chimeric assimilation) were considered cases of reduplicative paramnesia. The patients who were oriented in space or patients who were disoriented but accepted evaluator's explanation or changed their belief after being exposed to the referred counter-evidence were considered controls.

Clinical and demographic data were collected. The descriptions of the patients with reduplicative paramnesia were classified according to the subtypes defined in the literature, i.e. place reduplication, confabulatory mislocation and chimeric assimilation (Politis and Loane 2012). We also screened for other delusional misidentification syndromes, namely, Capgras syndrome, Fregoli syndrome, asomatognosia and somatoparaphrenia.

Regarding neuroimaging parameters, the grades of cerebral atrophy and small-vessel disease burden were visually rated (either on CT or MRI, as specified in the following section). The Global Cortical Atrophy scale was used to assess cortical atrophy (Pasquier et al. 1996). This scale was originally designed to grade cortical atrophy in stroke patients and consists of an ordinal scale, ranging from 0 (no atrophy) to 3 ('knife blade' atrophy), that includes a discrete assessment of the frontal, the parieto-occipital and the temporal regions. The Medial Temporal Lobe Atrophy score was also evaluated (Scheltens et al. 1992). It is a widely used ordinal scale to assess medial temporal lobe atrophy that ranges from 0 (no atrophy) to 4 (marked widening of the choroid fissure and of the temporal horn, marked atrophy and internal structure loss of the hippocampus). The Age-Related White Matter Changes was used to grade small-vessel disease burden (Wahlund et al. 2001). It evaluates both white matter disease and basal ganglia small-vessel lesions in two ordinal scales ranging from 0 (no lesions) to 3 (diffuse or confluent lesions). These three scales were chosen because they have good intra and interobserver reliability (Wahlund et al. 2001; Harper et al. 2015) and they have been recommended for the routine clinical assessment of CT and MRI images (Wahlund et al. 2017). The rater was blind to patients' outcome during the assessment.

Lesion topography analysis

Brain MRI or CT images were used to define stroke lesions. Delimitation was manually performed on axial slices with a thickness of 3mm. The researchers were blind to the status of the patient (i.e., case or control). MRI images were acquired in a Philips Achieva 3.0 Tesla or Philips Intera 1.5 Tesla scanner. The sequence of reference in MRI was the

diffusion-weighted imaging (de Haan and Karnath 2018). When MRI was not available, CT performed 24-72 hours after stroke onset was used. CT images were acquired in a Philips Brilliance 64-channel scanner.

Brain MRI and CT images were normalized to MNI152 space. For MRI, T1 images were used as the reference for normalization. We performed a first step of linear registration, applying an affine transformation (12 degrees of freedom), using FSL's *flirt* tool. A second step of non-linear registration was performed using FSL's *fnirt* tool (Jenkinson et al. 2012). For CT, a linear registration was performed applying the same parameters as before and using the CT-derived MNI152 template (de Haan and Karnath 2018). In both cases, the calculated deformation field was applied to the lesions.

Randomise is an FSL tool that allows nonparametric comparisons of brain images (Winkler et al. 2014). A two-sample unpaired analysis was performed using this tool to compare lesion maps of the two groups. Five thousand permutations were computed, a threshold-free cluster enhancement was applied, and the obtained p-values were family-wise error (FWE) corrected. Possible confounders were included in the model as covariates, namely, lesion volume, stroke clinical severity (measured by the National Institutes of Health Stroke Scale), imaging modality (MRI or CT) and stroke vascular territory. The analysis was whole-brain based.

A brain map of the areas whose lesion or sparing was significantly associated with reduplicative paramnesia was created.

A less conservative follow-up analysis was also performed, applying a False Discovery Rate (FDR) correction for multiple comparisons. FDR-corrected maps were computed using FSL's *fdr* tool.

To investigate neuroimaging differences between the three subtypes of reduplicative paramnesia, we also computed an F-test with *randomise*, contrasting patients with place reduplication, confabulatory mislocation and chimeric assimilation (Winkler et al. 2014). If the F-test revealed statistically significant intergroup differences, individual two sample tests were calculated to determine the direction of the effect.

We included prior brain lesions in the lesion mask. Since the neurobiological processes underlying acute and chronic stroke lesions differ, a sensitivity analysis including only patients with first-ever strokes was performed.

Structural disconnection analysis

Some neurobehavioural syndromes are better explained by the pattern of white matter disconnection rather than by a specific lesion localization (Herbet and Duffau 2020; Thiebaut de Schotten et al. 2020). With this in mind, we also compared the pattern of structural disconnection between the cases and controls.

The tool *Disconnectome* from the software package BCBtoolkit (http://toolkit.bcblab.com) indirectly calculates the probability of structural disconnection caused by focal lesions (Foulon et al. 2018). The probability of disconnection was derived from healthy subjects' tractography (n=178) from the Human Connectome Project 7T dataset (Vu et al. 2015). Tractography was processed as described by Karolis and colleagues (2019). This analysis produces a disconnectome map revealing disconnection patterns only when more than 50% of the tractographies of healthy subjects were disconnected.

A *randomise* two-sample test was computed to compare the disconnectome maps of the two groups using the same parameters and the same confounding covariates considered in the lesion topography analysis (Winkler et al. 2014). A brain map of areas whose disconnection was significantly associated with reduplicative paramnesia was created.

Similarly to the approach taken in the previous section, a F-test was calculated to investigate structural disconnection differences between the subtypes of reduplicative paramnesia.

We also computed a structural disconnection matrix. The Automated Anatomical Labelling atlas 3 (AAL3) was the chosen parcellation because it includes cortical and subcortical structures (Rolls et al. 2020). We used MRtrix's tool *tckedit* to select the tracts of each of 178 tractographies of reference that crossed the individual stroke lesions (Tournier et al. 2019). Then, MRtrix's tool *tck2connectome* was run to create a connectivity matrix. To calculate the proportion of disruption, we divided the number of disrupted streamlines by the total number of streamlines connecting each pair of regions. The mean of the 178 individual matrices was computed, in order to obtain single individual connectivity matrices. The difference in the proportion of disruption between the cases and controls and a two-sample unpaired statistics were calculated, applying a multiple comparisons Bonferroni-corrected p-value (p-value<3.5E-6).

Functional connectivity analysis

There is a considerable relationship between structural and functional disconnection, but the overlap is far from absolute (Suárez et al. 2020). Lesion network mapping of some neuropsychiatric syndromes, such as peduncular hallucinosis, has been achieved through functional connectivity analysis (Boes et al. 2015). Therefore, we complemented the connectivity characterization of reduplicative paramnesia with a functional connectivity study.

Stroke lesions were used as seeds. We calculated the correlation between the average time course of every lesion and the time course of the other brain voxels using the *Funcon* connectivity tool from BCBtoolkit (http://toolkit.bcblab.com; Foulon et al. 2018). We used 175 preprocessed 7.0 Tesla resting state functional MRIs from the Human Connectome Project S1200 dataset (Glasser et al. 2013). Preprocessing was performed according to the Human Connectome Project pipelines (Glasser et al. 2013). To create the functional disconnectome map of each patient, we followed the protocol developed by the Laboratory for Brain Network Imaging and Modulation (Fox 2018). Correlation values were converted to a normal distribution using Fisher's r to z transform. FSL's tool *randomise* one-sample test was used to compute statistically significant correlations, applying a threshold-free cluster enhancement. Statistical maps were thresholded and binarized at $t>\pm4.25$ to create positive and negative functional disconnectome maps (Fox et al. 2012; Darby et al. 2017). We chose the same threshold as Darby and colleagues in their work about delusional misidentifications syndromes, to allow a more direct comparison between studies (Darby et al. 2017). A *randomise* two-sample test was applied to compare the maps of the two groups using the same parameters and the same confounding covariates applied in the lesion topography and in the structural connectivity analyses. We run additional analyses without a t-value threshold and with alternative t-value thresholds of 4.16 ($p<0.00005$) and of 4.71 ($p<0.000005$) to evaluate the consistency of the results (Cohen and Fox 2020). A F-test to investigate intergroup functional connectivity differences between the subtypes of reduplicative paramnesia was computed as well.

It has been demonstrated that cognitive processing is enhanced when there is functional-structural coupling (Medaglia et al. 2018). In addition, it is expected that white matter disruption induces functional changes at the cortical level (Wu et al. 2020). Therefore, we performed a complementary analysis aimed to integrate functional and structural maps. We defined significant functional regions and adjacent white matter voxels as seeds for tractography in the seed-tracking algorithm provided by DSI Studio (http://dsi-

studio.labsolver.org). Then, we identified the areas of overlap between the obtained structural connectivity map and the map of significant structural disconnection.

Statistical analysis

Continuous variables were reported as the mean (standard deviation) or median [interquartile range] and compared using two-sample unpaired t-tests or Mann-Whitney tests, according to their distribution. Categorical variables were reported as frequencies and compared using chi-square or Fisher's tests, as appropriate.

A multivariate logistic regression model was built using Stata14®. Variables with a statistically significant association in the bivariate analysis or those that were considered clinically or biologically relevant were included using a step-up approach. Competing models were evaluated by their goodness-of-fit and complexity using Akaike information criterion.

Finally, the obtained model was cross-validated. We computed a support vector machine k-fold nested cross-validation using scikit-learn. We used *RepeatedStratifiedKFold* as a randomized cross-validation splitter, and 50 splits were performed, leaving 20% of the data out (Varoquaux et al. 2017). A structural disconnection map and a lesion spared map were computed in each cross-validation fold (i.e. 50 different structural disconnection and lesion spared maps were calculated). The maps derived solely from the training sample that was randomly selected at each iteration, so that the predictive capacity of the model was tested in a group of subjects (test sample) that did not contribute to the computation of these maps. We applied GridSearchCV for parameter hyperoptimization and C-Support Vector Classification as a classifier. A receiver operating characteristic (ROC) curve was plotted to evaluate the classifier's output, and the median and interquartile range of the area under the curve (AUC) scores were computed. The positive and negative predictive values of the model were also calculated.

Due to the hypothesis that psychiatric co-morbidities might increase the likelihood of delusional misidentifications of space, a subgroup analysis was performed comparing demographic, clinical and neuroimaging parameters between reduplicative paramnesia patients with and without prior psychiatric disease.

Alpha levels were set at 0.05 for statistical significance, and the p-value was corrected for multiple comparisons whenever appropriate, as specified in the previous sections.

Results

Out of 400 patients screened, 297 fulfilled our study criteria. The reasons for patient exclusion are presented in Table 9. Sixty-four out of the 297 patients presented with reduplicative paramnesia.

Table 9. Reasons for patient exclusion.

Reason for exclusion	**N**
Decreased level of consciousness	32
Acute confusional state	18
Severe dysarthria	12
Aphasia precluding assessment	7
Dementia	5
Epileptic seizures	3
Absence of stroke lesion in imaging	21
Brain images not available	5

Clinical features

The demographic, clinical and neuroimaging features of the cases and controls are presented in Table 10.

Table 10. Demographic, clinical and neuroimaging features

		Cases (n=64)	**Controls (n=233)**	**p-value**
Demographic features	Age (years)	78 [71-83]	68 [58-78]	<0.01
	Gender (F/M), n	31/33	99/134	0.40
Clinical features	Type of stroke (Isch/ICH), n	62/2	212/21	0.18
	Screening start (days)	2 [1-2]	2 [1-2]	0.18
	Length of admission (days)	8 [5-12]	7 [5-11]	0.44
	NIHSS admission	15 [12-18]	11[6-15]	<0.01
	NIHSS discharge	10 [5-15]	3 [1-8]	<0.01
	mRankin discharge	4 [3-4]	2 [1-4]	<0.01
	Anosognosia, n (%)	44 (69%)	73 (31%)	<0.01
	Neglect, n (%)	41 (64%)	109 (47%)	0.01

	Other DMS, n (%)	12 (21%)	6 (3%)	<0.01
	Fregoli syndrome	8 (14%)	1 (0.4%)	
	Asomatognosia	1 (1.7%)	2 (0.9%)	
	Somatoparaphrenia	2 (3%)	3 (1.3%)	
	Fregoli + asomatognosia	1 (1.7%)	0 (0%)	
	Ischaemic territory, n (%)			0.02
	MCA	45 (73%)	161 (76%)	
	ACA	0 (0%)	2 (1%)	
	PCA	1 (2%)	19 (9%)	
	Thalamic	1 (2%)	7 (3%)	
	MCA plus	11 (17%)	16 (8%)	
	Other	4 (6%)	7 (3%)	
	ICH location, n (%)			0.18
	Lobar	0 (0%)	13 (62%)	
	Deep	2 (100%)	8 (38%)	
Comorbidities	Prior psychiatric disease, n(%)	9 (14%)	26 (11%)	0.52
	Depression	8 (13%)	19 (8%)	
	Anxiety	0	6 (3%)	
	Bipolar disorder	1 (2%)	0	
	PTSD	0	1 (0.4%)	
Neuroimaging features	Modality (MRI/CT), n	23/41	118/115	0.06
	Lesion volume (cm3)	54[25-136]	17 [4-61]	<0.01
	ARWMC			
	White matter	1 [1-2]	1 [0-2]	0.19
	Basal ganglia	1 [0-2]	1 [0-2]	0.46
	Global cortical atrophy			
	Frontal	1 [0-2]	0 [0-1]	0.02
	Parieto-occipital	1 [1-2]	1 [0-2]	<0.01
	Temporal	1 [0-2]	0 [0-1]	0.04
	Medial temporal atrophy	2 [1-2]	1 [0-2]	<0.01

Values are presented as the median [interquartile range], unless otherwise specified. ACA, anterior cerebral artery; ARWMC, age-related white matter changes; DMS, delusional misidentification syndromes; F, female; ICH, intracerebral haemorrhage; Isch, ischaemic;

M, male; MCA, middle cerebral artery; NIHSS, National Institutes of Health stroke scale; mRankin, modified Rankin scale; PCA, posterior cerebral artery; PTSD, post-traumatic stress disorder.

The patients with reduplicative paramnesia were older, had more severe neurological deficits and had worse functional outcomes at discharge than controls. Anosognosia, neglect and other delusional misidentification syndromes were more frequent in patients with reduplicative paramnesia. There was no difference in terms of prior history of psychiatric disease. The patients with reduplicative paramnesia had higher lesion volumes and higher grades of cortical atrophy. There was no difference in terms of small vessel disease burden, both at the white matter and basal ganglia levels.

The median duration of reduplicative paramnesia was 2 days (interquartile range: 1-5 days) and ranged from 1 to at least 17 days. Nineteen patients maintained reduplicative paramnesia at the time of discharge (or transference to another hospital).

The most frequent subtype of reduplicative paramnesia was confabulatory mislocation (56%), followed by place reduplication (19%) and chimeric assimilation (13%).

In the subgroup of patients with prior psychiatric disease, none had a previous history of delusions. There was no statistically significant difference between reduplicative paramnesia patients with and without prior psychiatric disease in terms of age, frequency of anosognosia, clinical severity, lesion volume and small vessel disease burden.

Lesion topography

Lesion overlap maps of cases and controls are presented in Figure 19A. The comparison between the two groups, regressing for confounders, did not reveal any voxels significantly more often lesioned in the cases than controls (both in the primary FWE adjusted and in the follow-up FDR adjusted analyses). Conversely, there were voxels topographically located in the dorsal regions of the parietal and frontal lobes that were significantly more often lesioned in controls than in cases (FWE-corrected p-value<0.05; Figure 19B).

The proportion of MRI/CT scans in the groups of cases and controls were 23/41 and 118/115, respectively (p=0.06).

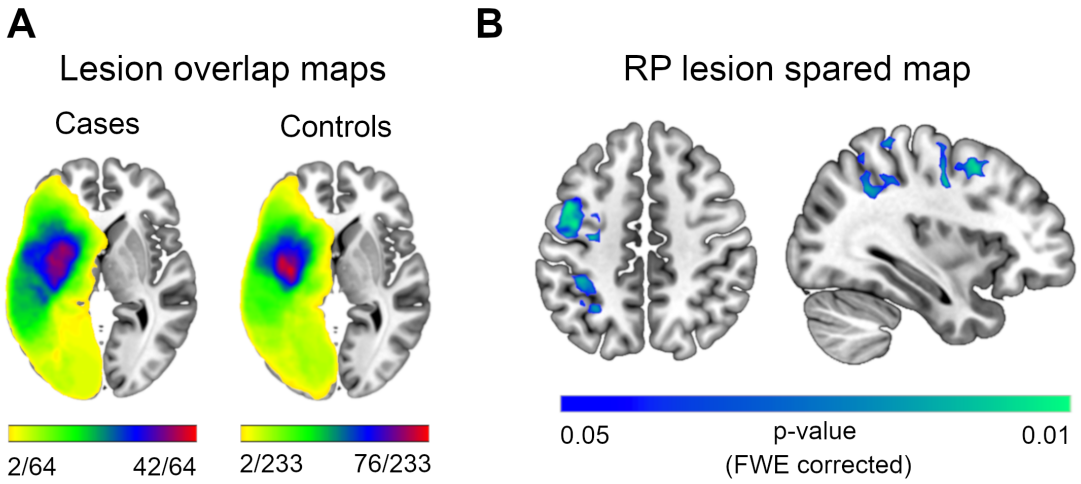

Figure 19. Lesion topography analysis. A – Lesion overlap maps of cases (left) and controls (right). B – Statistical mapping of areas significantly more often spared in cases of reduplicative paramnesia than in controls, regressing for confounders. RP, reduplicative paramnesia.

The sensitivity analysis including only patients with a first-ever stroke (n=276; 60 cases, 216 controls) revealed similar results.

There was no statistically significant intergroup difference between the three subtypes of reduplicative paramnesia or between reduplicative paramnesia patients with and without prior psychiatric disease.

Structural disconnection

The comparison of the structural disconnection maps between cases and controls, regressing for confounders, revealed a map of voxels significantly more often disconnected in cases than controls (FWE-corrected p-value<0.05; Figure 20A). There were no voxels significantly more often disconnected in the controls than in cases. Two main segments of disconnection were evident: right thalamo-frontal and right occipito-temporal (Figure 20B). The right thalamo-frontal segment overlapped the anterior thalamic radiations and the fronto-striatal projections (Figure 20C, left). The right occipito-temporal segment overlapped the inferior fronto-occipital fasciculus and the inferior longitudinal fasciculus (Figure 20C, right).

The sensitivity analysis including only patients with a first-ever stroke (n=276; 60 cases, 216 controls) revealed similar results.

All the lesions associated with reduplicative paramnesia hit at least one of these segments (Figure 21B). Most intersected both the right thalamo-frontal and the right occipito-temporal segments (81%, n=52). The remaining intersected the right occipito-temporal segment only (19%, n=12).

The structural disconnection matrix is presented in Figure 20D. The pairs of AAL3 nodes with the highest differences in terms of proportion of disconnection between the two groups were: a) the right fusiform gyrus with the right anterior orbitofrontal cortex; b) the right cuneus and superior occipital gyrus with the right superior temporal gyrus; c) the right thalamic ventral anterior nucleus with the right frontal middle gyrus; and d) the right midbrain with the right medial superior frontal gyrus (Figure 20E). The difference between the two groups was statistically significant (Bonferroni's corrected p-value<3.5E-6), with higher proportions of disconnection in patients with reduplicative paramnesia than in controls.

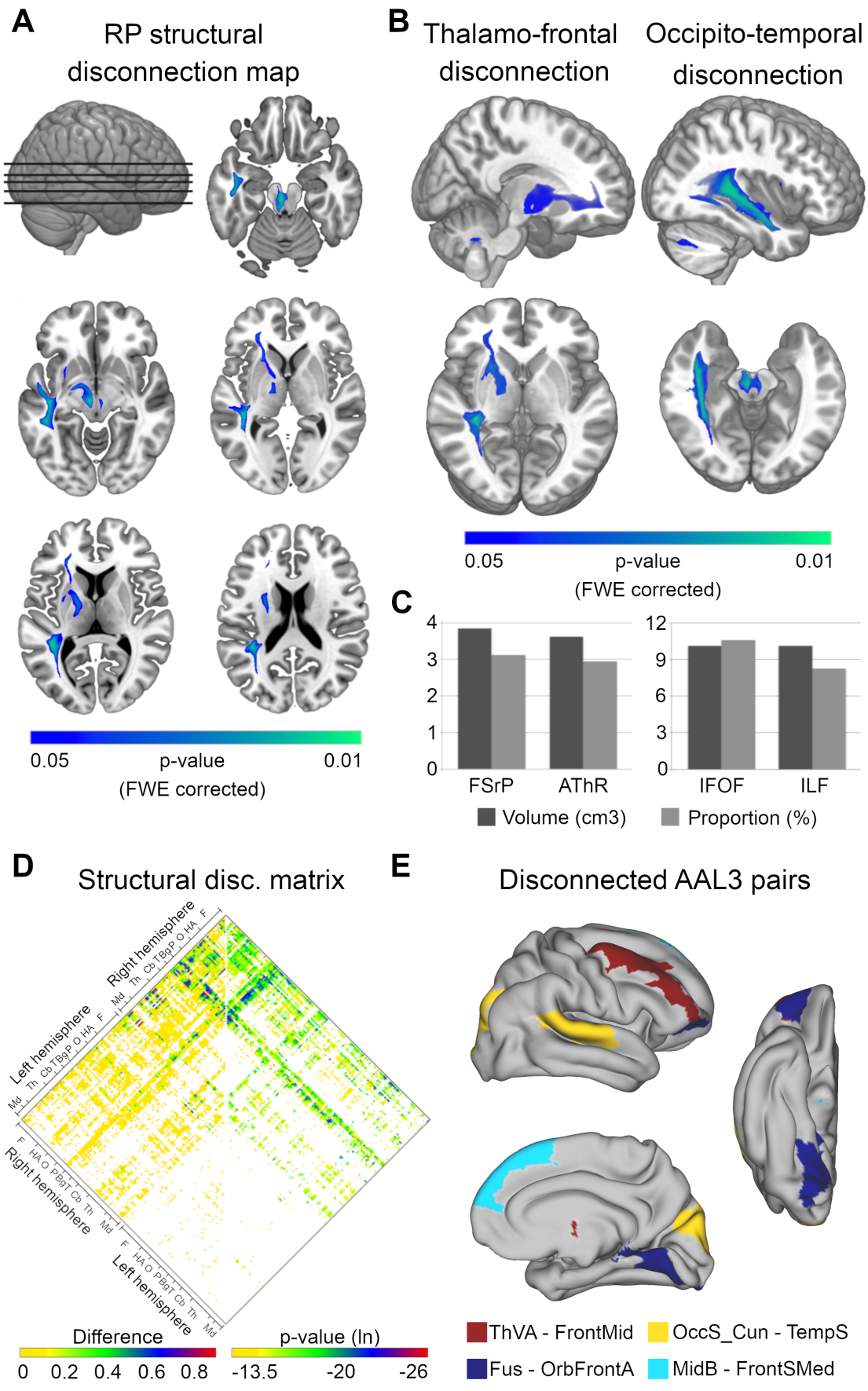
A
RP structural disconnection map
0.05
p-value
0.01
(FWE corrected)
B
Thalamo-frontal disconnection
Occipito-temporal disconnection
0.05
p-value
0.01
(FWE corrected)
C
4
3
2
1
0
FSrP
AThR
12
9
6
3
0
IFOF
ILF
Volume (cm3)
Proportion (%)
D
Structural disc. matrix
Right hemisphere
Left hemisphere
Left hemisphere
Right hemisphere
Difference
0 0.2 0.4 0.6 0.8
p-value (ln)
-13.5 -20 -26
E
Disconnected AAL3 pairs
ThVA - FrontMid
OccS_Cun - TempS
Fus - OrbFrontA
MidB - FrontSMed

Figure 20. Structural disconnection analysis. A – Statistical mapping of areas more often disconnected in patients with reduplicative paramnesia than controls, regressing for confounders. B – Three-dimensional representation of statistical mapping, evidencing the segments of the right thalamo-frontal and right occipito-temporal disconnection. C – Volume and proportion of the right fronto-striatal projections (FSrP), right anterior thalamic radiations (AThR), right inferior fronto-occipital fasciculus (IFOF) and right inferior longitudinal fasciculus (ILF) that are intersected by the statistical map of disconnection. D – Structural disconnection matrix. The left half represents the difference between the proportions of disconnection in cases and controls (cases minus controls). The right half represents the corresponding p-values (in a natural logarithmic scale). Each line represents an AAL3 node. Nodes were grouped into regions according to the corresponding labels (Bg, basal ganglia; Cb, cerebellum; F, frontal; HA, hipoccampal-amygdaline complex; Mid, midbrain; O, occipital; P, parietal; T, temporal; Th, thalamus). A complete indexing of AAL3 nodes is available in Table 11. E - Surface representation of the pairs with the highest difference of disconnection between the cases and controls. Each colour represents a pair of nodes. FrontMid, medial frontal gyrus; FrontSMed, medial surface of the superior frontal gyrus; Fus, fusiform gyrus; MidB, midbrain; OccS_Cun, superior occipital gyrus and cuneus; OrbFrontA, anterior orbitofrontal cortex; TempS, superior temporal gyrus; ThVA, thalamic ventral anterior nucleus. FWE, family-wise error; RP, reduplicative paramnesia.

In the analysis of intergroup differences between the different subtypes of reduplicative paramnesia, we found a statistically significant effect in a right frontal region that overlaps the thalamo-frontal circuit (Figure 21A). The individual two-sample analyses showed that the effect was driven by higher probabilities of disconnection of this circuit in patients with place reduplication or with confabulatory mislocation than in patients with chimeric assimilation.

There was no statistically significant difference between reduplicative paramnesia patients with and without prior psychiatric disease.

Table 11. Indexing of the structural disconnection matrix nodes represented in Figure 20. Numbers represent the position of each node in the matrix.

Matrix Position – AAL3 Labelling					
1	Precentral_L	58	Vermis_4_5	115	Occipital_Inf_R
2	Frontal_Sup2_L	59	Vermis_7	116	Fusiform_R
3	Frontal_Mid2_L	60	Vermis_9	117	Postcentral_R
4	Frontal_Inf_Oper_L	61	Thal_AV_L	118	Parietal_Sup_R
5	Frontal_Inf_Tri_L	62	Thal_LP_L	119	Parietal_Inf_R
6	Frontal_Inf_Orb2_L	63	Thal_VA_L	120	SupraMarginal_R
7	Rolandic_Oper_L	64	Thal_VL_L	121	Angular_R
8	Supp_Motor_L	65	Thal_VPL_L	122	Precuneus_R
9	Olfactory_L	66	Thal_IL_L	123	Paracentral_Lb_R
10	Frontal_Sup_Med_L	67	Thal_Re_L	124	Caudate_R
11	Frontal_Med_Orb_L	68	Thal_MDm_L	125	Putamen_R
12	Rectus_L	69	Thal_MDl_L	126	Pallidum_R
13	OFC_Med_L	70	Thal_LGN_L	127	Thalamus_R
14	OFC_Ant_L	71	Thal_MGN_L	128	Heschl_R
15	OFC_Post_L	72	Thal_PuA_L	129	Temporal_Sup_R
16	OFC_Lat_L	73	Thal_PuM_L	130	Temporal_P_Sup_R
17	Insula_L	74	Thal_PuL_L	131	Temporal_Mid_R
18	Cingulate_Ant_L	75	Thal_PuI_L	132	Temporal_P_Mid_R
19	Cingulate_Mid_L	76	ACC_subg_L	133	Temporal_Inf_R
20	Cingulate_Post_L	77	ACC_preg_L	134	Cerebelum_Cr1_R
21	Hippocampus_L	78	ACC_supc_L	135	Cerebelum_Cr2_R
22	ParaHippocampal_L	79	Vent_Str_L	136	Cerebelum_3_R
23	Amygdala_L	80	VTA_L	137	Cerebelum_4_5_R
24	Calcarine_L	81	SN_pc_L	138	Cerebelum_6_R
25	Cuneus_L	82	SN_pr_L	139	Cerebelum_7b_R
26	Lingual_L	83	Red_N_L	140	Cerebelum_8_R
27	Occipital_Sup_L	84	LC_L	141	Cerebelum_9_R
28	Occipital_Mid_L	85	Raphe_Dor	142	Cerebelum_10_R
29	Occipital_Inf_L	86	Raphe_Med	143	Vermis_1_2
30	Fusiform_L	87	Precentral_R	144	Vermis_4_5
31	Postcentral_L	88	Frontal_Sup2_R	145	Vermis_7

32	Parietal_Sup_L	89	Frontal_Mid2_R	146	Vermis_9
33	Parietal_Inf_L	90	Frontal_Inf_Oper_R	147	Thal_AV_R
34	SupraMarginal_L	91	Frontal_Inf_Tri_R	148	Thal_RP_R
35	Angular_L	92	Frontal_Inf_Orb2_R	149	Thal_VA_R
36	Precuneus_L	93	Rolandic_Oper_R	150	Thal_VL_R
37	Paracentral_Lb_L	94	Supp_Motor_R	151	Thal_VPL_R
38	Caudate_L	95	Olfactory_R	152	Thal_IL_R
39	Putamen_L	96	Frontal_Sup_Med_R	153	Thal_Re_R
40	Pallidum_L	97	Frontal_Med_Orb_R	154	Thal_MDm_R
41	Thalamus_L	98	Rectus_R	155	Thal_MDl_R
42	Heschl_L	99	OFC_Med_R	156	Thal_LGN_R
43	Temporal_Sup_L	100	OFC_Ant_R	157	Thal_MGN_R
44	Temporal_P_Sup_L	101	OFC_Post_R	158	Thal_PuA_R
45	Temporal_Mid_L	102	OFC_Lat_R	159	Thal_PuM_R
46	Temporal_P_Mid_L	103	Insula_R	160	Thal_PuL_R
47	Temporal_Inf_L	104	Cingulate_Ant_R	161	Thal_PuI_R
48	Cerebelum_Cr1_L	105	Cingulate_Mid_R	162	ACC_sub_R
49	Cerebelum_Cr2_L	106	Cingulate_Post_R	163	ACC_pre_R
50	Cerebelum_3_L	107	Hippocampus_R	164	ACC_sup_R
51	Cerebelum_4_5_L	108	ParaHippocampal_R	165	Vent_Str_R
52	Cerebelum_6_L	109	Amygdala_R	166	VTA_R
53	Cerebelum_7b_L	110	Calcarine_R	167	SN_pc_R
54	Cerebelum_8_L	111	Cuneus_R	168	SN_pr_R
55	Cerebelum_9_L	112	Lingual_R	169	Red_N_R
56	Cerebelum_10_L	113	Occipital_Sup_R	170	LC_R
57	Vermis_1_2	114	Occipital_Mid_R		

ACC; anterior cingulate cortex; Ant, anterior; AV, anteroventral; Cr, crus; IL, intralaminar; Dor, dorsal; Inf, inferior; L, left; Lat, lateral; Lb, lobule; LC, locus coeruleus; LGN, lateral geniculate nucleus; LP, lateral porterior; MDl, mediodorsal lateral; MDm, mediodorsal medial; Med, medial; MGN, medial geniculate nucleus; Mid, middle; N, nucleus; OFC, orbitofrontal; Orb, orbitalis; Oper, opercular; Orb, orbital; P, pole; pc, pars compacta; Post, posterior; pr, pars reticulata; preg, pregenual; PuA, pulvinar anterior; PuI, pulvinar inferior; PuL, pulvinar lateral; PuM, pulvinar medial; R, right; Re, reuniens; Str, striatum; SN, substantia nigra; subg, subgenual; Sup, superior; supc, supracallosal; Supp, supplementary;

Thal, thalamus; Tri, triangular; VA, ventral anterior; Vent, ventral; VL, ventral lateral; VPL, ventral posterolateral; VTA, ventral tegmental area.

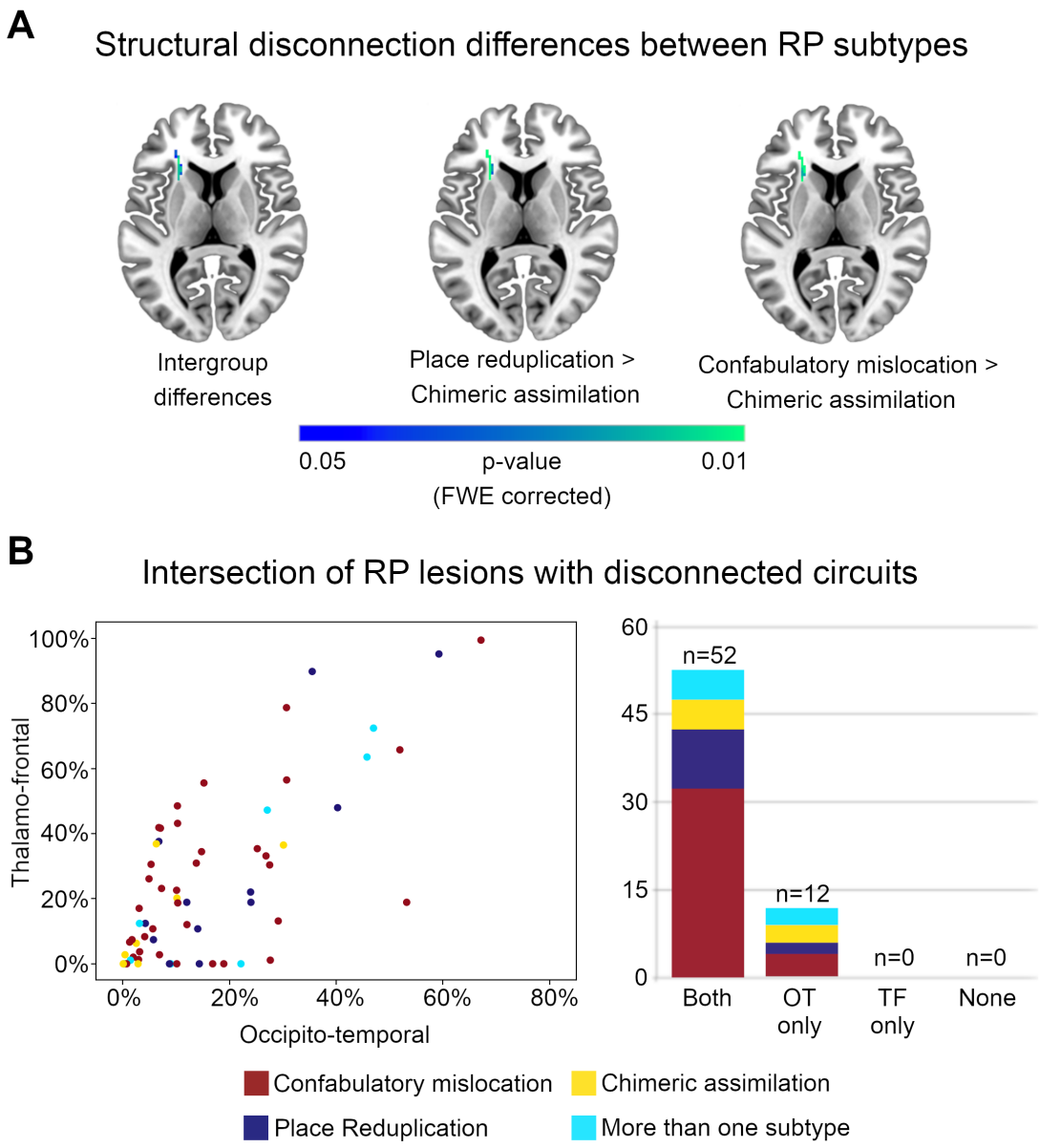

Figure 21. A – Structural disconnection differences between the different subtypes of reduplicative paramnesia; left: inter-group differences; centre: structural disconnection more frequent in place reduplication than in chimeric assimilation; right: structural disconnection more frequent in confabulatory mislocation than in chimeric assimilation. B – Intersection of reduplicative paramnesia lesions with the disconnected circuits of interest; left: percentage of the right occipito-temporal circuit and of the right thalamo-frontal circuit that are intersected by each lesion; right: number of patients in whom the stroke lesion hit both circuits, the right occipito-temporal circuit only, the right thalamo-

frontal circuit only or none of the circuits. OT, occipito-temporal circuit; TF, thalamo-frontal circuit.

Functional disconnection

The statistical comparison of the positive correlation maps, regressing for confounders, revealed one area significantly associated with reduplicative paramnesia that was located in the right precuneus (FWE-corrected p-value<0.05; Figure 22A). There was no significant association when the negative correlation maps were compared.

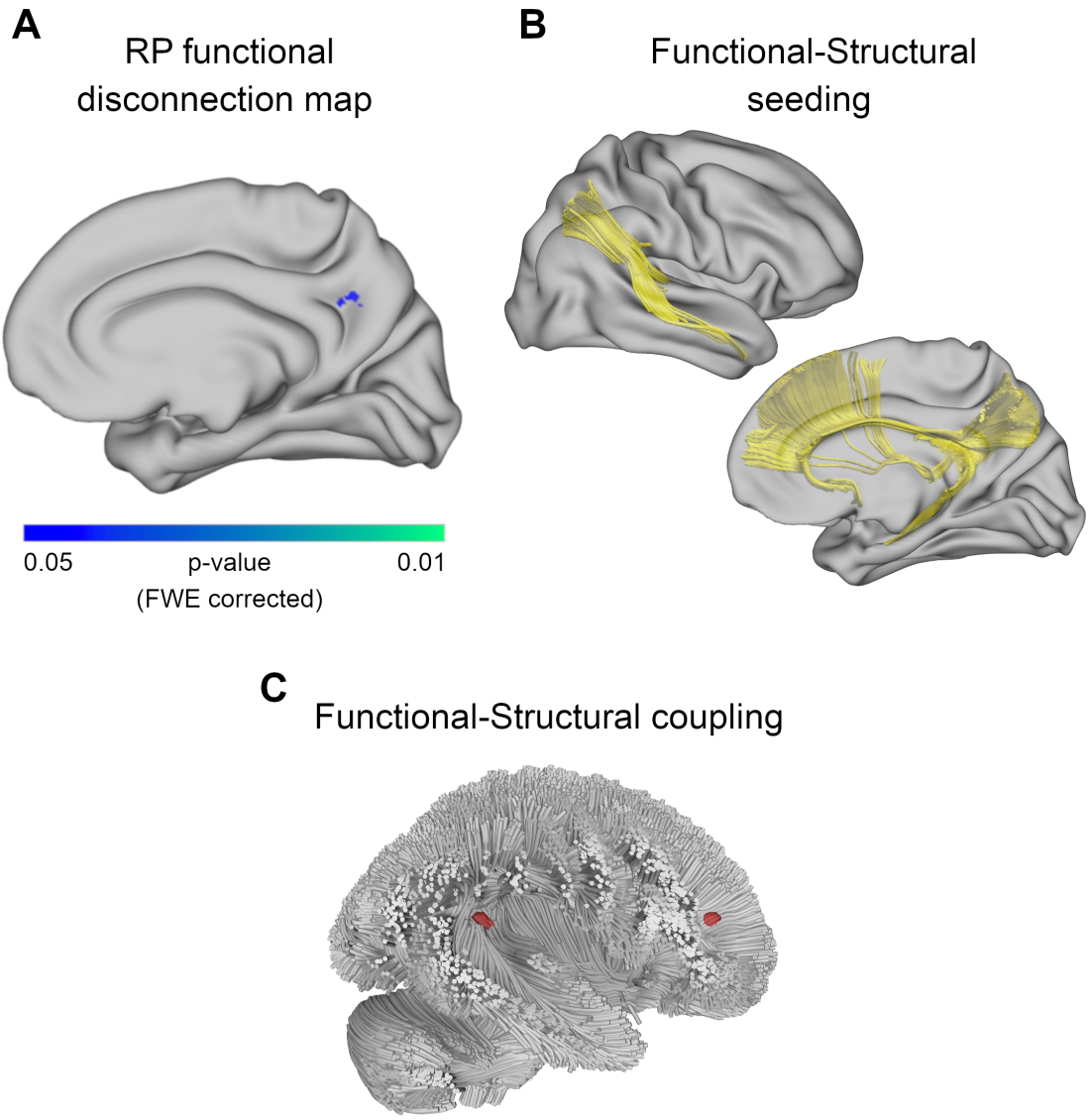

Figure 22. Functional disconnection analysis. A – Statistical map corresponding to the comparison of the positive correlation maps between patients and controls, regressing for

confounders, projected on a cortical surface. The mapped area is significantly associated with reduplicative paramnesia. B – White matter tracts seeding from the significant functional area. C – Areas of intersection (in red) of the structural connectivity map seeded from areas of significant functional disconnection with the map of significant structural disconnection. FWE, family-wise error; RP, reduplicative paramnesia.

White matter tracts seeded from the significant functional area in the right precuneus, included: a) a right lateral temporal bundle (Figure 22B, top) that partially overlapped the temporal region with significant structural disconnection (Figure 22C); and b) a right medial bundle (Figure 22B, bottom), that partially overlapped the frontal region with significant structural disconnection (Figure 22C).

The sensitivity analysis including only patients with a first-ever stroke (n=276; 60 cases, 216 controls) revealed similar results.

The additional analyses applying t-value thresholds of 4.16 and 4.71 showed similar results. The unthresholded analysis did not reveal statistically significant differences between cases and controls.

There was no statistically significant intergroup difference between the three subtypes of reduplicative paramnesia.

Multivariate model

The multivariate model with the best classification performance included the following independent variables: volume of an individual's structural disconnection map intersecting the reduplicative paramnesia structural disconnection map, volume of an individual's lesion intersecting the reduplicative paramnesia lesion spared map, age and anosognosia (Table 12). The total volume of the lesion, the total volume of the individual disconnectome map and the grade of cortical atrophy were not independent predictors of reduplicative paramnesia.

The validation of this model, namely, performing a support vector machine 50-fold nested cross-validation, revealed good discrimination accuracy with a median AUC of 0.80 (interquartile range: 0.75-0.85; Figure 23).

Table 12. Logistic model with the best classification performance

Variable	Odds ratio	95% CI	p-value
Structural disconnection intersecting reduplicative paramnesia structural disconnection map (cm3)	1.26	1.17 - 1.36	<0.01
Lesion intersecting reduplicative paramnesia lesion spared map (cm3)	0.79	0.68 - 0.92	<0.01
Age (years)	1.08	1.05 - 1.12	<0.01
Anosognosia (yes/no)	2.54	1.24 - 5.19	0.01

CI, confidence interval.

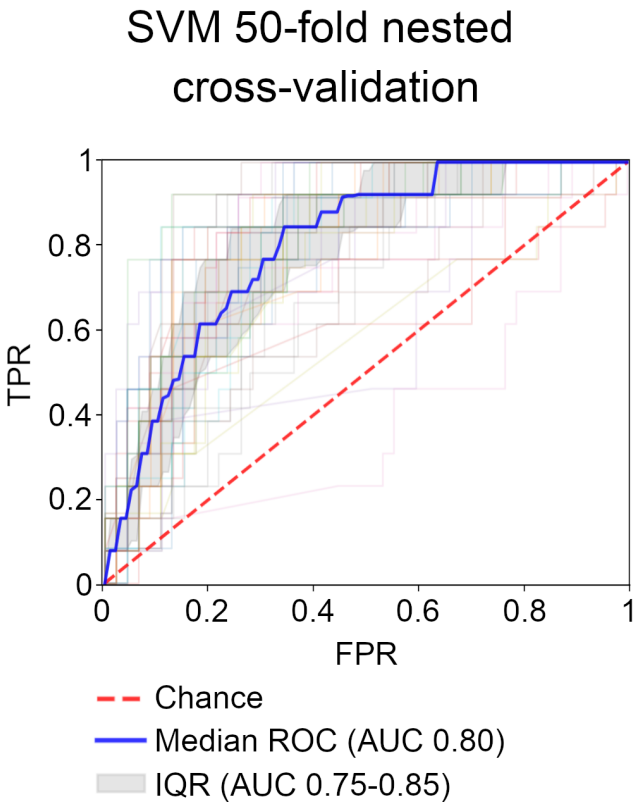

Figure 23. Multivariate model ROC curves from the 50-fold nested support vector machine cross-validation. ROC curves for individual folds are represented by different colours. FPR, false positive ratio; IQR, interquartile range; SVM, support vector machine; TPR, true positive ratio.

The model correctly classified 85% of the patients, presenting a positive predictive value of 70% and a negative predictive value of 87%. The variable with best

discriminability per se was the volume of an individual's structural disconnection map intersecting the reduplicative paramnesia structural disconnection map (AUC = 0.80).

Discussion

In this study, we investigated the anatomical basis of delusional misidentifications of space. We analysed lesion topography and structural and functional connectivity patterns, addressing the pathophysiological hypotheses that had been proposed to date. Three main findings emerged from this research. First, the structural disconnection map was the most important predictor of reduplicative paramnesia and was composed of two main streams, connecting the right anterior thalamus with the right prefrontal cortex and the right occipital cortex with the right temporal cortex. Second, reduplicative paramnesia was associated with functional disconnection with the right precuneus, and a functional-structural link was demonstrated at this level. Finally, we found that the independent predictors of reduplicative paramnesia were structural disconnection of the above-mentioned regions, lesion sparing of the right dorsal fronto-parietal areas, age and anosognosia.

At a neurobehavioural level, delusional misidentifications have been associated with defective binding of a proper emotional value to perceived visual information (Ellis and Young 1990). In reduplicative paramnesia, misidentified spaces are mostly reduplicated or mislocated to emotionally relevant places (Murai et al. 1997). The limbic system is a key circuit for emotional integration, particularly the limbic temporo-amygdala-orbitofrontal division (Catani et al. 2013). It has been shown that visual scenes that are affectively significant induce stronger amygdaline responses (Lim et al. 2009) and that lesions of the right inferior longitudinal fasciculus disturb visual-emotional integration (Bauer 1982; Fischer et al. 2016). The amygdala and the orbitofrontal cortex are densely connected by bidirectional pathways and synergistically regulate the cognitive control of emotions (Ochsner et al. 2012). The anterior nuclei of the thalamus belong to the limbic system (Papez 1937). They seem to modulate amygdala-orbitofrontal activity and participate in emotional-cognitive interactions (Child and Benarroch 2013). The connection of the anterior thalamic nuclei with the limbic regions of the prefrontal cortex is through the anterior thalamic projections that run in the anterior limb of the internal capsule (Catani et al. 2013). This pattern matches the thalamo-frontal stream identified in our study.

Translating these findings to the functional network organization of the brain, we have demonstrated that the anterior thalamus integrates the default mode network (Alves et al. 2019). The default mode network works as a multimodal integrator of domain-specific networks. The disruption of multimodal integration is phenomenologically evident in reduplicative paramnesia. For instance, patients recognize environmental landmarks and know where these landmarks are located but still misjudge their own position in space. Furthermore, they understand the counter-evidence that is shown but still do not update their belief.

The processes of identifying incongruent information and reality monitoring are mediated by the anterior prefrontal cortex (Simons et al. 2017). The anterior prefrontal cortex also has a determinant role in the self-referential processing of external stimuli through the activation of a network composed of the anterior right middle frontal gyrus, the medial superior frontal gyrus and the anterior orbitofrontal cortex (Vinogradov et al. 2006). Early reports identified frontal lesions as an important risk factor for reduplicative paramnesia (Benson et al. 1976), but several cases were described missing this feature (Politis and Loane 2012). Our results revealed that the significant determinant for the emergence of reduplicative paramnesia is the disconnection of distinct areas of the prefrontal cortex, rather than frontal lesion per se.

In addition to right fronto-thalamic disruption, the structural disconnection map associated with reduplicative paramnesia included a right occipito-temporal stream. Ventral visual pathways constitute a core system for visual categorization and mediate the connection of the occipital cortex with medial temporal structures involved in object-context memory, such as the hippocampus (Smith and Bulkin 2014). Furthermore, ventral visual pathways include longer fibres connecting the occipito-temporal cortex with the ventrolateral prefrontal cortex and with the orbitofrontal cortex (Borra et al. 2011). We showed that the occipito-temporal stream associated with reduplicative paramnesia overlaps both the right inferior longitudinal fasciculus and the inferior fronto-occipital fasciculus and that the right fusiform gyrus and the right anterior orbitofrontal cortex were among the pairs of regions with the highest difference in structural disconnection between the cases and controls. This anatomical relationship between posterior and anterior regions has important functional implications since perceptual integration is strictly linked with reality monitoring (Mesulam 2008). Such a relationship has been demonstrated in other delusional disorders, namely in schizophrenia (Fletcher and Frith 2009).

The ventral visual system is also the main mediator of allocentric spatial representations. Hippocampal cells are well known to fire in specific spatial locations (Ekstrom et al. 2003), while the parahippocampal cells are activated by objects that are implicitly or explicitly retrieved in decisive points during navigation (Janzen and Van Turennout 2004). The precuneus interacts with this system and seems to be important for updating the representation of objects in space (Wolbers et al. 2008). Defective allocentric positioning is manifested in patients with reduplicative paramnesia by their inability to properly localize themselves and the place where they are in the environment. Conversely, egocentric references seem to be intact in reduplicative paramnesia. Patients are able to correctly describe routes between different places, including routes starting from the place that they are misinterpreting (Benson et al. 1976). Egocentric spatial references are processed in the dorsal visual stream (Kravitz et al. 2011), and our data showed that lesion sparing of the right dorsal frontal and parietal regions is an independent predictor of reduplicative paramnesia. The right dorsal fronto-parietal network also contributes to the attentional shifts between external stimuli and internal representations, favouring the processing of internally generated mnemonic constructions (Wagner et al. 2005; Lückmann et al. 2014). We hypothesize that injury of this network may preclude the creation of the resilient internal spatial representations that could support the emergence of reduplicative paramnesia.

The pattern of structural disconnection differed between the subtypes of reduplicative paramnesia. We speculate that the stronger association of place reduplication and of confabulatory mislocation with disconnection of the thalamo-frontal stream might be due to higher limbic dysregulation in these subtypes. In place reduplication, there is a notable loss of familiarity for place, since patients typically believe that they are in a replica rather than in the original place (Devinsky 2009). Conversely, in confabulatory mislocation there is a resilient increase of familiarity for place, as patients usually misidentify a strange environment as a familiar one (Devinsky 2009). Chimeric assimilation might be more heavily related with a defective interpretation of allocentric spatial references and with dysfunction of the occipito-temporal stream.

In this imbalance of familiarity regulation, stroke patients tend to be particularly prone to hyperfamiliarity phenomena. The most frequent place of mislocation in our sample was patients' home. In addition, hyperfamiliarity misidentifications in other modalities, namely Fregoli syndrome, were more frequent than hypofamiliar delusions, such as Capgras

syndrome or somatoparaphrenia. The inverse pattern is observed in other diseases, namely in schizophrenia spectrum disorders (Kirov et al. 1994).

In addition to neuroimaging variables, age and anosognosia were independent predictors of reduplicative paramnesia. A systematic review of how ageing affects spatial navigation showed that allocentric strategies are particularly prone to deterioration (Colombo et al. 2017). Ageing may also increase the risk of deficits in neuropsychological domains associated with reduplicative paramnesia, namely, executive dysfunction, visual memory impairment and visuospatial deficits. In anosognosia, patients are resistant to demonstrations of their deficits. This shared behavioural feature with reduplicative paramnesia, as well as a common neuroanatomical limbic dysfunction (Pacella et al. 2019), may justify its predictive significance.

As limitations of our study, brain imaging does not reflect the full extent of brain dysfunction after stroke, and the delimitation of the visible lesion varies according to the modality used (Hillis et al. 2000). In addition, the results obtained in the thresholded functional connectivity analyses were not corroborated in the unthresholded analysis. The presence of large lesions may have affected the performance of lesion network mapping methodology in our sample (Boes 2020). Finally, this study was performed in a tertiary stroke unit and may not be representative of the entire stroke population.

In conclusion, on the basis of a large sample of patients with reduplicative paramnesia, we demonstrated that delusional misidentifications of space occur due to a pattern of disconnection involving fronto-thalamic limbic regions and occipito-temporal ventral visual structures of the right hemisphere. We propose that disruption of this network might explain the abnormal spatial-emotional binding and the defective updating of spatial representations that characterize delusional misidentifications of space.

4. Subcortical anatomy of multimodal integrative networks

4.1. Subcortical anatomy of the default mode network

Part of this section was published in the following article:

- Alves PN, Foulon C, Karolis V, Bzdok S, Margulies DS, Volle E, Thiebaut de Schotten M (2019) An improved neuroanatomical model of the default-mode network reconciles previous neuroimaging and neuropathological findings. Commun Biol 2:370. https://doi.org/10.1038/s42003-019-0611-3

Introduction

For the first time in 1979, David Ingvar used Xenon clearance to investigate resting wakefulness (Ingvar 1979). When aligned by scalp and skull markers, the 11 brains examined indicated an evident increase of the blood flow levels in the frontal lobe interpreted as a surrogate for undirected, spontaneous, conscious mental activity. Later, Positron Emission Tomography (PET) was used to map more systematically task-related activation in the brain, often with resting wakefulness as a control task. The contrast between task-related and resting wakefulness led to the description of deactivation (i.e. active at rest more than during the task) in a set of regions including retrosplenial cortex, inferior parietal cortex, dorsolateral frontal cortex, inferior frontal cortex, left inferior temporal gyrus, medial frontal regions and amygdala (Shulman et al. 1997a; Mazoyer et al. 2001) that quickly bore the name of default mode network (DMN; Raichle et al. 2001). In these studies, skull landmarks or structural MRI were used to align PET images in Talairach stereotaxic or in Montreal Neurological Institute (MNI) templates (Shulman et al. 1997a; Mazoyer et al. 2001). The advent of functional Magnetic Resonance Imaging, particularly of methods for analysing functional connectivity, led to the allocation of new structures to this network, such as the hippocampal formation (Greicius et al. 2004; Vincent et al. 2006; Buckner et al. 2008).

Today, the DMN has largely been a cortically-defined set of network nodes. Consisting of distinct regions/nodes distributed across the ventromedial and lateral prefrontal, posteromedial and inferior parietal, as well as lateral and medial temporal cortex, the DMN is considered a backbone of cortical integration (Andrews-Hanna et al. 2010; Margulies et al. 2016; Kernbach et al. 2018; Lopez-Persem et al. 2018). Its subcortical components are, however, less well characterized. Studies of whole-brain network organization reveal subregions of the cerebellum (Stoodley and Schmahmann 2009; Buckner et al. 2011) and striatum (Choi et al. 2012) that are functionally connected with the cortical regions of the DMN. Seed-based functional connectivity studies further demonstrate additional DMN-specific connectivity to several subcortical structures, including the amygdala (Roy et al. 2009; Bzdok et al. 2012) and striatum (Di Martino et al. 2008). The thalamus has also been shown to be structurally and functionally connected to DMN regions (Fransson 2005; Cunningham et al. 2016). These studies are important, as a cleaner characterization of the anatomy of the DMN is an essential step towards understanding its functional role and its involvement in brain diseases. Particularly, an increased activity characterises the regions that compose DMN during tasks involving autobiographical, episodic and semantic

memory, mind wandering, perspective-taking or future thinking (Shapira-Lichter et al., 2013; Shulman et al., 1997b; Bendetowicz et al. 2018). Conversely, DMN regions show a decreased neural activity during attention-demanding and externally-oriented tasks (Shulman et al. 1997b; Spreng et al. 2009). Finally, altered connectivity in the DMN has been observed in a large variety of brain diseases, including Alzheimer's disease, Parkinson's disease, schizophrenia, depression, temporal lobe epilepsy, attention deficit and hyperactivity disorder, drug addiction, among others (Broyd et al. 2009; Tessitore et al. 2012; Voets et al. 2012; Whitfield-Gabrieli and Ford 2012; Geng et al. 2017; Zhu et al. 2017). Hence, while prior research provides first hints towards a broader definition of the DMN system, further research is necessary to articulate the anatomical extent of specific subcortical contributions, and to understand the independent contribution of these structures in DMN function and pathologies.

Yet, since the DMN has repeatedly been characterized as a cohesive functional network (Buckner et al. 2008), an average of brain images relying exclusively on anatomical references and landmarks may be suboptimal (Brett et al. 2002; Thiebaut de Schotten and Shallice 2017) whether the method employed is a surface-based or volume-based registration (Brett et al. 2002; Despotovic et al. 2015). Small structures of the brain may be particularly susceptible to this misalignment, especially when MRI lacks contrast. Besides morphology, cytoarchitecture and function are poorly overlapping, especially in the DMN (Bzdok et al. 2015; Eickhoff et al. 2016). Consequently, functional areas present in every subject may not overlap after averaging all structurally aligned brain images in a group analysis (Brett et al. 2002; Braga and Buckner 2017). This biological misalignment can be particularly problematic for revealing significant small regions of the DMN (Figure 24A and B). A better alignment is also essential for the subcortical structures of the brain as their variability is still considerable (Amunts et al. 1999, 2005; Zaborszky et al. 2008; Croxson et al. 2017). Specifically, cytoarchitectonic studies have shown that only one-quarter of the volume of cholinergic nuclei overlaps in at least half of the individuals studied (Zaborszky et al. 2008). Similarly, structures such as mammillary bodies, nucleus basalis of Meynert, or anterior thalamic nuclei, can vary in size, morphology and locations, and are particularly prone to misalignment with the current methods of structural registration (Tagliamonte et al. 2013; Despotovic et al. 2015; Liu et al. 2015; Möttönen et al. 2015). Functional alignment methods have already been used to overcome the high interindividual variability of the morphology of some areas of heteromodal association

cortex and led to a more accurate mapping of resting-state functional connectivity (Mueller et al. 2013; Robinson et al. 2014; Langs et al. 2015). They also have led to better predictions of task activation patterns in group-analysis when compared to morphological alignment methods and have recently enabled much improved models of cortical parcellation (Langs et al. 2015; Glasser et al. 2016).

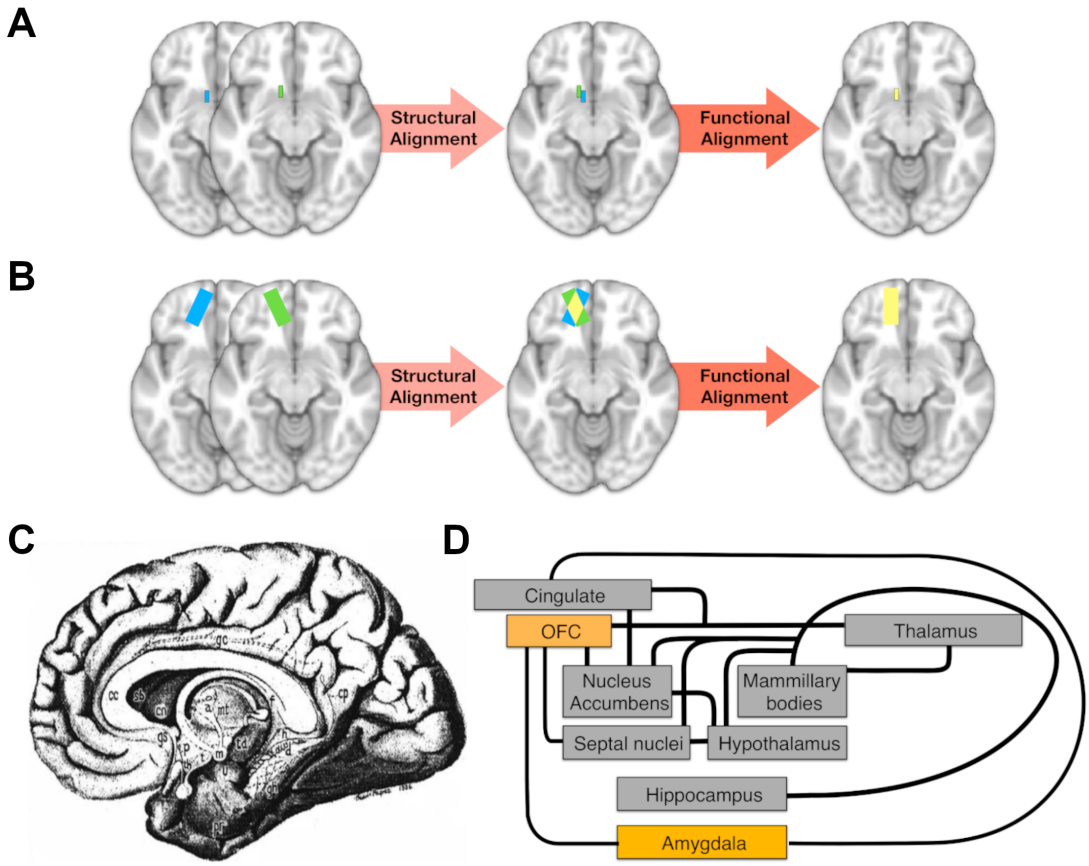

Figure 24. Illustration of intersubject alignment of brain images and of the unitary model of the limbic system. Blue and green rectangles represent the same functional area in two subjects, while yellow rectangles illustrate the overlap of the two individual areas after alignment. With structural alignment, there can be a complete misalignment of small functional areas (A) or partial misalignment of large functional areas (B) due to functional-anatomical variability or poor anatomical contrasts in MRI imaging. If an additional step of functional alignment is performed, an optimized overlap of functional areas is obtained. C - The limbic system (left panel) as originally depicted by Papez (1937) and (right panel) diagram of the unitary model of the limbic system (MacLean 1949, 1952; Haber et al. 1990, 1995; Kunishio and Haber 1994; Aggleton 2008; Catani et al. 2013).

To address several of these challenges that may impede proper group analysis if relying exclusively on MRI structural landmarks, we propose to revisit the anatomical scaffold of the DMN using a coregistration based on functional alignment. We hypothesised that using a functional alignment will reveal structures of basal forebrain and the Papez's circuits, namely anterior and mediodorsal thalamic nuclei and mammillary bodies, as constituent nodes of the DMN for several reasons. First, all these regions are highly interconnected which suggest they belong to the same functional system (Yakovlev 1948; Yakovlev and Locke 1961). Second, the current conceptualization of DMN anatomy resembles the unitary model of the limbic system (Figure 24C) which, through the coordination of its subregions, subserves the elaboration of emotion, memories and behaviour (Papez 1937; MacLean 1949, 1952; Catani et al. 2013). Third, the basal forebrain comprises a group of neurochemically diverse nuclei, involved in dopaminergic, cholinergic and serotoninergic pathways, that are crucial in the pathophysiology of the aforementioned diseases that affect the DMN connectivity. Finally, recent electrophysiological evidence has shown that in rats the basal forebrain exhibits the same pattern of gamma oscillations than DMN and that it influences the activity of anterior cingulate cortex (Nair et al. 2018).

Therefore, in this study, we used a functional alignment of resting state fMRI-based individual DMN maps to build a more comprehensive DMN model that includes the contribution of subcortical structures. To provide a complete window into the anatomy of the DMN, we explored the structural connectivity of our new model of the DMN using tractography imaging techniques and revealed that the thalamus and basal forebrain had high importance in term of values of node degree and centrality for the DMN.

Methods

Subjects and MRI acquisition

MRI images of subjects without neurological or psychiatric disease were obtained (age mean±SD 29±6 years, range 22-42 years; 11 female, 9 male) with a Siemens 3 Tesla Prisma system equipped with a 64-channel head coil.

An axial 3D T1-weighted imaging dataset covering the whole head was acquired for each participant (286 slices, voxel resolution=0.7mm^3, echo time=2.17ms, repetition time=2400ms, flip angle=9°).

Resting state functional MRI images were obtained using T2*-weighted echo-planar imaging (EPI) with blood oxygenation level-dependent (BOLD) contrast. EPIs (repetition

time/echo time=2050/25ms) comprised 42 axial slices acquired with a multiband pulse (Feinberg et al. 2010; Moeller et al. 2010; Setsompop et al. 2012; Xu et al. 2013) covering the entire cerebrum (voxel size=3mm^3) including 290 brain scan volumes in one run of 10 minutes.

A diffusion-weighted imaging acquisition sequence, fully optimised for tractography, provided isotropic (1.7×1.7×1.7mm) resolution and coverage of the whole head with a posterior-anterior phase of acquisition, with an echo time of 75ms. A repetition time equivalent to 3500ms was used. At each slice location, six images were acquired with no diffusion gradient applied (b-value of 0 s/mm^2). Additionally, 60 diffusion-weighted images were acquired, in which gradient directions were uniformly distributed on the hemisphere with electrostatic repulsion. The diffusion weighting was equal to a b-value of 2000 s/mm^2. This sequence was fully repeated with reversed phase-encode blips. This provides us with two datasets with distortions going in opposite directions. From these pairs, the susceptibility-induced off-resonance field was estimated using a method similar to that described in Andersson et al. (2003) and corrected on the whole diffusion-weighted dataset using the tool TOPUP and EDDY as implemented in FSL (Smith et al. 2004).

Resting-state functional MRI analysis - overview

Resting state functional MRI images were corrected for artefacts in Funcon-Preprocessing tool of the Brain Connectivity and Behaviour toolkit (http://toolkit.bcblab.com; Foulon et al., 2018; Jenkinson et al., 2002; Woolrich et al., 2009). Then, they were registered to T1 high resolution individual structural images and normalized to MNI152 standard space using Advanced Normalization Tools (ANTs; http://stnava.github.io/ANTs; Avants and Gee, 2004; Avants et al., 2010). Preprocessing steps in detail:

a) fMRI images were first motion corrected using *mcflirt* (Jenkinson et al. 2002), then corrected for slice timing, smoothed with a full half width maximum equal to 1.5 times the largest voxel dimension and finally filtered for low temporal frequencies using a gaussian-weighted local fit to a straight line. These steps are available in *feat*, as part of FSL package (Woolrich et al. 2009).

b) fMRI images were linearly registered to the T1 images, and subsequently to the MNI152 template (2mm) using affine and diffeomorphic transformations (Klein et al.

2009; Avants et al. 2011). Confounding signals were discarded from fMRI by regressing out a confound matrix from the functional data. The confound matrix included the estimated motion parameters obtained from the previously performed motion correction, the first eigenvariate of the white matter and cerebrospinal fluid, as well as their first derivative. Eigenvariates were extracted using *fslmeants* combined with the --eig option. White matter and cerebrospinal fluid eigenvariates were extracted using masks based on the T1 derived 3-classes segmentation thresholded to a probability value of 0.9, registered to the resting state fMRI images and binarised. Finally, the first derivative of the motion parameters, white matter and cerebrospinal fluid signal was calculated by linear convolution between their time course and a [-1 0 1] vector.

c) Since the resting state fMRI signal can be heavily affected by motion, even following motion correction between temporally adjacent volumes (van Dijk et al. 2012), we estimated the signal fluctuation associated with motion and regressed it out from the fMRI. To this aim, we employed a recently developed and validated procedure based on data-driven Independent Component Analysis, termed ICA-Aroma (Pruim et al. 2015). This method performs an Independent Component Analysis decomposition of the data and estimates which components reflect motion-related noise in the fMRI signal on the basis of a robust set of spatial and temporal features. This is made possible due the distinctiveness of the motion-related components isolated by Independent Component Analysis on the fMRI signal (Salimi-khorshidi et al. 2014). This approach outperforms other methods such as the regression of the motion parameter estimates, while limiting in the same time the loss in degrees of freedom (Pruim et al. 2015). Compared to spike removal methods such as scrubbing (Power et al. 2012), ICA-Aroma has the advantage of preserving the temporal structure of the fMRI signal.

Individual DMN maps in the structural space

Individual subject-tailored/fitted DMN maps were obtained by correlation with seed regions of interest of a functional parcellated brain template. The regions used for the seed-based functional connectivity analysis were those defined as DMN regions in the resting-state parcellation map by Gordon and collaborators (Gordon et al. 2016; Shine et al. 2016; Tomasi and Volkow 2018). Gordon and collaborators created these parcellations according to abrupt changes in resting state's time course profile, each parcel having a homogenous time course profile. This general-purpose atlas provides a total of 40 DMN nodes (20 in

each hemisphere). The DMN nodes as defined by Gordon et al. are displayed in Figure 25 and Table 13.

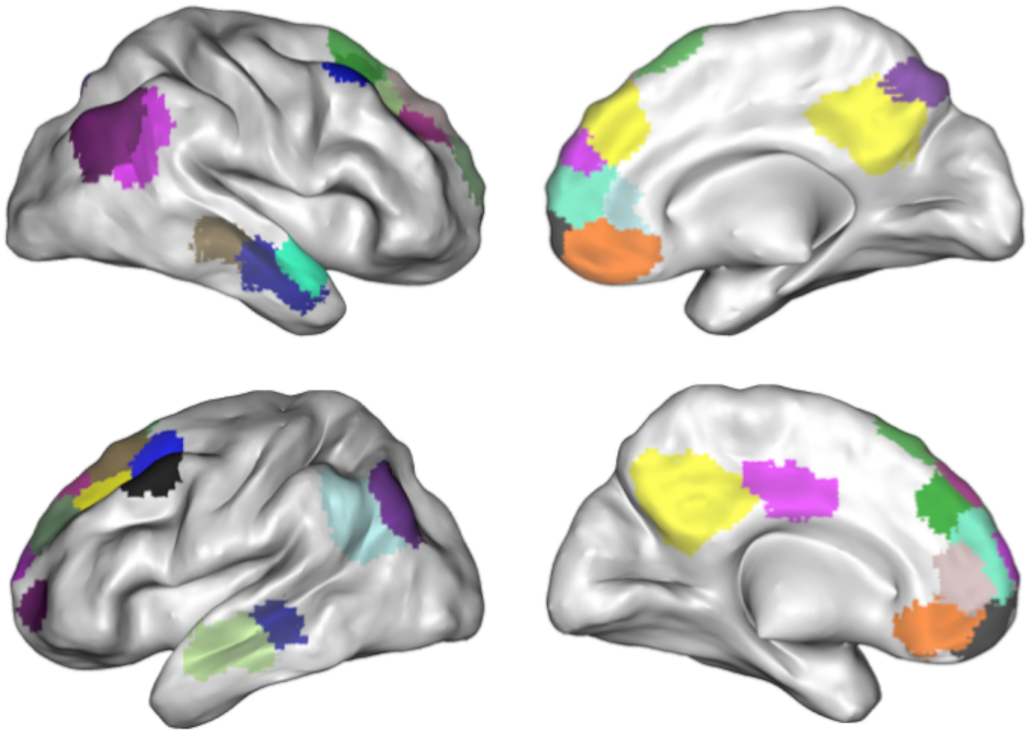

Figure 25. DMN nodes according to the functional parcellated cortical template of Gordon et al (2016), represented on an inflated cortical surface. Right hemisphere is represented in the upper images and the left hemisphere in the bottom.

These 40 regions were used as seeds. The correlation map for each seed was obtained using the Funcon-Connectivity tool of the Brain Connectivity and Behaviour toolkit (http://toolkit.bcblab.com; Foulon et al., 2018). This tool calculates the Pearson's correlation between the mean resting state fMRI time-course of the seed with the rest of the brain to generate the functional connectivity map for every seed (Foulon et al. 2018).

The DMN map of each participant was obtained by calculating the median of the 40 seed-based correlation maps of each individual using FSL (Jenkinson et al. 2012). We then calculated the median across the DMN maps of the 20 participants to obtain the median DMN map in the MNI152 space. The median was used, instead of the mean, because it is less sensitive to outliers, being a better centrality measure for small sample sizes (Kenney 1939).

Table 13. MNI coordinates of the centres of gravity and volume of DMN cortical nodes. These nodes, defined by Gordon and collaborators, were used as seeds for building correlation maps.

Left hemisphere				
DMN seed	**MNI (X)**	**MNI (Y)**	**MNI (Z)**	**Volume (mm^3)**
Seed 1	-7	-50	34	4152
Seed 2	-12	28	57	1368
Seed 3	-48	-58	32	3240
Seed 4	-5	43	35	1312
Seed 5	-3	-15	38	1336
Seed 6	-20	29	47	1360
Seed 7	-40	-74	37	2048
Seed 8	-28	55	-1	568
Seed 9	-6	58	-9	2000
Seed 10	-7	37	-9	1008
Seed 11	-60	-28	-9	1248
Seed 12	-56	-11	-16	2488
Seed 13	-13	48	40	1384
Seed 14	-20	53	27	1088
Seed 15	-7	55	19	1936
Seed 16	-14	64	15	904
Seed 17	-7	44	7	864
Seed 18	-27	28	39	832
Seed 19	-29	15	52	896
Seed 20	-39	15	49	1192
Right hemisphere				
DMN seed	**MNI (X)**	**MNI (Y)**	**MNI (Z)**	**Volume (mm^3)**
Seed 21	8	-50	34	4096
Seed 22	12	23	60	1472
Seed 23	8	41	4	1136
Seed 24	23	21	50	968
Seed 25	52	-53	28	1736
Seed 26	61	-26	-6	896

Seed 27	9	-68	50	752
Seed 28	45	-67	35	2776
Seed 29	8	63	-5	1800
Seed 30	6	44	-13	2104
Seed 31	58	-8	-17	1896
Seed 32	22	33	41	720
Seed 33	21	45	35	560
Seed 34	14	62	19	1128
Seed 35	9	54	13	1232
Seed 36	7	54	30	824
Seed 37	13	45	45	1160
Seed 38	7	41	37	992
Seed 39	31	19	49	840
Seed 40	53	1	-15	952

Individual DMN maps in the "functional space"

To achieve the proposed optimized map of the DMN, the same twenty individual maps were functionally aligned with each other in a new "functional space".

Individual DMN maps (obtained in the previous section) were aligned with each other using ANTs' script *buildtemplateparallel.sh*, defining cross-correlation as the similarity measure and greedy SyN as the transformation model (Avants et al. 2008, 2011; Klein et al. 2009). This approach consists in an iterative (n=4) diffeomorphic transformation to a common space. The group map was obtained by calculating the median of all DMN maps after functional alignment.

The resulting maps correspond to alignment of the 20 individual DMN maps in a "functional space".

Functional connectivity comparison of the two DMN

We applied a 0.3 threshold on the functional connectivity strength for both the functional and structural-based DMN maps. This value was chosen because it corresponds to a medium effect size (Cohen 1992). Time-series of resting state fMRI of each individual

in the different regions of interest identified in the DMN maps were extracted and the mean value of the voxels of each region was obtained, using the command *fslstats* (with the options –k and –M) (Jenkinson et al. 2012). Cortical regions of interest were defined according to the previous anatomical models of the DMN (Buckner et al. 2008; Andrews-Hanna et al. 2010). Subcortical regions of interest were defined manually based on the experienced judgment of the neuroanatomists among the authors combined with the careful comparison with previously published atlases (Nieuwenhuys et al. 2008; Catani and Thiebaut de Schotten 2012). Correlation and partial correlation coefficients were determined as measures of functional connectivity.

Two matrices, representing the median correlation values in the MNI152 space and in the functional space, were created using BrainNet Viewer (Xia et al. 2013). A paired t-test was calculated for each cell of the two connectivity matrices using Python's Scipy package, version 0.19.1 (https://www.scipy.org/; *scipy.stats.ttest_rel*). A p-value corrected for multiple comparisons at a threshold of <0.0001 (Bonferroni correction) was used. Circos software was used to illustrate functional connections in the functional space (http://circos.ca/; Krzywinski, 2009).

Anatomical validation in thalamic, basal forebrain and mesencephalic areas

Meynert nuclei, medial septal nuclei and diagonal band of Broca probabilistic maps were derived from the work of Zaborszky and colleagues, the Harvard-Oxford probabilistic atlas was employed for nucleus accumbens, Talairach atlas registered to the MNI152 space for mammillary bodies and thalamic nuclei, and Harvard Ascending Arousal Network Atlas for ventral tegmental area (Talairach and Tournoux 1988; Desikan et al. 2006; Lancaster et al. 2007; Zaborszky et al. 2008; Edlow et al. 2012). A percentage of volume overlap between the DMN map and each nucleus of interest was subsequently calculated for each subject. The same threshold of a Pearson's correlation of 0.3 was applied for this analysis, as specified in the previous section.

Tractography analysis

Diffusion Weighted Images were corrected for signal drift (Vos et al. 2017), motion and eddy current artefacts using ExploreDTI (http://www.exploredti.com; Leemans et al., 2009).

Whole-brain tractography was performed on the software StarTrack using a deterministic approach (https://www.mr-startrack.com). A damped Richardson-Lucy algorithm was applied for spherical deconvolutions (Dell'Acqua et al. 2010). A fixed fibre response corresponding to a shape factor of α=1.5x10-3 mm^2/s was adopted. The defined number of iterations was 150 and the geometric damping parameter was 8. The absolute threshold was defined as 3 times the spherical fibre orientation distribution of a grey matter isotropic voxel and the relative threshold as 8% of the maximum amplitude of the fibre orientation distribution (Thiebaut de Schotten et al. 2014). A modified Euler algorithm was used (Dell'Acqua et al. 2013). An angle threshold of 35°, a step size of 0.85mm, and a minimum length of 20mm were chosen.

Diffusion tensor images were registered to the MNI152 standard space and, then, into the "functional space" applying the affine and diffeomorphic deformation generated in the previous sections, using the tool *tractmath* as part of the software package Tract Querier (Wassermann et al. 2016).

The same regions of interest used for functional connectivity calculation were also used for the tractography analysis.

The command *tckedit* of MRtrix toolbox (http://www.mrtrix.org/; Tournier et al., 2012) was used to extract the tracts of interest. The –include arguments were composed by combinations of DMN regions of interest to guarantee that the selected streamlines crossed at least two DMN regions of interest.

In order to have a group-representative map for each tract, individual tracts were converted into maps using *tckmap* command of MRtrix toolbox (http://www.mrtrix.org/; Calamante et al., 2010). Each voxel was binarised in 1 or 0 according to being or not being intersected by a streamline (Thiebaut de Schotten et al. 2011b). Lastly, a one sample t-test was calculated using FSL *randomise*, with variance smoothing of 4mm (Thiebaut de Schotten et al. 2011b). The resulting group-representative tract maps using this method were shown to have a good anatomical correspondence with histological atlas of white matter tracts (Bürgel et al. 2006; Thiebaut de Schotten et al. 2011b). BrainVisa was used to create the corresponding illustration of the tracts that reached significance (Rivière et al. 2011).

Graph theory analysis of structural connectivity

To explore whether the new putative regions of the DMN are essential structures and potential areas of vulnerability in the network, we investigated the hub properties of the network nodes using graph theory measures, namely node degree and betweenness centrality (Bullmore and Sporns 2009). Node degree refers to the number of connections between a given node and the other nodes of the network. Betweenness centrality is the fraction of all shortest paths in the network that pass through a given node (Bullmore and Sporns 2009).

For each participant, an anatomical connectome matrix of the DMN was built using the *tck2connectome* command of MRtrix (http://www.mrtrix.org/; Tournier et al., 2012). Each region of interest was defined as a node. Only the streamlines that ended in both regions of interest were considered (Gong et al. 2009; Shu et al. 2011). The matrices were binarised depending on the existence or absence of streamlines connecting two regions of interest (Gong et al. 2009; Shu et al. 2011). The defined threshold for the binarisation was 1 because the number of streamlines does not reflect the connectivity strength or the true number of axonal projections between two brain regions (Gong et al. 2009; Jones et al. 2013), and previous evidence has shown that changing the streamline count threshold for binarisation (between 1 and 5) does not change the overall results of the network analysis. Brain Connectivity Toolbox for Python (https://pypi.python.org/pypi/bctpy) was used to obtain the network measures. The functions *degrees_und* and *betweenness_bin* were run, respectively, for each individual matrix (Rubinov and Sporns 2010). The median values for each measure were obtained. The illustration of the network was made using Surf Ice (https://www.nitrc.org/projects/surfice/)

Results

Anatomical comparison between the two alignment methods

DMN connectivity maps obtained from structural and functional alignments are displayed in Figure 26A-C. In both maps, classical areas of the DMN were observed, namely: posterior cingulate cortex and retrosplenial cortex; ventromedial, anteromedial, and dorsal prefrontal cortex; temporal pole; middle temporal gyrus; hippocampus and parahippocampal cortex; amygdala; and the posterior parietal cortex.

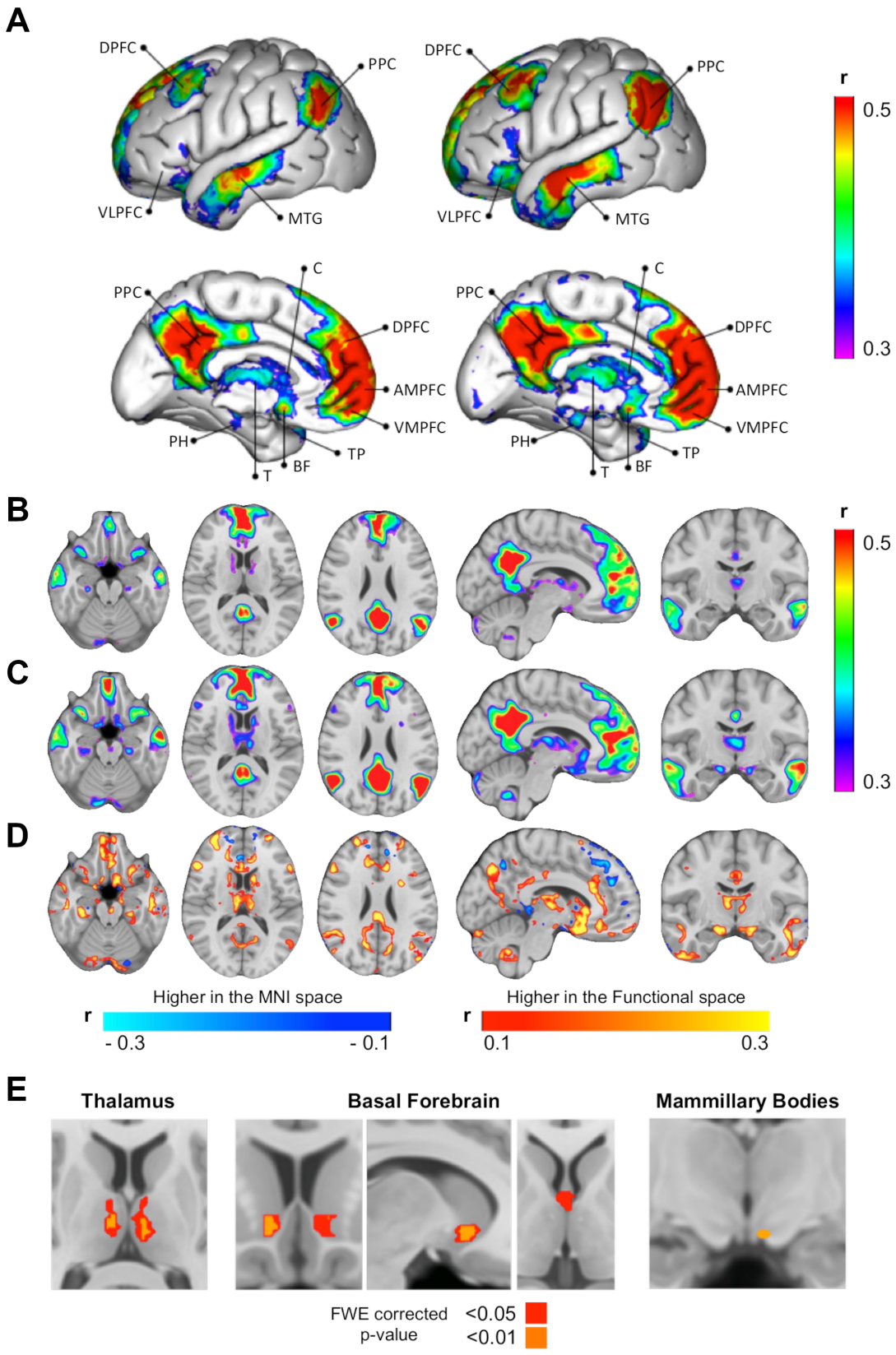

Figure 26. Maps of the DMN structurally or functionally aligned. A - 3D view of the two DMN left panel corresponds to the structural space alignment, right panel to the functional space alignment. B - brain sections of the structurally aligned DMN. C - brain sections of

the functionally aligned DMN. D - subtraction of the structurally and the functionally aligned DMN maps. E - statistical comparison (paired t-test) between the two methods of alignment (structurally and functionally aligned DMN) in the three hypothesized regions, with colours indicating statistically significant differences at two levels of significance: <0.05 and <0.01, family-wise error (FWE) corrected p-values (higher in the functional space). DPFC, Dorsal Prefrontal Cortex; PPC, Posterior Parietal Cortex; VLPFC, Ventro-Lateral Prefrontal Cortex; MTG, Middle Temporal Gyrus; PCC, Posterior Cingulate Cortex; C, Caudate; DPFC, Dorsal Prefrontal Cortex; AMPFC, Antero-Median Prefrontal Cortex; VMPFC, Ventro-Median Prefrontal Cortex; TP, Temporal Pole; BF, Basal Forebrain; T, Thalamus; PH, Parahippocampal.

Figure 26D illustrates the simple voxel-based subtraction between the DMN connectivity maps obtained from structural and functional alignments. Higher average connectivity was achieved in the functionally aligned DMN map in large areas, such as medial prefrontal cortex and posterior cingulate cortex, mostly in the border zones. In fact, the highest differences in connectivity between structural and functional aligned DMN were at the level of the basal forebrain and thalamus. These areas were poorly or even not represented with alignment in the MNI152 space, but were visible after the functional alignment. DMN connectivity was also visible in the medial mesencephalic region, as well in inferior regions in the caudate nuclei, ventrolateral prefrontal cortex, cerebellar tonsils and cerebellar hemispheres. As expected, a significant difference was found between the two maps bilaterally in the thalamus and in the basal forebrain, and in a peripheral zone of the left mammillary body (Figure 26E, Table14).

Unthresholded statistical maps of the comparison between the two methods of alignment - structurally and functionally aligned DMN - are available at neurovault.org (https://neurovault.org/collections/OCAMCQFK/).

Table 14. Clusters of the statistical maps obtained when comparing the two methods of alignment. Coordinates represent the centre of gravity and 'p-value' of the lowest value found in the cluster.

Cluster index	Voxels	p-value	MNI (X)	MNI (Y)	MNI (Z)
Basal forebrain - Right nucleus accumbens	43	0.001	9	13	-7
Basal forebrain - Left nucleus accumbens	21	0.007	-9	16	-6
Basal forebrain - Medial septal nuclei	38	0.007	0	-1	1
Limbic thalamus - Right	72	0.001	8	-12	9
Limbic thalamus - Left	146	<0.001	-7	-14	8
Mammillary bodies - Left	3	0.001	-5	-11	-14

Functional connectivity of the DMN in the functional space

Twenty-four regions of interest were defined based on the DMN we obtained in the functional space and concordant with the previous anatomical models of the DMN (Buckner et al. 2008; Andrews-Hanna et al. 2010). Nine additional regions were defined as being solely revealed after the functional alignment. These regions included the left and right thalamus, the left and right basal forebrain, the midbrain, the left and right ventral lateral prefrontal cortex and the left and right caudate nucleus (inferior regions of the nuclei), resulting in a total of 33 regions of interest. The association strength determined by Pearson's correlation between the resting state fMRI time-series of the regions of interest (i.e. functional connectivity) were higher with alignment in the functional space, compared with structural space, in all pairs of regions (Figure 27A).

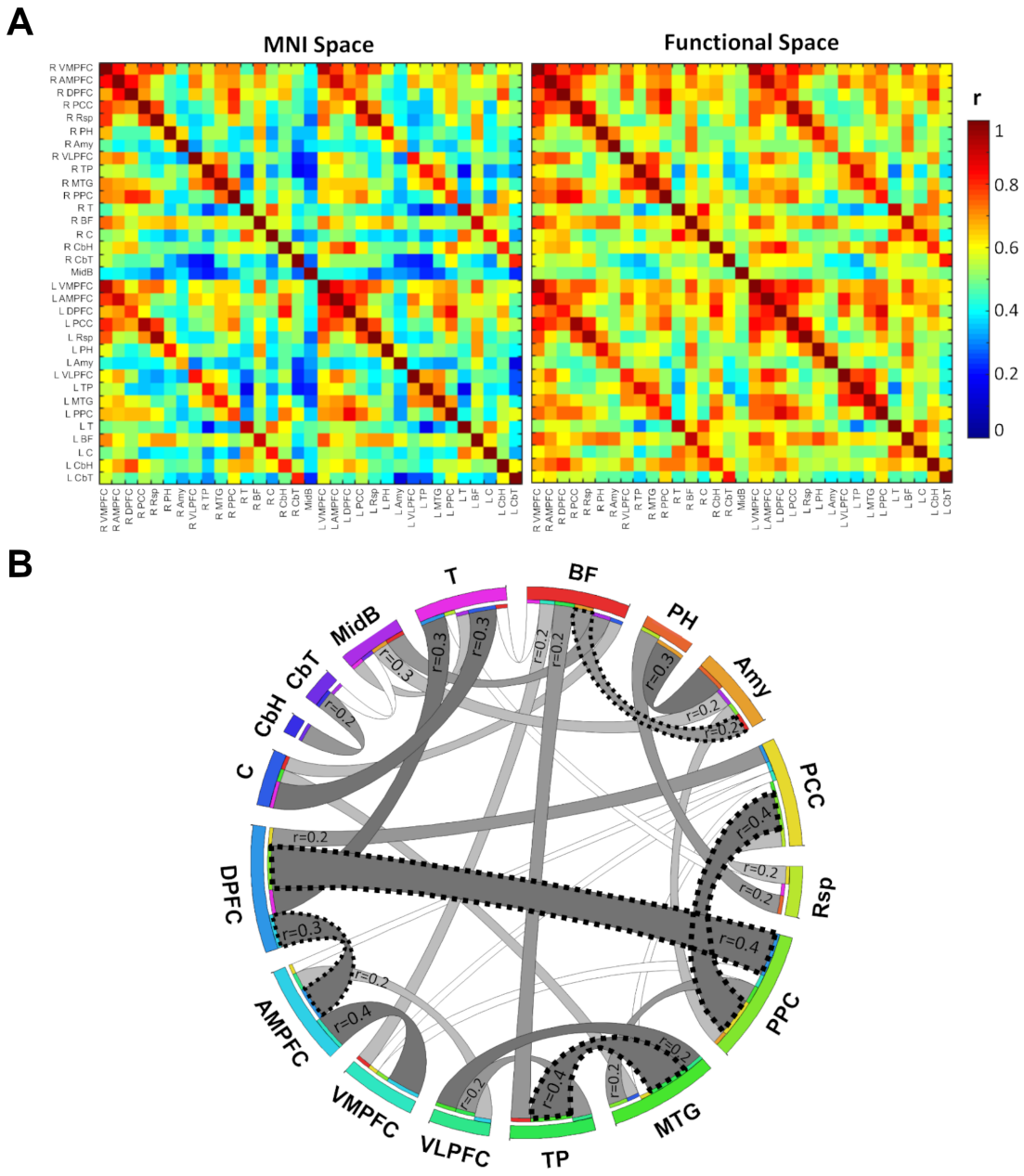

Figure 27. Functional connectivity. A - Matrices of the Pearson's correlations between resting state fMRI time series of the regions of interest in the structural and in the functional space. B - Graph representation of the partial correlations between regions of interest in the functional space (connections with partial correlation above 0.2 are depicted; darker grey tones represent stronger connections). Statistically significant partial correlations have a dashed borderline (one-sample t test; $p<0.0001$, which corresponds to the Bonferroni corrected level of significance). The left side structures are not represented, for a clearer visualisation. DPFC dorsal prefrontal cortex, PPC posterior parietal cortex, VLPFC ventrolateral prefrontal cortex, Rsp retrosplenial cortex, MTG middle temporal gyrus, PCC posterior cingulate cortex, C caudate, DPFC dorsal prefrontal cortex, AMPFC

antero-median prefrontal cortex, VMPFC ventro-median prefrontal cortex, TP temporal pole, BF basal forebrain, T thalamus, PH parahippocampal region, CbH cerebellar hemisphere, CbT cerebellar tonsil, Amy amygdala, MidB midbrain. n =20 participants.

The difference was statistically significant in 18% of pairs after Bonferroni correction for multiple comparisons (p-value<0.0001). Table 15 represents the MNI coordinates of the centres of gravity of all the regions of interest in the DMN map.

Table 15. Regions of interest. MNI coordinates represent the centre of gravity of each region.

Region of interest	**Voxels**	**MNI (X)**	**MNI (Y)**	**MNI (Z)**
Left Ventro-Medial Prefrontal Cortex	2267	-11	55	-5
Right Ventro-Medial Prefrontal Cortex	2673	11	53	-6
Left Antero-Medial Prefrontal Cortex	2243	-10	50	20
Right Antero-Medial Prefrontal Cortex	2144	10	50	19
Left Dorsal Prefrontal Cortex	3818	-20	31	46
Right Dorsal Prefrontal Cortex	3084	23	32	46
Left Posterior Cingulate Cortex	2484	-5	-50	35
Right Posterior Cingulate Cortex	2224	7	-51	34
Left Retrosplenial Cortex	845	-6	-55	12
Right Retrosplenial Cortex	638	6	-54	13
Left Posterior Parietal Cortex	2448	-46	-64	33
Right Posterior Parietal Cortex	1733	50	-59	34
Left Middle Temporal Gyrus	2406	-58	-21	-15
Right Middle Temporal Gyrus	2170	59	-17	-18
Left Temporal Pole	348	-38	17	-34
Right Temporal Pole	318	43	15	-35
Left Ventro-Lateral Cortex	706	-36	23	-16
Right Ventro-Lateral Cortex	487	37	25	-16
Left Parahippocampal Region	355	-24	-30	-16
Right Parahippocampal Region	287	26	-26	-18
Left Amygdala	66	-15	-9	-18
Right Amygdala	58	17	-8	-16

Left Caudate	303	-11	12	7
Right Caudate	266	13	11	9
Left Cerebellar Hemisphere	906	-26	-82	-33
Right Cerebellar Hemisphere	1500	29	-79	-34
Left Cerebellar Tonsil	184	-6	-57	-45
Right Cerebellar Tonsil	278	8	-53	-48
Left Thalamus	382	-7	-14	8
Right Thalamus	305	7	-11	8
Left Basal Forebrain	456	-7	12	-12
Right Basal Forebrain	351	7	9	-12
Midbrain	65	-1	-22	-21

Regarding the hypothesized areas, the left basal forebrain had significantly higher correlations with the right antero-medial prefrontal cortex, with the right posterior parietal cortex and with the midbrain area, while the right basal forebrain had significantly higher correlations with the right temporal pole and with the left cerebellar hemisphere. The left thalamus had significantly higher correlations with the left parahippocampal region, with the left temporal pole, with the right and the left antero-medial prefrontal cortex, with the left and the right ventro-lateral prefrontal cortex and with the right posterior parietal cortex, while the right thalamus had significantly higher correlations with the right and the left antero-medial prefrontal cortex, with the left temporal pole and with the left cerebellar tonsil. No significant difference was found for partial correlations.

Anatomical validation in thalamic, basal forebrain and mesencephalic areas

Figure 28 illustrates the intersection of the new DMN map after its translation to the MNI group space using individual inverse transformation matrices specific for each individual.

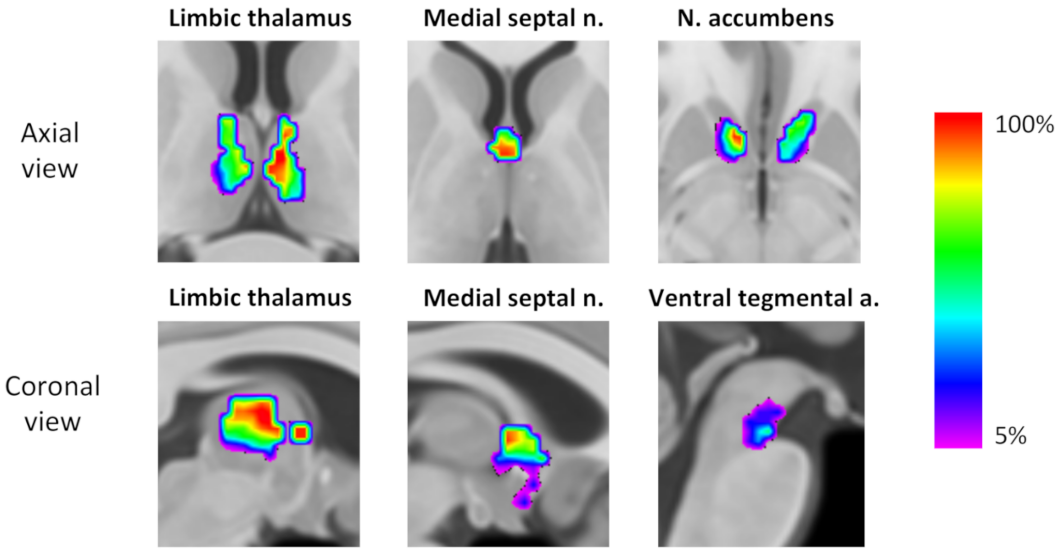

Figure 28. Density maps of the functionally-aligned individual DMN networks superimposed in the MNI152 space. Colour bar represents the percentage of individuals with a significant correlation in each voxel. This map is freely available at https://neurovault.org/collections/CTTXXAYJ/.

Table 16. Proportion of individual DMN maps intersecting, average proportion of the intersection and average volume of the intersection for each nucleus.

Nuclei	**Percentage of individual DMN maps intersecting the nuclei**	**Percentage of nuclei volume intersected - median [IQR]**	**Absolute volume of intersection - median [IQR]**
L middle septal nuclei	100%	22% [15-29]	248mm^3 [169-327]
R middle septal nuclei	100%	26% [21-30]	291mm^3 [235-336]
L mediodorsal thalamic	100%	64% [53-77]	696mm^3 [577-838]
R mediodorsal thalamic	100%	33% [11-42]	401mm^3 [134-511]
L anterior thalamic	100%	80% [75-88]	160mm^3 [150-176]
R anterior thalamic	95%	62% [28-60]	193mm^3 [87-187]
L nucleus accumbens	100%	51% [15-84]	367mm^3 [108-605]
R nucleus accumbens	95%	49% [33-58]	333mm^3 [224-394]
Ventral Tegmental Area	90%	17% [6-24]	48mm^3 [17-67]
L mammillary body	50%	2% [0-9]	4mm^3 [0-17]
L Meynert nucleus	40%	0% [0-1]	0mm^3[0-22]
R Meynert nucleus	45%	0% [0-4]	0mm^3 [0-97]

IQR, interquartile range; L, Left; R, Right.

All subjects' DMN spatially overlapped with the templates of the left anterior thalamic nucleus, mediodorsal thalamic nuclei, medial septal nuclei and left nucleus accumbens (Table 16; Talairach and Tournoux 1988; Desikan et al. 2006; Lancaster et al. 2007; Zaborszky et al. 2008; Edlow et al. 2012). The number of subjects with an intersection with the right anterior thalamic nucleus, right nucleus accumbens and ventral tegmental area was also very high (95%, 95% and 90% respectively), while the intersection with the other basal forebrain nuclei occurred in approximately half of the subjects, possibly due to their very small size.

Tractography

We explored the structural connectivity of our new model of the DMN using tractography imaging techniques. The regions of interest were the same used for functional connectivity analysis. Figure 29 represents the structural connectivity of the network.

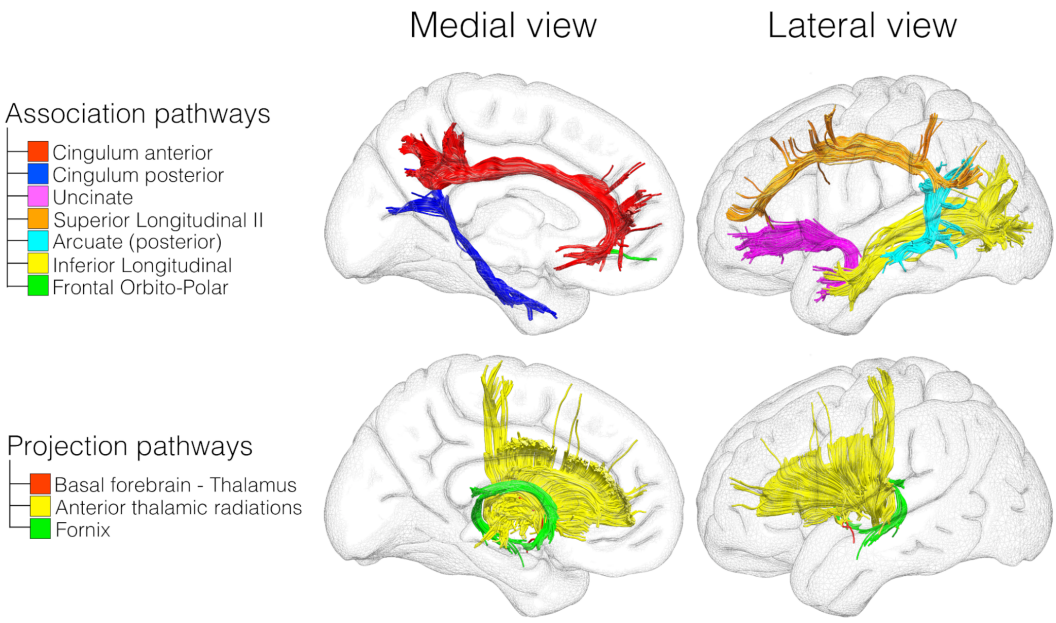

Figure 29. Structural connections supporting the DMN. The upper panel corresponds to the association pathways connecting the cortical regions of the DMN. The lower panel illustrates the projection pathways mediating the connections between subcortical and cortical regions of the DMN.

Results indicated that both anterior and posterior portions of the cingulum, as well as inferior longitudinal fasciculus, the second branch of the superior longitudinal fasciculus, the posterior segment of arcuate fasciculus, the uncinate fasciculus and some fibres of the frontal orbito-polar tract (Figure 27, upper panel) connected the different nodes of the DMN. Additionally, the anatomical connectivity of the basal forebrain and the thalamus with other regions of interest included: the anterior thalamic projections, connecting thalamus with medial prefrontal cortex; the cingulum, connecting basal forebrain with medial prefrontal cortex and posterior cingulate cortex; the fornix, connecting basal forebrain (specifically the region correspondent to the medial septal nuclei) to the hippocampus; and fibres connecting basal forebrain and thalamus, some of the most medial possibly corresponding to the bundle of Vicq D'Azyr (Figure 29, lower panel).

Graph theory analysis

Figure 30 represents the analysis of the DMN structural network with a graph theory approach using the 33 regions of interest defined from the DMN in the functional space.

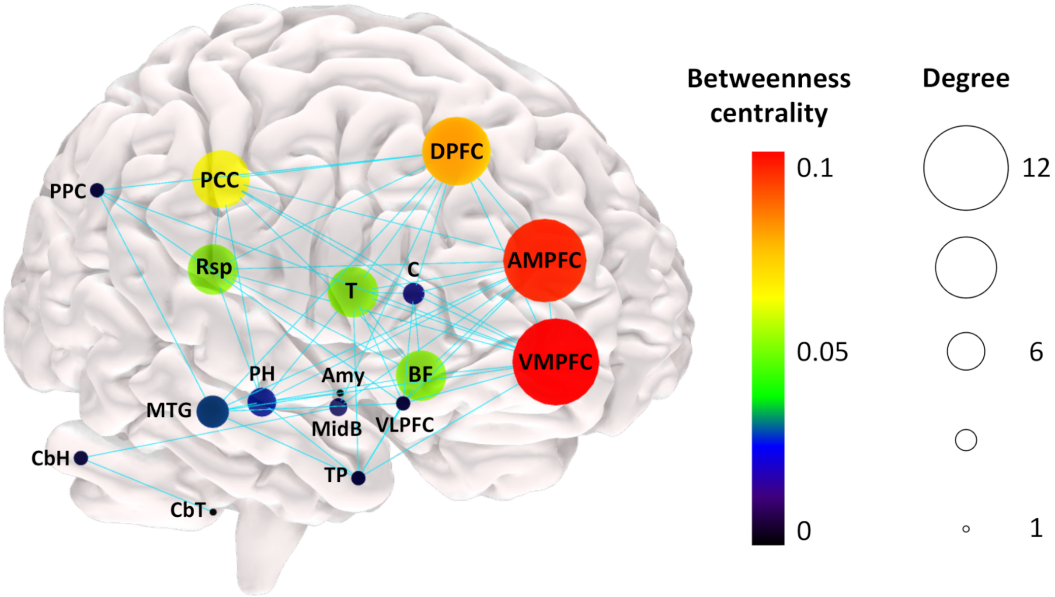

Figure 30. Graph theory analysis of structural connectivity. The node size represents node degree and the node colour illustrates node betweenness centrality. The edges denote presence of structural connection. DPFC, dorsal prefrontal cortex; PPC, posterior parietal cortex; VLPFC, ventro-lateral prefrontal cortex; Rsp, retrosplenial cortex; MTG, middle temporal gyrus; PCC, posterior cingulate cortex; C, caudate; DPFC, dorsal prefrontal

cortex; AMPFC, antero-medial prefrontal cortex; VMPFC, ventro-medial prefrontal cortex; TP, temporal pole; BF, basal forebrain; T, thalamus; PH, parahippocampal region; CbH, cerebellar hemisphere; CbT, cerebellar tonsil; Amy, amygdala; MidB, midbrain.

Results indicate that high degrees and high betweenness centrality in the network were obtained for the basal forebrain and thalamic regions, alongside the medial prefrontal cortex and the posterior cingulate–retrosplenial cortex as well as in regions which were previously considered as hubs in the DMN.

More precisely, the [maximum-minimum] range of distribution of node degrees was [12 - 1] and the median [interquartile range] was 5 [8 - 2]. The node degrees of the left and right thalamus were 9 and 7, and of the left and right basal forebrain were 8 and 7, respectively (Table 17).

Table 17. Node degree and betweenness centrality of the network nodes.
Data is presented as median [interquartile range].

Nodes	**Node degree**	**Betweenness centrality**
Right Ventro-Medial Prefrontal Cortex	12 [10 – 14]	0.104 [0.087 – 0.126]
Left Ventro-Medial Prefrontal Cortex	12 [11 – 14]	0.070 [0.041 – 0.123]
Right Antero-Medial Prefrontal Cortex	12 [9 – 13]	0.060 [0.029 – 0.093]
Left Antero-Medial Prefrontal Cortex	11 [10 – 12]	0.040 [0.025 – 0.058]
Left Dorsal Prefrontal Cortex	10 [9 – 11]	0.075 [0.055 – 0.095]
Right Dorsal Prefrontal Cortex	10 [8 – 11]	0.057 [0.033 – 0.116]
Left Posterior Cingulate Cortex	9 [8 – 10]	0.025 [0.014 – 0.055]
Left Thalamus	9 [7 – 11]	0.029 [0.016 – 0.047]
Left Basal Forebrain	8 [7 – 9]	0.032 [0.021 – 0.058]
Right Posterior Cingulate Cortex	8 [7 – 10]	0.028 [0.012 – 0.047]
Left Retrosplenial Cortex	8 [7 – 9]	0.020 [0.008 – 0.039]
Right Basal Forebrain	7 [5 – 8]	0.024 [0.011 – 0.054]
Right Retrosplenial Cortex	7 [6 – 8]	0.020 [0.008 – 0.035]
Right Thalamus	7 [5 – 9]	0.033 [0.016 – 0.057]
Left Caudate	5 [4 – 6]	0.003 [0.001 – 0.015]
Left Parahippocampal region	5 [4 – 6]	0.003 [0.001 – 0.042]
Right Middle Temporal Gyrus	5 [3 – 6]	0.020 [0.007 – 0.042]

Left Middle Temporal Gyrus	4 [4 – 6]	0.013 [0.005 – 0.060]
Left Ventro-Lateral Prefrontal Cortex	4 [3 – 4]	0.002 [0.001 – 0.017]
Right Parahippocampal region	4 [3 – 5]	0.004 [0.001 – 0.017]
Left Temporal Pole	3 [2 – 5]	0.002 [0.000 – 0.014]
Right Caudate	3 [2 – 4]	0.001 [0.000 – 0.002]
Left Posterior Parietal Cortex	3 [2 – 3]	0.002 [0.000 – 0.018]
Midbrain	3 [1 – 5]	0.000 [0.000 – 0.059]
Right Cerebellar hemisphere	2 [1 – 3]	0.000 [0.000 – 0.031]
Right Temporal Pole	2 [0 – 5]	0.003 [0.000 – 0.032]
Right Posterior Parietal Cortex	2 [2 – 3]	0.001 [0.000 – 0.005]
Right Ventro-Lateral Prefrontal Cortex	2 [2 – 3]	0.000 [0.000 – 0.002]
Left Amygdala	1 [1 – 2]	0.000 [0.000 – 0.000]
Left Cerebellar Hemisphere	1 [1 – 2]	0.000 [0.000 – 0.004]
Left Tonsil	1 [0 – 1]	0.000 [0.000 – 0.000]
Right Amygdala	1 [0 – 1]	0.000 [0.000 – 0.000]
Right Tonsil	1 [0 – 1]	0.000 [0.000 – 0.000]

Therefore, thalamus and basal forebrain are among the structures in the network that have connections with a high number of nodes. For betweenness centrality, the [maximum-minimum] range of distribution was [0.104 - 0] and the median [interquartile range] was 0.004 [0.03 - 0.001]. The betweenness centrality of the left and right thalamus was 0.03 and of the left and right basal forebrain were 0.03 and 0.02, respectively (Table 17). Hence, thalamus and basal forebrain make part of a high fraction of shortest paths in the network, that is, the shortest connections between two nodes.

Discussion

In this study, we revisited the constituent elements of the default mode network using an optimized method of coregistration in a functional space, besides the conventional structural alignment. Three main findings emerge from this research in healthy humans. First, higher functional connectivity correlation and sharper anatomical details were achieved when registering the DMN maps in a functional space. Second, we confirmed the hypothesis that structures of basal forebrain and anterior and mediodorsal thalamic nuclei belong to the DMN. Lastly, we characterised in detail the structural connectivity

underlying functional connectivity. Based on these findings, we provided a more comprehensive neurobiological model of the DMN that bridge the gap between local differences in subcortical structures and global differences in the DMN reported in clinical studies.

The difference between alignment in the functional space and the structural space was characterised by an increase of the connectivity strength across the brain as well as in many subcortical areas classically not considered to be constituent nodes of the DMN. As previously reported, this confirmed that registration in the functional space provides a more accurate interindividual anatomical description and is recommended when doing functional connectivity analyses (Mueller et al. 2013; Langs et al. 2015).

The maps of the DMN registered in the functional space revealed previously underappreciated parts of this network such as basal forebrain and anterior and mediodorsal thalamic nuclei. Tractography analysis yielded structural connectivity of these new DMN regions to the other regions of the network. Mainly, the cingulum connected the basal forebrain with medial prefrontal cortex, posterior cingulate region, retrosplenial cortex, and hippocampus and parahippocampal regions (Catani et al. 2002, 2012). The fornix linked basal forebrain, specifically the medial septal nuclei, with the hippocampus and parahippocampal regions (Aggleton 2000; Saunders and Aggleton 2007; Catani et al. 2013). The anterior thalamic projections connected the thalamus with medial and ventrolateral prefrontal regions (Behrens et al. 2003) and finally some of the most medial fibres connecting the basal forebrain with the thalamus, probably corresponded to the mammillothalamic tract of Vicq D'Azyr (Vicq D'Azyr 1786; Balak et al. 2018).

Our graph theory approach (Bullmore and Sporns 2009) applied to the measures of structural connectivity revealed a high node degree of the basal forebrain and the thalamus in the network, as well as high betweenness centrality (Rubinov and Sporns 2010). These results indicate that basal forebrain and thalamus have high centrality within the network, and therefore can have an important role for network integration and resilience (Hagmann et al. 2008; Bullmore and Sporns 2009; Rubinov and Sporns 2010), along with the classically defined hubs such as the medial prefrontal region as well as posterior cingulate and retrosplenial region (van Oort et al. 2014).

The involvement of basal forebrain and anterior and mediodorsal thalamus in the DMN has theoretical and functional repercussions beyond the purely anatomical level. For instance, Kernbach and colleagues recently demonstrated that grey-matter variability across the DMN can well predict population variation in the microstructural properties of

the anterior thalamic radiation and the fornix in 10,000 people (Kernbach et al. 2018). As another example, Margulies and colleagues studied functional gradients along cortical surface and found that DMN areas were at the opposite end of primary motor/sensory areas in a spectrum of connectivity differentiation and that DMN areas exhibit the most considerable geodesic distance at the cortical level, being equidistant to the unimodal cortical areas (Margulies et al. 2016). These investigators suggested that the DMN acts as a neural relay for transmodal information. We speculate that thalamus and basal forebrain may follow the same model at a subcortical level, integrating functional networks related to primary functions and brainstem inputs to the associative areas (Dringenberg and Olmstead 2003; Mease et al. 2016). The involvement of the anterior and mediodorsal thalamic nuclei as well as the basal forebrain are concordant with the role of the DMN in memory processes (Schacter et al. 2007; Andrews-Hanna et al. 2010), as all these regions are relays of the unitary model of the limbic system (MacLean 1949, 1952; Catani et al. 2013). Previous reports of engagement of the mediodorsal thalamic nucleus and the DMN during memory tasks and the memory deficits provoked by lesions of the anterior and the mediodorsal thalamic nuclei also support this claim (Rabin et al., 2010; Spreng and Grady, 2010; Child and Benarroch, 2013; Danet et al., 2015). At a neurochemical level, the basal forebrain is also a principal actor in the production of acetylcholine (Zaborszky et al. 2015). Acetylcholine has a physiological and a neuropharmacological effect on memory processes. For instance, cholinergic system mediates rhythmic oscillation in the hippocampus that facilitates encoding (Hasselmo 2006; Zaborszky et al. 2008). The basal forebrain also contains GABAergic and glutamatergic neurons that mediate hippocampal theta synchronization through an indirect septo-hippocampal pathway (Dannenberg et al. 2015). By providing evidence of the involvement of medial septal cholinergic nucleus and its structural connection to the hippocampus in our DMN model, the present work indicates a match between connectivity, neurochemistry and cognition.

The same correspondence between connectivity, neurochemistry and cognition applies to the relation between DMN and emotional modulation (Mars et al. 2012; Bzdok et al. 2013; Raichle 2015; Alcalá-López et al. 2017; Spies et al. 2017; Zhao et al. 2017). The nucleus accumbens is a central output for the dopaminergic projections and is involved in emotion regulation and affect integration (Laviolette 2007; Floresco 2015). The nucleus accumbens also receives glutamatergic inputs from the hippocampus and the prefrontal cortex (Britt et al. 2012) belonging to the DMN. Surprisingly, our analysis also revealed the ventral tegmental area, which is also a dopaminergic nucleus with projections to the

nucleus accumbens and the medial prefrontal cortex (Morales and Margolis 2017). This association with the mesolimbic dopaminergic pathway is reinforced by our results of functional connectivity, since ventromedial prefrontal cortex and midbrain were among the structures with highest partial correlations with basal forebrain. Hence, combining present and previous findings, we speculate that the DMN, as defined by functional connectivity, might have a putative role in the integration of cholinergic and dopaminergic systems dedicated to memory and emotion.

The new DMN's subcortical structures identified in the current work have cognitive and neurochemical roles that open a new window to the understanding of distinct brain pathologies affecting DMN connectivity (Table 18). Indeed, functional connectivity in each area of the DMN is an estimate of the global coherence of the DMN. Since we demonstrated that limbic thalamus and basal forebrain are nodes with high degree and high centrality in the DMN, damage in these structures should lead to a drastic decrease of functional connectivity in the whole DMN (van den Heuvel and Sporns 2013). For instance, Alzheimer's disease is associated with degeneration of the cholinergic system, including the medial septal nuclei, even in the earliest clinical stages of Mild Cognitive Impairment (Grothe et al. 2010) and apparently related to decreased functional coherence and deactivation in hub regions of DMN (He et al. 2007b; Persson et al. 2008). The high centrality of the basal forebrain in the DMN network may explain this early link between DMN and Alzheimer's disease. In schizophrenia, also associated with decreased DMN connectivity and activation (Bluhm et al. 2007; Pomarol-Clotet et al. 2008), neuropathological evidence suggests an abnormal glutamatergic-dopaminergic interaction at the level of nucleus accumbens (McCollum and Roberts 2015). Additionally, the ventral tegmental area is connected to the nucleus accumbens through the mesolimbic system, the classical dopaminergic pathway associated with schizophrenia, and functional data shows a decrease of connectivity between ventral tegmental area and several brain regions, including the thalamus, in unmedicated patients with schizophrenia (Hadley et al. 2014). The pathophysiology of others diseases, such as drug addiction, depression, temporal lobe epilepsy and attention deficit and hyperactivity disorder involve modifications in the nucleus accumbens, medial septal nuclei or the thalamic nuclei that connect limbic regions as well as dysfunctional connectivity of the DMN (specified in Table 18; Butler et al., 2013; Dinkelacker et al., 2015; Ivanov et al., 2010; Scofield et al., 2016; Vialou et al., 2010; Voets et al., 2012; Volkow et al., 2011; Yamamura et al., 2016; Zhu et al., 2016). Hence, the involvement of the basal forebrain and the thalamic nuclei in the DMN appears

to bridge the gap between the subcortical anatomical differences and the global differences in the DMN previously reported.

Table 18. Pathophysiological associations of the subcortical structures of DMN.

Disease associated with DMN dysfunction	**Pathophysiological associations with subcortical DMN**	**References**
Alzheimer's disease	Degeneration of cholinergic system (including medial septal nuclei), even in MCI stage	Grothe et al., 2010
	Dysfunction of limbic thalamus in early stages of the disease	Aggleton et al., 2016
	Decreased functional coherence and deactivation in hub regions of DMN	He et al., 2007; Persson et al., 2008
Schizophrenia	Abnormalities in glutamatergic-dopaminergic interaction in Nucleus Accumbens	McCollum and Roberts, 2015
	Decreased functional connectivity between ventral tegmental area and thalamus	Hadley et al., 2014
	Decreased connectivity and activation of hub regions of DMN	Bluhm et al., 2007; Pomarol-Clotet et al., 2008
Temporal Lobe Epilepsy (TLE)	Dysfunctional increase in hippocampus - mediodorsal thalamus connectivity	Dinkelacker et al., 2015
	Stimulation of anterior thalamic nucleus is efficacious in treatment of TLE	Osorio et al., 2007; Salanova et al., 2015
	Enlargement of medial septal nuclei in TLE	Butler et al., 2013
	Decreased functional connectivity between hippocampus and DMN	Voets et al., 2012
Depression	Resting activity of the thalamus predicts response to anti-depressant medication	Yamamura et al., 2016
	Nucleus accumbens mediates response to stress and to anti-depressant medication	Vialou et al., 2010

MCI, mild cognitive impairment

Interestingly, the thalamus and the basal forebrain are phylogenetically older than many cortical structures and especially those that compose the DMN (Butler 2008; Karten 2015; Yamamoto et al. 2017). The inclusion of these structures in the anatomical model of the DMN can open a window to the exploration of DMN in other mammalian species as well (Rilling et al. 2007; Vincent et al. 2007; Lu et al. 2012; Buckner and Margulies 2018). The medial thalamus has already been shown to be part of the mouse's DMN (Gozzi and Schwarz 2016), as found in resting state fMRI studies (Sforazzini et al. 2014; Liska et al. 2015; Bertero et al. 2018). Our results are also concordant with recent neurophysiological evidence in rats about the influence of basal forebrain in the regulation of the DMN (Nair et al. 2018). Namely, it has been shown that gamma-band local field potentials in the basal forebrain exerts influence on one of the hub regions of rat's DMN, the anterior cingulate cortex (Nair et al. 2018). The cellular basis for the association of these two areas has been characterized with retrograde tracing studies (Chandler and Waterhouse 2012; Chandler et al. 2013). In humans, it has been demonstrated that basal forebrain has a major functional coupling with the anterior cingulate cortex and with ventromedial prefrontal cortex (Markello et al. 2018). We speculate that the putative differences in the basal forebrain projections may be one explanation for the more diffuse DMN activation at the midline level in rats, when compared to humans (Lu et al. 2012).

One limitation of the present work is that the overlap between the DMN map and the nuclei studied is based on comparison with templates or variability maps, and not with the individual location of the nucleus in the explored subjects. The limited capacity of structural MRI to differentiate these small nuclei does not allow such comparison. Besides, the reverse transformation of the DMN from the functional space to the MNI space may not be exact, due to inherent limitations of inverse transformations. Although these limitations may decrease the accuracy of the intersection quantification with discrete nuclei, they did not alter the apparent overlap with basal forebrain and with the thalamus. Furthermore, demonstrating that the additional step of functional alignment results in higher correlation values is somewhat circular. However, our purpose was to demonstrate that this increase in correlation revealed subcortical structures that were previously neglected in the literature. The intra-individual functional connectivity variation across time may also be a source of bias (Braga and Buckner 2017). However, this factor and the lack of uniformity regarding the optimal functional alignment method have not precluded the achievement of higher accurate results in previous studies (Mueller et al. 2013; Robinson et al. 2014; Langs et al. 2015; Glasser et al. 2016). Finally, tractography analyses

can produce inaccurate results (Jones and Cercignani 2010; Maier-Hein et al. 2017). In order to avoid these caveats, we employed methods that have previously demonstrated high anatomical reliability when compared to axonal tracing and with post-mortem dissections (Thiebaut de Schotten et al. 2011a; Catani et al. 2012; Dell'Acqua et al. 2013; Karolis et al. 2019).

In conclusion, this work demonstrates that the registration of individual DMN maps in a functional space improves the definition of the anatomy of DMN by including additional structures, such as the thalamus and basal forebrain.

4.2. Subcortical anatomy of the ventral and dorsal attention networks

Part of this section is included in the following manuscript:

- Alves PN, Forkel JS, Corbetta M, Thiebaut de Schotten M (2022) The subcortical and neurochemical organisation of the ventral and dorsal attention networks. Commun Biol 5:1343. https://doi.org/10.1038/s42003-022-04281-0 (accepted).

Introduction

"*Everyone knows what attention is. It is the taking possession by the mind, in clear and vivid form, of one out of what seem several simultaneously possible objects or trains of thought."* (James 1890).

The pioneer elucidations of the paramount role of attention for the maintenance of a coherent behaviour fostered an endeavour, taken by different fields of neuroscience, to understand the neural basis of attentional processes (Petersen and Posner 2012). Neuroimaging studies prompted the identification of two fundamental macroscale networks - the dorsal attention network and the ventral attention network (Corbetta and Shulman 2002). The dorsal attention network (DAN) acts as a top-down modulator and participates in goal-driven tasks. The ventral attention network (VAN) is a stimulus-driven system and mediates reorientation to relevant or unexpected events. Neuroanatomically, the core regions of the DAN are the intraparietal sulcus, the superior parietal lobe, and the frontal eye fields (Corbetta et al. 2000; Buschman and Miller 2007), while the temporo-parietal junction and the ventrolateral prefrontal cortex constitute the central regions of the VAN (Downar et al. 2000).

Yet, evidence from diverse grounds suggests that purely concentric-based models might be insufficient to explain the neuroanatomical framework of attentional mechanisms. First, neuronal electrical recordings in primates showed that subcortical structures have crucial roles in the neural mechanisms of attention. For instance, inactivation of the superior colliculus during motion-change detection markedly disturbs visual attention without affecting the neuronal activity in the visual cortex (Zénon and Krauzlis 2012). Furthermore, it has been demonstrated that attentional states modulate the cellular activity of the thalamic pulvinar nuclei (Bender and Youakim 2001), while different patterns of neuronal discharge in the locus coeruleus promote changes between selective and scanning attention (Aston-Jones et al. 1999; Vazey et al. 2018). Second, pathophysiological data from human brain disease supports the foremost relevance of deep brain nuclei. Neglect is a clinical syndrome characterized by pathological hemispatial inattention and might arise from exclusively subcortical lesions, namely in the pulvinar or in the striatum (Healton et al. 1982; Ferro et al. 1984; Karnath et al. 2002). Moreover, the patients with attention deficit hyperactivity disorder present morphological alterations of the pulvinar, a change that is influenced by the severity of the disease and the use of stimulants (Ivanov et al. 2010). Third, phylogenetic distant species, such as pigeons, have markedly different cortical morphologies, but exhibit patterns of attention errors and reaction times that are

similar to humans (Blough 1977). Even with close mammals, such as the macaques, relevant functional attention dissimilarities have been found at the cortical level, namely concerning the VAN (Patel et al. 2015).

Average group alignments of functional connectivity maps exclusively based on structural landmarks might fail to represent the full architecture of a functional network (Brett et al. 2002; Thiebaut de Schotten and Shallice 2017). Subcortical nuclei are particular prone to structural misalignment due to their low dimension, lower anatomical definition in structural MRI and intersubject cytoarchitectonic variability (Carmack et al. 2004; Amunts et al. 2005; Zaborszky et al. 2008). Functional alignment improves structural-functional correspondence of heteromodal association cortical areas across subjects (Mueller et al. 2013; Robinson et al. 2014; Langs et al. 2015; Glasser et al. 2016). At the subcortical level, we demonstrated that the employment of functional alignment methods uncovered the deep brain nuclei that integrate the default mode network (Alves et al. 2019).

Finally, knowledge about the DAN and the VAN neurochemistry is limited to primate studies that indicated a noradrenergic innervation of the DAN and the VAN, including the temporo-parietal junction and frontal lobe (Morrison and Foote 1986; Foote and Morrison 1987; Bouret and Sara 2005). Additionally, noradrenaline has been proposed as a critical trigger of the reorientation of attention (Bouret and Sara 2005; Corbetta et al. 2008). However, despite its essential neuroscientific and medical importance (Sanefuji et al. 2017), the neurochemical signatures of the VAN and the DAN have never been contrasted in humans.

Therefore, we explored the subcortical anatomy of attention networks by aligning the individual resting-state functional maps of the VAN and the DAN in a common functional space. We hypothesized that basal ganglia and brainstem nuclei, namely the pulvinar, the striatum, the superior colliculus and the locus coeruleus, were functional constituents of attention networks. An optimized model of the VAN and the DAN was uncovered together with the structural, functional, graph centrality and neurochemical properties of theirs subcortical structures.

Methods

Resting-state fMRI

We used 110 7T resting-state fMRIs from the Human Connectome Project S1200 dataset (Glasser et al. 2013). Images were preprocessed and registered to the MNI152 space as specified in the Human Connectome Project protocol (http://www.humanconnectome.org/storage/app/media/documentation/s1200/HCP_S1200_Release_Reference_Manual.pdf; Glasser et al. 2013).

VAN and DAN maps in the structural space

VAN and DAN maps were computed using the seeding regions of interest defined in the functional cortical parcellation map provided by Gordon and colleagues (2016). This template includes 23 VAN parcels (11 in the left hemisphere and 12 in the right hemisphere) and 32 DAN parcels (19 in the left hemisphere and 13 in the right hemisphere). This parcellation was performed according to the patterns of resting-state functional connectivity, each parcel having a homogeneous resting-state functional connectivity arrangement and being separated from neighbour parcels by abrupt changes of their connectivity profile (Gordon et al. 2016).

We calculated functional correlation maps seeded from each of the VAN cortical parcels, using the Funcon-Connectivity tool of the Brain Connectivity and behaviour toolkit (http://toolkit.bcblab.com; Foulon et al. 2018). This tool computes the Pearson's correlation between the mean resting state activity of the seed region and the other voxels of the brain. Then, the median of the 23 functional connectivity maps (generated from the 23 VAN seeds) was computed, in order to obtain the VAN representative map of each subject. The median was the chosen central tendency measure, because it is less affected by outliers than the mean (Kenney 1939). One hundred and ten individual VAN maps in the MNI152 were obtained (i.e. one per subject). To obtain DAN maps, the same steps were performed, using the 32 DAN seeds.

DAN and VAN maps in the functional space

The 110 individual VAN maps were aligned with each other in a functional space (Mueller et al. 2013; Robinson et al. 2014; Langs et al. 2015; Glasser et al. 2016). We used the Advanced Normalization Tools' (ANTs) script *buildtemplateparallel.sh* to perform an

iterative (n=4) diffeomorphic transformation to a common space (Avants et al. 2011; Alves et al. 2019). Cross-correlation was set as the similarity measure and greedy SyN as the transformation model (Avants et al. 2008; Klein et al. 2009). The resulting transformation warps were applied to the MNI152 aligned VAN maps, using the ANTs' script *WarpImageMultiTransform*, to obtain the representation of the 110 individual VAN maps in the common functional space. The same steps were performed with the DAN maps.

To calculate group statistical VAN and DAN maps, we performed a permutation inference analysis using the FSL's tool *randomise* one-sample and applying a Threshold-Free Cluster Enhancement (Jenkinson et al. 2012). To evaluate the similarity between the VAN and the DAN statistical maps, the t-maps were converted to z-maps and a conjunction analysis was computed (Nichols et al. 2005). The illustrations were made in SurfIce (https://www.nitrc.org/projects/surfice/) and MRIcroGL (https://www.nitrc.org/projects/mricrogl/).

Anatomical validation of the subcortical structures

To identify thalamic nuclei, we used the DISTAL (Deep brain stimulation Intrinsic Template Atlas; Ewert et al. 2018) and the THOMAS (Thalamus Optimized Multi Atlas Segmentation; Su et al. 2019) atlases. The DISTAL atlas is a high-resolution template of subcortical structures in the MNI space used as a reference to localize targets for deep brain stimulation (Ewert et al. 2018). Its segmentation was performed manually, based on histology, structural imaging and diffusion-weighted imaging (Chakravarty et al. 2006; Ewert et al. 2018). The THOMAS atlas is a template of thalamic nuclei derived from the manual segmentation of 20 White-Matter-Nulled Magnetization Prepared Rapid Gradient Echo (MP-RAGE) 7T datasets, warped to the MNI space (Su et al. 2019). Its segmentation accuracy is high compared to the Morel histological atlas (Morel et al. 1997; Su et al. 2019).

To map the brainstem nuclei, we used the WIKIBrainStem atlas (Lechanoine et al. 2021). This template is based on mesoscopic T2-weighted and diffusion-weighted images obtained from the ultra-high-field scanning (11.7T) of an *ex vivo* specimen. It provides detailed segmentation rules of 99 brainstem structures (Lechanoine et al. 2021).

Tractography analysis

Functional interactions in the brain are shaped by the underlying structural properties, both at the cellular and at the neuroanatomical levels (Suárez et al. 2020; Thiebaut de Schotten et al. 2020). We analysed the structural connectivity of the VAN and the DAN, including the newly identified subcortical structures.

Tractography was computed using 177 diffusion-weighted images from the 7T dataset of the Human Connectome Project (Vu et al. 2015). The scanning parameters are detailed in Vu et al. 2015. Preprocessing was performed according to the default Human Connectome Project pipeline (v3.19.0; Glasser et al. 2013). Tractography was processed as described in Thiebaut de Schotten et al. 2020. Briefly, a whole brain determinist approach was employed, using the StarTrack software (https://mr-startrack.com), and applying a damped Richardson-Lucy algorithm for spherical deconvolution (Dell'Acqua et al. 2010). Then, the individual whole-brain streamline tractographies were registered to the MNI152 space. First, they were converted into density maps, in which the voxel densities corresponded to the number of streamlines crossing each voxel (Thiebaut de Schotten et al. 2020). Second, individual density maps were aligned in a common template using the Greedy symmetric diffeomorphic normalization of the Advanced Normalization Tools pipeline (Avants et al. 2011). Third, the resulting template was co-registered to the MNI152 2mm template using the FSL's tool *flirt* (Jenkinson et al. 2002). Finally, the resulting transformation warps were applied to the individual whole-brain streamline tractographies using the Tract Querier package (Wassermann et al. 2016).

Then, we computed the structural connectome of the VAN and the DAN models. The cortical nodes were defined according to the parcellation of Gordon and colleagues (2016). To determine the subcortical regions of interest (ROI), we selected the statistically significant voxels of the subcortical structures identified in the previous sections with a median Pearson's correlation higher than 0.1. This correlation threshold was applied to avoid including voxels significantly associated with the network, but with very weak correlations (Cohen 1988). The streamlines that crossed at least two ROIs (cortico-cortical, cortico-subcortical or subcortical-subcortical) were selected using the MRtrix3's tool *tckedit* (Tournier et al. 2019). Afterwards, the selected streamlines were volume-mapped into the MNI space using the MRtrix3's tool *tckmap* (Tournier et al. 2019). The volume maps were binarized and a group level overlap map was computed.

ROI-to-ROI structural and functional connectivity analysis

To analyse ROI-to-ROI structural connectivity, we used the MRtrix3's tool *tck2connectome*. The cortical and subcortical ROIs were defined as stated in the previous section. Regarding ROI-to-ROI functional connectivity, we computed the partial correlation between the network nodes using the nilearn's function *ConnectivityMeasure* (Pedregosa et al. 2011). The illustrations of the connectivity matrices were created with Matplolib 3.4.2 (Hunter 2007).

Graph theory analysis of structural connectivity

To analyse if the newly identified subcortical nuclei would be core regions in the networks, we performed a graph theory analysis of the hub properties of the VAN and the DAN nodes. Two measures were used, the degree centrality and the betweenness centrality (Bullmore and Sporns 2009). Degree centrality denotes the fraction of nodes connected to the node of interest. Betweenness centrality is the fraction of all-pairs shortest paths that pass through the node of interest (Bullmore and Sporns 2009).

The 177 individual binarized structural connectivity matrices were converted into undirected connectivity graphs and both measures were calculated, using the NetworkX package (https://networkx.org/). Then, we calculated the median value of both measures across the 177 network graphs, for each node. The illustrations of the network graphs were created with Surf Ice (https://www.nitrc.org/projects/surfice/).

Structural correlations with the neurotransmitter system

Subcortical structures play critical roles in the neurotransmitter systems. The brainstem nuclei are the main sources of neurotransmitter synthesis and send axonal projections to the cortex and the basal ganglia. The basal ganglia are central targets of the neurotransmitter axonal projections and mediate their physiological effects.

Hansen and colleagues have recently mapped the macroscale neuroanatomy of the neurotransmitter receptors and transporters (Hansen et al. 2021). Based on positron emission topography (PET) and single-photon emission computerized tomography (SPECT) scans derived from more than 1200 healthy individuals, they provided an atlas of nine neurotransmitter systems aligned in the MNI space (Hansen et al. 2021).

Here, we studied the relationship between the subcortical structural projections of the proposed neuroanatomical models and the spatial distribution of the neurotransmitter

systems. First, we selected the newly identified brainstem nuclei that synthesize neurotransmitters, according to the cytochemical evidence in the literature. Second, we computed the structural projections of these nuclei to the remaining nodes of the VAN and the DAN, i.e. we selected the streamlines that crossed the brainstem nuclei of interest and every other node of the network, using the MRtrix3's tool *tckedit* (Tournier et al. 2019). Then, we used the MRtrix3's tool *tckmap* to map those streamlines into the MNI space (Tournier et al. 2019). The binarized structural connectome maps were overlapped and a group representative map expressing the proportion of structural projections was created. Finally, we computed the Spearman's correlation between the spatial distribution of the created structural projection map and the neurotransmitter maps provided by Hansen and colleagues, using the neuromaps' tool *compare_images* (Hansen et al. 2021; https://netneurolab.github.io/neuromaps/). The graphical representations were created with Matplolib 3.4.2 and with Datashader 0.13.0 (Hunter 2007; https://datashader.org).

Results

VAN anatomical map

The statistical map of the VAN, after functional alignment, is represented in Figure 31 (left column).

At the cerebral cortical level, the peaks of statistical association were found in the temporo-parietal junction, in the inferior frontal gyrus, in the anterior part of the superior frontal gyrus and the superior temporal gyrus (Figure 31A). Additionally, peaks of statistical association were also present in the crus I and crus II of the cerebellar cortex (Figure 31D).

At the thalamus and basal ganglia level, we found areas with high statistical association in the head of caudate nuclei and in the pulvinar (Figure 31B). In the brainstem, the high statistical association was found in voxels overlapping the superior colliculi, the interpeduncular nucleus, the pedunculopontine-cuneiforn nuclei complex, the nucleus pontis oralis, the gigantocellular nuclei and the raphe pallidus and median nuclei (Figure 31C). Table 19 represents the centres of gravity coordinates of the subcortical regions of interest. The VAN statistical and correlation maps are available at https://neurovault.org/collections/XONZLGPJ/.

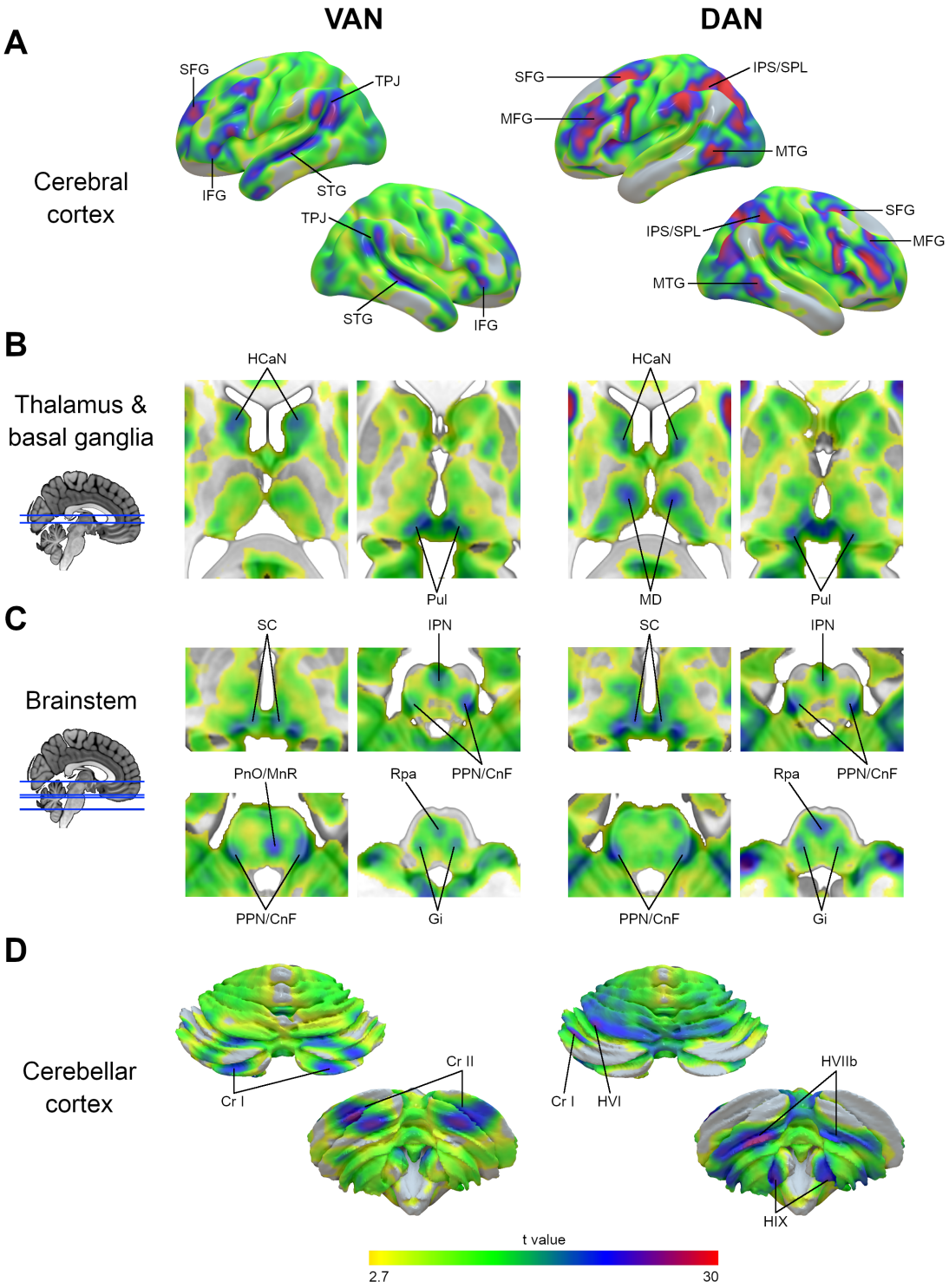

Figure 31. VAN (left) and DAN (right) maps after functional alignment, at different anatomical levels, namely cerebral cortical surface (A), thalamus and basal ganglia (B), brainstem (C) and cerebellar cortical surface (D). The colourmap gradient represents the t-values distribution. CnF, cuneiform nucleus; Cr I, cerebellar crus I lobule; Cr II, cerebellar crus II lobule; DAN, dorsal attention network; Gi, gigantocellular nucleus; HCaN, head of caudate nucleus; HIIb, cerebellar lobule IIb; HVI, cerebellar lobule VI; HIX, cerebellar

lobule IX; IFG, inferior frontal gyrus; IPN, interpeduncular nucleus; IPS, intraparietal sulcus; MnR, median raphe nucleus; MD, mediodorsal nucleus of the thalamus; MTG, middle temporal gyrus; PnO, nucleus pontis oralis; PPN, pedunculopontine nucleus; Pul, pulvinar; Rpa, raphe pallidus nucleus; SC, superior colliculus; SFG, superior frontal gyrus; SPL, superior parietal lobule; STG, superior temporal gyrus; TPJ, temporoparietal junction; VAN, ventral attention network.

Table 19. MNI coordinates of the VAN subcortical regions centres of gravity.

Regions of interest	**MNI (X)**	**MNI (Y)**	**MNI (Z)**
HCaN L	-11	8	13
Pul L	-4	-30	1
SC L	-9	-31	-3
PPN/CnF L	-14	-29	-25
Gi L	-10	-25	-36
Cr I L	-31	-73	-31
Cr II L	-21	-79	-42
IPN	1	-19	-21
MnR	-3	-29	-28
Rpa	1	-28	-43
HCaN R	13	11	12
Pul R	6	-29	1
SC R	13	-30	-3
PPN/CnF R	13	-31	-25
Gi R	11	-24	-35
Cr I R	30	-74	-30
Cr II R	24	-79	-41

CnF, cuneiform nucleus; Cr I, cerebellar crus I lobule; Cr II, cerebellar crus II lobule; Gi, gigantocellular nucleus; HCaN, head of caudate nucleus; IPN, interpeduncular nucleus; L, left; MnR, median raphe nucleus; PnO, nucleus pontis oralis; PPN, pedunculopontine nucleus; Pul, pulvinar; R, right; Rpa, raphe pallidus nucleus; SC, superior colliculus.

DAN anatomical map

The statistical map of the DAN, after functional alignment, is represented in the Figure 31 (right column).

At the cerebral cortical level, the peaks of statistical association were found in the intraparietal sulcus and superior parietal lobule, in the middle and superior frontal gyrus, and in the posterior part of inferior temporal sulcus (Figure 31A). Peaks of statistical association were also found in the cerebellar cortex areas VIIb, IX, left VI and left crus I lobules (Figure 31D).

At the thalamus and basal ganglia level, we found areas with high statistical association in the head of caudate nuclei and in the thalamic pulvinar and mediodorsal nuclei (Figure 31B). In the brainstem, high statistical association was found in voxels overlapping the superior colliculi, the interpeduncular nucleus, the pedunculopontine-cuneiforn nuclei complex, the gigantocellular nuclei and the raphe pallidus nuclei (Figure 31C). Table 2 represents the centres of gravity of the subcortical regions of interest. The DAN statistical and correlation maps are available at https://neurovault.org/collections/XONZLGPJ/.

Table 20. MNI coordinates of the DAN subcortical regions centres of gravity.

Regions of interest	**MNI (X)**	**MNI (Y)**	**MNI (Z)**
HCaN L	-10	4	10
MD L	-9	-18	8
Pul L	-4	-30	1
SC L	-8	-31	-3
PPN/CnF L	-14	-30	-25
Gi L	-10	-24	-35

Cr I L	-39	-64	-29
HVI L	-25	-62	-24
HVIIb L	-24	-66	-49
HIX L	-11	-51	-50
IPN	1	-19	-21
Rpa	1	-28	-42
HCaN R	12	7	10
MD R	9	-16	8
Pul R	6	-29	1
SC R	11	-30	-3
PPN/CnF R	14	-30	-25
Gi R	11	-25	-34
HVIIb R	25	-68	-49
HIX R	11	-53	-51

CnF, cuneiform nucleus; Cr I, cerebellar crus I lobule; Gi, gigantocellular nucleus; HCaN, head of caudate nucleus; HVI, cerebellar lobule VI; HIX, cerebellar lobule IX; IPN, interpeduncular nucleus; L, left; MD, mediodorsal nucleus of the thalamus; PPN, pedunculopontine nucleus; Pul, pulvinar; R, right; Rpa, raphe pallidus nucleus; SC, superior colliculus.

The conjunction analysis showed that most of the subcortical peaks of statistical association were shared by both networks (Figure 32), explicitly overlapping the pulvinar, the superior colliculi, the interpeduncular nuclei, the pedunculopontine-cuneiform nuclei complex, the gigantocellular nuclei and the raphe pallidus nuclei.

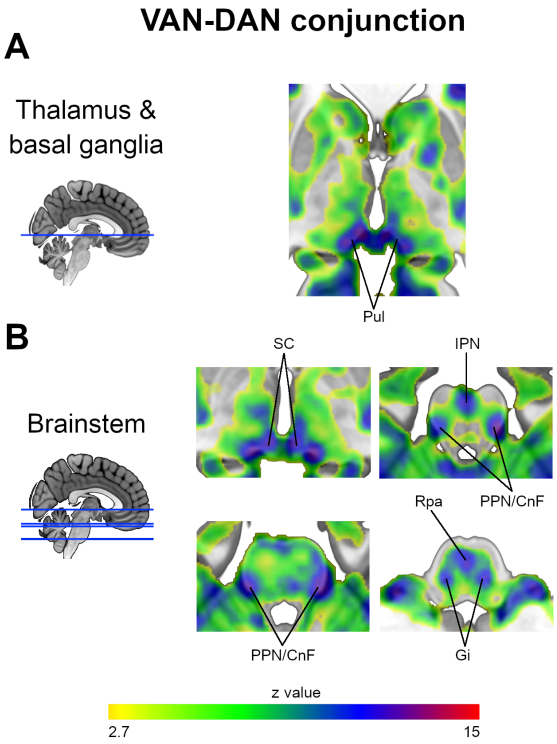

Figure 32. Conjunction analysis of the VAN and DAN statistical maps, at the thalamus and basal ganglia (A) and at the brainstem (B) levels. The colourmap gradient represents the z-values distribution. CnF, cuneiform nucleus; DAN, dorsal attention network; Gi, gigantocellular nucleus; IPN, interpeduncular nucleus; PPN, pedunculopontine nucleus; Pul, pulvinar; Rpa, raphe pallidus nucleus; SC, superior colliculus; VAN, ventral attention network.

Structural and functional connectivity of the VAN nodes

The structural connectivity map of the VAN is represented in Figure 33A.

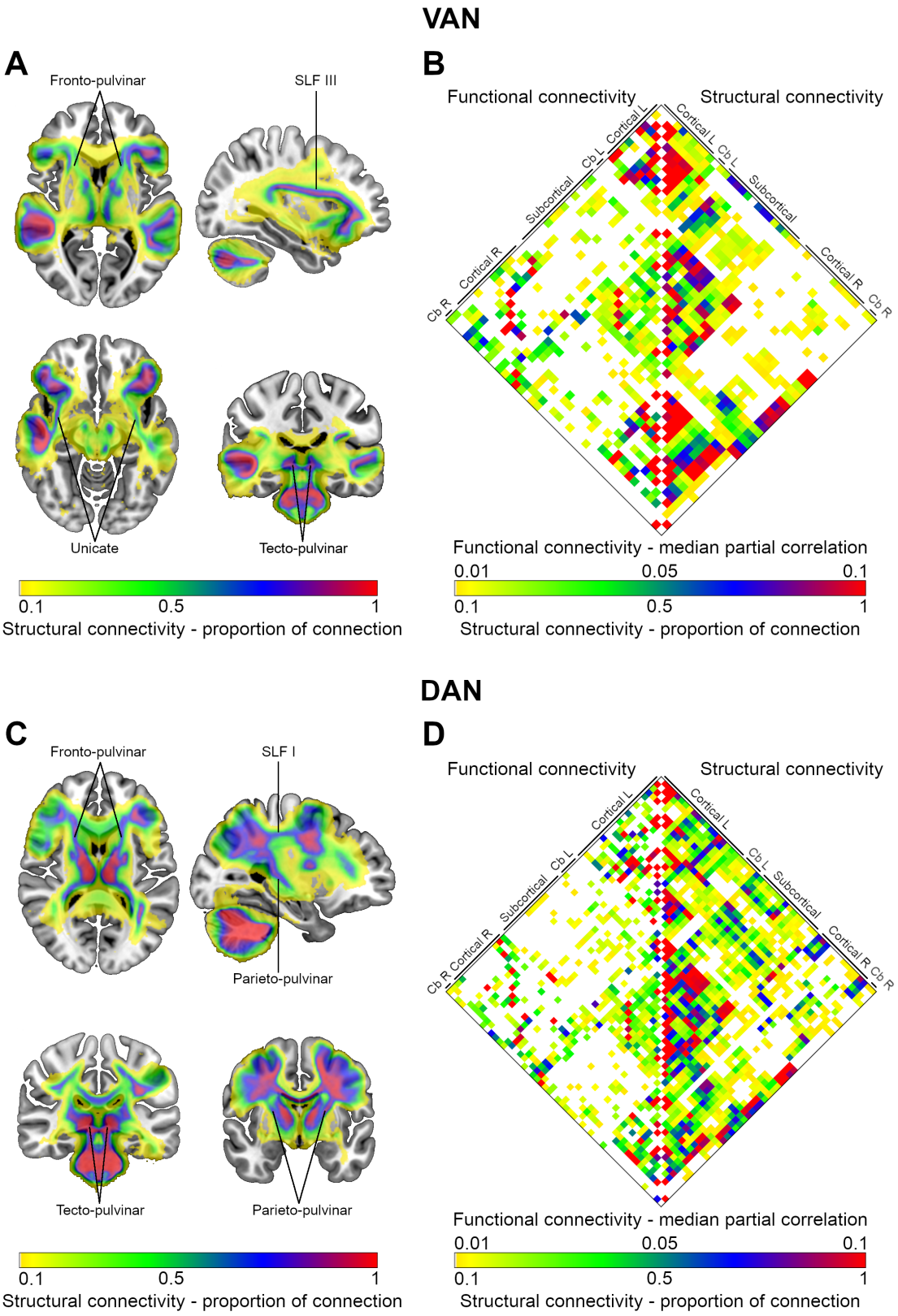

Figure 33. Structural and functional connectivity of the VAN and DAN nodes. A - Structural connectivity map of the VAN. B - Matrix with the node-to-node functional and structural connectivity of the VAN, represented on the left and right halves, respectively. C

- Structural connectivity map of the DAN. D - Matrix with the node-to-node functional and structural connectivity of the DAN, represented on the left and right halves, respectively. The nodes of the matrices were labelled in groups according to their anatomical location, for a clearer reading. A full list with node labels is available in the Tables 21 and 22. Colour gradients represent the structural connectivity (expressed as the proportion of connection) or the functional connectivity (expressed as the median partial correlation). Cb, cerebellum; L, left; R, right; SLF, superior longitudinal fasciculus.

Table 21. Detailed list of the nodes represented in the VAN connectivity matrices

Group label	**Node**	**Group label**	**Node**	**Group label**	**Node**
Cortical L	Parcel 23	**Subcortical**	HCaN L	**Cortical R**	Parcel 221
	Parcel 60		Pul L		Parcel 222
	Parcel 61		SC L		Parcel 226
	Parcel 62		PPN/CnF L		Parcel 228
	Parcel 75		Gi L		Parcel 229
	Parcel 79		IPN		Parcel 231
	Parcel 80		MnR		Parcel 237
	Parcel 85		Rpa		Parcel 241
	Parcel 86		HCaN R		Parcel 242
	Parcel 158		Pul R		Parcel 243
	Parcel 161		SC R		Parcel 332
Cb L	Cr I L		PPN/CnF R		Parcel 333
	Cr II L		Gi R	**Cb R**	Cr I R
					Cr II R

Nodes are ordered according to their position in the connectivity matrix. Numerated parcel correspond to the cortical parcels of the VAN, described by Gordon and colleagues (2016).

Cb, cerebellum; CnF, cuneiform nucleus; Cr I, cerebellar crus I lobule; Cr II, crus II lobule; Gi, gigantocellular nucleus; HCaN, head of caudate nucleus; IPN, interpeduncular nucleus; L, left; MnR, median raphe nucleus; PnO, nucleus pontis oralis; PPN, pedunculopontine nucleus; Pul, pulvinar; R, right; Rpa, raphe pallidus nucleus; SC, superior colliculus.

Table 22. Detailed list of the nodes represented in the DAN connectivity matrices

Group label	**Node**	**Group label**	**Node**	**Group label**	**Node**
Cortical L	Parcel 41	**Subcortical**	HCaN L	**Cortical R**	Parcel 189
	Parcel 42		MD L		Parcel 199
	Parcel 43		Pul L		Parcel 203
	Parcel 49		SC L		Parcel 208
	Parcel 51		PPN/CnF L		Parcel 211
	Parcel 52		Gi L		Parcel 236
	Parcel 55		IPN		Parcel 250
	Parcel 74		Rpa		Parcel 252
	Parcel 87		HCaN R		Parcel 253
	Parcel 88		MD R		Parcel 262
	Parcel 91		Pul R		Parcel 266
	Parcel 92		SC R		Parcel 271
	Parcel 95		PPN/CnF R		Parcel 275
	Parcel 100		Gi R	**Cb R**	HVIIb R
	Parcel 106				HIX R
	Parcel 107				
	Parcel 110				

	Parcel 113
	Parcel 155
Cb L	Cr I L
	HVI L
	HVIIb L
	HIX L

Nodes are ordered according to their position in the connectivity matrix. Numerated parcel correspond to the cortical parcels of the DAN, described by Gordon and colleagues (2016). Cb, cerebellum; CnF, cuneiform nucleus; Cr I, cerebellar crus I lobule; Gi, gigantocellular nucleus; HCaN, head of caudate nucleus; HVI, cerebellar lobule VI; HVIIb, cerebellar lobule VIIb; HIX, cerebellar lobule IX; IPN, interpeduncular nucleus; L, left; MD, medial dorsal nucleus of the thalamus; PPN, pedunculopontine nucleus; Pul, pulvinar; R, right; Rpa, raphe pallidus nucleus; SC, superior colliculus.

The cortical regions of the VAN were connected by the third branch of the Superior Longitudinal Fasciculus and by the uncinate fasciculus (Figure 33A). Fronto-pulvinar and tecto-pulvinar projections established the connections with or between subcortical structures (Figure 33A).

The node-to-node structural and functional connectivity patterns are represented in Figure 33B.

The maps of the VAN ROIs and of the structural connectivity analysis are available at https://neurovault.org/collections/XONZLGPJ/.

Structural and functional connectivity of DAN nodes

The structural connectivity map of the DAN is represented in Figure 33C.

The cortical regions of the DAN established connections through the first branch of the Superior Longitudinal Fasciculus (Figure 33C). Fronto-pulvinar, parieto-pulvinar and tecto-pulvinar projections mediated the links with or between subcortical structures (Figure 33C).

The node-to-node structural and functional connectivity patterns are shown in the figure 33D.

The maps of the DAN ROIs and of the structural connectivity analysis are available at https://neurovault.org/collections/XONZLGPJ/.

Graph theory analysis

Figure 34 illustrates the graph theory representation of the VAN and DAN structural connectivity.

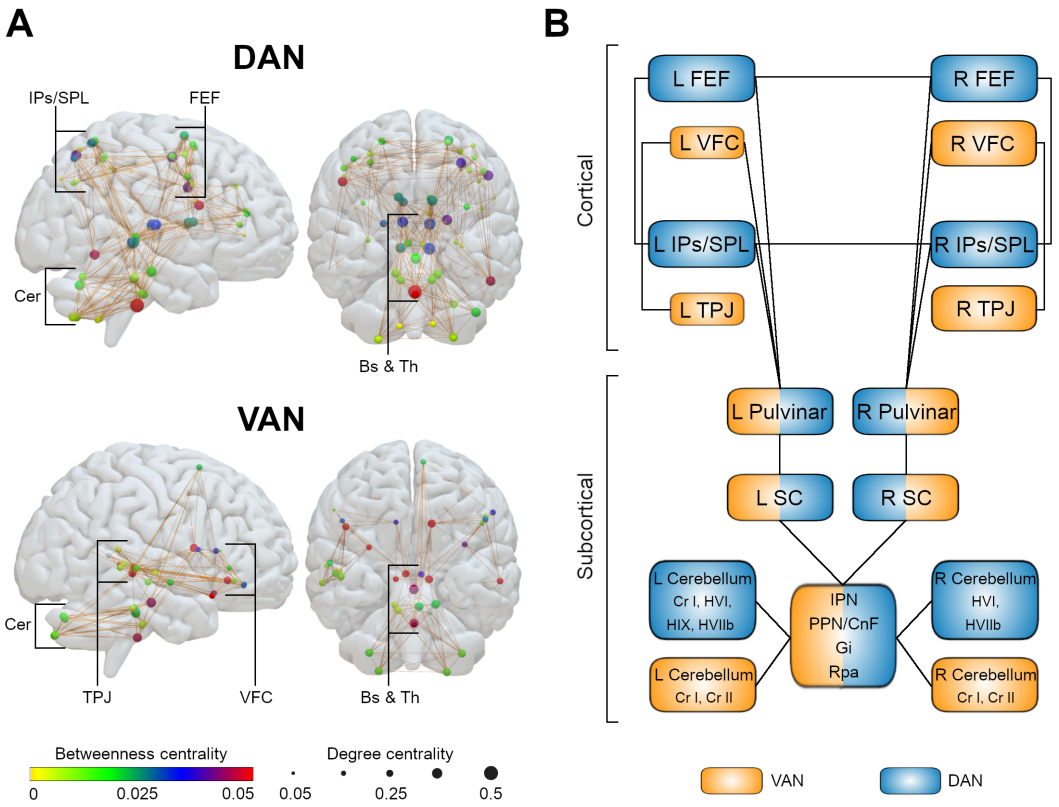

Figure 34. A - Graph theory analysis of the VAN and DAN structural connectivity. Circles illustrate nodes. Circle colours represent the median betweenness centrality of each node (according to the colour gradient), while circle dimension represent the median degree centrality. Brown lines represent node-to-node structural connections that were presented in at least half of the subjects. B – Anatomical model of the VAN and DAN. CnF, cuneiform nucleus; DAN, dorsal attention network; Gi, gigantocellular nucleus; HCaN, head of caudate nucleus; IPN, interpeduncular nucleus; MnR, median raphe nucleus; MD, medial dorsal nucleus of the thalamus; PnO, nucleus pontis oralis; PPN, pedunculopontine

nucleus; Pul, pulvinar; Rpa, raphe pallidus nucleus; SC, superior colliculus; VAN, ventral attention network.

In the VAN, the subcortical structures with the highest median betweenness centrality were the right pulvinar and the left caudate nucleus head (the second and the third highest of all nodes, respectively) and the ones with the highest median degree centrality were the interpeduncular nucleus and the left pedunculopontine-cuneiform nuclei complex (the first and the second highest of all nodes, respectively).

In the DAN, the subcortical structures with the highest median betweenness centrality were the raphe pallidus nucleus and the right mediodorsal nucleus of the thalamus (the first and the seventh highest of all nodes, respectively) and the ones with the highest median degree centrality were the raphe pallidus nucleus and the left superior colliculus (the first and the second highest of all nodes, respectively).

Overall, the subcortical structures had high centrality values in both networks. The betweenness centrality and degree centrality values of all nodes in the VAN and in the DAN are detailed in Tables 23 and 24.

Table 23. Centrality measures of the VAN nodes

Node	Betweenness centrality	Degree centrality	Node	Betweenness centrality	Degree centrality
Parcel 62	0.102	0.23	**Cr I R**	0.014	0.28
Pul R	0.085	0.26	**Parcel 231**	0.013	0.26
HCaN L	0.070	0.28	**Cr II L**	0.012	0.28
SC L	0.069	0.28	**Parcel 237**	0.012	0.10
Parcel 242	0.067	0.26	**Cr I L**	0.011	0.28
Parcel 243	0.051	0.21	**Cr II R**	0.011	0.28
SC R	0.050	0.21	**Parcel 333**	0.010	0.23
Rpa	0.046	0.31	**Parcel 85**	0.010	0.18
IPN	0.045	0.33	**Parcel 222**	0.006	0.23

Parcel 80	0.042	0.21	**Parcel 229**	0.005	0.23
HCaN R	0.036	0.18	**Gi R**	0.004	0.26
Parcel 75	0.036	0.21	**PPN/CnF R**	0.004	0.23
Pul L	0.034	0.23	**Parcel 226**	0.003	0.21
Parcel 241	0.029	0.18	**Parcel 228**	0.003	0.21
Parcel 79	0.028	0.21	**Gi L**	0.000	0.18
MnR	0.021	0.31	**Parcel 158**	0.000	0.05
Parcel 23	0.020	0.21	**Parcel 161**	0.000	0.10
Parcel 332	0.020	0.23	**Parcel 221**	0.000	0.18
PPN/CnF L	0.020	0.31	**Parcel 60**	0.000	0.05
Parcel 86	0.015	0.18	**Parcel 61**	0.000	0.05

Nodes are ordered according to their betweenness centrality value. Numerated parcel correspond to the cortical parcels of the VAN, described by Gordon and colleagues (2016). CnF, cuneiform nucleus; Cr I, cerebellar crus I lobule; Cr II, cerebellar crus II lobule; Gi, gigantocellular nucleus; HCaN, head of caudate nucleus; IPN, interpeduncular nucleus; L, left; MnR, median raphe nucleus; PnO, nucleus pontis oralis; PPN, pedunculopontine nucleus; Pul, pulvinar; R, right; Rpa, raphe pallidus nucleus; SC, superior colliculus.

Table 24. Centrality measures of the DAN nodes.

Node	Betweenness centrality	Degree centrality	Node	Betweenness centrality	Degree centrality
Rpa	0.056	0.47	**Parcel 74**	0.010	0.22
Parcel 275	0.049	0.33	**PPN/CnF L**	0.009	0.31
Parcel 100	0.046	0.33	**Parcel 253**	0.009	0.18
Parcel 87	0.041	0.35	**HVI L**	0.009	0.27
Parcel 106	0.041	0.35	**Parcel 110**	0.009	0.20

Parcel 41	0.038	0.35	**Gi L**	0.009	0.29
MD R	0.032	0.37	**Gi R**	0.008	0.27
SC L	0.031	0.41	**PPN/CnF R**	0.007	0.29
MD L	0.030	0.39	**Parcel 42**	0.007	0.22
Parcel 252	0.028	0.25	**Parcel 199**	0.007	0.22
Parcel 189	0.026	0.31	**HVIIb L**	0.006	0.31
SC R	0.025	0.35	**Parcel 107**	0.006	0.20
Cd L	0.025	0.35	**Parcel 155**	0.006	0.18
Cd R	0.025	0.31	**Parcel 88**	0.005	0.18
Parcel 49	0.023	0.31	**HVIIb R**	0.005	0.29
Cr I L	0.019	0.33	**Pul L**	0.005	0.22
Parcel 236	0.017	0.22	**Parcel 250**	0.004	0.14
Parcel 51	0.016	0.24	**Parcel 113**	0.003	0.16
IPN	0.015	0.35	**Parcel 52**	0.003	0.14
Pul R	0.015	0.27	**Parcel 92**	0.003	0.18
Parcel 208	0.014	0.25	**HIX L**	0.002	0.24
Parcel 91	0.013	0.27	**Parcel 95**	0.002	0.14
Parcel 262	0.013	0.18	**HIX R**	0.002	0.22
Parcel 43	0.012	0.24	**Parcel 55**	0.002	0.10
Parcel 271	0.011	0.24	**Parcel 211**	0.001	0.10
Parcel 203	0.011	0.24	**Parcel 266**	0.000	0.06

Nodes are ordered according to their betweenness centrality value. Numerated parcel correspond to the cortical parcels of the VAN, described by Gordon and colleagues (2016). CnF, cuneiform nucleus; Cr I, cerebellar crus I lobule; Gi, gigantocellular nucleus; HCaN, head of caudate nucleus; HVI, cerebellar lobule VI; HVIIb, cerebellar lobule VIIb; HIX,

cerebellar lobule IX; IPN, interpeduncular nucleus; L, left; MD, medial dorsal nucleus of the thalamus; PPN, pedunculopontine nucleus; Pul, pulvinar; R, right; Rpa, raphe pallidus nucleus; SC, superior colliculus.

Correlation with the neurotransmitter system

The brainstem nuclei identified in the VAN anatomical map that synthetize neurotransmitters are the pedunculopontine nuclei (cholinergic, glutamatergic and GABAergic; Benarroch 2013), the cuneiform nuclei (glutamatergic and GABAergic; Chang et al. 2020), the gigantocellular nucleus (glutamatergic and GABAergic; Martin et al. 2011), the median raphe nucleus (serotoninergic; Van De Kar and Lorens 1979) and the raphe pallidus nucleus (serotoninergic; Heym et al. 1982).

The spatial correlations of these VAN brainstem nuclei structural projections with the neurotransmitter systems are represented in figure 35A. The highest spatial correlations (figure 35B) were with the distribution of the acetylcholine alpha-4 beta-2 nicotinic receptors (Spearman's $r=0.23$, $p<0.001$; PET derived map from Hillmer et al. 2016) and with the distribution of the dopamine transporters (Spearman's $r=0.20$, $p<0.001$, SPECT derived map from Dukart et al. 2018; Spearman's $r=0.17$, $p<0.001$, PET derived map from Sasaki et al. 2012). There was also a positive spatial correlation with the distribution of the vesicular acetylcholine transporters (Spearman's $r=0.16$, $p<0.001$, PET derived map from Bedard et al. 2019; Spearman's $r=0.13$,$p<0.001$, PET derived map from Tuominen and Guimond; Spearman's $r=0.05$, $p<0.001$, PET derived map from Aghourian et al. 2017) and with the distribution of fluorodopa uptake (Spearman's $r=0.08$, $p<0.001$, PET derived map from Gómez et al. 2015).

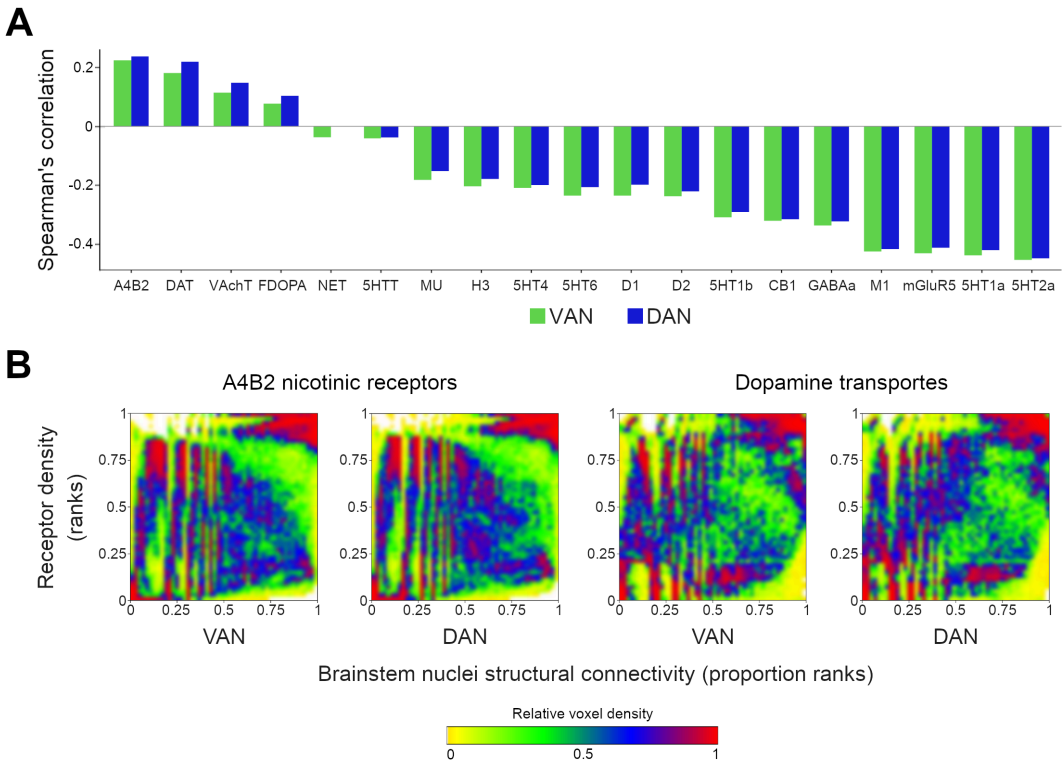

Figure 35. Correlation between the structural projections of the brainstem nuclei and the neurotransmitter systems. A - Spearman's correlation with the available maps of neurotransmitter receptors and transporters; for the receptors or transporters with two or more maps available, the mean correlation was calculated. B - Graphical representation of the highest correlations, i.e. with the acetylcholine alpha-4 beta-2 nicotinic receptor map (top) and with the dopamine transporter map (bottom). The colourmap represents the relative voxel density at each point of the graph. 5HT1a, serotonin 1a receptors; 5HT1b, serotonin 1b receptors; 5HT2a, serotonin 2a receptors; 5HTT, serotonin transporters; A4B2, acetylcholine alpha-4 beta-2 nicotinic receptors; CB1, cannabinoid receptors 1; D1, dopamine receptors 1; D2, dopamine receptors 2; DAT, dopamine transporters; FDOPA, fluorodopa; GABAa, GABAa receptors; H3, histamine receptors 3; M1, muscarinic receptors 1; mGluR5, metabotropic glutamate receptors 5; MU, mu-opioid receptors; NET, norepinephrine transporters; VAchT, vesicular acetylcholine transporters.

The brainstem nuclei identified in the DAN anatomical map that synthetize neurotransmitters are the pedunculopontine nuclei, the cuneiform nuclei, the gigantocellular nucleus and the raphe pallidus nucleus (corresponding neurotransmitters and references stated in the first paragraph of this section).

The highest spatial correlations of these DAN brainstem nuclei (figure 35) projections were also with the distribution of the acetylcholine alpha-4 beta-2 nicotinic receptors (Spearman's r=0.24, p<0.001; PET derived map from Hillmer et al. 2016) and with the distribution of the dopamine transporters (Spearman's r=0.23, p<0.001, SPECT derived map from Dukart et al. 2018; Spearman's r=0.21, p<0.001, PET derived map from Sasaki et al. 2012). There was also a positive spatial correlation with distribution of the vesicular acetylcholine transporters (Spearman's r=0.19, p<0.001, PET derived map from Bedard et al. 2019; Spearman's r=0.17,p<0.001, PET derived map from Tuominen and Guimond; Spearman's r=0.08, p<0.001, PET derived map from Aghourian et al. 2017) and with the distribution of fluorodopa uptake (Spearman's r=0.10 , p<0.001, PET derived map from Gómez et al. 2015).

Discussion

In this study, we reexamined the neuroanatomy of the VAN and of the DAN by co-registering individual network maps in a common functional space. Based on the convergence of functional, structural and neurochemical findings, we propose an optimized model of these networks. First, we confirmed the initial hypothesis that subcortical structures, namely the pulvinar, the superior colliculi, the head of caudate nuclei and a group of brainstem nuclei are constituent elements of the attentional networks. Second, we characterized the structural connections underlying functional connectivity. Deep brain nuclei are densely connected and proved to be structural network hubs. Third, we showed that the identified brainstem nuclei projections are spatially correlated with the distribution of the acetylcholine alpha-4 beta-2 nicotinic receptors and of the dopamine transporters.

Pulvinar is a high order thalamic relay nucleus, participating in cortico-thalamo-cortical circuits that modulate information processing (Sherman 2007). Citoarchitectonically, it is divided into four regions: the anterior pulvinar, the inferior pulvinar, the medial pulvinar and the lateral pulvinar (Stepniewska and Kaas 1997). The medial pulvinar is particularly important in the establishment of connections with heteromodal association areas, such as the superior and inferior temporal, the inferior parietal, the dorsolateral prefrontal and the orbitofrontal cortices (Bridge et al. 2016). In our model, the pulvinar regions with highest statistical association were medial and we demonstrated that they were structurally connected with VAN cortical areas, through fronto-pulvinar projections, and with DAN

cortical areas, by fronto-pulvinar and parieto-pulvinar projections (Bos and Benevento 1975; DeVito 1978; Lemaire et al. 2011).

As previously stated, pulvinar lesions may provoke hemispatial attention deficits (Karnath et al. 2002). Decades ago, Sprague impressively found that lesion-provoked hemispatial neglect in cats was attenuated by removing the contralateral superior colliculus (Sprague 1966; Krauzlis et al. 2013). This effect was later observed in humans (Weddell 2004). In our model, the pulvinar established connections with the superior colliculi through tecto-pulvinar fibres (Luppino et al. 1988), reinforcing the involvement of pulvinar - superior colliculus interactions in attention processes.

The so-called Sprague effect is in part mediated by the pedunculopontine nuclei (Durmer and Rosenquist 2001; Valero-Cabré et al. 2020), which is one of the brainstem nuclei included in our model. The pedunculopontine nuclei posses a population of cholinergic neurons in their caudal portion that give rise to a distinctive network that regulate attentional states and enhance the processing of salient stimuli (Mena-Segovia and Bolam 2017). The descending projections from these cholinergic neurons innervate the nucleus pontis oralis (Mena-Segovia et al. 2008) and the gigantocellular nuclei (Martinez-Gonzalez et al. 2014), while their dorsal ascending projections innervate the colliculi (Jeon et al. 1993; Motts and Schofield 2009) and several nuclei of the thalamus, including the pulvinar and the mediodorsal nuclei (Steriade et al. 1988). The pattern of the pedunculopontine projections closely matches the brainstem and thalamic map evidenced in our analysis.

The proposed relationship between the subcortical nuclei of the attention networks and the acetylcholinergic system was reinforced by the neurotransmitter system correlation analysis. The highest spatial correlation of both networks was with the acetylcholine alpha-4 beta-2 nicotinic receptors and both were also spatially correlated with the distribution of the vesicular acetylcholine transporters. The acetylcholine alpha-4 beta-2 nicotinic receptors have a well-established relationship with sustained attention processes. Acetylcholine alpha-4 beta-2 nicotinic receptors agonists reduce distractibility of adult monkeys during the performance of matching-to-sample tasks with distractors (Prendergast et al. 1998) and increase the firing rate of dorsolateral prefrontal neurons during sustained attention tasks, an effect that is reversed by the co-administration of receptor antagonists (Sun et al. 2017). In humans, transdermal nicotine administration improves attentiveness (Levin et al. 1998; Valentine and Sofuoglu 2017).

The projections of the VAN and DAN brainstem nuclei were also spatially correlated with the distribution of the dopamine transporters and fluorodopa uptake. This finding is consistent with the psychopharmacological knowledge about attention. Methylphenidate is the first-line treatment for attention deficit hyperactivity disorder (Cortese et al. 2018). Pharmacologically, it is a noradrenaline-dopamine reuptake inhibitor, with higher potency for dopamine transporters (Gatley et al. 1996; Faraone 2018). Modafinil is a selective inhibitor of dopamine transporters (Zolkowska et al. 2009) and also produces attention enhancement effects (Turner et al. 2004; Repantis et al. 2010). Further studies are needed to understand how the interplay between the nicotinic acetylcholine and the dopamine systems occurs in attention networks, but it might be mediated by their interaction at the levels of the striatum (Zoli et al. 2002; Exley and Cragg 2008) and midbrain (Blaha and Winn 1993; Forster and Blaha 2003).

The characterization of the subcortical anatomy of attention networks in the human brain fosters the exploration of a common structural-functional attentional framework across species. Attention is far from being a specific cognitive ability of human beings (Washburn and Taglialatela 2006). Species with either close or distant common ancestors in the phylogenetic tree, such as monkeys, rats and pigeons, are able to scan, select and maintain attention in surrounding environmental stimuli (Mackintosh 1965; Blough 1977; Washburn and Taglialatela 2006; Wasserman and Castro 2021). A common subcortical attention framework may surpass the challenge to find the cortical homologues of the human VAN and DAN in other species (Patel et al. 2015).

The subcortical nuclei described in our model probably have different hierarchical and functional roles. First, most of them are shared by the VAN and the DAN, while the cortical regions of these networks are largely segregated (Vossel et al. 2014). Second, certain distinctive attention disorders, such as hemispatial neglect, rarely occur after brainstem lesions (Ringman et al. 2004). Brainstem nuclei are putatively closer linked with more primary components of attention, such as arousal and alertness (Boucetta et al. 2014; Petzold et al. 2015; Cox et al. 2016).

A limitation of our study is the inability to untangle the different roles of and the dynamic interactions between the proposed subcortical structures. While the cortical regions of the DAN and the VAN are quite neatly segregated (Vossel et al. 2014) the subcortical nuclei described in our model probably contributed to both the VAN and the DAN. Future investigations using our model to explore the BOLD signal during task-related fMRI in humans or direct electrical recordings in animals might dissociate the

hierarchical organisation and functional role of subcortical regions better than resting-state fMRI.

In conclusion, this work proposes an improved neuroanatomical model of the VAN and the DAN that includes the pulvinar, the superior colliculi, the head of caudate nuclei and a group of brainstem nuclei interrelated with the acetylcholine nicotinic and with the dopamine transporter systems. This novel framework reconciles behavioural, electrophysiological and psychopharmacological data, and provides a common background to understand the neural basis of attention across different species and brain pathologies.

5. Spatial delusions and acute stroke treatment

Part of this section is included in the following manuscript (submitted):

- Alves PN, Fonseca AC, Pinho-e-Melo T, Martins IP. Novel patterns of stroke neural damage link endovascular thrombectomy to the occurrence of spatial delusions. *Submitted.*

Introduction

Endovascular thrombectomy has markedly changed the paradigm of acute stroke treatment (Powers et al. 2019), leading to better functional outcomes (Badhiwala et al. 2015; Rodrigues et al. 2016), milder neurological deficits (Berkhemer et al. 2015) and smaller infarct volumes (Nogueira et al. 2018). However, the impact of revascularization techniques goes far beyond these global outcome measures.

Behavioural changes are debilitating stroke sequelae (Krakauer and Hillis 2014) and their occurrence is closely linked to specific patterns of damage in strategic brain regions (Weaver et al. 2021) and neural networks (Thiebaut de Schotten et al. 2020). Importantly, endovascular thrombectomy may change the classical distribution of stroke lesions (Puntonet et al. 2019). Catheter manipulations close to vessels' ostia and thrombus fragmentation during extraction may prompt new infarcts in primarily unaffected arterial territories (Puntonet et al. 2019). How these changes interfere with the behavioural neurology of stroke is largely unknown.

Delusions of space, or reduplicative paramnesias, are disturbing right hemisphere syndromes (Pick 1903) that result from a dual stream disconnection of right fronto-thalamic and occipito-temporal fibres (Alves et al. 2021a, b). Recently, we prospectively assessed the presence of this syndrome during the acute phase of right hemisphere stroke and found a prevalence of 23% (Alves et al. 2021a), which was surprisingly high considering previous observations (Murai et al. 1997; Dragicevic and Hoffmann 2015; Stangeland et al. 2018).

Here, we aimed to investigate if the performance of endovascular thrombectomy was associated with the occurrence of reduplicative paramnesia, and if this putative relationship could be explained by novel patterns of lesion and structural disconnection.

Methods

Study sample and design

This research work is a subanalysis of a prospective, cumulative, case-control study that aimed to evaluate the neural basis of spatial delusions after right hemisphere stroke (Alves et al. 2021a). The study was performed from December/2016 to February/2020 in a stroke unit of a university hospital in Lisbon, Portugal. Briefly, we consecutively evaluated 400 patients with right hemispheric ischemic or hemorrhagic strokes, admitted with less than 72 hours of symptoms onset, for the presence of spatial delusions. The screening was

performed during the first 72 hours of admission and then at regular intervals of 48 hours using a structured interview, until patients' discharge (Alves et al. 2021a). The exclusion criteria were: acute confusional state (delirium); decreased level of consciousness; subarachnoid hemorrhage; epileptic seizures during admission; aphasia or severe dysarthria precluding evaluation; severe visual deficit, precluding confrontation with counter-evidence stimuli; history of dementia; absence of a stroke lesion in brain imaging, or unavailable brain images (Alves et al. 2021a).

Of the 297 patients that fulfilled the study criteria, 64 cases of spatial delusions and 233 controls were identified. Additional cases were prospectively included from March/2020 to June/2021 (n=17). For the present case-control analysis, we selected the ischemic stroke patients (cases, n=78; controls, n=212).

Our center follows the standard of care guidelines of stroke treatment (Powers et al. 2019; Turc et al. 2019).

The study was approved by the Ethics Committee of the Lisbon Academic Medical Centre.

Clinical characterization

Demographic and stroke clinical data were collected, namely, age, gender, NIHSS at admission and discharge, stroke vascular territory and acute treatment.

In Lisbon, endovascular thrombectomy is performed by four hospitals, in rotation shifts (including our centre). Inter-hospital transfers are frequent between these centres and with smaller peripheral hospitals. Due to the putative contribution of inter-hospital transfers to the onset of space misinterpretations, this variable was also registered.

Patients solely submitted to arterial puncture and angiography (due to proximal extracranial artery obstruction or unfavourable anatomy, or due to spontaneous recanalization) were included in the no thrombectomy group, because the study hypotheses were based on the putative lesion pattern changes induced by thrombus manipulation and extraction.

Neuroimaging analysis

Stroke lesion delimitation was performed on the diffusion diffusion-weighted imaging sequence of brain MRI (preferentially) or on the brain CT images performed 24-72 hours

after stroke onset (MRI, n=122; CT, n=168). Standard linear and nonlinear transformations were used to normalize lesion mask into the MNI152 space (Jenkinson et al. 2012).

Structural disconnectomes were computed using a tract-wise approach, with the BCBtoolkit's tool *Disconnectome* (Foulon et al. 2018). Each lesion was superimposed on a group of 178 healthy subjects' tractography from the Human Connectome Project 7 Tesla dataset and the voxel-wise probability maps of disconnection were calculated. The voxels disconnected in a least half of tractography maps were included (Thiebaut de Schotten et al. 2020).

Endovascular thrombectomy and reduplicative paramnesia

The bivariate association between endovascular thrombectomy (independent variable) and spatial delusions (dependent variable) was determined with a chi-square test. In the multivariate analysis, a logistic regression was performed including the covariates: age, clinical severity (measured by the NIHSS at admission), vascular territory, inter-hospital transfer and endovenous thrombolysis. These variables were chosen based on clinical and statistical rationale, namely previously demonstrated clinical association and statistical correlation with the dependent and independent variables.

Endovascular thrombectomy and brain structural changes

A voxel-wise logistic regression was performed to analyse the association between endovascular thrombectomy (independent variable) and brain structural changes (lesion or structural disconnection as dependent variable). Clinical severity, stroke vascular territory and endovenous thrombolysis treatment were included as covariates.

Correlation and conjunction analyses

First, we analysed if the voxel-wise reduplicative paramnesia proportion maps were correlated with the endovascular thrombectomy proportion maps, using the neuromaps' tool 'compare_images' (Hansen et al. 2021; https://netneurolab.github.io/neuromaps/). These correlations were compared with the control correlations using *cocor* (Diedenhofen and Musch 2015).

Then, we determined if the endovascular thrombectomy statistical maps spatially overlapped the reduplicative paramnesia disconnection statistical map (available at

https://neurovault.org/collections/DCRSGZBD/; Alves et al. 2021a). Both were converted into z-maps and a conjunction analysis was performed. Significantly shared clusters were identified with a Gaussian Random Field theory approach, using FSL's function *cluster* (Jenkinson et al. 2012).

Statistical significance and software

Alpha levels were set at 0.05 for statistical significance. Stata14® and the python package *statsmodels* (https://www.statsmodels.org/) were used to perform the statistical analysis.

Results

Demographic and clinical features

The detailed descriptive statistics and bivariate analysis of the demographic and clinical features of the cases and controls are available in Table 25. Patients that presented reduplicative paramnesia were older, had higher NIHSS scores at admission, and were subjected to endovascular thrombectomy and interhospital transfer more frequently. There were no significant differences in the NIHSS at hospital discharge and in the frequency of treatment with endovenous thrombolysis.

The detailed descriptive statistics and bivariate analysis about endovascular treatment in cases and controls are available in Table 26. Endovascular thrombectomy was performed in the anterior circulation in most patients (right middle cerebral artery, n=92, 69%; right internal carotid artery, n=40, 30%; basilar artery, n=2, 1%). There was no significant difference between cases and controls in terms of occluded vessels, treated vessel, TICI score, reperfusion technique (stent retriever and/or aspiration), and number of passages.

Table 25. Demographic and clinical features of cases and controls

	Cases (n=78)	**Controls (n=212)**	**p-value**
Age (years-old)	78 [71-83]	69 [59-78]	<0.001
Gender (F/M)	37/41	93/119	0.588
NIHSS admission	16 [13-18]	11 [6-16]	<0.001
NIHSS discharge	4 [1-10]	5 [2-11]	0.308
Vascular territory			0.004
ACA R	0 (0%)	2 (1%)	
AChA R	0 (0%)	1 (0.5%)	
MCA R	61 (78%)	161 (76%)	
MCA RL + PICA	1 (1%)	0 (0%)	
MCA R + ACA R	7 (9%)	6 (3%)	
MCA R + ACA R + PCA R	1 (1%)	7 (3%)	
MCA + AChA R	0 (0%)	1 (0.5%)	
MCA R + PCA R	4 (5%)	3 (1%)	
MCA R + PICA R	0 (0%)	3 (1%)	
PCA R	2 (3%)	26 (12%)	
PCA R + PICA R	0 (0%)	1 (0.5%)	
Basilar artery + PCA R	2 (3%)	0 (0%)	
Basilar artery + PCA RL	0 (0%)	1 (0.5%)	
Endovenous thrombolysis	42 (54%)	133 (63%)	0.170
Endovascular thrombectomy	54 (69%)	80 (38%)	<0.001
Interhospital transfer	44 (56%)	83 (39%)	0.009

ACA, anterior cerebral artery; AChA, anterior choroidal artery; L, left; MCA, middle cerebral artery; PCA, posterior cerebral artery; PICA, posterior inferior cerebellar artery; R, right.

Table 26. Endovascular thrombectomy features of cases and controls.

	Cases (n=54)	**Controls (n=80)**	**p-value**
Occluded intracranial segment			0.248
Basilar artery, top	2 (4%)	0 (0%)	
Internal carotid artery, top	16 (30%)	24 (30%)	
M1	28 (52%)	48 (60%)	
M1 + A2	1 (2%)	0 (0%)	
M1 + A3	1 (2%)	0 (0%)	
M1 + A4	0 (0%)	1 (1%)	
M2	5 (9%)	7 (9%)	
M2 + A1	1 (2%)	0 (0%)	
Treated intracranial segment			0.364
Basilar artery, top	2 (4%)	0 (0%)	
Internal carotid artery, top	16 (30%)	24 (30%)	
M1	30 (56%)	49 (61%)	
M2	5 (9%)	7 (9%)	
M2 + A1	1 (2%)	0 (0%)	
TICI score			0.835
0	5 (9%)	3 (4%)	
1	0 (0%)	1 (1%)	
2a	2 (4%)	2 (3%)	
2b	26 (48%)	16 (20%)	
2c	11 (20%)	9 (11%)	
3	36 (67%)	23 (29%)	
Treatment technique*			0.150
Aspiration	29 (56%)	38 (54%)	
Stent retriever	9 (17%)	21 (30%)	
Aspiration + stent retriever	14 (27%)	11 (16%)	
Number of attempts*	2 [1-4]	2 [1-3]	0.736

* 12 missing values.

Multivariate statistical association

Endovascular thrombectomy was an independent predictor of reduplicative paramnesia in the multivariate analysis (Table 27).

Table 27. Multivariate regression for the occurrence of reduplicative paramnesia (dependent variable).

Independent variables	Odds Ratio	Confidence interval (95%)	p-value
Endovascular thrombectomy	2.46	[1.18, 5.16]	0.017
Endovenous thrombolysis	0.62	[0.34, 1.15]	0.128
NIHSS at admission	1.12	[1.05, 1.19]	<0.001
Age	1.07	[1.04, 1.09]	<0.01
Inter-hospital transfer	0.91	[0.46, 1.78]	0.777
Vascular territory	1.06	[0.30, 3.73]	0.922

The variables endovascular thrombectomy, intravenous thrombolysis, inter-hospital transfer and vascular territory were dichotomous. The dichotomy in vascular territory was between infarct of the middle cerebral artery territory *vs* other territories.

Maps' spatial correlation

Endovascular thrombectomy was associated with lower probabilities of lesion and structural disconnection of frontal, parietal and temporal regions and with higher probabilities in deep subcortical and insular regions (regressing for NIHSS at admission, endovenous thrombolysis and stroke territory; Figure 36).

The lesion proportion map of the patients submitted to endovascular thrombectomy had a significantly higher spatial correlation with the lesion proportion map of cases than controls (Figure 37A; Spearman's r cases=0.96, controls=0.85; $p<0.001$). The same relationship was observed with structural disconnection proportion maps (Figure 37B; Spearman's r cases=0.98, controls=0.94; $p<0.001$).

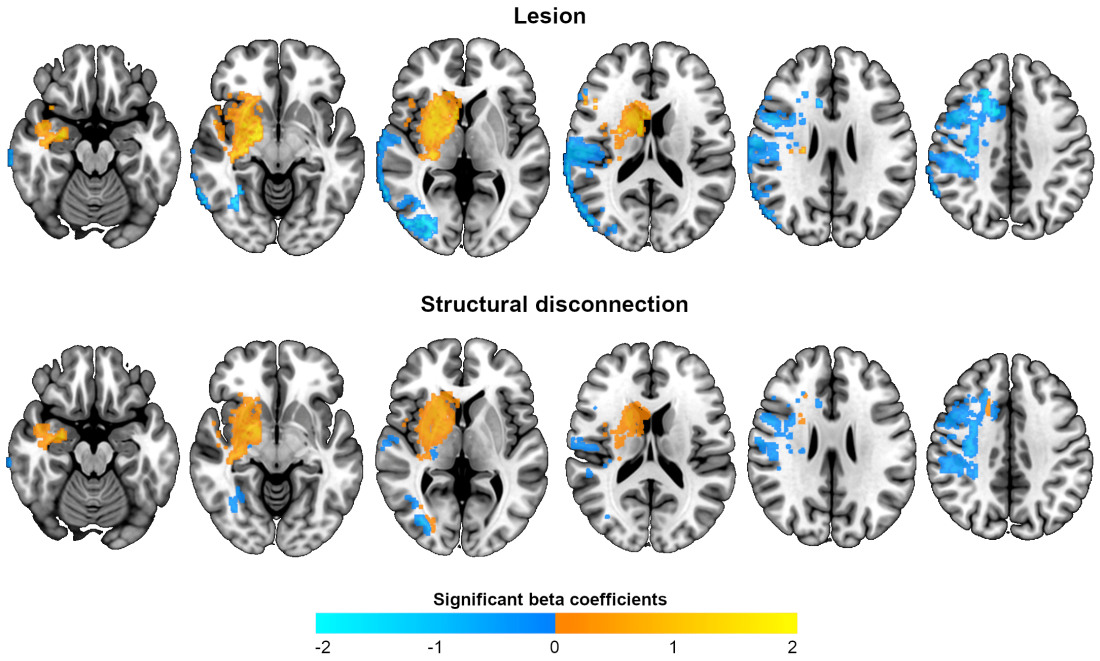

Figure 36. Beta coefficient maps for the association of endovascular thrombectomy with lesion (top) and structural disconnection (bottom), regressing for clinical severity, stroke vascular territory and endovenous thrombolysis treatment. Only the statistically significant voxels are represented.

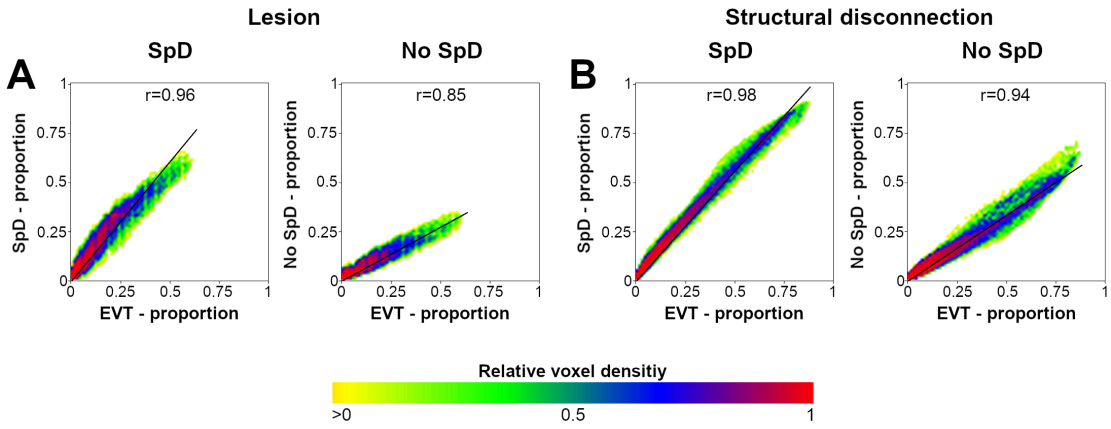

Figure 37. Spatial correlations between the proportion maps of the patients submitted to endovascular thrombectomy and the proportion maps of cases and controls, regarding voxel lesion (A) and voxel structural disconnection (B). EVT, endovascular thrombectomy; r, Spearman's correlation; SpD, spatial delusions.

Shared clusters of lesion and disconnection

The conjunction analysis showed that both the endovascular thrombectomy lesion and structural disconnection maps had significant clusters of intersection with the reduplicative paramnesia disconnection map (Figure 38). The lesion cluster overlapped the anterior limb of the internal capsule and the anterior temporal regions (Figure 38A). The structural disconnection cluster involved thalamo-orbitofrontal and anteroinferior temporal fibres (Figure 38B).

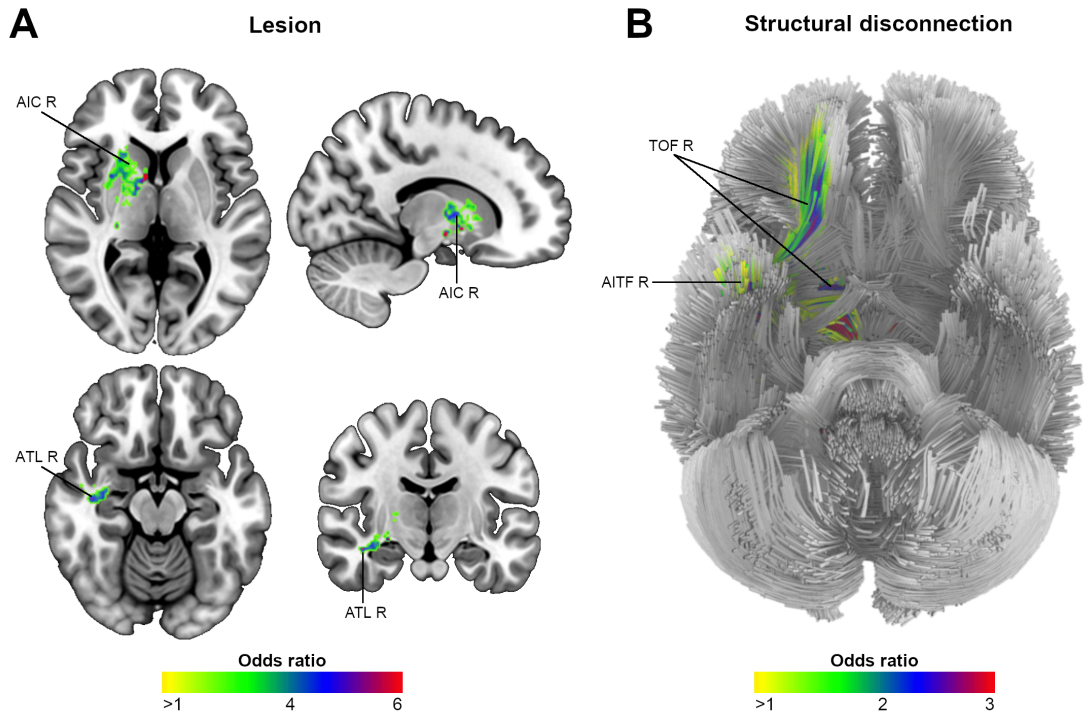

Figure 38. Statistically significant clusters of the conjunction analysis between the structural disconnectome map of reduplicative paramnesia and the endovascular thrombectomy associated lesion maps, regressing for NIHSS at admission, endovenous thrombolysis and stroke territory (A); and between the structural disconnectome map of reduplicative paramnesia with the endovascular thrombectomy associated lesion maps, regressing for the same variables (B). The colourmaps represent odds ratios. AIC, anterior limb of the internal capsule; AITF, anteroinferior temporal fibres; ATL, anterior temporal lobe; R, right; TOF, thalamo-orbitofrontal fibres.

Discussion

In this study, we demonstrated an association between the occurrence of spatial delusions and the performance of endovascular thrombectomy after right hemisphere stroke. We showed the existence of shared clusters of lesion and structural disconnection, which overlapped the anterior limb of the internal capsule, disrupting thalamo-orbitofrontal fibres, and anterior temporal regions.

Most of the arterial ostia supplying these anatomical regions emerge from the M1 segment of the middle cerebral artery. The internal capsule anterior limb receives blood supply from perforating lenticulostriate arteries, which variably arise from the anterior and the middle cerebral arteries (Shapiro et al. 2020). The anterior temporal region is irrigated by the anterior temporal and temporopolar arteries, which most frequently emerge before middle cerebral artery bifurcation (Tanriover et al. 2003).

Proximal middle cerebral artery branches seem to be particularly prone to ischemia in endovascular thrombectomy. Nearly half of new territory infarcts are associated with catheter manipulation past arterial ostia (Kaesmacher et al. 2020) and more than one fifth of patients submitted to middle cerebral artery thrombectomy have lenticulostriate infarcts proximal to the occluded segment, in arteries that were permeable before the recanalization (Kleine et al. 2017).

As limitation, this work was performed in a tertiary stroke unit and may not be representative of the entire stroke population.

Despite the undoubted effectiveness of endovascular thrombectomy, it may condition new patterns of lesion and putatively modulate the behavioural neurology of stroke. Our work demonstrates how it affects the occurrence of spatial delusions after right hemisphere stroke.

IV. General discussion and conclusions

In this thesis, we investigated the neurology of stroke-associated spatial delusions. We analysed their clinical presentation and neural basis, studied the neuroanatomy of putatively related multimodal integrative functional networks, and explored their association with endovascular thrombectomy.

Clinical phenomenology of spatial delusions

Our results show that spatial delusions have characteristic patterns of presentation. The places of mislocation typically are affectively relevant and most patients localize them closer to their home than to the hospital (studies 1 and 2). The abnormal modulation of place-emotion binding putatively leads to an adaptive behaviour of mislocation to a psychologically more pleasant place (Paterson and Zangwill 1944; Ovelacg et al. 1988).

The time duration of stroke-associated spatial delusions is generally short (study 2). This feature is shared with other right hemisphere disconnection syndromes involving belief and reality monitoring disturbances, such as anosognosia for hemiplegia (Vocat et al. 2010; Pacella et al. 2019). We showed that their duration was moderately correlated with the magnitude of structural-functional decoupling of belief-related networks. Inferior temporal fibres were the major drivers of this relationship. Left hemisphere disconnection may contribute to syndrome prolongation by further unleashing false explanations (Devinsky 2009).

Most patients maintain a correct semantic knowledge about hospital location and orientation in time, and nearly half were able to describe spatial routes mentally (study 2). This evidence highlights the specificity of the syndrome to place-related misinterpretation.

Confabulatory mislocation is the most frequent delusion subtype after stroke, followed by place reduplication and chimeric assimilation (study 2). Although these three clinical subtypes represent different poles of pathological familiarity for space (Devinsky 2009), case clustering based on structural decoupling of familiar and unfamiliar-associated functional networks poorly matched clinical categorization. We provided a comprehensive description of the patients' response patterns according to the spatial delusion subtype. Representative examples were reported, which may facilitate the clinical diagnosis of the syndrome.

Neural basis of spatial delusions

We showed that delusions of space after stroke are associated with structural disconnection of right thalamo-orbitofrontal and right occipito-temporal fibres (study 3). This dual-stream pattern of disconnection putatively constitutes the two-hit model neurobiological basis (Coltheart et al. 2011).

The orbitofrontal cortex and the anterior temporal lobe compose the temporo-amygdala-orbitofrontal division of the limbic system. They are fundamental for cognitive-emotional integration (Catani et al. 2013) and participate in evaluating false beliefs, reality monitoring and attribution of proper familiarity values to visual stimuli (Petrides et al. 2002; Hartwright et al. 2012; Kandylaki et al. 2015; Simons et al. 2017). Notably, the activity of the temporo-amygdala-orbitofrontal system is modulated by thalamic nuclei (Romanski et al. 1997; Child and Benarroch 2013; Arcaro et al. 2018). We propose that fronto-thalamic disconnection might cause an imbalance of the temporo-amygdala-orbitofrontal system.

The occipito-temporal pathways are critical in visual environmental perception and allocentric positioning (Epstein and Kanwisher 1998; Evensmoen et al. 2021). A proper implicit spatial interpretation depends on integrating place-related information with the belief and familiarity limbic networks. We propose that disconnection of the occipito-temporal pathways might cause an abnormal interaction between place-related networks and the limbic temporo-amygdala-orbifrontal system, leading to disturbed covert identifications of spatial stimuli.

The dual-stream pattern of structural disconnection matches the results obtained in the analysis of cases reported in the literature (study 1). The spatial delusions-associated structural changes mediate functional decoupling of the belief, familiarity and place networks (study 1), further supporting the temporo-orbitofrontal limbic disconnection model.

Subcortical anatomy of multimodal integrative functional networks

In studies 4.1 and 4.2, we unveiled the subcortical anatomy of multimodal integrative functional networks, namely the default mode network and the ventral and dorsal attention networks.

We found that basal forebrain nuclei and the anterior and mediodorsal thalamic nuclei integrate the default mode network (study 4.1). The proposed configuration matches the

unitary model of the limbic system (MacLean 1949; Yakovlev and Locke 1961). The default mode network works as a transmodal integrator of semantic, episodic and autobiographical memory with emotion and social cognition (Margulies et al. 2016). The identified deep brain nuclei are the probable mediators of this function at the subcortical level.

In addition, we demonstrated that the pulvinar, the superior colliculi, the head of caudate nuclei and a cluster of brainstem nuclei incorporate the ventral and dorsal attention networks (study 4.2). Neurochemically, our results reveal that their brainstem nuclei projections are spatially correlated with the acetylcholine nicotinic and dopamine transporter systems. Along with the cortical structures of the attention networks, we propose that this subcortical circuits take part in the prioritization of relevant sensory inputs and in the selection of external information according to internal goals and expectations (Corbetta and Shulman 2002; Petersen and Posner 2012).

The cortico-subcortical structural connections of the default mode network and the ventral attention network include thalamic connections with ventral regions of the frontal lobe (studies 4.1 and 4.2), raising the hypothesis of a common connectivity background between these networks and spatial delusions. Further studies would be important to endorse this hypothesis by contrasting resting-state connectivity during spatial delusions and after their resolution.

Association of spatial delusions with endovascular thrombectomy

In study 5, we established an association between the occurrence of spatial delusions after stroke and the performance of endovascular thrombectomy. Despite the remarkable benefits of endovascular thrombectomy for ameliorating the neurological sequela of stroke, thrombus manipulation and extraction may change the classical pattern of stroke neural damage (Kleine et al. 2017; Puntonet et al. 2019). Our results show that endovascular thrombectomy shares anatomical clusters of higher lesion probability with the structural disconnectome map of spatial delusions. This relationship occurred at the anterior limb of the internal capsule, disrupting thalamo-orbitofrontal fibres, and at anterior temporal regions. Perforating lenticulostriate arteries and the anterior temporal and temporo-polar arteries irrigate these regions. They commonly arise from the middle cerebral artery's proximal segment and seem to be particularly vulnerable to post-procedure ischemia (Kleine et al. 2017).

Figures 39 and 40 illustrate the main findings and interpretations of this thesis.

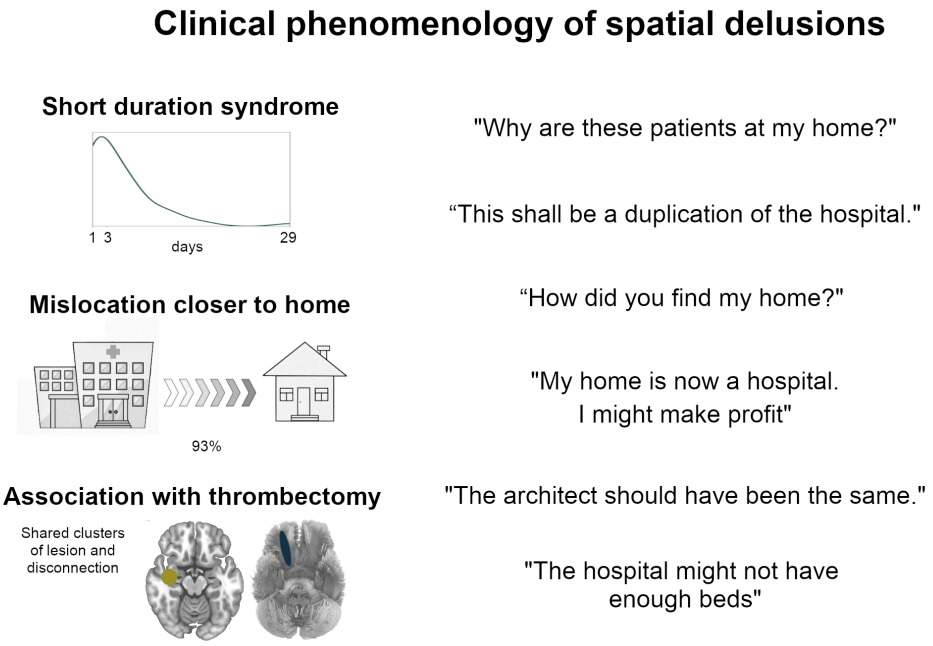

Figure 39. Summary of the clinical and phenomenological features of spatial delusions after stroke.

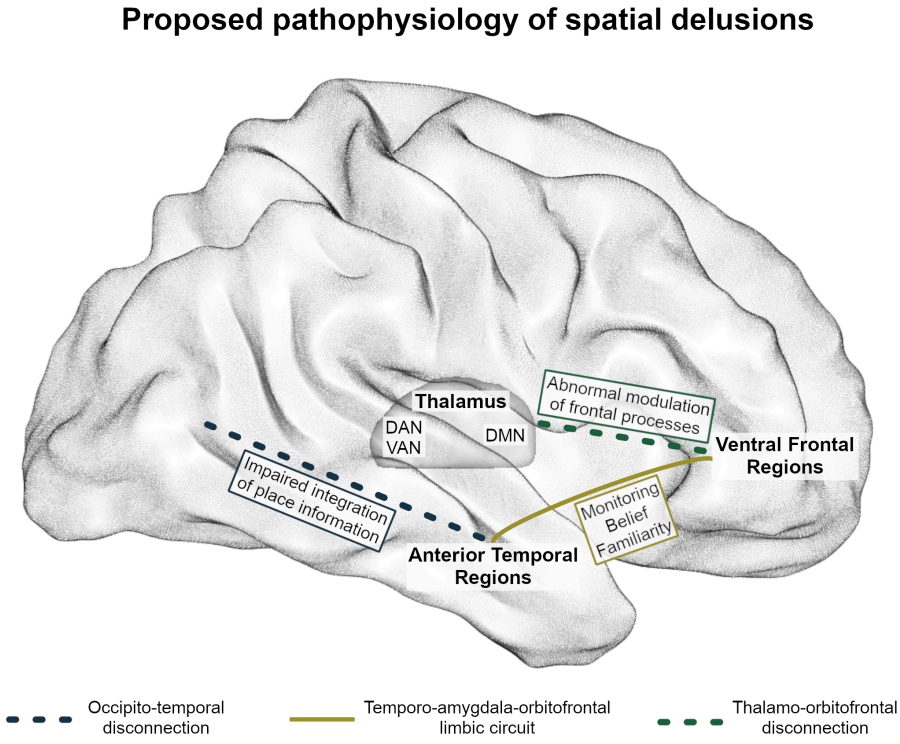

Figure 40. Illustration of the proposed pathophysiology of spatial delusions. DAN, dorsal attention network; DMN, default mode network; VAN, ventral attention network.

In conclusion, our results provide a more comprehensive understanding of the clinical and phenomenological features of stroke-associated spatial delusions, which may foster the awareness and the proper diagnosis of the syndrome. The novel knowledge about stroke-associated spatial delusions neural basis may contribute to disentangling the pathophysiology of delusional misidentifications and spatial misinterpretation disorders.

References

Aggleton J (2000) The Amygdala: A Functional Analysis, 2nd edn. Oxford University Press, New York

Aggleton JP (2008) Understanding anterograde amnesia: Disconnections and hidden lesions. Q J Exp Psychol 61:1441–1471. https://doi.org/10.1080/17470210802215335

Aggleton JP, Pralus A, Nelson AJD, Hornberger M (2016) Thalamic pathology and memory loss in early Alzheimer's disease: Moving the focus from the medial temporal lobe to Papez circuit. Brain 139:1877–1890. https://doi.org/10.1093/brain/aww083

Aghourian M, Legault-Denis C, Soucy JP, et al (2017) Quantification of brain cholinergic denervation in Alzheimer's disease using PET imaging with [18F]-FEOBV. Mol Psychiatry 22:1531–1538. https://doi.org/10.1038/mp.2017.183

Aguirre GK, D'Esposito M (1999) Topographical disorientation: a synthesis and taxonomy. Brain 122:1613–1628. https://doi.org/10.1093/brain/122.9.1613

Aimard G, Vighetto A, Confavreux C, Devic M (1981) Spatial disorientation. Report of 5 cases. Rev Neurol 137:97–111

Alcalá-López D, Smallwood J, Jefferies E, et al (2017) Computing the Social Brain Connectome Across Systems and States. Cereb Cortex 1–26. https://doi.org/10.1093/cercor/bhx121

Alderson-Day B, Diederen K, Fernyhough C, et al (2016) Auditory hallucinations and the Brain's resting-state networks: findings and methodological observations. Schizophr Bull 42:1110–1123. https://doi.org/10.1093/schbul/sbw078

Alves PN, Fonseca AC, Silva DP, et al (2021a) Unravelling the neural basis of spatial delusions after stroke. Ann Neurol 89:1181–1194. https://doi.org/10.1002/ana.26079

Alves PN, Foulon C, Karolis V, et al (2019) An improved neuroanatomical model of the default-mode network reconciles previous neuroimaging and neuropathological findings. Commun Biol 2:370. https://doi.org/10.1038/s42003-019-0611-3

Alves PN, Silva DP, Fonseca AC, Martins IP (2021b) Mapping delusions of space onto a structural disconnectome that decouples familiarity and place networks. Cortex 146:250–260. https://doi.org/10.1016/j.cortex.2021.11.008

Amunts K, Kedo O, Kindler M, et al (2005) Cytoarchitectonic mapping of the human amygdala, hippocampal region and entorhinal cortex: Intersubject variability and

probability maps. Anat Embryol (Berl) 210:343–352. https://doi.org/10.1007/s00429-005-0025-5

Amunts K, Schleicher A, Bürgel U, et al (1999) Broca's region revisited: Cytoarchitecture and intersubject variability. J Comp Neurol 412:319–341. https://doi.org/10.1002/(SICI)1096-9861(19990920)412:2<319::AID-CNE10>3.0.CO;2-7

Andersson JLR, Skare S, Ashburner J (2003) How to correct susceptibility distortions in spin-echo echo-planar images: Application to diffusion tensor imaging. Neuroimage 20:870–888. https://doi.org/10.1016/S1053-8119(03)00336-7

Andre JM, Beis JM, Morin N, Paysant J (2000) Buccal hemineglect. Arch Neurol 57:1734–1741. https://doi.org/10.1001/archneur.57.12.1734

Andrews-Hanna JR, Reidler JS, Sepulcre J, et al (2010) Functional-Anatomic Fractionation of the Brain's Default Network. Neuron 65:550–562. https://doi.org/10.1016/j.neuron.2010.02.005

Angelaki DE, Cullen KE (2008) Vestibular system: the many facets of a multimodal sense. Annu Rev Neurosci 31:125–150. https://doi.org/10.1146/annurev.neuro.31.060407.125555

Arcaro MJ, Pinsk MA, Chen J, Kastner S (2018) Organizing principles of pulvino-cortical functional coupling in humans. Nat Commun 9:1–14. https://doi.org/10.1038/s41467-018-07725-6

Aston-Jones G, Rajkowski J, Cohen J (1999) Role of locus coeruleus in attention and behavioral flexibility. Biol Psychiatry 46:1309–1320. https://doi.org/10.1016/S0006-3223(99)00140-7

Avants B, Gee JC (2004) Geodesic estimation for large deformation anatomical shape averaging and interpolation. Neuroimage 23:139–150. https://doi.org/10.1016/j.neuroimage.2004.07.010

Avants BB, Epstein CL, Grossman M, Gee JC (2008) Symmetric diffeomorphic image registration with cross-correlation: Evaluating automated labeling of elderly and neurodegenerative brain. Med Image Anal 12:26–41. https://doi.org/10.1016/j.media.2007.06.004

Avants BB, Tustison NJ, Song G, et al (2011) A reproducible evaluation of ANTs similarity metric performance in brain image registration. Neuroimage 54:2033–2044. https://doi.org/10.1016/j.neuroimage.2010.09.025

Avants BB, Yushkevich P, Pluta J, et al (2010) The optimal template effect in

hippocampus studies of diseased populations. Neuroimage 49:2457–2466. https://doi.org/10.1016/j.neuroimage.2009.09.062

Badhiwala JH, Nassiri F, Alhazzani W, et al (2015) Endovascular thrombectomy for acute ischemic stroke ameta-analysis. JAMA - J Am Med Assoc 314:1832–1843. https://doi.org/10.1001/jama.2015.13767

Badre D, Wagner AD (2004) Selection, Integration, and Conflict Monitoring. Neuron 41:473–487. https://doi.org/10.1016/s0896-6273(03)00851-1

Balak N, Balkuv E, Karadag A, et al (2018) Mammillothalamic and Mammillotegmental Tracts as New Targets for Dementia and Epilepsy Treatment. World Neurosurg 110:133–144. https://doi.org/10.1016/j.wneu.2017.10.168

Barahona-Corrêa JB, Cotovio G, Costa RM, et al (2020) Right-sided brain lesions predominate among patients with lesional mania: evidence from a systematic review and pooled lesion analysis. Transl Psychiatry 10:. https://doi.org/10.1038/s41398-020-0811-0

Barbay M, Taillia H, Nédélec-Ciceri C, et al (2018) Prevalence of poststroke neurocognitive disorders using national institute of neurological disorders and stroke-Canadian stroke network, VASCOG criteria (Vascular Behavioral and Cognitive Disorders), and optimized criteria of cognitive deficit. Stroke 49:1141–1147. https://doi.org/10.1161/STROKEAHA.117.018889

Bartolomeo P, Vito S De, Seidel T (2016) Space-related confabulations after right hemisphere damage. Cortex 87:166–173. https://doi.org/10.1016/j.cortex.2016.07.007

Bates E, Wilson SM, Saygin AP, et al (2003) Voxel-based lesion–symptom mapping. Nat Neurosci 11–12

Bauer RM (1982) Visual Hypoemotionality as a Symptom of Visual-Limbic Disconnection in Man. Arch Neurol 39:702–708. https://doi.org/10.1001/archneur.1982.00510230028009

Baum GL, Cui Z, Roalf DR, et al (2020) Development of structure–function coupling in human brain networks during youth. Proc Natl Acad Sci U S A 117:771–778. https://doi.org/10.1073/pnas.1912034117

Bedard MA, Aghourian M, Legault-Denis C, et al (2019) Brain cholinergic alterations in idiopathic REM sleep behaviour disorder: a PET imaging study with 18 F-FEOBV. Sleep Med 58:35–41. https://doi.org/10.1016/j.sleep.2018.12.020

Behrens TEJ, Johansen-Berg H, Woolrich MW, et al (2003) Non-invasive mapping of connections between human thalamus and cortex using diffusion imaging. Nat

Neurosci 6:750–757. https://doi.org/10.1038/nn1075

Benarroch EE (2013) Pedunculopontine nucleus: Functional organization and clinical implications. Neurology 80:1148–1155. https://doi.org/10.1212/WNL.0b013e3182886a76

Bender DB, Youakim M (2001) Effect of attentive fixation in macaque thalamus and cortex. J Neurophysiol 85:219–234. https://doi.org/10.1152/jn.2001.85.1.219

Benson DF (1977) The Third Alexia. Arch Neurol 34:327–331. https://doi.org/10.1001/archneur.1977.00500180021004

Benson DF, Gardner H, Meadows JC (1976) Reduplicative paramnesia. Neurology 26:147–151

Berkhemer OA, Fransen PSS, Beumer D, et al (2015) A Randomized Trial of Intraarterial Treatment for Acute Ischemic Stroke. N Engl J Med 372:11–20. https://doi.org/10.1056/nejmoa1411587

Bertero A, Liska A, Pagani M, et al (2018) Autism-associated 16p11.2 microdeletion impairs prefrontal functional connectivity in mouse and human. Brain 141:2055–2065. https://doi.org/10.1093/brain/awy111

Berthoz A, Israel I, Georges-François P, et al (1995) Spatial memory of body linear displacement: what is being stored? Science 269:95–8. https://doi.org/10.1126/science.7604286

Berti A, Bottini G, Gandola M, et al (2005) Shared cortical anatomy for motor awareness and motor control. Science 309:488–491. https://doi.org/10.1126/science.1110625

Bez Y, Nurmedov S (2007) Reduplicative paramnesia in a case with corpus callosum lesion. Yeni Symp J 45:174–176

Bisiach E, Luzzatti C (1978) Unilateral Neglect of Representational Space. Cortex 14:129–133. https://doi.org/10.1016/S0010-9452(78)80016-1

Biswal B, Yetkin FZ, Haughton VM, Hyde JS (1995) Functional connectivity in the motor cortex of resting human brain using echo-planar MRI. Magn Reson Med 34:537–41

Blaha CD, Winn P (1993) Modulation of dopamine efflux in the striatum following cholinergic stimulation of the substantia nigra in intact and pedunculopontine tegmental nucleus-lesioned rats. J Neurosci 13:1035–1044. https://doi.org/10.1523/jneurosci.13-03-01035.1993

Blough DS (1977) Visual search in the pigeon: Hunt and peck method. Science (80-) 196:1013–4. https://doi.org/10.1126/science.860129

Bluhm RL, Miller J, Lanius RA, et al (2007) Spontaneous low-frequency fluctuations in

the BOLD signal in schizophrenic patients: Anomalies in the default network. Schizophr Bull 33:1004–1012. https://doi.org/10.1093/schbul/sbm052

Boes AD (2020) Lesion network mapping: where do we go from here? Brain 1–4. https://doi.org/10.1093/brain/awaa350

Boes AD, Prasad S, Liu H, et al (2015) Network localization of neurological symptoms from focal brain lesions. Brain 138:3061–75. https://doi.org/10.1093/brain/awv228

Bohbot VD, Kalina M, Stepankova K, et al (1998) Spatial memory deficits in patients with lesions to the right hippocampus and to the right parahippocampal cortex. Neuropsychologia 36:1217–1238. https://doi.org/10.1016/S0028-3932(97)00161-9

Borghesani V, Monti A, Fortis P, Miceli G (2019) Reduplicative paramnesia for places: A comprehensive review of the literature and a new case report. Clin Neurol Neurosurg 181:7–20. https://doi.org/10.1016/j.clineuro.2019.03.022

Borra E, Gerbella M, Rozzi S, Luppino G (2011) Anatomical evidence for the involvement of the macaque ventrolateral prefrontal area 12r in controlling goal-directed actions. J Neurosci 31:12351–12363. https://doi.org/10.1523/JNEUROSCI.1745-11.2011

Bos J, Benevento LA (1975) Projections of the medial pulvinar to orbital cortex and frontal eye fields in the rhesus monkey (Macaca mulatta). Exp Neurol 49:487–496. https://doi.org/10.1016/0014-4886(75)90103-X

Boucetta S, Cissé Y, Mainville L, et al (2014) Discharge profiles across the sleep-waking cycle of identified cholinergic, GABAergic, and glutamatergic neurons in the pontomesencephalic tegmentum of the rat. J Neurosci 34:4708–4727. https://doi.org/10.1523/JNEUROSCI.2617-13.2014

Bouret S, Sara SJ (2005) Network reset: A simplified overarching theory of locus coeruleus noradrenaline function. Trends Neurosci 28:574–582. https://doi.org/10.1016/j.tins.2005.09.002

Braga RM, Buckner RL (2017) Parallel Interdigitated Distributed Networks within the Individual Estimated by Intrinsic Functional Connectivity. Neuron 95:457-471.e5. https://doi.org/10.1016/j.neuron.2017.06.038

Brandt T, Schautzer F, Hamilton DA, et al (2005) Vestibular loss causes hippocampal atrophy and impaired spatial memory in humans. Brain 128:2732–2741. https://doi.org/10.1093/brain/awh617

Brett M, Johnsrude IS, Owen AM (2002) The problem of functional localization in the human brain. Nat Rev Neurosci 3:243–249

Bridge H, Leopold DA, Bourne JA (2016) Adaptive Pulvinar Circuitry Supports Visual

Cognition. Trends Cogn Sci 20:146–157. https://doi.org/10.1016/j.tics.2015.10.003

Britt JP, Benaliouad F, McDevitt RA, et al (2012) Synaptic and Behavioral Profile of Multiple Glutamatergic Inputs to the Nucleus Accumbens. Neuron 76:790–803. https://doi.org/10.1016/j.neuron.2012.09.040

Broca P (1861) Perte de la parole: ramollissement chronique et destruction partielle du lobe anterieur gauche du cerveau. Bulletins de la Societe d'anthropologie, 1re serie. Paris, pp 235–8

Broyd SJ, Demanuele C, Debener S, et al (2009) Default-mode brain dysfunction in mental disorders: A systematic review. Neurosci Biobehav Rev 33:279–296. https://doi.org/10.1016/j.neubiorev.2008.09.002

Buckner RL, Andrews-Hanna JR, Schacter DL (2008) The brain's default network: Anatomy, function, and relevance to disease. Ann N Y Acad Sci 1124:1–38. https://doi.org/10.1196/annals.1440.011

Buckner RL, Carroll DC (2007) Self-projection and the brain. Trends Cogn Sci 11:49–57. https://doi.org/10.1016/j.tics.2006.11.004

Buckner RL, Krienen FM, Castellanos A, et al (2011) The organization of the human cerebellum estimated by intrinsic functional connectivity. J Neurophysiol 106:2322–2345. https://doi.org/10.1152/jn.00339.2011.

Buckner RL, Margulies DS (2019) Macroscale cortical organization and a default-like apex transmodal network in the marmoset monkey. Nat Commun 10:1–12. https://doi.org/10.1038/s41467-019-09812-8

Buckner RL, Margulies DS (2018) Macroscale Cortical Organization and a Default-Like Transmodal Apex Network in the Marmoset Monkey. bioRxiv. https://doi.org/10.1101/415141

Budson A, Roth H, Rentz D, Ronthal M (2000) Disruption of the ventral visual stream in a case of reduplicative paramnesia. Ann N Y Acad Sci 911:447–452. https://doi.org/10.1111/j.1749-6632.2000.tb06742.x

Bullmore E, Sporns O (2009) Complex brain networks: Graph theoretical analysis of structural and functional systems. Nat Rev Neurosci 10:186–198. https://doi.org/10.1038/nrn2575

Bürgel U, Amunts K, Hoemke L, et al (2006) White matter fiber tracts of the human brain: Three-dimensional mapping at microscopic resolution, topography and intersubject variability. Neuroimage 29:1092–1105. https://doi.org/10.1016/j.neuroimage.2005.08.040

Burgess N (2014) The 2014 Nobel Prize in Physiology or Medicine: a spatial model for cognitive neuroscience. Neuron 84:1120–1125. https://doi.org/10.1016/j.neuron.2014.12.009

Buschman TJ, Miller EK (2007) Top-down versus bottom-up control of attention in the prefrontal and posterior parietal cortices. Science (80-) 315:1860–1864. https://doi.org/10.1126/science.1138071

Butler AB (2008) Evolution of the thalamus: a morphological and functional review. Thalamus Relat Syst. https://doi.org/10.1017/S1472928808000356

Butler T, Zaborszky L, Wang X, et al (2013) Septal nuclei enlargement in human temporal lobe epilepsy without mesial temporal sclerosis. Neurology 80:487–491. https://doi.org/10.1212/WNL.0b013e31827f0ed7

Buxbaum LJ, Ferraro MK, Veramonti T, et al (2004) Hemispatial neglect: Subtypes, neuroanatomy, and disability. Neurology 62:749–756. https://doi.org/10.1212/01.WNL.0000113730.73031.F4

Bzdok D, Heeger A, Langner R, et al (2015) Subspecialization in the human posterior medial cortex. Neuroimage 106:55–71. https://doi.org/10.1016/j.neuroimage.2014.11.009

Bzdok D, Laird AR, Zilles K, Fox PT (2012) An Investigation of the Structural , Connectional , and Functional Subspecialization in the Human Amygdala. Hum Brain Mapp 34:3247–66. https://doi.org/10.1002/hbm.22138

Bzdok D, Langner R, Schilbach L, et al (2013) Segregation of the human medial prefrontal cortex in social cognition. Front Hum Neurosci 7:1–17. https://doi.org/10.3389/fnhum.2013.00232

Calamante F, Tournier JD, Jackson GD, Connelly A (2010) Track-density imaging (TDI): Super-resolution white matter imaging using whole-brain track-density mapping. Neuroimage 53:1233–1243. https://doi.org/10.1016/j.neuroimage.2010.07.024

Cambier J, Elghozi D, Strube E (1980) Lesions of the right thalamus with at non-dominant hemisphere syndrome: a report of three cases with a discussion of the concept of thalamic negligence. Rev Neurol(Paris) 136:105–16

Caplan LR, van Gijn J (2012) Stroke Syndromes, 3rd edn. Cambridge University Press, New York

Carmack PS, Spence J, Gunst RF, et al (2004) Improved agreement between Talairach and MNI coordinate spaces in deep brain regions. Neuroimage 22:367–371. https://doi.org/10.1016/j.neuroimage.2004.01.022

Catani M, Dell'Acqua F, Thiebaut de Schotten M (2013) A revised limbic system model for memory, emotion and behaviour. Neurosci Biobehav Rev 37:1724–1737. https://doi.org/10.1016/j.neubiorev.2013.07.001

Catani M, Dell'Acqua F, Vergani F, et al (2012) Short frontal lobe connections of the human brain. Cortex 48:273–291. https://doi.org/10.1016/j.cortex.2011.12.001

Catani M, Ffytche DH (2005) The rises and falls of disconnection syndromes. Brain 128:2224–2239. https://doi.org/10.1093/brain/awh622

Catani M, Howard RJ, Pajevic S, Jones DK (2002) Virtual in Vivo interactive dissection of white matter fasciculi in the human brain. Neuroimage 17:77–94. https://doi.org/10.1006/nimg.2002.1136

Catani M, Thiebaut de Schotten M (2012) Atlas of Human Brain Connections, 1st edition. Oxford University Press

Catani M, Thiebaut de Schotten M (2008) A diffusion tensor imaging tractography atlas for virtual in vivo dissections. Cortex 44:1105–1132. https://doi.org/10.1016/j.cortex.2008.05.004

Chakravarty MM, Bertrand G, Hodge CP, et al (2006) The creation of a brain atlas for image guided neurosurgery using serial histological data. Neuroimage 30:359–376. https://doi.org/10.1016/j.neuroimage.2005.09.041

Chandler D, Waterhouse BD (2012) Evidence for broad versus segregated projections from cholinergic and noradrenergic nuclei to functionally and anatomically discrete subregions of prefrontal cortex. Front Behav Neurosci 6:1–9. https://doi.org/10.3389/fnbeh.2012.00020

Chandler DJ, Lamperski CS, Waterhouse BD (2013) Identification and distribution of projections from monoaminergic and cholinergic nuclei to functionally differentiated subregions of prefrontal cortex. Brain Res 1522:38–58. https://doi.org/10.1016/j.brainres.2013.04.057

Chang SJ, Cajigas I, Opris I, et al (2020) Dissecting Brainstem Locomotor Circuits: Converging Evidence for Cuneiform Nucleus Stimulation. Front Syst Neurosci 14:1–8. https://doi.org/10.3389/fnsys.2020.00064

Chawla N V. (2005) Data mining for imbalanced datasets: An overview. Springer US

Chawla N V., Bowyer KW, Hall LO, Kegelmeyer WP (2002) SMOTE: Synthetic Minority Over-sampling Technique. J Artif Intell Res 16:321–357. https://doi.org/10.1613/jair.953

Chen X, Zirnsak M, Moore T (2018) Dissonant Representations of Visual Space in

Prefrontal Cortex during Eye Movements. Cell Rep 22:2039–2052. https://doi.org/10.1016/j.celrep.2018.01.078

Child ND, Benarroch EE (2013) Anterior nucleus of the thalamus: Functional organization and clinical implications. Neurology 81:1869–1876. https://doi.org/10.1212/01.wnl.0000436078.95856.56

Choi EY, Yeo BTT, Buckner RL (2012) The organization of the human striatum estimated by intrinsic functional connectivity. J Neurophysiol 108:2242–2263. https://doi.org/10.1152/jn.00270.2012

Cohen AL, Fox MD (2020) Reply: The influence of sample size and arbitrary statistical thresholds in lesion- network mapping. Brain 1–6. https://doi.org/10.1093/brain/awaa095

Cohen AL, Soussand L, Corrow SL, et al (2019) Looking beyond the face area: Lesion network mapping of prosopagnosia. Brain 142:3975–3990. https://doi.org/10.1093/brain/awz332

Cohen J (1988) Statistical power analysis for the behavioural sciences, 2nd edn. Lawrence Erlbaum Associates

Cohen J (1992) A power prime. Psychol bull 112:155–159

Colombo D, Serino S, Tuena C, et al (2017) Egocentric and allocentric spatial reference frames in aging: A systematic review. Neurosci Biobehav Rev 80:605–621. https://doi.org/10.1016/j.neubiorev.2017.07.012

Coltheart M (2010) The neuropsychology of delusions. Ann N Y Acad Sci 1191:16–26. https://doi.org/10.1111/j.1749-6632.2010.05496.x

Coltheart M, Langdon R, Mckay R (2011) Delusional Belief. Annu Rev Psychol 62:271–298. https://doi.org/10.1146/annurev.psych.121208.131622

Corbetta M, Kincade JM, Ollinger JM, et al (2000) Voluntary orienting is dissociated from target detection in human posterior parietal cortex. Nat Neurosci 3:. https://doi.org/10.1038/73009

Corbetta M, Patel G, Shulman GL (2008) The Reorienting System of the Human Brain: From Environment to Theory of Mind. Neuron 58:306–324. https://doi.org/10.1016/j.neuron.2008.04.017

Corbetta M, Ramsey L, Callejas A, et al (2015) Common behavioral clusters and subcortical anatomy in stroke. Neuron 85:927–41. https://doi.org/10.1016/j.neuron.2015.02.027

Corbetta M, Shulman GL (2002) Control of goal-directed and stimulus-driven attention in

the brain. Nat Rev Neurosci 3:201–15. https://doi.org/10.1038/nrn755

Corbetta M, Shulman GL (2011) Spatial neglect and attention networks

Cordes D, Haughton VM, Arfanakis K, et al (2001) Frequencies Contributing to Functional Connectivity in the Cerebral Cortex in '"Resting-state"' Data. AJNR Am J Neuroradiol 22:1326–33. https://doi.org/10.1007/s10854-014-1833-2

Cortese S, Adamo N, Del Giovane C, et al (2018) Comparative efficacy and tolerability of medications for attention-deficit hyperactivity disorder in children, adolescents, and adults: a systematic review and network meta-analysis. The Lancet Psychiatry 5:727–738. https://doi.org/10.1016/S2215-0366(18)30269-4

Cotard J (1882) Du Delire des Negations. Arch du Neurol Paris 4:282–296

Cox J, Pinto L, Dan Y (2016) Calcium imaging of sleep-wake related neuronal activity in the dorsal pons. Nat Commun 7:1–7. https://doi.org/10.1038/ncomms10763

Croxson PL, Forkel SJ, Cerliani L, Thiebaut de Schotten M (2017) Structural Variability Across the Primate Brain: A Cross-Species Comparison. Cereb Cortex 1–13. https://doi.org/10.1093/cercor/bhx244

Cunningham SI, Tomasi D, Volkow ND (2016) Structural and Functional Connectivity of the Precuneus and Thalamus to the Default Mode Network. Hum Brain Mapp 38:938–56. https://doi.org/10.1002/hbm.23429

Damasio AR (1992) Aphasia. N Engl J Med 326:531–539. https://doi.org/10.1056/NEJM199202203260806

Damoiseaux JS, Rombouts SARB, Barkhof F, et al (2006) Consistent resting-state networks across healthy subjects. Proc Natl Acad Sci 103:13848–13853

Danet L, Barbeau E, Eustache P, et al (2015) Thalamic amnesia after infarct: The role of the mammillothalamic tract and mediodorsal nucleus. Neurology 85:2107–15. https://doi.org/10.1212/WNL.0000000000002730

Dannenberg XH, Pabst M, Braganza O, et al (2015) Synergy of Direct and Indirect Cholinergic Septo-Hippocampal Pathways Coordinates Firing in Hippocampal Networks. J Neurosci 35:8394–8410. https://doi.org/10.1523/JNEUROSCI.4460-14.2015

Darby R, Prasad S (2016) Lesion-related delusional misidentification syndromes: a comprehensive review of reported cases. J Neuropsychiatry Clin Neurosci 28:217–22. https://doi.org/10.1176/appi.neuropsych.15100376

Darby RR, Joutsa J, Fox MD (2019) Network localization of heterogeneous neuroimaging findings. Brain 142:70–9. https://doi.org/10.1093/brain/awy292

Darby RR, Laganiere S, Pascual-Leone A, et al (2017) Finding the imposter: brain connectivity of lesions causing delusional misidentifications. Brain 140:497–507. https://doi.org/10.1093/brain/aww288

de Haan B, Karnath HO (2018) A hitchhiker's guide to lesion-behaviour mapping. Neuropsychologia 115:5–16. https://doi.org/10.1016/j.neuropsychologia.2017.10.021

de Haan EHF, Young AW, Newcombe F (1991) Covert and overt recognition in prosopagnosia. Brain 114:2575–2591. https://doi.org/10.1093/brain/114.6.2575

De Renzi E, Scotti G, Spinnler H (1969) Perceptual and associative disorders of visual recognition: Relationship to the side of the cerebral lesion. Neurology 19:. https://doi.org/10.1212/WNL.19.7.634

Dell'Acqua F, Scifo P, Rizzo G, et al (2010) A modified damped Richardson-Lucy algorithm to reduce isotropic background effects in spherical deconvolution. Neuroimage 49:1446–1458. https://doi.org/10.1016/j.neuroimage.2009.09.033

Dell'Acqua F, Simmons A, Williams SCR, Catani M (2013) Can spherical deconvolution provide more information than fiber orientations? Hindrance modulated orientational anisotropy, a true-tract specific index to characterize white matter diffusion. Hum Brain Mapp 34:2464–2483. https://doi.org/10.1002/hbm.22080

DeMarco AT, Turkeltaub PE (2018) A multivariate lesion symptom mapping toolbox and examination of lesion-volume biases and correction methods in lesion-symptom mapping. Hum Brain Mapp 39:4169–4182. https://doi.org/10.1002/hbm.24289

Desikan RS, Ségonne F, Fischl B, et al (2006) An automated labeling system for subdividing the human cerebral cortex on MRI scans into gyral based regions of interest. Neuroimage 31:968–980. https://doi.org/10.1016/j.neuroimage.2006.01.021

Despotovic I, Goossens B, Philips W (2015) Review Article MRI Segmentation of the Human Brain : Challenges , Methods , and Applications. Comput Math Methods Med 2015:1–23. https://doi.org/10.1155/2015/450341

Devinsky O (2009) Delusional misidentifications and duplications: right brain lesions, left brain delusions. Neurology 72:80–7. https://doi.org/10.1212/01.wnl.0000338625.47892.74

DeVito JL (1978) A horseradish peroxidase-autoradiographic study of parietopulvinar connections in saimiri sciureus. Exp Brain Res 32:581–590. https://doi.org/10.1007/BF00239554

Di Martino A, Scheres A, Margulies DS, et al (2008) Functional Connectivity of Human Striatum: A Resting State fMRI Study. Cereb Cortex 18:2735–2747.

https://doi.org/10.1093/cercor/bhn041

Diedenhofen B, Musch J (2015) Cocor: A comprehensive solution for the statistical comparison of correlations. PLoS One 10:1–12. https://doi.org/10.1371/journal.pone.0121945

Dinkelacker V, Valabregue R, Thivard L, et al (2015) Hippocampal-thalamic wiring in medial temporal lobe epilepsy: Enhanced connectivity per hippocampal voxel. Epilepsia 56:1217–1226. https://doi.org/10.1111/epi.13051

Direcção Geral de Saúde (2014) Portugal - Doenças Cérebro-Cardiovasculares em números – 2014

Doeller CF, Barry C, Burgess N (2010) Evidence for grid cells in a human memory network. Nature 463:657–661. https://doi.org/10.1038/nature08704

Downar J, Crawley AP, Mikulis DJ, Davis KD (2000) A multimodal cortical network for the detection of changes in the sensory environment. Nat Neurosci 3:277–283. https://doi.org/10.1038/72991

Dragicevic N, Hoffmann M (2015) Characterization of content specific delusions after right hemispheric ischemic stroke. Neurology 84:

Dringenberg HC, Olmstead MC (2003) Integrated contributions of basal forebrain and thalamus to neocortical activation elicited by pedunculopontine tegmental stimulation in urethane-anesthetized rats. Neuroscience 119:839–853. https://doi.org/10.1016/S0306-4522(03)00197-0

Dronkers NF, Plaisant O, Iba-Zizen MT, Cabanis EA (2007) Paul Broca's historic cases: High resolution MR imaging of the brains of Leborgne and Lelong. Brain 130:1432–1441. https://doi.org/10.1093/brain/awm042

Dukart J, Holiga Š, Chatham C, et al (2018) Cerebral blood flow predicts differential neurotransmitter activity. Sci Rep 8:1–11. https://doi.org/10.1038/s41598-018-22444-0

Durmer JS, Rosenquist AC (2001) Ibotenic acid lesions in the pedunculopontine region result in recovery of visual orienting in the hemianopic cat. Neuroscience 106:765–781. https://doi.org/10.1016/S0306-4522(01)00321-9

Edlow BL, Takahashi E, Wu O, et al (2012) Neuroanatomic connectivity of the human ascending arousal system critical to consciousness and its disorders. J Neuropathol Exp Neurol 71:531–546. https://doi.org/10.1097/NEN.0b013e3182588293

Eichenbaum H (2017) On the Integration of Space, Time, and Memory. Neuron 95:1007–1018. https://doi.org/10.1016/j.neuron.2017.06.036

Eichenbaum H, Dudchenko P, Wood E, et al (1999) The Hippocampus, Memory, Review and Place Cells: Is It Spatial Memory or a Memory Space? Neuron 23:209–226. https://doi.org/10.1016/s0896-6273(00)80773-4

Eickhoff SB, Laird AR, Fox PT, et al (2016) Functional Segregation of the Human Dorsomedial Prefrontal Cortex. Cereb Cortex 26:304–21. https://doi.org/10.1093/cercor/bhu250

Eickhoff SB, Yeo BTT, Genon S (2018) Imaging-based parcellations of the human brain. Nat Rev Neurosci 19:672–686. https://doi.org/10.1038/s41583-018-0071-7

Ekstrom AD, Arnold AEGF, Iaria G (2014) A critical review of the allocentric spatial representation and its neural underpinnings: toward a network-based perspective. Front Hum Neurosci 8:803

Ekstrom AD, Kahana MJ, Caplan JB, et al (2003) Cellular networks underlying human spatial navigation. Nature 425:184–188. https://doi.org/10.1038/nature01964

Ellis HD, Young AW (1990) Accounting for delusional misidentifications. Br J Psychiatry 157:239–248. https://doi.org/10.1192/bjp.157.2.239

Ellis HD, Young AW, Quayle AH, De Pauw KW (1997) Reduced autonomic responses to faces in Capgras delusion. Proc R Soc B Biol Sci 264:1085–1092. https://doi.org/10.1098/rspb.1997.0150

Epstein R, Kanwisher N (1998) Acortical representationof the local visual environment Russell. Nature 392:6–9

Evensmoen HR, Rimol LM, Winkler AM, et al (2021) Allocentric representation in the human amygdala and ventral visual stream. Cell Rep 34:. https://doi.org/10.1016/j.celrep.2020.108658

Ewert S, Plettig P, Li N, et al (2018) Toward defining deep brain stimulation targets in MNI space: A subcortical atlas based on multimodal MRI, histology and structural connectivity. Neuroimage 170:271–282. https://doi.org/10.1016/j.neuroimage.2017.05.015

Exley R, Cragg SJ (2008) Presynaptic nicotinic receptors: A dynamic and diverse cholinergic filter of striatal dopamine neurotransmission. Br J Pharmacol 153:283–297. https://doi.org/10.1038/sj.bjp.0707510

Faraone S V. (2018) The pharmacology of amphetamine and methylphenidate: Relevance to the neurobiology of attention-deficit/hyperactivity disorder and other psychiatric comorbidities. Neurosci Biobehav Rev 87:255–270. https://doi.org/10.1016/j.neubiorev.2018.02.001

Feeney EJ, Groman SM, Taylor JR, Corlett PR (2017) Explaining delusions: Reducing uncertainty through basic and computational neuroscience. Schizophr Bull 43:263–272. https://doi.org/10.1093/schbul/sbw194

Feigin VL, Norrving B, Mensah GA (2017) Global Burden of Stroke. Circ Res 120:439–448. https://doi.org/10.1161/CIRCRESAHA.116.308413

Feinberg DA, Moeller S, Smith SM, et al (2010) Multiplexed echo planar imaging for sub-second whole brain fmri and fast diffusion imaging. PLoS One 5:. https://doi.org/10.1371/journal.pone.0015710

Feinberg TE (2013) Neuropathologies of the self and the right hemisphere: a window into productive personal pathologies. Front Hum Neurosci 7:. https://doi.org/10.3389/fnhum.2013.00472

Ferro JM, Martins IP, Távora L (1984) Neglect in children. Ann Neurol 15:281–284. https://doi.org/10.1002/ana.410150314

Fischer DB, Perez DL, Prasad S, et al (2016) Right inferior longitudinal fasciculus lesions disrupt visual-emotional integration. Soc Cogn Affect Neurosci 11:945–951. https://doi.org/10.1093/scan/nsw011

Fisher CM (1982) Disorientation for Place. Arch Neurol 39:33–6

Fletcher PC, Frith CD (2009) Perceiving is believing: A Bayesian approach to explaining the positive symptoms of schizophrenia. Nat Rev Neurosci 10:48–58. https://doi.org/10.1038/nrn2536

Floresco SB (2015) The Nucleus Accumbens: An Interface Between Cognition, Emotion, and Action. Annu Rev Psychol 66:25–52. https://doi.org/10.1146/annurev-psych-010213-115159

Foote SL, Morrison JH (1987) Extrathalamic modulation of cortical function. Annu Rev Neurosci 10:67–95. https://doi.org/10.1146/annurev.ne.10.030187.000435

Forster GL, Blaha CD (2003) Pedunculopontine tegmental stimulation evokes striatal dopamine efflux by activation of acetylcholine and glutamate receptors in the midbrain and pons of the rat. Eur J Neurosci 17:751–762. https://doi.org/10.1046/j.1460-9568.2003.02511.x

Förstl H, Beats B (1992) Charles Bonnet's description of Cotard 's delusion and reduplicative paramnesia in an elderly patient (1788). Br J Psychiatry 160:416–418. https://doi.org/10.1192/bjp.160.3.416

Fotopoulou A (2014) Time to get rid of the "Modular" in neuropsychology: A unified theory of anosognosia as aberrant predictive coding. J Neuropsychol 8:1–19.

https://doi.org/10.1111/jnp.12010

Foulon C, Cerliani L, Kinkingnéhun S, et al (2018) Advanced lesion symptom mapping analyses and implementation as BCBtoolkit. Gigascience 7:1–17. https://doi.org/10.1093/gigascience/giy004

Fox MD (2018) Mapping symptoms to brain networks with the human connectome. N Eng J Med 379:2237–45. https://doi.org/10.1056/NEJMra1706158

Fox MD, Buckner RL, White MP, et al (2012) Efficacy of transcranial magnetic stimulation targets for depression is related to intrinsic functional connectivity with the subgenual cingulate. Biol Psychiatry 72:595–603. https://doi.org/10.1016/j.biopsych.2012.04.028

Fox MD, Raichle ME (2007) Spontaneous fluctuations in brain activity observed with functional magnetic resonance imaging. Nat Rev Neurosci 8:700–711

Fransson P (2005) Spontaneous low-frequency BOLD signal fluctuations: An fMRI investigation of the resting-state default mode of brain function hypothesis. Hum Brain Mapp 26:15–29. https://doi.org/10.1002/hbm.20113

Funahashi S (2013) Space representation in the prefrontal cortex. Prog Neurobiol 103:131–155. https://doi.org/10.1016/j.pneurobio.2012.04.002

Fyhn M, Molden S, Witter MP, et al (2004) Spatial representation in the entorhinal cortex. Science (80-) 305:1258–1264. https://doi.org/10.1126/science.1099901

Gatley SJ, Pan D, Chen R, et al (1996) Affinities of methylphenidate derivatives for dopamine, norepinephrine and serotonin transporters. Life Sci 58:231–239. https://doi.org/10.1016/0024-3205(96)00052-5

Geng X, Hu Y, Gu H, et al (2017) Salience and default mode network dysregulation in chronic cocaine users predict treatment outcome. Brain 140:1513–1524. https://doi.org/10.1093/brain/awx036

Geschwind N (1971) Aphasia. N Engl J Med 284:654–656. https://doi.org/10.1056/NEJM197103252841206

Glasser MF, Coalson TS, Robinson EC, et al (2016) A multi-modal parcellation of human cerebral cortex. Nature 536:171–178. https://doi.org/10.1038/nature18933

Glasser MF, Sotiropoulos SN, Wilson JA, et al (2013) The minimal preprocessing pipelines for the Human Connectome Project. Neuroimage 80:105–124. https://doi.org/10.1016/j.neuroimage.2013.04.127

Gómez FJG, Acevedo-Báñez I, Martínez-Castillo R, et al (2015) The role of 18FDG, 18FDOPA PET/CT and 99mTc bone scintigraphy imaging in Erdheim-Chester

disease. Eur J Radiol 84:1586–1592. https://doi.org/10.1016/j.ejrad.2015.04.022

Gong G, He Y, Concha L, et al (2009) Mapping Anatomical Connectivity Patterns of Human Cerebral Cortex Using In Vivo Diffusion Tensor Imaging Tractography. Cereb Cortex 19:524–536. https://doi.org/10.1093/cercor/bhn102

Goodale M, Milner A, Jakobson L, Carey D (1991) A neurological dissociation between perceiving objects and grasping them. Nature 349:154–6. https://doi.org/10.1038/349154a0

Gooddy W, Reinhold M (1952) Some aspects of human orientation in space I - sensation and movement. Brain 75:472–509

Gordon EM, Laumann TO, Adeyemo B, et al (2016) Generation and Evaluation of a Cortical Area Parcellation from Resting-State Correlations. Cereb Cortex 26:288–303. https://doi.org/10.1093/cercor/bhu239

Gozzi A, Schwarz AJ (2016) Large-scale functional connectivity networks in the rodent brain. Neuroimage 15:496–509. https://doi.org/10.1016/j.neuroimage.2015.12.017

Greicius MD, Srivastava G, Reiss AL, Menon V (2004) Default-mode network activity distinguishes Alzheimer ' s disease from healthy aging : Evidence from functional MRI. Proc Natl Acad Sci U S A 101:4637–4642. https://doi.org/10.1073/pnas.0308627101

Griffis JC, Metcalf N V., Corbetta M, Shulman GL (2019) Structural disconnections explain brain network dysfunction after stroke. Cell Rep 28:2527–40. https://doi.org/10.1016/j.celrep.2019.07.100

Grothe M, Zaborszky L, Atienza M, et al (2010) Reduction of basal forebrain cholinergic system parallels cognitive impairment in patients at high risk of developing alzheimer's disease. Cereb Cortex 20:1685–1695. https://doi.org/10.1093/cercor/bhp232

Haber SN, Kunishio K, Mizobuchi M (1995) The Orbital and Medial Prefrontal Basal Ganglia Circuit Through the Primate. Neuroscience 39:323–338

Haber SN, Wolfe DP, Groenewegen HJ (1990) The relationship between ventral striatal efferent fibers and the distribution of peptide-positive woolly fibers in the forebrain of the rhesus monkey. Neuroscience 39:323–338

Hadley JA, Nenert R, Kraguljac N V., et al (2014) Ventral tegmental area/midbrain functional connectivity and response to antipsychotic medication in schizophrenia. Neuropsychopharmacology 39:1020–1030. https://doi.org/10.1038/npp.2013.305

Hafting T, Fyhn M, Molden S, et al (2005) Microstructure of a spatial map in the

entorhinal cortex. Nature 436:801–806. https://doi.org/10.1038/nature03721

Hagmann P, Cammoun L, Gigandet X, et al (2008) Mapping the structural core of human cerebral cortex. PLoS Biol 6:1479–1493. https://doi.org/10.1371/journal.pbio.0060159

Hansen JY, Shafiei G, Markello RD, et al (2021) Mapping neurotransmitter systems to the structural and functional organization of the human neocortex. bioRxiv 2021.10.28.466336. https://doi.org/10.1101/2021.10.28.466336

Harper L, Barkhof F, Fox NC, Schott JM (2015) Using visual rating to diagnose dementia: A critical evaluation of MRI atrophy scales. J Neurol Neurosurg Psychiatry 86:1225–1233. https://doi.org/10.1136/jnnp-2014-310090

Harris S, Sheth SA, Cohen MS (2008) Functional neuroimaging of belief, disbelief, and uncertainty. Ann Neurol 63:141–147. https://doi.org/10.1002/ana.21301

Hartwright CE, Apperly IA, Hansen PC (2012) Multiple roles for executive control in belief-desire reasoning: Distinct neural networks are recruited for self perspective inhibition and complexity of reasoning. Neuroimage 61:921–930. https://doi.org/10.1016/j.neuroimage.2012.03.012

Hasselmo ME (2006) The role of acetylcholine in learning and memory. Curr Opin Neurobiol 16:710–715. https://doi.org/10.1016/j.conb.2006.09.002

He BJ, Snyder AZ, Vincent JL, et al (2007a) Breakdown of Functional Connectivity in Frontoparietal Networks Underlies Behavioral Deficits in Spatial Neglect. Neuron 53:905–918. https://doi.org/10.1016/j.neuron.2007.02.013

He H, Garcia EA (2019) Learning from Imbalanced Data. IEEE Trans Know Data Eng 21:1263–1284. https://doi.org/10.1109/tkde.2008.239

He Y, Wang L, Zang Y, et al (2007b) Regional coherence changes in the early stages of Alzheimer's disease: A combined structural and resting-state functional MRI study. Neuroimage 35:488–500. https://doi.org/10.1016/j.neuroimage.2006.11.042

Healton EB, Navarro C, Bressman S, Brust JCM (1982) Subcortical neglect. Neurology 32:776–778. https://doi.org/10.1212/wnl.32.7.776

Heilman KM, Valenstein E (2012) Clinical neuropsychology. Oxford University Press, New York

Herbet G, Duffau H (2020) Revisiting the functional anatomy of the human brain: Toward a meta-networking theory of cerebral functions. Physiol Rev 100:1181–1228. https://doi.org/10.1152/physrev.00033.2019

Heym J, Steinfels GF, Jacobs BL (1982) Activity of serotonin-containing neurons in the

nucleus raphe pallidus of freely moving cats. Brain Res 251:259–276. https://doi.org/10.1016/0006-8993(82)90743-0

Hillis AE, Barker PB, Beauchamp NJ, et al (2000) MR perfusion imaging reveals regions of hypoperfusion associated with aphasia and neglect. Neurology 55:782–788. https://doi.org/10.1212/WNL.55.6.782

Hillis AE, Caramazza A (1991) Category-specific naming and comprehension impairment: A double dissociation. Brain 114:2081–2094. https://doi.org/10.1093/brain/114.5.2081

Hillmer AT, Esterlis I, Gallezot JD, et al (2016) Imaging of cerebral α4β2* nicotinic acetylcholine receptors with (−)-[18F]Flubatine PET: Implementation of bolus plus constant infusion and sensitivity to acetylcholine in human brain. Neuroimage 141:71–80. https://doi.org/10.1016/j.neuroimage.2016.07.026

Hudson AJ, Grace GM (2000) Misidentification syndromes related to face specific area in the fusiform gyrus. J Neurol Neurosurg Psychiatry 69:645–8. https://doi.org/10.1136/jnnp.69.5.645

Hunter J (2007) Matplotlib: a 2D graphics environment. Comput Sci Eng 9:90–95. https://doi.org/10.1109/MCSE.2007.55

Ingvar DH (1979) "Hyperfrontal" distribution of the cerebral grey matter flow in resting wakefulness; on the functional anatomy of the conscious state. Acta Neurol Scand 60:12–25. https://doi.org/10.1111/j.1600-0404.1979.tb02947.x

Ivanov I, Bansal R, Hao X, et al (2010) Morphological Abnormalities of the Thalamus in Youths With Attention Deficit Hyperactivity Disorder. Image Process 397–408. https://doi.org/10.1176/appi.ajp.2009.09030398

Jacobs J, Kahana MJ, Ekstrom AD, et al (2010) A sense of direction in human entorhinal cortex. Proc Natl Acad Sci U S A 107:6487–6492. https://doi.org/10.1073/pnas.0911213107

Jacquin A, Virat-Brassaud ME, Rouaud O, et al (2014) Vascular aphasia outcome after intravenous recombinant tissue plasminogen activator thrombolysis for ischemic stroke. Eur Neurol 71:288–295. https://doi.org/10.1159/000357428

James T, Humphrey G, Gati J, et al (2002) Differential effects of viewpoint on object-driven activation in dorsal and ventral Streams. Neuron 35:793–801. https://doi.org/10.1016/S0896-6273(02)00803-6

James W (1890) The principles of psychology. Henry Holt and Company, New York

Janzen G, Van Turennout M (2004) Selective neural representation of objects rellevant for

navigation. Nat Neurosci 7:673–677. https://doi.org/10.1038/nn1257

Jenkinson M, Bannister P, Brady M, Smith S (2002) Improved optimization for the robust and accurate linear registration and motion correction of brain images. Neuroimage 17:825–841. https://doi.org/10.1016/S1053-8119(02)91132-8

Jenkinson M, Beckmann CF, Behrens TEJ, et al (2012) Fsl. Neuroimage 62:782–790. https://doi.org/10.1016/j.neuroimage.2011.09.015

Jeon CJ, Spencer RF, Mize RR (1993) Organization and synaptic connections of cholinergic fibers in the cat superior colliculus. J Comp Neurol 333:360–374. https://doi.org/10.1002/cne.903330305

Jimenez-Marin A, Rivera D, Boado V, et al (2018) Hyperconnectivity of the default mode network in multiorgan dysfunction syndrome. bioRxiv. https://doi.org/10.1101/418160

Jocic Z, Staton R (1993) Reduplication after right middle cerebral artery infarction. Brain Cogn 23:222–30. https://doi.org/10.1006/brcg.1993.1056

Jones DK, Cercignani M (2010) Twenty-five pitfalls in the analysis of diffusion MRI Data. NMR Biomed 23:803–820. https://doi.org/10.1002/nbm.1543

Jones DK, Knösche TR, Turner R (2013) White matter integrity, fiber count, and other fallacies: The do's and don'ts of diffusion MRI. Neuroimage 73:239–254. https://doi.org/10.1016/j.neuroimage.2012.06.081

Kaesmacher J, Kurmann C, Jungi N, et al (2020) Infarct in new territory after endovascular stroke treatment: A diffusion-weighted imaging study. Sci Rep 10:1–10. https://doi.org/10.1038/s41598-020-64495-2

Kandylaki KD, Nagels A, Tune S, et al (2015) Processing of false belief passages during natural story comprehension: An fMRI study. Hum Brain Mapp 36:4231–4246. https://doi.org/10.1002/hbm.22907

Kapur N, Turner A, King C (1988) Reduplicative paramnesia: possible anatomical and neuropsychological mechanisms. J Neurol Neurosurg Psychiatry 51:579–81. https://doi.org/10.1136/jnnp.51.4.579

Karnath HO, Himmelbach M, Rorden C (2002) The subcortical anatomy of human spatial neglect: Putamen, caudate nucleus and pulvinar. Brain 125:350–360. https://doi.org/10.1093/brain/awf032

Karolis VR, Corbetta M, Thiebaut de Schotten M (2019) The architecture of functional lateralisation and its relationship to callosal connectivity in the human brain. Nat Commun 10:1417–1424. https://doi.org/10.1038/s41467-019-09344-1

Karten HJ (2015) Vertebrate brains and evolutionary connectomics : on the origins of the mammalian ‘ neocortex .’ Phil Trans R Soc B 370:

Kenney J (1939) Mathematics of Statistics. Chapman & Hall, London

Kernbach JM, Yeo BTT, Smallwood J, et al (2018) Subspecialization within default mode nodes characterized in 10 , 000 UK Biobank participants. Proc Natl Acad Sci U S A 115:12295–12300. https://doi.org/10.1073/pnas.1804876115

Kirov G, Jones P, Lewis SW (1994) Prevalence of delusional misidentification syndromes. Psychopathology 27:148–149. https://doi.org/10.1159/000284862

Klein A, Andersson J, Ardekani BA, et al (2009) Evaluation of 14 nonlinear deformation algorithms applied to human brain MRI registration. Neuroimage 46:786–802. https://doi.org/10.1016/j.neuroimage.2008.12.037

Kleine JF, Beller E, Zimmer C, Kaesmacher J (2017) Lenticulostriate infarctions after successful mechanical thrombectomy in middle cerebral artery occlusion. J Neurointerv Surg 9:234–239. https://doi.org/10.1136/neurintsurg-2015-012243

Krakauer JW, Hillis AE (2014) The future of stroke treatment: Bringing evaluation of behavior back to stroke neurology. JAMA Neurol 71:1473–4. https://doi.org/10.1001/jamaneurol.2014.2343

Krauzlis RJ, Lovejoy LP, Zénon A (2013) Superior Colliculus and Visual Spatial Attention. Annu Rev Neurosci 36:. https://doi.org/10.1146/annurev-neuro-062012-170249.Superior

Kravitz DJ, Saleem KS, Baker CI, Mishkin M (2011) A new neural framework for visuospatial processing. Nat Rev Neurosci 12:217–230. https://doi.org/10.1038/nrn3008

Krzywinski M et al (2009) Circos: an Information Aesthetic for Comparative Genomics. Genome Res 19:1639–1645. https://doi.org/10.1101/gr.092759.109.19

Kunishio K, Haber SN (1994) Primate Cingulostriatal Projection : Limbic Striatal Versus Sensorimotor Striatal Input. J Comp Neurol 350:337–356

Lackner JR, Dizio P (2005) Vestibular, proprioceptive, and haptic contributions to spatial orientation. Annu Rev Psychol 56:115–47. https://doi.org/10.1146/annurev.psych.55.090902.142023

Lamar M, Dannhauser TM, Walker Z, et al (2011) Memory complaints with and without memory impairment: The impact of leukoaraiosis on cognition. J Int Neuropsychol Soc 17:1104–1112. https://doi.org/10.1017/S1355617711001123

Lancaster JL, Tordesillas-Gutiérrez D, Martinez M, et al (2007) Bias between MNI and

talairach coordinates analyzed using the ICBM-152 brain template. Hum Brain Mapp 28:1194–1205. https://doi.org/10.1002/hbm.20345

Langs G, Golland P, Ghosh S (2015) Predicting Activation Across Individuals with Resting-State Functional Connectivity Based Multi-Atlas Label Fusion. Med Image Comput Comput Assist Interv 9350:313–320. https://doi.org/10.1007/978-3-319-24571-3

Laviolette SR (2007) Dopamine modulation of emotional processing in cortical and subcortical neural circuits: Evidence for a final common pathway in schizophrenia? Schizophr Bull 33:971–981. https://doi.org/10.1093/schbul/sbm048

Lechanoine F, Jacquesson T, Beaujoin J, et al (2021) WIKIBrainStem: An online atlas to manually segment the human brainstem at the mesoscopic scale from ultrahigh field MRI. Neuroimage 236:. https://doi.org/10.1016/j.neuroimage.2021.118080

Lee K, Shinbo M, Kanai H, Nagumo Y (2011) Reduplicative paramnesia after a right frontal lesion. Cogn Behav Neurol 24:35–9. https://doi.org/10.1097/WNN.0b013e31821129b7

Leemans A, Jeurissen B, Sijbers J, Jones D (2009) ExploreDTI: a graphical toolbox for processing, analyzing, and visualizing diffusion MR data. In: 17th Scientific Meeting, International Society for Magnetic Resonance in Medicine. Hawaii, USA, p 3537

Leiguarda R (1983) Environmental reduplication associated with a right thalamic haemorrhage. J Neurol Neurosurg Psychiatry 46:1154. https://doi.org/10.1136/jnnp.46.12.1154

Lemaire JJ, Cosnard G, Sakka L, et al (2011) White matter anatomy of the human deep brain revisited with high resolution DTI fibre tracking. Neurochirurgie 57:52–67. https://doi.org/10.1016/j.neuchi.2011.04.001

Lerch JP, Van Der Kouwe AJW, Raznahan A, et al (2017) Studying neuroanatomy using MRI. Nat Neurosci 20:314–326. https://doi.org/10.1038/nn.4501

Levin ED, Conners CK, Silva D, et al (1998) Transdermal nicotine effects on attention. Psychopharmacology (Berl) 140:135–141. https://doi.org/10.1007/s002130050750

Liew SL, Anglin JM, Banks NW, et al (2018) A large, open source dataset of stroke anatomical brain images and manual lesion segmentations. Sci Data 5:1–11. https://doi.org/10.1038/sdata.2018.11

Likitcharoen Y, Phanthumchinda K (2004) Environmental reduplication in a patient with right middle cerebral artery occlusion. J Med Assoc Thai 87:1526–9

Lim SL, Padmala S, Pessoa L (2009) Segregating the significant from the mundane on a

moment-to-moment basis via direct and indirect amygdala contributions. Proc Natl Acad Sci U S A 106:16841–16846. https://doi.org/10.1073/pnas.0904551106

Liska A, Galbusera A, Schwarz AJ, Gozzi A (2015) Functional connectivity hubs of the mouse brain. Neuroimage 115:281–291. https://doi.org/10.1016/j.neuroimage.2015.04.033

Liu AKL, Chang RCC, Pearce RKB, Gentleman SM (2015) Nucleus basalis of Meynert revisited: anatomy, history and differential involvement in Alzheimer's and Parkinson's disease. Acta Neuropathol 129:527–540. https://doi.org/10.1007/s00401-015-1392-5

Lopez-Larson MP, Shah LM, Weeks HR, et al (2017) Abnormal Functional Connectivity Between Default and Salience Networks in Pediatric Bipolar Disorder. Biol Psychiatry Cogn Neurosci Neuroimaging 2:85–93. https://doi.org/10.1016/j.bpsc.2016.10.001

Lopez-Persem A, Verhagen L, Amiez C, et al (2018) The human ventro medial prefrontal cortex sulcal morphology and its influence on its functional organization . bioRxiv 1–36. https://doi.org/10.1101/417824

Lowe MJ, Dzemidzic M, Lurito JT, et al (2000) Correlations in low-frequency BOLD fluctuations reflect cortico-cortical connections. Neuroimage 12:582–587. https://doi.org/10.1006/nimg.2000.0654

Lu H, Zou Q, Gu H, et al (2012) Rat brains also have a default mode network. Proc Natl Acad Sci 109:3979–3984. https://doi.org/10.1073/pnas.1200506109

Lückmann HC, Jacobs HIL, Sack AT (2014) The cross-functional role of frontoparietal regions in cognition: Internal attention as the overarching mechanism. Prog Neurobiol 116:66–86. https://doi.org/10.1016/j.pneurobio.2014.02.002

Luppino G, Matelli M, Carey RG, et al (1988) New view of the organization of the pulvinar nucleus in Tupaia as revealed by tectopulvinar and pulvinar‐cortical projections. J Comp Neurol 273:67–86. https://doi.org/10.1002/cne.902730107

Luque A, Carrasco A, Martín A, de las Heras A (2019) The impact of class imbalance in classification performance metrics based on the binary confusion matrix. Pattern Recognit 91:216–231. https://doi.org/10.1016/j.patcog.2019.02.023

Ma H, Campbell BCV, Parsons MW, et al (2019) Thrombolysis Guided by Perfusion Imaging up to 9 Hours after Onset of Stroke. N Engl J Med 380:1795–1803. https://doi.org/10.1056/nejmoa1813046

Mackintosh NJ (1965) Selective attention in animal discrimination learning. Psychol Bull 64:124–150. https://doi.org/10.1037/h0022347

MacLean P (1949) Psychosomatic disease and the "visceral brain." Recent developments bearing on the Papez theory of emotion. Psychosom Med 11:338–353

MacLean P (1952) Some psychiatric implications of physiological studies on frontotemporal portion of limbic system (Visceral brain). Electroencephalogr Clin Neurophysiol 4:407–418. https://doi.org/10.1016/0013-4694(52)90073-4

Maier-Hein KH, Neher PF, Descoteaux M (2017) The challenge of mapping the human connectome based on diffusion tractography. Nat Commun 8:1349–1361. https://doi.org/10.1038/s41467-017-01285-x

Mair G, Von Kummer R, Morris Z, et al (2018) Effect of IV alteplase on the ischemic brain lesion at 24-48 hours after ischemic stroke. Neurology 91:E2067–E2077. https://doi.org/10.1212/WNL.0000000000006575

Margulies DS, Ghosh SS, Goulas A, et al (2016) Situating the default-mode network along a principal gradient of macroscale cortical organization. Proc Natl Acad Sci 113:12574–12579. https://doi.org/10.1073/pnas.1608282113

Markello RD, Spreng RN, Luh W, et al (2018) Segregation of the human basal forebrain using resting state functional MRI. Neuroimage 173:287–297. https://doi.org/10.1016/j.neuroimage.2018.02.042

Mars RB, Neubert F-X, Noonan MP, et al (2012) On the relationship between the "default mode network" and the "social brain." Front Hum Neurosci 6:1–9. https://doi.org/10.3389/fnhum.2012.00189

Martin EM, Devidze N, Shelley DN, et al (2011) Molecular and neuroanatomical characterization of single neurons in the mouse medullary gigantocellular reticular nucleus. J Comp Neurol 519:2574–2593. https://doi.org/10.1002/cne.22639

Martinez-Gonzalez C, Van Andel J, Bolam JP, Mena-Segovia J (2014) Divergent motor projections from the pedunculopontine nucleus are differentially regulated in Parkinsonism. Brain Struct Funct 219:1451–1462. https://doi.org/10.1007/s00429-013-0579-6

Martins IP, Farrajota L (2007) Proper and common names: A double dissociation. Neuropsychologia 45:1744–1756. https://doi.org/10.1016/j.neuropsychologia.2006.12.016

Martins IP, Fonseca J, Morgado J, et al (2017) Language improvement one week after thrombolysis in acute stroke. Acta Neurol Scand 135:339–345.

https://doi.org/10.1111/ane.12604

Mazoyer B, Zago L, Mellet E, et al (2001) Cortical networks for working memory and executive functions sustain the conscious resting state in man. Brain Res Bull 54:287–298. https://doi.org/10.1016/S0361-9230(00)00437-8

McCarthy RA, Warrington EK (1986) Visual associative agnosia: A clinico-anatomical study of a single case. J Neurol Neurosurg Psychiatry 49:1233–1240. https://doi.org/10.1136/jnnp.49.11.1233

McCollum LA, Roberts RC (2015) Uncovering the role of the nucleus accumbens in schizophrenia: A postmortem analysis of tyrosine hydroxylase and vesicular glutamate transporters. Schizophr Res 169:369–373. https://doi.org/10.1016/j.schres.2015.08.041

Mease RA, Metz M, Groh A (2016) Cortical Sensory Responses Are Enhanced by the Higher-Order Thalamus. Cell Rep 14:208–215. https://doi.org/10.1016/j.celrep.2015.12.026

Medaglia JD, Huang W, Karuza EA, et al (2018) Functional alignment with anatomical networks is associated with cognitive flexibility. Nat Hum Behav 2:156–164. https://doi.org/10.1038/s41562-017-0260-9

Mena-Segovia J, Bolam JP (2017) Rethinking the Pedunculopontine Nucleus: From Cellular Organization to Function. Neuron 94:7–18. https://doi.org/10.1016/j.neuron.2017.02.027

Mena-Segovia J, Sims HM, Magill PJ, Bolam JP (2008) Cholinergic brainstem neurons modulate cortical gamma activity during slow oscillations. J Physiol 586:2947–2960. https://doi.org/10.1113/jphysiol.2008.153874

Menon V (2011) Large-scale brain networks and psychopathology: A unifying triple network model. Trends Cogn Sci 15:483–506. https://doi.org/10.1016/j.tics.2011.08.003

Mesulam M (2008) Representation, inference, and transcendent encoding in neurocognitive networks of the human brain. Ann Neurol 64:367–378. https://doi.org/10.1002/ana.21534

Mesulam MM, Thompson CK, Weintraub S, Rogalski EJ (2015) The Wernicke conundrum and the anatomy of language comprehension in primary progressive aphasia. Brain 138:2423–2437. https://doi.org/10.1093/brain/awv154

Moeller S, Yacoub E, Olman CA, et al (2010) Multiband multislice GE-EPI at 7 tesla, with 16-fold acceleration using partial parallel imaging with application to high spatial and

temporal whole-brain FMRI. Magn Reson Med 63:1144–1153. https://doi.org/10.1002/mrm.22361

Morales M, Margolis EB (2017) Ventral tegmental area: Cellular heterogeneity, connectivity and behaviour. Nat Rev Neurosci 18:73–85. https://doi.org/10.1038/nrn.2016.165

Morel A, Magnin M, Jeanmonod D (1997) Multiarchitectonic and stereotactic atlas f the human thalamus. J Comp Neurol 387:588–630. https://doi.org/10.1002/(SICI)1096-9861(19971103)387:4<588::AID-CNE8>3.0.CO;2-Z

Moritz KP, Pockles CF, Maimon S (1788) Gnothi Sauton oder Magazin zur Erfahrungsseelenkunde als em Lesebuch fur Gelehrte und Ungelehrte. Berlin

Morrison JH, Foote SL (1986) Noradrenergic and serotoninergic innervation of cortical, thalamic, and tectal visual structures in old and new world monkeys. J Comp Neurol 243:117–138. https://doi.org/10.1002/cne.902430110

Moser DJ, Cohen RA, Malloy P, et al (1998) Reduplicative paramnesia: longitudinal neurobehavioral and neuroimaging analysis. J Geriatr Psychiatry Neurol 11:174–80. https://doi.org/10.1177/089198879901100402

Moser EI, Roudi Y, Witter MP, et al (2014) Grid cells and cortical representation. Nat Rev Neurosci 15:466–481. https://doi.org/10.1038/nrn3766

Möttönen T, Katisko J, Haapasalo J, et al (2015) Defining the anterior nucleus of the thalamus (ANT) as a deep brain stimulation target in refractory epilepsy: Delineation using 3 T MRI and intraoperative microelectrode recording. NeuroImage Clin 7:823–829. https://doi.org/10.1016/j.nicl.2015.03.001

Motts SD, Schofield BR (2009) Sources of cholinergic input to the inferior colliculus. Neuroscience 160:103–114. https://doi.org/10.1016/j.neuroscience.2009.02.036

Mueller S, Wang D, Fox MD, et al (2013) Individual Variability in Functional Connectivity Architecture of the Human Brain. Neuron 77:586–595. https://doi.org/10.1016/j.neuron.2012.12.028

Murai T, Toichi M, Sengoku A, et al (1997) Reduplicative paramnesia in patients with focal brain damage. Neuropsychiatry Neuropsychol Behav Neurol 10:190–6

Nagahama Y, Okina T, Suzuki N, et al (2007) Classification of psychotic symptoms in dementia with Lewy bodies. Am J Geriatr Psychiatry 15:961–967. https://doi.org/10.1097/JGP.0b013e3180cc1fdf

Nagahama Y, Okina T, Suzuki N, Matsuda M (2010) Neural correlates of psychotic symptoms in dementia with Lewy bodies. Brain 133:557–567.

https://doi.org/10.1093/brain/awp295

Nair J, Klaassen A-L, Arato J, et al (2018) Basal forebrain contributes to default mode network regulation. Proc Natl Acad Sci 2018:201712431. https://doi.org/10.1073/pnas.1712431115

Nichols T, Brett M, Andersson J, et al (2005) Valid conjunction inference with the minimum statistic. Neuroimage 25:653–660. https://doi.org/10.1016/j.neuroimage.2004.12.005

Nieuwenhuys R, Voogd J, van Huijzen C (2008) The Human Central Nervous System: A Synopsis and Atlas, 4th editio. Steinkopff

Nighoghossian N, Trouillas P, Vighetto A, Philippon B (1992) Spatial delirium following a right subcortical infarct with frontal deactivation. J Neurol Neurosurg Psychiatry 55:334–5. https://doi.org/10.1136/jnnp.55.4.334

Nishio Y, Mori E (2012) Delusions of death in a patient with right hemisphere infarction. Cogn Behav Neurol 25:216–223. https://doi.org/10.1097/WNN.0b013e31827504c7

Nogueira RG, Jadhav AP, Haussen DC, et al (2018) Thrombectomy 6 to 24 Hours after Stroke with a Mismatch between Deficit and Infarct. N Engl J Med 378:11–21. https://doi.org/10.1056/nejmoa1706442

Nozais V, Forkel SJ, Foulon C, et al (2021) Functionnectome as a framework to analyse the contribution of brain circuits to fMRI. Commun Biol 1–12. https://doi.org/10.1038/s42003-021-02530-2

O'Keefe J, Burgess N (1996) Geometric determinants of the place fields of hippocampal neurons. Nature 381:425–8. https://doi.org/10.1038/381425a0

O'Keefe J, Dostrovsky J (1971) The hippocampus as a spatial map: prelim- inary evidence from unit activity in the freely-moving rat. Brain Res 34:171–175

Ochsner KN, Silvers JA, Buhle JT (2012) Functional imaging studies of emotion regulation: a synthetic review and evolving model of the cognitive control of emotion. Ann N Y Acad Sci 1251:E1–E24. https://doi.org/10.1111/j.1749-6632.2012.06751.x

Osmon DC (1996) Understanding symptoms of medial frontal lobe disorder: a clinical case study. J Clin Psychol Med Settings 3:23–39. https://doi.org/10.1007/BF01989287

Osorio I, Overman J, Giftakis J, Wilkinson SB (2007) High frequency thalamic stimulation for inoperable mesial temporal epilepsy. Epilepsia 48:1561–1571. https://doi.org/10.1111/j.1528-1167.2007.01044.x

Ovelacg E, Gallois P, Berteloot E, et al (1988) Le delire des lieux: apport de la bebitmetrie cerebrale. Cortex 24:329–337. https://doi.org/10.1016/S0010-9452(88)80041-8

Pacella V, Foulon C, Jenkinson PM, et al (2019) Anosognosia for hemiplegia as a tripartite disconnection syndrome. Elife 8:1–13. https://doi.org/10.7554/elife.46075

Papez J (1937) A proposed mechanism of emotion. Arch Neurol Psychiatry 258:725–743

Pasquier F, Leys D, Weerts J, et al (1996) Inter and intraobserver reproducibility of cerebral atrophy assessment on MRI scans with hemispheric infarcts. Eur Neurol 36:268–72

Patel GH, Yang D, Jamerson EC, et al (2015) Functional evolution of new and expanded attention networks in humans. Proc Natl Acad Sci 112:E5377–E5377. https://doi.org/10.1073/pnas.1516559112

Paterson A, Zangwill O (1944) Recovery of spatial orientation in the post-traumatic confusional state. Brain 67:54–68

Peckins CS, Khorashadi L, Wolpow ER (2016) A case of reduplicative paramnesia for home. Cogn Behav Neurol 29:150–7. https://doi.org/10.1097/WNN.0000000000000102

Pedregosa F, Varoquaux G, Gramfort A, et al (2011) Scikit-learn: Machine Learning in Python. J Mach Learn Res 12:2825–2830. https://doi.org/10.1145/2786984.2786995

Pendlebury ST, Rothwell PM (2019) Incidence and prevalence of dementia associated with transient ischaemic attack and stroke: analysis of the population-based Oxford Vascular Study. Lancet Neurol 18:248–258. https://doi.org/10.1016/S1474-4422(18)30442-3

Perini G, Carlini A, Pomati S, et al (2016) Misidentification Delusions: Prevalence in Different Types of Dementia and Validation of a Structured Questionnaire. Alzheimer Dis Assoc Disord 30:331–337. https://doi.org/10.1097/WAD.0000000000000141

Perrotin A, Desgranges B, Landeau B, et al (2015) Anosognosia in Alzheimer disease: Disconnection between memory and self-related brain networks. Ann Neurol 78:477–486. https://doi.org/10.1002/ana.24462

Persson J, Lind J, Larsson A, et al (2008) Altered deactivation in individuals with genetic risk for Alzheimer's disease. Neuropsychologia 46:1679–1687. https://doi.org/10.1016/j.neuropsychologia.2008.01.026

Petersen SE, Posner MI (2012) The attention system of the human brain: 20 years after. Annu Rev Neurosci 35:73–89. https://doi.org/10.1146/annurev-neuro-062111-150525

Petrides M (2005) Lateral prefrontal cortex: Architectonic and functional organization. Philos Trans R Soc B Biol Sci 360:781–795. https://doi.org/10.1098/rstb.2005.1631

Petrides M, Alivisatos B, Frey S (2002) Differential activation of the human orbital, mid-

ventrolateral, and mid-dorsolateral prefrontal cortex during the processing of visual stimuli. Proc Natl Acad Sci U S A 99:5649–5654. https://doi.org/10.1073/pnas.072092299

Petzold A, Valencia M, Pál B, Mena-Segovia J (2015) Decoding brain state transitions in the pedunculopontine nucleus: Cooperative phasic and tonic mechanisms. Front Neural Circuits 9:68. https://doi.org/10.3389/fncir.2015.00068

Pick A (1903) Clinical studies III. On reduplicative paramnesia. Brain 26:260–7

Pignat JM, Ptak R, Leemann B, et al (2013) Modulation of environmental reduplicative paramnesia by perceptual experience. Neurocase 19:445–450. https://doi.org/10.1080/13554794.2012.690428

Politis M, Loane C (2012) Reduplicative paramnesia: A review. Psychopathology 45:337–343. https://doi.org/10.1159/000337748

Pollock A, St George B, Fenton M, Firkins L (2012) Top ten research priorities relating to life after stroke. Lancet Neurol 11:209. https://doi.org/10.1016/S1474-4422(12)70029-7

Pomarol-Clotet E, Salvador R, Sarró S, et al (2008) Failure to deactivate in the prefrontal cortex in schizophrenia: Dysfunction of the default mode network? Psychol Med 38:1185–1193. https://doi.org/10.1017/S0033291708003565

Power JD, Barnes KA, Snyder AZ, et al (2012) Spurious but systematic correlations in functional connectivity MRI networks arise from subject motion. Neuroimage 59:2142–2154. https://doi.org/10.1016/j.neuroimage.2011.10.018

Power JD, Cohen AL, Nelson SM, et al (2011) Functional network organization of the human brain. Neuron 72:665–678. https://doi.org/10.1016/j.neuron.2011.09.006.Functional

Powers WJ, Rabinstein AA, Ackerson T, et al (2019) Guidelines for the early management of patients with acute ischemic stroke: 2019 update to the 2018 guidelines for the early management of acute ischemic stroke a guideline for healthcare professionals from the American Heart Association/American Stroke A

Prendergast MA, Jackson WJ, Terry Jr A V, et al (1998) Central nicotinic receptor agonists ABT-418, ABT-089, and (–)-nicotine reduce distractibility in adult monkeys. Psychopharmacol 136:50–58. https://doi.org/10.1007/s002130050538

Prigatano G (2010) The study of anosognosia. Oxford University Press, New York

Pruim RHR, Mennes M, Buitelaar JK, Beckmann CF (2015) Evaluation of ICA-AROMA and alternative strategies for motion artifact removal in resting state fMRI.

Neuroimage 112:278–287. https://doi.org/10.1016/j.neuroimage.2015.02.063

Puntonet J, Richard ME, Edjlali M, et al (2019) Imaging Findings after Mechanical Thrombectomy in Acute Ischemic Stroke: Clinical Implications and Perspectives. Stroke 50:1618–1625. https://doi.org/10.1161/STROKEAHA.118.024754

Rabin JS, Gilboa A, Stuss DT, et al (2010) Common and Unique Neural Correlates of Autobiographical Memory and Theory of Mind. J Cogn Neurosci 22:1095–1111. https://doi.org/10.1162/jocn.2009.21344

Raichle ME (2015) The Brain's Default Mode Network. Annu Rev Neurosci 38:433–447. https://doi.org/10.1146/annurev-neuro-071013-014030

Raichle ME, MacLeod AM, Snyder AZ, et al (2001) A default mode of brain function. Proc Natl Acad Sci U S A 98:676–82. https://doi.org/10.1073/pnas.98.2.676

Rasquin SMC, Verhey FRJ, Van Oostenbrugge RJ, et al (2004) Demographic and CT scan features related to cognitive impairment in the first year after stroke. J Neurol Neurosurg Psychiatry 75:1562–1567. https://doi.org/10.1136/jnnp.2003.024190

Repantis D, Schlattmann P, Laisney O, Heuser I (2010) Modafinil and methylphenidate for neuroenhancement in healthy individuals: A systematic review. Pharmacol Res 62:187–206. https://doi.org/10.1016/j.phrs.2010.04.002

Rilling JK, Barks SK, Parr LA, et al (2007) A comparison of resting-state brain activity in humans and chimpanzees. Proc Natl Acad Sci 104:17146–17151

Ringman JM, Saver JL, Woolson RF, et al (2004) Frequency risk factors, anatomy, and course of unilateral neglect in an acute stroke cohort. Neurology 63:468–474

Rivière D, Geffroy D, Denghien I, et al (2011) Anatomist: a python framework for interactive 3D visualization of neuroimaging data. In: Python in Neuroscience workshop

Robinson EC, Jbabdi S, Glasser MF, et al (2014) MSM: A new flexible framework for Multimodal Surface Matching. Neuroimage 100:414–426. https://doi.org/10.1016/j.neuroimage.2014.05.069

Rodrigues FB, Neves JB, Caldeira D, et al (2016) Endovascular treatment versus medical care alone for ischaemic stroke: Systematic review and meta-analysis. BMJ 353:. https://doi.org/10.1136/bmj.i1754

Roeltgen DP, Lacey EH (2010) Reading, writing, and their disorders. Contin Lifelong Learn Neurol 16:59–68. https://doi.org/10.1212/01.CON.0000368260.15544.35

Rojkova K, Volle E, Urbanski M, et al (2016) Atlasing the frontal lobe connections and their variability due to age and education: a spherical deconvolution tractography

study. Brain Struct Funct 221:1751–1766. https://doi.org/10.1007/s00429-015-1001-3

Rolls ET, Huang CC, Lin CP, et al (2020) Automated anatomical labelling atlas 3. Neuroimage 206:. https://doi.org/10.1016/j.neuroimage.2019.116189

Romanski LM, Giguere M, Bates JF, Goldman-Rakic PS (1997) Topographic organization of medial pulvinar connections with the prefrontal cortex in the rhesus monkey. J Comp Neurol 379:313–332. https://doi.org/10.1002/(SICI)1096-9861(19970317)379:3<313::AID-CNE1>3.0.CO;2-6

Rorden C, Bonilha L, Fridriksson J, et al (2012) Age-specific CT and MRI templates for spatial normalization. Neuroimage 61:957–965. https://doi.org/10.1038/mp.2011.182.doi

Roy AK, Shehzad Z, Margulies DS, et al (2009) Functional connectivity of the human amygdala using resting state fMRI. Neuroimage 45:614–626. https://doi.org/10.1016/j.neuroimage.2008.11.030

Rubinov M, Sporns O (2010) Complex network measures of brain connectivity: Uses and interpretations. Neuroimage 52:1059–1069. https://doi.org/10.1016/j.neuroimage.2009.10.003

Sacks O, Hirsch J (2008) A neurology of belief. Ann Neurol 63:129–130. https://doi.org/10.1002/ana.21378

Salanova V, Witt T, Worth R, et al (2015) Long-term efficacy and safety of thalamic stimulation for drug-resistant partial epilepsy. Neurology 84:1017–1025. https://doi.org/10.1212/WNL.0000000000001334

Salimi-khorshidi G, Douaud G, Beckmann CF, et al (2014) Automatic denoising of functional MRI data: Combining independent component analysis and hierarchical fusion of classifiers. Neuroimage 90:449–468. https://doi.org/10.1016/j.neuroimage.2013.11.046

Sanefuji M, Craig M, Parlatini V, et al (2017) Double-dissociation between the mechanism leading to impulsivity and inattention in Attention Deficit Hyperactivity Disorder: A resting-state functional connectivity study. Cortex 86:290–302. https://doi.org/10.1016/j.cortex.2016.06.005

Sasaki T, Ito H, Kimura Y, et al (2012) Quantification of dopamine transporter in human brain using PET with 18F-FE-PE2I. J Nucl Med 53:1065–1073. https://doi.org/10.2967/jnumed.111.101626

Saunders R, Aggleton J (2007) Origin and topography of fibers contributing to the fornix in macaque monkeys. Hippocampus 17:396–411. https://doi.org/10.1002/hipo.20276

Schacter DL, Addis DR, Buckner RL (2007) Remembering the past to imagine the future: the prospective brain. Nat Rev Neurosci 8:657–61

Scheltens P, Kuiper M, Ch Wolters E, et al (1992) Atrophy of medial temporal lobes on MRI in "probable" Alzheimer's disease and normal ageing: diagnostic value and neuropsychological correlates. J Neurol Neurosurg Psychiatry 55:967–972. https://doi.org/10.1136/jnnp.55.10.967

Scofield MD, Heinsbroek JA, Gipson CD, et al (2016) The Nucleus Accumbens: Mechanisms of Addiction across Drug Classes Reflect the Importance of Glutamate Homeostasis. Pharmacol Rev 68:816–871. https://doi.org/10.1124/pr.116.012484

Seitz RJ (2021) Beliefs: A challenge in neuropsychological disorders. J. Neuropsychol.

Seitz RJ, Sondermann V, Wittsack HJ, Siebler M (2009) Lesion patterns in successful and failed thrombolysis in middle cerebral artery stroke. Neuroradiology 51:865–871. https://doi.org/10.1007/s00234-009-0576-x

Sellal F, Fontaine SF, Van Der Linden M, et al (1996) To be or not to be at home? A neuropsychological approach to delusion for place. J Clin Exp Neuropsychol 18:234–48. https://doi.org/10.1080/01688639608408278

Sepulcre J, Sabuncu MR, Yeo TB, et al (2012) Stepwise connectivity of the modal cortex reveals the multimodal organization of the human brain. J Neurosci 32:10649–10661. https://doi.org/10.1523/JNEUROSCI.0759-12.2012

Setsompop K, Gagoski BA, Polimeni JR, et al (2012) Blipped-controlled aliasing in parallel imaging for simultaneous multislice echo planar imaging with reduced g-factor penalty. Magn Reson Med 67:1210–1224. https://doi.org/10.1002/mrm.23097

Sforazzini F, Schwarz AJ, Galbusera A, et al (2014) Distributed BOLD and CBV-weighted resting-state networks in the mouse brain. Neuroimage 87:403–415. https://doi.org/10.1016/j.neuroimage.2013.09.050

Shapira-Lichter I, Oren N, Jacob Y, et al (2013) Portraying the unique contribution of the default mode network to internally driven mnemonic processes. Proc Natl Acad Sci 110:4950–4955. https://doi.org/10.1073/pnas.1209888110

Shapiro M, Raz E, Nossek E, et al (2020) Neuroanatomy of the middle cerebral artery: Implications for thrombectomy. J Neurointerv Surg 12:768–773. https://doi.org/10.1136/neurintsurg-2019-015782

Sharp DJ, Bonnelle V, De Boissezon X, et al (2010) Distinct frontal systems for response inhibition, attentional capture, and error processing. Proc Natl Acad Sci U S A 107:6106–6111. https://doi.org/10.1073/pnas.1000175107

Sherman SM (2007) The thalamus is more than just a relay. Curr Opin Neurobiol 17:417–422. https://doi.org/10.1016/j.conb.2007.07.003

Shine JM, Bissett PG, Bell PT, et al (2016) The dynamics of functional brain networks: integrated network states during cognitive task performance. Neuron 92:544–554. https://doi.org/10.1016/j.neuron.2016.09.018

Shu N, Liu Y, Li K, et al (2011) Diffusion tensor tractography reveals disrupted topological efficiency in white matter structural networks in multiple sclerosis. Cereb Cortex 21:2565–2577. https://doi.org/10.1093/cercor/bhr039

Shulman G, Corbetta M, Buckner RL, et al (1997a) Top-down modulation of early sensory cortex. Cereb cortex 7:193–206. https://doi.org/10.1093/cercor/7.3.193

Shulman G, Fiez JA, Corbetta M, et al (1997b) Common Blood Flow Changes across Visual Tasks : II . Decreases in Cerebral Cortex. J Cogn Neurosci 9:648–663. https://doi.org/10.1162/jocn.1997.9.5.648

Simons DJ, Wang RF (1998) Perceiving real-world viewpoint changes. Psychol Sci 9:315–320

Simons JS, Garrison JR, Johnson MK (2017) Brain Mechanisms of Reality Monitoring. Trends Cogn Sci 21:462–473. https://doi.org/10.1016/j.tics.2017.03.012

Smallwood J, Bernhardt BC, Leech R, et al (2021) The default mode network in cognition: a topographical perspective. Nat Rev Neurosci 22:503–513. https://doi.org/10.1038/s41583-021-00474-4

Smith DM, Bulkin DA (2014) The form and function of hippocampal context representations. Neurosci Biobehav Rev 40:52–61. https://doi.org/10.1016/j.neubiorev.2014.01.005

Smith SM, Fox PT, Miller KL, et al (2009) Correspondence of the brain's functional architecture during activation and rest. Proc Natl Acad Sci U S A 106:13040–13045. https://doi.org/10.1073/pnas.0905267106

Smith SM, Jenkinson M, Woolrich MW, et al (2004) Advances in functional and structural MR image analysis and implementation as FSL. Neuroimage 23:208–219. https://doi.org/10.1016/j.neuroimage.2004.07.051

Sperber C, Karnath HO (2017) Impact of correction factors in human brain lesion-behavior inference. Hum Brain Mapp 38:1692–1701. https://doi.org/10.1002/hbm.23490

Spetsieris PG, Ko JH, Tang CC, et al (2015) Metabolic resting-state brain networks in health and disease. Proc Natl Acad Sci U S A 112:2563–2568. https://doi.org/10.1073/pnas.1411011112

Spies M, Kraus C, Geissberger N, et al (2017) Default mode network deactivation during emotion processing predicts early antidepressant response. Transl Psychiatry 7:e1008. https://doi.org/10.1038/tp.2016.265

Sprague JM (1966) Interaction of cortex and superior colliculus in mediation of visually guided behavior in the cat. Science (80-) 153:1544–1547. https://doi.org/10.1126/science.153.3743.1544

Spreng RN, Grady CL (2010) Patterns of Brain Activity Supporting Autobiographical Memory, Prospection, and Theory of Mind, and Their Relationship to the Default Mode Network. J Cogn Neurosci 22:1112–1123. https://doi.org/10.1162/jocn.2009.21282

Spreng RN, Mar RA, Kim ASN (2009) The Common Neural Basis of Autobiographical Memory, Prospection, Navigation, Theory of Mind, and the Default Mode: A Quantitative Meta-analysis. J Cogn Neurosci 21:489–510. https://doi.org/10.1162/jocn.2008.21029

Stangeland H, Orgeta V, Bell V (2018) Poststroke psychosis: A systematic review. J Neurol Neurosurg Psychiatry 89:879–885. https://doi.org/10.1136/jnnp-2017-317327

Staton RD, Brumback RA, Wilson H (1982) Reduplicative paramnesia: a disconnection syndrome of memory. Cortex 18:23–35. https://doi.org/10.1016/S0010-9452(82)80016-6

Stepniewska I, Kaas JH (1997) Architectonic subdivisions of the inferior pulvinar in New World and Old World monkeys. Vis Neurosci 14:1043–1060. https://doi.org/10.1017/s0952523800011767

Steriade M, Paré D, Parent A, Smith Y (1988) Projections of cholinergic and non-cholinergic neurons of the brainstem core to relay and associational thalamic nuclei in the cat and macaque monkey. Neuroscience 25:47–67. https://doi.org/10.1016/0306-4522(88)90006-1

Stoodley CJ, Schmahmann JD (2009) NeuroImage Functional topography in the human cerebellum : A meta-analysis of neuroimaging studies. Neuroimage 44:489–501. https://doi.org/10.1016/j.neuroimage.2008.08.039

Stumps A, Saad E, Rothlein D, et al (2020) Characterizing developmental prosopagnosia beyond face perception: Impaired recollection but intact familiarity recognition. Cortex 130:64–77. https://doi.org/10.1016/j.cortex.2020.04.016

Su JH, Thomas FT, Kasoff WS, et al (2019) Thalamus Optimized Multi Atlas Segmentation (THOMAS): fast, fully automated segmentation of thalamic nuclei

from structural MRI. Neuroimage 194:272–282. https://doi.org/10.1016/j.neuroimage.2019.03.021

Suárez L, Markello R, Betzel R, Misic B (2020) Linking structure and function in macroscale brain. Trends Cogn Sci 24:302–315. https://doi.org/10.1016/j.tics.2020.01.008

Sun Y, Yang Y, Galvin VC, et al (2017) Nicotinic α4β2 cholinergic receptor influences on dorsolateral prefrontal cortical neuronal firing during a working memory task. J Neurosci 37:5366–5377. https://doi.org/10.1523/JNEUROSCI.0364-17.2017

Tagliamonte M, Sestieri C, Romani GL, et al (2013) MRI anatomical variants of mammillary bodies. Brain Struct Funct 220:85–90. https://doi.org/10.1007/s00429-013-0639-y

Talairach J, Tournoux P (1988) Co-planar stereotaxic atlas of the human brain. Thieme, New York

Tanriover N, Kawashima M, Rhoton AL, et al (2003) Microsurgical anatomy of the early branches of the middle cerebral artery: Morphometric analysis and classification with angiographic correlation. J Neurosurg 98:1277–1290. https://doi.org/10.3171/jns.2003.98.6.1277

Taube J, Muller R, Ranck JJ (1990) Head-direction cells recorded from the postsubiculum in freely moving rats. I. Description and quanti- tative analysis. J Neurosci 10:420–435

Taube JS (2007) The head direction signal: Origins and sensory-motor integration. Annu Rev Neurosci 30:181–207. https://doi.org/10.1146/annurev.neuro.29.051605.112854

Tessitore A, Esposito F, Vitale C, et al (2012) Default-mode network connectivity in cognitively unimpaired patients with Parkinson disease. Neurology 79:2226–2232. https://doi.org/10.1212/WNL.0b013e31827689d6

The NINDS rt-PA Stroke Study (1995) Recombinant tissue plasminogen activator for acute ischemic stroke. N Eng J Med 333:1581–7. https://doi.org/10.1056/NEJM199512143332401

Thiebaut de Schotten M, Acqua FD, Forkel SJ, et al (2011a) A lateralized brain network for visuospatial attention. Nat Neurosci 14:1245–47. https://doi.org/10.1038/nn.2905

Thiebaut de Schotten M, Ffytche D, Bizzi A, et al (2011b) Atlasing location, asymmetry and inter-subject variability of white matter tracts in the human brain with MR diffusion tractography. Neuroimage 54:49–59. https://doi.org/10.1016/j.neuroimage.2010.07.055

Thiebaut de Schotten M, Foulon C, Nachev P (2020) Brain disconnections link structural connectivity with function and behaviour. Nat Commun 11:5094. https://doi.org/10.1038/s41467-020-18920-9

Thiebaut de Schotten M, Shallice T (2017) Identical, similar or different? Is a single brain model sufficient? Cortex 86:172–175. https://doi.org/10.1016/j.cortex.2016.12.002

Thiebaut de Schotten M, Tomaiuolo F, Aiello M, et al (2014) Damage to white matter pathways in subacute and chronic spatial neglect: A group study and 2 single-case studies with complete virtual "in vivo" tractography dissection. Cereb Cortex 24:691–706

Thomas Yeo BT, Krienen FM, Sepulcre J, et al (2011) The organization of the human cerebral cortex estimated by intrinsic functional connectivity. J Neurophysiol 106:1125–1165. https://doi.org/10.1152/jn.00338.2011

Tomasi D, Volkow ND (2018) Association between brain activation and functional connectivity. Cereb Cortex 1–13. https://doi.org/10.1093/cercor/bhy077

Tournier JD, Calamante F, Connelly A (2012) MRtrix: Diffusion tractography in crossing fiber regions. Int J Imaging Syst Technol 22:53–66. https://doi.org/10.1002/ima.22005

Tournier JD, Smith R, Raffelt D, et al (2019) MRtrix3: A fast, flexible and open software framework for medical image processing and visualisation. Neuroimage 202:. https://doi.org/10.1016/j.neuroimage.2019.116137

Tranel D, Damasio H, Damasio AR (1995) Double dissociation between overt and covert face recognition. J Cogn Neurosci 7:425–432. https://doi.org/10.1162/jocn.1995.7.4.425

Turc G, Bhogal P, Fischer U, et al (2019) European Stroke Organisation (ESO) - European Society for Minimally Invasive Neurological Therapy (ESMINT) Guidelines on Mechanical Thrombectomy in Acute Ischemic Stroke. J Neurointerv Surg 1–30. https://doi.org/10.1136/neurintsurg-2018-014569

Turner DC, Clark L, Dowson J, et al (2004) Modafinil improves cognition and response inhibition in adult attention-deficit/hyperactivity disorder. Biol Psychiatry 55:1031–1040. https://doi.org/10.1016/j.biopsych.2004.02.008

Umarova RM, Schumacher L V., Schmidt CSM, et al (2021) Interaction between cognitive reserve and age moderates effect of lesion load on stroke outcome. Sci Rep 11:1–10. https://doi.org/10.1038/s41598-021-83927-1

Valentine G, Sofuoglu M (2017) Cognitive Effects of Nicotine: Recent Progress. Curr

Neuropharmacol 16:403–414. https://doi.org/10.2174/1570159x15666171103152136

Valero-Cabré A, Toba MN, Hilgetag CC, Rushmore RJ (2020) Perturbation-driven paradoxical facilitation of visuo-spatial function: Revisiting the 'Sprague effect.' Cortex 122:10–39. https://doi.org/10.1016/j.cortex.2019.01.031

Van De Kar LD, Lorens SA (1979) Differential serotonergic innervation of individual hypothalamic nuclei and other forebrain regions by the dorsal and median midbrain raphe nuclei. Brain Res 162:45–54. https://doi.org/10.1016/0006-8993(79)90754-6

van den Heuvel MP, Sporns O (2013) Network hubs in the human brain. Trends Cogn Sci 17:683–696. https://doi.org/10.1016/j.tics.2013.09.012

van Dijk KRA, Sabuncu MR, Buckner RL (2012) The influence of head motion on intrinsic functional connectivity MRI. Neuroimage 59:431–438. https://doi.org/10.1016/j.neuroimage.2011.07.044

van Oort ESB, van Cappellen van Walsum AM, Norris DG (2014) An investigation into the functional and structural connectivity of the Default Mode Network. Neuroimage 90:381–389. https://doi.org/10.1016/j.neuroimage.2013.12.051

Varoquaux G, Raamana PR, Engemann DA, et al (2017) Assessing and tuning brain decoders: Cross-validation, caveats, and guidelines. Neuroimage 145:166–179. https://doi.org/10.1016/j.neuroimage.2016.10.038

Vatansever D, Menon DK, Manktelow AE, et al (2015) Default mode dynamics for global functional integration. J Neurosci 35:15254–15262. https://doi.org/10.1523/JNEUROSCI.2135-15.2015

Vazey EM, Moorman DE, Aston-Jones G (2018) Phasic locus coeruleus activity regulates cortical encoding of salience information. Proc Natl Acad Sci U S A 115:E9439–E9448. https://doi.org/10.1073/pnas.1803716115

Vialou V, Robison AJ, Laplant QC, et al (2010) DeltaFosB in brain reward circuits mediates resilience to stress and antidepressant responses. Nat Neurosci 13:745–752. https://doi.org/10.1038/nn.2551

Vicq D'Azyr F (1786) Traité d'anatomie et de physiologie, avec des planches coloriées représentant au naturel les divers organes de l'Homme et des Animaux. François-Ambroise Didot, Paris

Vighetto A, Aimard G, Confavreux C, Devic M (1980) Une observation anatomo-clinique de Fabulation (Ou Délire) Topografique. Cortex 16:501–7. https://doi.org/10.1016/S0010-9452(80)80052-9

Vighetto A, Henry E, Garde P, Aimard G (1985) Spatial delusion: sign of lesions of the

non-dominant hemisphere. Rev Neurol(Paris) 141:476–81

Vincent JL, Patel GH, Fox MD, et al (2007) Intrinsic functional architecture in the anaesthetized monkey brain. Nature 447:83–88. https://doi.org/10.1038/nature05758

Vincent JL, Snyder AZ, Fox MD, et al (2006) Coherent Spontaneous Activity Identifies a Hippocampal-Parietal Memory Network. J Neurophysiol 96:3517–3531. https://doi.org/10.1152/jn.00048.2006

Vinogradov S, Luks TL, Simpson G V., et al (2006) Brain activation patterns during memory of cognitive agency. Neuroimage 31:896–905. https://doi.org/10.1016/j.neuroimage.2005.12.058

Vocat R, Saj A, Vuilleumier P (2013) The riddle of anosognosia: Does unawareness of hemiplegia involve a failure to update beliefs? Cortex 49:1771–1781. https://doi.org/10.1016/j.cortex.2012.10.009

Vocat R, Staub F, Stroppini T, Vuilleumier P (2010) Anosognosia for hemiplegia: A clinical-anatomical prospective study. Brain 133:3578–3597. https://doi.org/10.1093/brain/awq297

Voets NL, Beckmann CF, Cole DM, et al (2012) Structural substrates for resting network disruption in temporal lobe epilepsy. Brain 135:2350–2357. https://doi.org/10.1093/brain/aws137

Volkow ND, Wang GJ, Newcorn JH, et al (2011) Motivation deficit in ADHD is associated with dysfunction of the dopamine reward pathway. Mol Psychiatry 16:1147–1154. https://doi.org/10.1038/mp.2010.97

Vos SB, Tax CMW, Luijten PR, et al (2017) The Importance of Correcting for Signal Drift in Diffusion MRI. Magn Reson Med 77:285–299. https://doi.org/10.1002/mrm.26124

Vossel S, Geng JJ, Fink GR (2014) Dorsal and ventral attention systems: Distinct neural circuits but collaborative roles. Neuroscientist 20:150–159. https://doi.org/10.1177/1073858413494269

Vu AT, Auerbach E, Lenglet C, et al (2015) High resolution whole brain diffusion imaging at 7T for the Human Connectome Project. Neuroimage 122:318–331. https://doi.org/10.1016/j.neuroimage.2015.08.004

Wagner AD, Shannon BJ, Kahn I, Buckner RL (2005) Parietal lobe contributions to episodic memory retrieval. Trends Cogn Sci 9:445–453. https://doi.org/10.1016/j.tics.2005.07.001

Wahlund LO, Barkhof F, Fazekas F, et al (2001) A new rating scale for age-related white matter changes applicable to MRI and CT. Stroke 32:1318–1322.

https://doi.org/10.1161/01.STR.32.6.1318

Wahlund LO, Westman E, van Westen D, et al (2017) Imaging biomarkers of dementia: recommended visual rating scales with teaching cases. Insights Imaging 8:79–90. https://doi.org/10.1007/s13244-016-0521-6

Washburn DA, Taglialatela LA (2006) Attention as it is manifest across species. In: Wasserman EA, Zentall TR (eds) Comparative cognition: Experimental explorations of animal intelligence. Oxford University Press, New York, pp 127–142

Wasserman EA, Castro L (2021) Assessing Attention in Category Learning by Animals. Curr Dir Psychol Sci 30:495–502. https://doi.org/10.1177/09637214211045686

Wassermann D, Makris N, Rathi Y, et al (2016) The white matter query language: a novel approach for describing human white matter anatomy. Brain Struct Funct 221:4705–4721. https://doi.org/10.1007/s00429-015-1179-4

Weaver NA, Kuijf HJ, Aben HP, et al (2021) Strategic infarct locations for post-stroke cognitive impairment: a pooled analysis of individual patient data from 12 acute ischaemic stroke cohorts. Lancet Neurol 20:448–459. https://doi.org/10.1016/S1474-4422(21)00060-0

Weddell RA (2004) Subcortical modulation of spatial attention including evidence that the Sprague effect extends to man. Brain Cogn 55:497–506. https://doi.org/10.1016/j.bandc.2004.02.075

Whitfield-Gabrieli S, Ford JM (2012) Default mode network activity and connectivity in psychopathology. Annu Rev Clin Psychol 8:49–76. https://doi.org/10.1146/annurev-clinpsy-032511-143049

Winkler AM, Ridgway GR, Webster MA, et al (2014) Permutation inference for the general linear model. Neuroimage 92:381–397. https://doi.org/10.1016/j.neuroimage.2014.01.060

Witwer BP, Moftakhar R, Hasan KM, et al (2002) Diffusion-tensor imaging of white matter tracts in patients with cerebral neoplasm. J Neurosurg 97:568–575. https://doi.org/10.3171/jns.2002.97.3.0568

Wolbers T, Hegarty M, Büchel C, Loomis JM (2008) Spatial updating: How the brain keeps track of changing object locations during observer motion. Nat Neurosci 11:1223–1230. https://doi.org/10.1038/nn.2189

Woolrich MW, Jbabdi S, Patenaude B, et al (2009) Bayesian analysis of neuroimaging data in FSL. Neuroimage 45:S173–S186. https://doi.org/10.1016/j.neuroimage.2008.10.055

Wu D, Fan L, Song M, et al (2020) Hierarchy of connectivity-function relationship of the human cortex revealed through predicting activity across functional domains. Cereb Cortex 30:4607–4616. https://doi.org/10.1093/cercor/bhaa063

Xia M, Wang J, He Y (2013) BrainNet Viewer: A Network Visualization Tool for Human Brain Connectomics. PLoS One 8:. https://doi.org/10.1371/journal.pone.0068910

Xu J, Moeller S, Auerbach EJ, et al (2013) Evaluation of slice accelerations using multiband echo planar imaging at 3T. Neuroimage 83:991–1001. https://doi.org/10.1016/j.neuroimage.2013.07.055

Yakovlev PI (1948) Motility, behaviour and the brain: stereodynamic organization and neural correlates of behaviour. J Nerve Men Dis 107:313–35

Yakovlev PI, Locke S (1961) Limbic Nuclei of Thalamus and Connections of Limbic Cortex III. Corticocortical Connections of the Anterior Cingulate Gyrus, the Cingulum, and the Subcallosal Bundle in Monkey. Arch Neurol 5:364–400

Yamada M, Murai T, Ohigashi Y (2003) Postoperative reduplicative paramnesia in a patient with a right frontotemporal lesion. Psychogeriatrics 3:127–131. https://doi.org/10.1111/j.1479-8301.2003.00017.x

Yamamoto K, Solal B, Philippe V (2017) New perspective on the regionalization of the anterior forebrain in Osteichthyes. Dev Growth Regen 59:175–187. https://doi.org/10.1111/dgd.12348

Yamamura T, Okamoto Y, Okada G, et al (2016) Association of thalamic hyperactivity with treatment-resistant depression and poor response in early treatment for major depression: a resting-state fMRI study using fractional amplitude of low-frequency fluctuations. Transl Psychiatry 6:e754. https://doi.org/10.1038/tp.2016.18

Yarkoni T, Poldrack RA, Nichols TE, et al (2011) Large-scale automated synthesis of human functional neuroimaging data. Nat Methods 8:665–670. https://doi.org/10.1038/nmeth.1635

Young AW, Hellawell DJ, Wright S, Ellis HD (1994) Reduplication of visual stimuli. Behav Neurol 7:135–142. https://doi.org/10.3233/BEN-1994-73-405

Zaborszky L, Csordas A, Mosca K, et al (2015) Neurons in the Basal Forebrain Project to the Cortex in a Complex Topographic Organization that Re fl ects Corticocortical Connectivity Patterns : An Experimental Study Based on Retrograde Tracing and 3D Reconstruction. Cereb Cortex 25:118–37. https://doi.org/10.1093/cercor/bht210

Zaborszky L, Hoemke L, Mohlberg H, et al (2008) Stereotaxic probabilistic maps of the magnocellular cell groups in human basal forebrain. Neuroimage 42:1127–1141.

https://doi.org/10.1016/j.neuroimage.2008.05.055

Zénon A, Krauzlis RJ (2012) Attention deficits without cortical neuronal deficits. Nature 489:434–437. https://doi.org/10.1038/nature11497

Zhao J, Tomasi D, Wiers CE, et al (2017) Correlation between traits of emotion-based impulsivity and intrinsic default-mode network activity. Neural Plast 2017:. https://doi.org/10.1155/2017/9297621

Zhu X, Zhu Q, Shen H, et al (2017) Rumination and Default Mode Network Subsystems Connectivity in First-episode, Drug-Naive Young Patients with Major Depressive Disorder. Sci Rep 7:43105. https://doi.org/10.1038/srep43105

Zhu Y, Wienecke CFR, Nachtrab G, Chen X (2016) A thalamic input to the nucleus accumbens mediates opiate dependence. Nature 530:219–222. https://doi.org/10.1038/nature16954

Zoli M, Moretti M, Zanardi A, et al (2002) Identification of the nicotinic receptor subtypes expressed on dopaminergic terminals in the rat striatum. J Neurosci 22:8785–8789. https://doi.org/10.1523/jneurosci.22-20-08785.2002

Zolkowska D, Jain R, Rothman RB, et al (2009) Evidence for the involvement of dopamine transporters in behavioral stimulant effects of modafinil. J Pharmacol Exp Ther 329:738–746. https://doi.org/10.1124/jpet.108.146142

Attachments

The following pages include the *facsimile* of the published article, in the following order:

1) Alves PN, Silva DP, Fonseca AC, Martins IP (2021) Mapping delusions of space onto a structural disconnectome that decouples familiarity and place networks. Cortex 146:250–260. https://doi.org/10.1016/j.cortex.2021.11.008.

2) Alves PN, Fonseca AC, Pinho-e-Melo T, Martins IP (2022) Clinical features and neural correlates of stroke-associated spatial delusions. Eur J Neurol 30(1):125–133. https://doi.org/10.1111/ene.15557.

3) Alves PN, Fonseca AC, Silva DP, Andrade MR, Pinho-e-Melo T, Thiebaut de Schotten M, Martins IP (2021) Unravelling the neural basis of spatial delusions after stroke. Ann Neurol 89:1181–1194. https://doi.org/10.1002/ana.26079.

4) Alves PN, Foulon C, Karolis V, Bzdok S, Margulies DS, Volle E, Thiebaut de Schotten M (2019) An improved neuroanatomical model of the default-mode network reconciles previous neuroimaging and neuropathological findings. Commun Biol 2:370. https://doi.org/10.1038/s42003-019-0611-3.

5) Alves PN, Forkel JS, Corbetta M, Thiebaut de Schotten M (2022) The subcortical and neurochemical organisation of the ventral and dorsal attention networks. Commun Biol 5:1343. https://doi.org/10.1038/s42003-022-04281-0.

CORTEX 146 (2022) 250–260

Available online at www.sciencedirect.com

ScienceDirect

Journal homepage: www.elsevier.com/locate/cortex

Research Report

Mapping delusions of space onto a structural disconnectome that decouples familiarity and place networks

Pedro N. Alves [a,b,c,*], *Daniela P. Silva* [b], *Ana C. Fonseca* [b,c] *and Isabel P. Martins* [a,b,c]

[a] *Language Research Laboratory, Faculty of Medicine, Universidade de Lisboa, Lisbon, Portugal*
[b] *Department of Neurosciences and Mental Health, Neurology, Hospital de Santa Maria, CHULN, Lisbon, Portugal*
[c] *Instituto de Medicina Molecular João Lobo Antunes, Faculty of Medicine, Universidade de Lisboa, Lisbon, Portugal*

ARTICLE INFO

Article history:
Received 29 June 2021
Reviewed 12 August 2021
Revised 4 October 2021
Accepted 12 November 2021
Action editor Stephanie Forkel
Published online 27 November 2021

Keywords:
Spatial orientation
Connectivity
Delusions of space
Reduplicative paramnesia

ABSTRACT

Interpretation of space is an important determinant of human behaviour. Delusions of space, or reduplicative paramnesias, are a particularly disturbing form of spatial disorientation characterized by the patients' strong belief of place reduplication, transformation or mislocation. Their occurrence following focal brain damage provides a unique opportunity to unveil the structural-functional basis of space misinterpretations.

First, we identified reports of lesion-associated reduplicative paramnesias with brain images available through a systematic review of the literature (n = 24). Each lesion was matched with 4 stroke controls and the sample was randomly split in an exploratory (n = 60) and in a validation (n = 60) dataset. Second, we used 178 7T tractographies to compute structural disconnectome maps and analysed lesion topography and disconnection patterns. Delusions of space were significantly associated with structural disconnection of right ventrolateral prefrontal and right temporal regions, and this finding was replicated in the validation sample. Third, we performed a functional meta-analysis of syndrome-related terms. We demonstrated that the structural disconnectomes of delusions of space were spatially correlated with the functional meta-analytic maps of familiarity and place, and replicated the previous evidence that the lesion topography maps are spatially correlated with belief-related functional networks. No association was found with control terms.

These results reveal that structural disconnection putatively mediates functional changes associated with reduplicative paramnesias and provide a possible neural basis for the content specificity for places that characterizes these delusional beliefs.

* *Corresponding author*. Laboratório de Estudos de Linguagem, Serviço de Neurologia, Hospital de Santa Maria, CHULN, Avenida Professor Egas Moniz, 1649-028 Lisboa, Portugal.
E-mail address: pedronascimentoalves@gmail.com (P.N. Alves).
https://doi.org/10.1016/j.cortex.2021.11.008
0010-9452/

1. Introduction

Spatial disorientation is a striking manifestation of brain disease, which profoundly disturbs patients' behaviour. Delusions of space, also known as reduplicative paramnesia, are a particularly disrupting subtype of spatial disorientation. Patients present prominent misinterpretations of space, believing that they are in a different place from the real one, and their conviction is unchangeable even after being exposed to evidence that would clearly prove otherwise (Pick, 1903). They may believe that they are in a replica or duplication of a certain place (i.e., place reduplication), in a space that results from the combination or fusion of two distinct places (i.e., chimeric assimilation), or in a place that is substantially different from the real one (i.e., confabulatory mislocation; Politis & Loane, 2012).

Observational studies have demonstrated that reduplicative paramnesia is a frequent manifestation of different brain disorders, either of degenerative or focal aetiology. In a cohort of patients with right hemispheric focal brain injuries (either right-side or bilateral) who were admitted to a rehabilitation centre (mostly stroke and traumatic brain injuries), Murai and colleagues reported a prevalence of 17% (Murai, Toichi, Sengoku, Miyoshi, & Morimune, 1997). In Dementia with Lewy bodies, the described prevalence is 20% (Nagahama et al., 2007), while in the moderate stages of Alzheimer's disease it might be as high as 30% (Perini et al., 2016). At the neuropsychological level, reduplicative paramnesia has been associated with neuropsychological deficits in executive functions and in non-verbal episodic memory tasks (Borghesani, Monti, Fortis, & Miceli, 2019). However, the neuroanatomical basis of this syndrome remains elusive (Bartolomeo, Vito, & Seidel, 2016). On the one hand, delusions misidentifications have been associated with functional disturbances of familiarity and belief evaluation networks (Darby, Laganiere, Pascual-Leone, Prasad, & Fox, 2017), but how this relationship is established at the structural level is uncertain. On the other hand, the neural basis of the content specificity for places that characterizes the delusional beliefs of reduplicative paramnesia is undetermined.

The occurrence of delusions of space after focal brain lesions constitutes a particular opportunity to unveil the neuroanatomical circuits underlying their phenomenological and functional features. Here, we aimed to study the structural connectivity patterns of reported lesion-associated reduplicative paramnesias, and to analyse their spatial relationship with functionally related network maps.

2. Materials and methods

2.1. Search strategy and selection criteria

To identify cases of reduplicative paramnesia associated with focal brain lesions, we performed a systematic review. Protocol development and result reports were done according to The Preferred Reporting Items for Systematic Reviews and Meta-Analyses (PRISMA) guidelines (PRISMA checklist provided in the Supplemental Table 1).

The search term 'reduplicative paramnesia' and the related search terms 'reduplicative phenomenon', 'chimeric assimilation', 'confabulatory mislocation', 'extravagant spatial localization', 'delusional misidentification', 'space confabulation', 'spatial confabulation' and 'spatial delirium' were applied in the databases Pubmed, EMBASE, PsycInfo and Web of Science. First, the abstracts were screened. If there was not enough information in the abstract, the full text was consulted. The specific search formulae, the inclusion and exclusion criteria, and the data extracted are available in the Supplemental Tables 2 and 3.

Our database search retrieved a total of 1949 references, 932 repeated references were removed and the free search resulted in 7 new references. The total number of analysed references was 1024. A total of 708 references were excluded after abstract screening and 166 after assessing the full text. Of the 57 articles included, most were case reports and case series. The flow diagram of study selection is displayed in Supplemental Fig. 1. The total number of patients with reduplicative paramnesia was 123. Of these, 67 were associated with focal brain lesions. Twenty-four cases had MRI or CT images available (MRI, n = 10; CT, n = 14). All images were reported separately, i.e., none corresponded to group-level analyses.

2.2. Neuroimaging analysis

2.2.1. Lesion topography

The reports with brain images available were selected. Each lesion was mapped onto a common brain atlas, the MNI152 1 mm standard space. Two clinicians with experience in the analysis of brain images (PNA and DPS) performed lesion tracing. The slices that best matched the published images in each article (either, axial, coronal or sagittal) were chosen by consensus between the two clinicians. Neuroanatomical landmarks were used as reference for slice selection (Boes et al., 2015). Then, both authors independently performed lesion tracing on the selected slices using FSLeyes (https://fsl.fmrib.ox.ac.uk/fsl/fslwiki/FSLeyes). Inter-observer agreement was analysed by calculating the Dice similarity coefficient (Liew et al., 2018):

$$DC = \frac{2|X \cap Y|}{|X| + |Y|}$$

where X and Y represent the voxels selected by each investigator, and DC represents the similarity coefficient that ranges from 0 (no overlap) to 1 (perfect overlap). The percentage of voxels for which the investigators disagreed was also calculated. Lesions were extended 2 mm perpendicular to the planes they were registered. According to Boes and colleagues, this method allows a conservative balance between inflated and scarce lesion overlap when lesions are extracted from the literature, as performed in our study (Boes et al., 2015).

For statistical analysis, two different control datasets were used. We used a database of 233 stroke lesions prospectively collected in our stroke unit. Patients were recruited from December 2016 to February 2020. Reduplicative paramnesia is a right-hemisphere syndrome (Bartolomeo et al., 2016). The database included ischaemic stroke and intracerebral haemorrhage lesions with right hemisphere involvement (either

right-sided or bilateral). Patients were systematically evaluated for reduplicative paramnesia and none of the included patients presented reduplicative paramnesia during the period of their hospitalization (median length of hospitalization = 7 days, interquartile range 5–11 days). Lesion delimitation was performed manually based on MRI (preferentially) or CT images in the native space. Then, the images were registered to the MNI152 space. For MRI, the sequence of reference for lesion delimitation was the diffusion-weighted imaging (de Haan & Karnath, 2018). T1 images were linearly registered applying an affine transformation (12 degrees of freedom) using FSL FLIRT tool (Jenkinson, Beckmann, Behrens, Woolrich, & Smith, 2012). Then, a non-linear registration was performed using FSL FNIRT tool. For CT images, a linear registration with an affine transformation was performed (de Haan & Karnath, 2018). Finally, the deformation fields were applied to the lesion masks.

In addition, we used the open-source dataset ATLAS (Anatomical Tracings of Lesions After Stroke; Liew et al., 2018). ATLAS is a multicentre neuroimaging collection, derived from 11 cohorts worldwide, that includes 304 ischaemic stroke lesions of different arterial territories. Lesions were manually delimited based on high resolution T1-weighted structural MRI, and 229 of them were normalized to the MNI152 space. No behavioural data is publicly available in this dataset.

For proper comparison of reduplicative paramnesia lesions extracted from the literature, we selected the slices from the stroke controls dataset where there were lesions in the reduplicative paramnesia group (Barahona-Corrêa et al., 2020). Then, they were matched for lesion volume and for hemispheric lateralization (either right, left or bilateral). Each reduplicative paramnesia lesion was matched with four control stroke lesions, two from our inward dataset and two from the ATLAS dataset.

Randomise is a FSL tool that computes nonparametric permutation inference on neuroimaging data (Winkler, Ridgway, Webster, Smith, & Nichols, 2014). To calculate brain areas significantly associated with reduplicative paramnesia, a permutation test comparing cases and stroke controls was performed using this tool (Winkler et al., 2014). Five thousand permutations were computed, applying a threshold-free cluster enhancement, and the statistical maps were family-wise error corrected.

To evaluate the generalization of our results, the sample was split in two groups: the exploratory sample and the validation sample. Splitting was performed randomly, controlling for lesion volume. First, we run randomise in the exploratory sample. If there were statistically significant differences between cases and stroke controls, we analysed if the results were replicable in the validation sample, i.e., if the regions that were found in the exploratory sample also presented statically significant differences in the validation sample.

Age is a proxy of brain reserve and is an important determinant of cognitive disturbances after focal brain lesions (Umarova et al., 2021). Therefore, we also performed a regression analysis, using FSL's tool randomise, in which we included patients' age as a covariate in the model (de Haan & Karnath, 2018). In this analysis, we could not include the control stroke lesions from ATLAS dataset, because the information about the age of these patients is not publicly available. Since no information is available about the putative occurrence of reduplicative paramnesia in the ATLAS dataset, this sensitivity analysis also allowed a comparison with control stroke patients that were systematically assessed for the presence of the syndrome.

2.2.2. *Structural connectivity*

Disconnectome (http://www.bcblab.com; Foulon et al., 2018; Thiebaut de Schotten et al., 2014) is a tool that superimposes brain lesion maps onto tractography reconstructions obtained from a group of healthy controls and indirectly estimates which fibre tracts would be disrupted by a focal lesion. The output is a structural disconnection map representing the probability of each voxel being disconnected by a certain lesion. We derived disconnection maps from the 7T dataset of the Human Connectome Project (n = 178; Vu et al., 2015). Tractographies were obtained using a whole-brain deterministic approach, using the StarTrack software (https://mr-startrack.com), and applying a spherical deconvolution methodology, specifically a damped Richardson-Lucy algorithm. They were made available with BCBtoolkit (http://www.bcblab.com) and the full details of pre-processing are described in Karolis, Corbetta, & Thiebaut de Schotten, 2019. Voxels were included in the disconnectome map if they were disconnected in more than 50% of tractographies (Foulon et al., 2018).

Randomise was used to perform the permutation test comparing the structural disconnection maps between cases and stroke controls, using the same settings and the same cross-validation approach detailed in section about the lesion topography analysis. In addition, we performed a regression analysis including patients' age as a covariate in the model, as specified in the previous section. Since tumours may displace surrounding white matter tracts (Witwer et al., 2002) and bias the structural connectivity analysis, a supplemental analysis excluding tumoral lesions was also computed.

2.2.3. *Classification performance of the lesion topography and of the structural disconnection maps*

To evaluate the classification performance of the neuroimaging models, i.e., their accuracy to correctly identify cases of reduplicative paramnesia in an independent lesion sample, voxel-wise balanced accuracy maps were computed using lesion topography maps or structural disconnection maps as predictors. Logistic regression was the classification algorithm applied, and the output variable was the occurrence of reduplicative paramnesia. First, the models were trained (i.e., the logistic weights were estimated) in the exploratory sample. Then, the performance of the logistic model to correctly classify a neuroimaging input as corresponding or not to a case of reduplicative paramnesia (at a voxel level) was evaluated in the validation sample. Therefore, the classification performance was evaluated in a group of neuroimaging maps that did not contribute to the building of the model.

Our dataset was imbalanced, in a ratio of 1 case to 4 controls. Evaluation of classification performance in imbalanced datasets can be misleading, because most predictive techniques have a poor performance on the minority class (He & Garcia, 2019). To address this issue, we used the Synthetic Minority Over-sampling Technique (SMOTE) algorithm to

perform a synthetic over-sampling of the minority class in the exploratory sample, by linearly interpolating new minority instances between the 5 nearest neighbours, as recommended (Chawla, Bowyer, Hall, & Kegelmeyer, 2002; Luque, Carrasco, Martín, & de lasHeras, 2019). Balanced accuracy was chosen as the classification metric, to avoid the spuriously high accuracy estimations that may occur in the evaluation of imbalanced datasets (Chawla, 2005). The analysis was performed using scikit-learn .24.1 package (Pedregosa et al., 2011).

2.2.4. *Structural–functional coupling*

Neurosynth (http://neurosynth.org/) is an automated and validated tool to extract large-scale neuroimaging data from the literature (Yarkoni, Poldrack, Nichols, Essen, & Wager, 2011). Based on text-mining and machine-learning techniques, it generates meta-analytic maps of functional studies whose abstract mention a certain term of interest.

Darby and colleagues (Darby et al., 2017) studied the relationship between the functional meta-analytic maps of familiarity and belief evaluation and the functional connectivity maps of 17 lesion-induced delusional misidentifications. They found an overlap between them, however it is unknown how this relationship is established at the structural level, i.e., if it is mediated directly by the lesions or by structural disconnection. Here, we used Neurosynth to generate functional meta-analytic maps of similar terms, namely 'familiarity' and 'belief'. There are several forms of delusional misidentifications, which manifest for different kinds of stimuli. Reduplicative paramnesia is a delusional misidentification of space and places. Therefore, these two terms – 'space' and 'place' – were also included. Other monothematic delusional misidentification syndromes manifest for other kinds of stimuli (Devinsky, 2009): Capgras and Fregoli syndromes for faces, somatoparaphrenia for parts of the body, most commonly limbs; and Cotard syndrome for interoceptive stimuli. To test the hypothesis that reduplicative paramnesia would be associated with 'place' or 'space'-related functional networks, but not with networks related to 'faces', 'limb', 'body' and 'interoceptive', these terms were included too.

Since reduplicative paramnesia was also associated with neuropsychological deficits in executive functions and in non-verbal episodic memory tasks (Borghesani et al., 2019), we performed a supplemental analysis including the Neurosynth terms 'executive functions' and 'memory task'.

The Neurosynth extracted maps are thresholded to correct for multiple comparisons, using a False Discovery Rate criterion of .01. This threshold is applied by default in Neurosynth (http://neurosynth.org/). No additional threshold was applied.

Then, we analysed the spatial correlation between the functional meta-analytic maps of the terms of interest and the lesion topography maps. In addition, we performed the same analysis with the structural disconnection maps. Since Neurosynth maps predominantly represent areas of cortical activation, while the tractography-derived masks mainly correspond to white matter regions, we projected the disconnectome maps to the cortical ribbon. First, we converted streamline tractographies into streamline density volumes, in which voxel values corresponded to the number of fibres crossing each voxel (Nozais, Forkel, Foulon, Schotten, & Petit, 2021). This step was performed using the MRtrix3 command tckmap (Tournier et al., 2019). Second, all individual streamline density volumes were aligned with each other by performing a diffeomorphic normalization (Nozais et al., 2021). This step was computed using the Advance Normalisation Tools' script buildtemplateparallel.sh, and defining cross-correlation as the similarity measure and greedy SyN as the transformation model (Avants et al., 2011). With this, we obtained an average template of the streamline density volumes. Third, we registered the average template to the MNI152 1 mm standard space, using FSL's tool flirt (Jenkinson et al., 2012; Nozais et al., 2021), and applied the transformation warp to the individual disconnection maps. With this, we obtained disconnectome maps projected into grey matter. Then, we analysed the spatial correlation between the functional meta-analytic maps of the terms of interest and the projected disconnectome maps.

Finally, we also analysed if the relative spatial overlap of the lesion topography and of the structural disconnection maps with the meta-analytic functional maps was significantly different, in the cases of reduplicative paramnesia. The Dice similarity coefficient was calculated and a paired comparison was performed.

2.3. *Statistical analysis*

Continuous variables were reported as mean (standard deviation) or median [interquartile range] and compared using two-tailed Mann–Whitney test or two-tailed unpaired-t test, as appropriate. Categorical variables were reported as frequencies.

Alpha levels were set at .05 for statistical significance. In the neuroimaging analysis, a family-wise error rate approach was used to correct for multiple comparisons. For the comparison of other variables, a Bonferroni correction was applied.

The statistical approach to build and evaluate the classification performance of the neuroimaging models was presented previously, in the corresponding section.

3. Results

3.1. *Demographic and phenomenological characteristics*

The median age of the 67 patients reported was 66 [53–72] years old and the median time duration of delusions of space was 60 [30–113] days (reported in 31 cases). The phenomenological features of the reported cases are presented in Table 1.

The aetiologies of the lesions with brain images available (n = 24) were: stroke, n = 17; tumour, n = 3; trauma, n = 2; encephalitis, n = 1; and subarachnoid haemorrhage with focal parenchymal lesions, n = 1. A summarizing table, detailing the type of study, the number of patients assessed, the

Table 1 – Phenomenological characteristics of delusions of space.

Subtype of reduplicative paramnesia (reported in 67)	Reduplication	35 (52%)
	Chimeric assimilation	9 (13%)
	Confabulatory mislocation	9 (13%)
	Reduplication and confabulatory mislocation	7 (10%)
	Reduplication and chimeric assimilation	3 (4%)
	Confabulatory mislocation and chimeric assimilation	4 (6%)
Content of delusions of space (reported in 67)	Reduplication of the hospital	31 (46%)
	Reduplication of the patient's home	8 (20%)
	Combination of hospital and patient's home spaces	8 (12%)
	Mislocation of the hospital to a familiar place	2 (3%)
	Misidentification of home as another familiar place	2 (3%)
	Misidentification of the hospital as patient's home	2 (3%)
	Reduplication of other places	1 (1%)
	Combinations of other places	1 (1%)
	Other mislocations	2 (3%)
	Other misidentifications	1 (1%)
	Mixture of two of the previous delusional contents	9 (13%)
Association with other delusional misidentification syndromes (reported in 66)	Capgras syndrome	2 (3%)
	Reduplication of people	7 (11%)
	Fregoli syndrome	2 (3%)
	Reduplication of body parts	3 (5%)
	Intermetamorphosis	3 (5%)
	Cotard syndrome	2 (3%)
	Self-misidentification	1 (2%)
	Fregoli syndrome and reduplication of body parts	1 (2%)
	Unspecified misidentification of people	11 (17%)
	No association with other delusional misidentification syndromes	34 (52%)
Psychiatric history (reported in 49)	Previous suicide attempt (unspecified disease; no history of delusions)	1 (2%)
	No antecedents of major psychiatric disease	48 (98%)

patients' age and schooling, the lesion aetiologies and locations, and the results of the neuropsychological assessment for each case is provided in the Supplemental Table 5.

3.2. *Lesion topography*

Individual lesions are represented in Supplemental Fig. 2. The Dice similarity coefficient for lesion delimitation was .79 [.77–.84] (median [interquartile range]). The percentage of voxels for which the raters disagreed was 18% [12–27%] (median [interquartile range]). Almost all lesions were right sided or bilateral, except one (ischaemic stroke) that was located in the left temporo-parieto-occipital junction (Budson, Roth, Rentz, & Ronthal, 2000). This patient presented clinical evidence of right hemisphere dominance, namely right side neglect and impaired visual memory with preserved verbal memory.

The maximum value of overlap at a voxel-level was 3/24, in the right ventrolateral prefrontal, right temporal lateral and right insular regions (Supplemental Fig. 3a).

The permutation analysis of the exploratory sample revealed that: a) a region of the right lateral temporal lobe was more frequently lesioned in cases than in stroke controls; b) a region of the right dorsal striatum was more frequently lesioned in stroke controls than in cases (Supplemental Fig. 3b). However, these findings were not replicated in the validation sample and no statistically significant differences were found in the regression analysis including age as a covariate.

3.3. *Structural disconnectome*

In the structural connectivity analysis, the permutation test of the exploratory sample revealed that reduplicative paramnesia was significantly associated with higher probabilities of disconnection of: a) a right ventral temporo-occipital region; b) a right ventrolateral prefrontal region (Fig. 3a, top row). A similar statistically significant disconnection map was obtained in the regression analysis including age as a covariate (Supplemental Fig. 4), as well as in the supplemental analysis considering the delimitations of each rater separately. Conversely, reduplicative paramnesia was significantly associated with lower probabilities of disconnection of dorsal inter-hemispheric pathways (Fig. 1a, bottom row). These results were replicated in the validation sample (Fig. 1b), but not when age was included as a covariate in the regression analysis.

The results of the sensitivity analysis excluding tumoral lesions were similar (Supplemental Fig. 5), as well as when the discrete lesion delimitations of each researcher were considered separately (Supplemental Fig. 6).

3.4. *Classification performance of the lesion topography and of the structural disconnection maps*

The structural disconnectome model demonstrated a maximum balanced accuracy value in the validation sample of .78 (Fig. 2a). The voxels with higher balanced accuracy were located in two clusters: a) a right temporal cluster with an

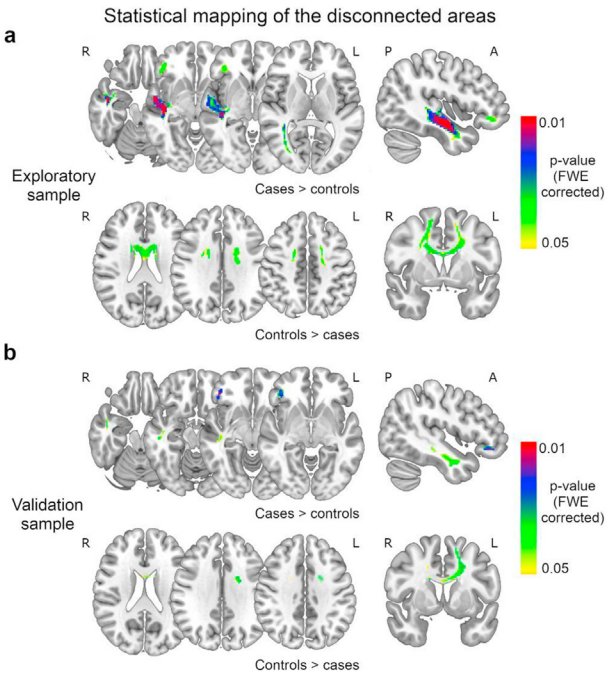

Fig. 1 – Structural disconnection analysis. (a) Statistical brain maps of voxels with significantly higher probabilities of disconnection in cases than in stroke controls (top row) and with significantly higher probabilities of disconnection in stroke controls than in cases (bottom row). (b) Statistical brain maps of the replication analysis performed in the validation sample. A, anterior; L, left; P, posterior; R, right.

overall balanced accuracy of .77, a sensitivity of .75 and a specificity of .79; b) a right ventrolateral prefrontal cluster, with an overall balanced accuracy of .75, a sensitivity of .67 and a specificity of .83 (Fig. 2b).

The lesion topography model revealed lower capacity to predict delusions of space with a maximum balanced accuracy value of .69.

3.5. *Structural–functional coupling*

The meta-analytic functional maps are provided in the Supplemental Fig. 7. The number of studies from which the meta-analytic maps derived were: belief, n = 83; familiarity, n = 188; place, n = 189; space, n = 303; faces, n = 864; limb, n = 127; body, n = 552; interoceptive, n = 81.

The lesions associated with spatial delusions had significantly higher spatial overlap with the belief-related functional network than stroke controls (Fig. 3a). There was no significant difference for familiarity, place and space-related functional networks.

Regarding structural disconnection, the disconnectome maps associated with delusions of space had significantly higher spatial overlap with the familiarity-related and with the place-related functional networks than stroke controls (Fig. 3a).

For the control terms, that would be the content-related equivalents for other monothematic delusional misidentifications, there was no significant difference of spatial overlap regarding lesion topography or structural disconnection (Fig. 3b). No significant difference was also found for the 'executive functions' and 'memory task'-related functional maps.

Comparing the relative spatial overlap (Dice similarity coefficient) with the meta-analytic functional maps, the structural disconnection maps had a higher coefficient of overlap with the familiarity and with the place-related functional networks than the lesion topography maps (Fig. 4). No significant difference was found for the belief and for the space-related functional maps.

4. Discussion

In this work, we performed a case-control analysis of the neural basis of reduplicative paramnesias. First, we found that they are associated with structural disconnection of right temporal and right ventrolateral prefrontal areas. This pattern of disconnection was replicated in an independent validation sample. Second, we showed that structural disconnectomes provide the anatomical framework to explain associated functional changes. Specifically, we demonstrated the existence of a spatial relationship between the structural disconnectome maps of reduplicative paramnesias and the familiarity and place-related functional networks.

Reduplicative paramnesia is a right hemisphere syndrome (Bartolomeo et al., 2016; Feinberg, 2013), however a sole lesion

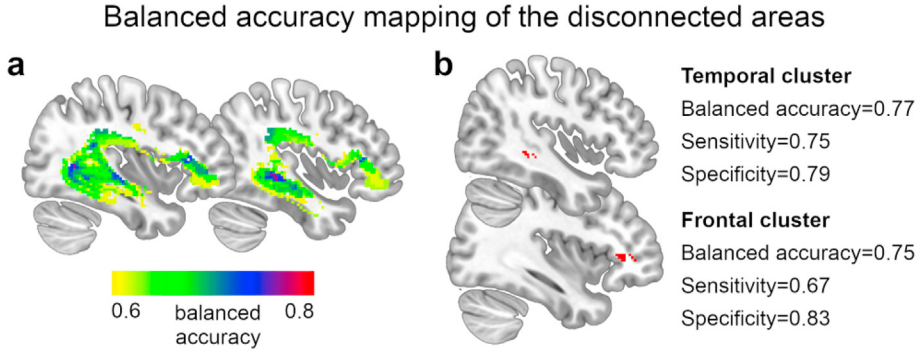

Fig. 2 – Balanced accuracy mapping of the structural disconnectome model. (a) Voxel-wise representation of the balanced accuracy scores. (b) Balanced accuracy score, sensitivity and specificity of the right temporal and of the right ventrolateral prefrontal clusters.

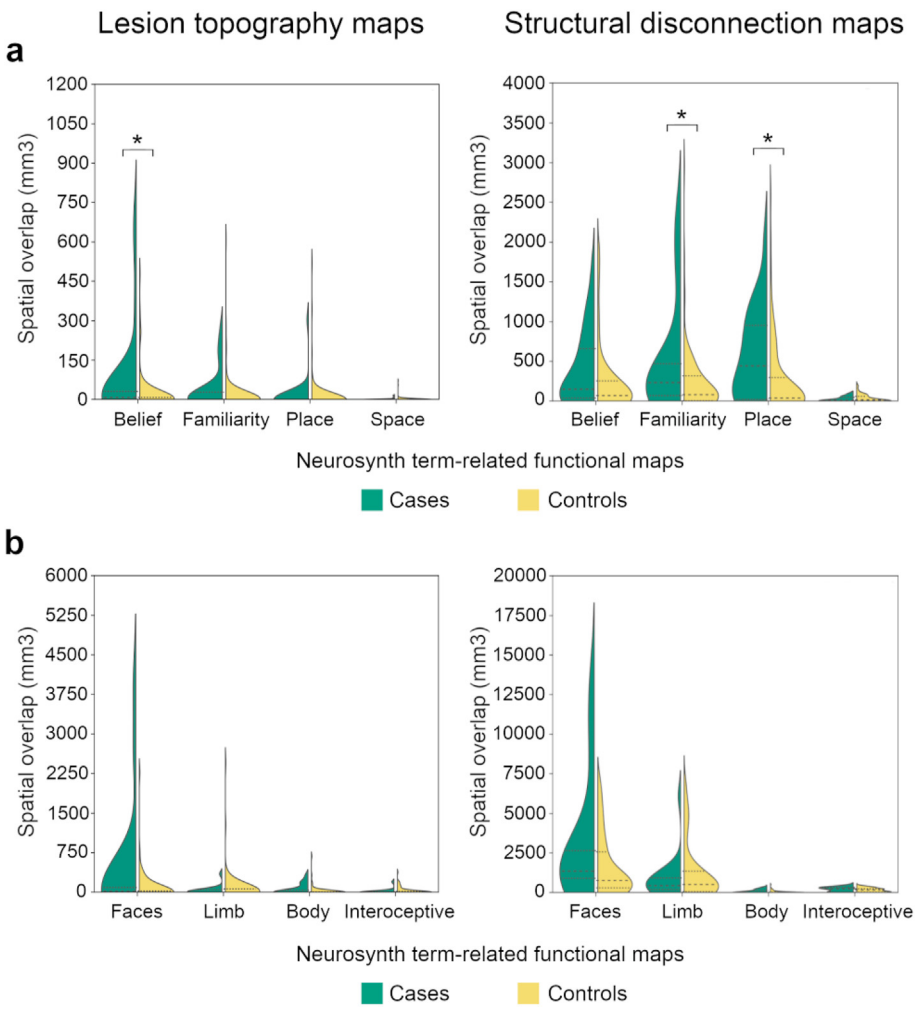

Fig. 3 – Spatial overlap between the meta-analytic functional maps and the lesion topography maps (left) and the projected structural disconnection maps (right). (a) Comparison regarding spatial delusions-related terms. (b) Comparison regarding the control terms that would be the content-related equivalents for other monothematic delusional misidentifications. Data is presented in violin plots. The dashed lines represent quartiles and the asterisks represent statistically significant differences between cases and stroke controls (Bonferroni-corrected *p*-value <.0125).

location or the lesion location per se may not be a satisfactory neuroanatomical explanation for this type of spatial disorientation (Griffis, Metcalf, Corbetta, & Shulman, 2019; Thiebaut de Schotten, Foulon, & Nachev, 2020). Our results provide evidence to support that reduplicative paramnesia is a disconnection syndrome.

Darby and colleagues (Darby et al., 2017) previously showed the association between delusional misidentification syndromes and functional disconnection of the right ventrolateral prefrontal cortex and of the left retrosplenial cortex (Darby et al., 2017). Here, we showed that the right ventrolateral prefrontal region is also structurally disconnected, which provides evidence for the existence of structure–function coupling in this region and reinforces its pathophysiological relevance (Baum et al., 2020). The two-hit model of delusional belief states that two factors contribute to the emergence of delusional misidentifications (Coltheart, Langdon, & Mckay, 2011). The first is an abnormal covert (i.e., implicit) recognition of the misidentified stimuli (Ellis & Young, 1990). The second is an impairment of the belief and familiarity evaluation processes (Coltheart et al., 2011). Evidence suggests that the neural basis of the second factor is the dysfunction of the right lateral prefrontal cortex (Coltheart, 2010) and our results support it. The ventrolateral prefrontal cortex is activated during the presentation of unexpected perceptual events and during implicit false belief processing (Kandylaki et al., 2015; Sharp et al., 2010). We also replicated the previous finding that delusional misidentification lesions were spatially correlated with belief-related networks (Darby et al., 2017). In addition, the right ventrolateral prefrontal cortex has an important role in reality monitoring (Badre & Wagner, 2004). Its damage or disconnection has been associated with anosognosia for hemiplegia (Berti et al., 2005; Pacella et al., 2019; Prigatano, 2010), a disorder characterized by the patients' failure to acknowledge limb paralysis, even after being clearly confronted with the deficit. Our results fits this

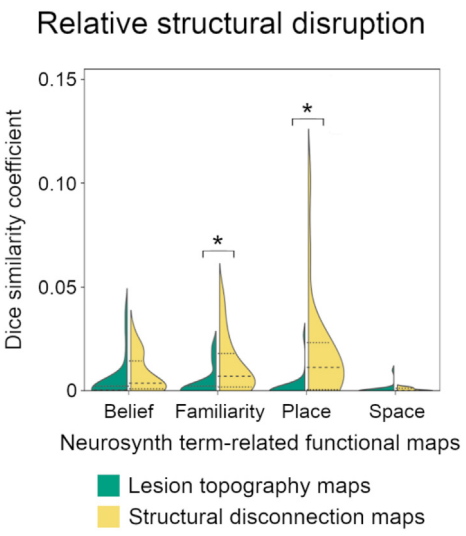

Fig. 4 – Comparison of the relative spatial overlap (Dice similarity coefficient) of the meta-analytic functional maps between the lesion topography and the projected structural disconnection maps in the cases of reduplicative paramnesia. The dashed lines represent quartiles and the asterisks represent statistically significant differences (Bonferroni-corrected *p*-value <.0125).

evidence, since both disorders share a disturbance in reality awareness and belief update (Fotopoulou, 2014; Vocat, Saj, & Vuilleumier, 2013).

The right ventrolateral prefrontal cortex is also a core area to emotional regulation, and seems to be particularly important when personal significance factors are involved in belief reasoning (Hartwright, Apperly, & Hansen, 2012) and to explicit decisions on the relative familiarity of stimuli (Petrides, Alivisatos, & Frey, 2002). It establishes bi-directional connections with ventral limbic structures (Petrides, 2005) and with limbic nuclei of the thalamus through the anterior thalamic radiations (Rojkova et al., 2016), and integrates the Default Mode Network, a fundamental network for trans-modal processing of limbic information (Alves et al., 2019). Ellis and Young proposed that a defective attribution of appropriate emotional valences to stimuli was involved in the pathogenesis of delusional misidentification syndromes (Devinsky, 2009; Young, Hellawell, Wright, & Ellis, 1994). Darby and colleagues (Darby et al., 2017) established a functional association between delusional misidentifications and familiarity networks. We demonstrated that this association is neuroanatomically mediated by structural disconnection.

The delusional content of reduplicative paramnesia is very specific for places, distinguishing it from other monothematic delusional misidentifications. Still according to the two-hit model, all delusional misidentification syndromes would have a first factor that determines the content of delusional belief (Coltheart et al., 2011). Here, we provide the first group-level evidence showing that there is a spatial correlation between reduplicative paramnesia and place-related functional networks. Ventral occipito-temporal pathways are fundamental for orientation in allocentric spatial references (Ekstrom, Arnold, & Iaria, 2014) and to the emotional recognition of visual cues (Herbet & Duffau, 2020). We propose that the disconnection of this pathway may impair a proper update and integration of visual information in allocentric, place-related networks. The dual pattern of disconnection that was found validates what we have recently described in acute stroke patients (Alves et al., 2021).

Other authors have hypothesized that delusional misidentifications results from unbalanced activity of the two hemispheres, with right hemisphere hypofunction and left hemisphere overactivity (Devinsky, 2009; Young et al., 1994). We found that dorsal fronto-parietal inter-hemispheric connections were more frequently spared in cases of reduplicative paramnesia, when compared with stroke controls. This might mediate dysfunctional interhemispheric communication, but this finding was not replicated when age was included in the model. Further studies are needed.

As limitations of our study, the meta-analytic functional maps do not reflect the complex associations and the dynamic interactions of brain systems. The lesion mapping analysis was also constrained by the available images in the cases reports. Although we replicated 2D lesion tracing methodologies that have been applied to study cognitive and behavioural syndromes about which the available neuroanatomical evidence is scarce (Boes et al., 2015; Cohen et al., 2019; Darby, Joutsa, & Fox, 2019), the lesion masks may not represent the full 3D geometry of the original lesions. In addition, we cannot guarantee that the control stroke patients did not develop reduplicative paramnesia after the period of systematic assessment. These bias may increase the risk of false negative results (Cohen et al., 2019). It is also known that the years of education, as well as co-occurring cognitive deficits, may correlate with the cognitive syndrome of interest (Borghesani et al., 2019; de Haan & Karnath, 2018; Umarova et al., 2021). However, the absence of information about the years of schooling, the heterogeneity of the reported neuropsychological evaluations and the number of cases available precluded the inclusion of these covariates in the neuroimaging model.

In conclusion, our work suggests that delusions of space may be associated with structural disconnection of right ventrolateral prefrontal and right temporal regions and that these structural connectivity changes might mediate functional interactions with familiarity and place-related networks. These results shed light on the neural basis of spatial orientation disorders and of delusional misidentifications.

CRediT author statement

Pedro N Alves: Conceptualization, Methodology, Formal analysis, Investigation, Writing – Original Draft, Funding acquisition. **Daniela P Silva:** Investigation, Writing – Review and Editing. **Ana C Fonseca:** Conceptualization, Methodology, Writing – Review and Editing. **Isabel P Martins:** Conceptualization, Methodology, Writing – Review and Editing, Supervision.

Data availability

The nifti maps of reduplicative paramnesia cases are publicly available at: https://identifiers.org/neurovault.collection:

11259. The nifti maps of control stroke lesions are not publicly available because the conditions of our ethical approval do not permit the public archiving of this data. They can be requested from the corresponding author if ethical committee approval is obtained. The code necessary to reproduce the results of this article also contains ethically sensitive information and is therefore covered by the same ethical restriction.

Anonymized data to reproduce structural-functional decoupling analyses are publicly available at: https://osf.io/a8wc4/

Pre-registration

No part of the study procedures or analyses was pre-registered prior to the research being conducted.

Data reporting

We report how we determined our sample size, all data exclusions, all inclusion/exclusion criteria, whether inclusion/exclusion criteria were established prior to data analysis, all manipulations, and all measures in the study.

Declaration of competing interest

The authors declare that no conflict of interest exists.

Acknowledgements

This work was supported by the following grants: "PRÉMIO JOÃO LOBO ANTUNES 2018" – SCML; "Bolsa de Investigação em Doencas Vasculares Cerebrais 2017" – SPAVC.

Supplementary data

Supplementary data to this article can be found online at https://doi.org/10.1016/j.cortex.2021.11.008.

REFERENCES

Alves, P. N., Fonseca, A. C., Silva, D. P., Andrade, M. R., Pinho-e-Melo, T., Thiebaut de Schotten, M., et al. (2021). Unravelling the neural basis of spatial delusions after stroke. *Annals of Neurology*, 1–14. https://doi.org/10.1002/ana.26079

Alves, P. N., Foulon, C., Karolis, V., Bzdok, D., Margulies, D. S., Volle, E., et al. (2019). An improved neuroanatomical model of the default-mode network reconciles previous neuroimaging and neuropathological findings. *Communications Biology*, 1–14. https://doi.org/10.1038/s42003-019-0611-3

Avants, B. B., Tustison, N. J., Song, G., Cook, P. A., Klein, A., & Gee, J. C. (2011). A reproducible evaluation of ANTs similarity metric performance in brain image registration. *NeuroImage*, 54(3), 2033–2044. https://doi.org/10.1016/j.neuroimage.2010.09.025

Badre, D., & Wagner, A. D. (2004). Selection, integration, and conflict monitoring. *Neuron*, 41(3), 473–487. https://doi.org/10.1016/s0896-6273(03)00851-1

Barahona-Corrêa, J. B., Cotovio, G., Costa, R. M., Ribeiro, R., Velosa, A., Silva, V. C.e., et al. (2020). Right-sided brain lesions predominate among patients with lesional mania: Evidence from a systematic review and pooled lesion analysis. *Translational Psychiatry*, 10(1). https://doi.org/10.1038/s41398-020-0811-0

Bartolomeo, P., Vito, S. De, & Seidel, T. (2016). Space-related confabulations after right hemisphere damage. *Cortex*, 87, 166–173. https://doi.org/10.1016/j.cortex.2016.07.007

Baum, G. L., Cui, Z., Roalf, D. R., Ciric, R., Betzel, R. F., Larsen, B., et al. (2020). Development of structure–function coupling in human brain networks during youth. *Proceedings of the National Academy of Sciences of the United States of America*, 117(1), 771–778. https://doi.org/10.1073/pnas.1912034117

Berti, A., Bottini, G., Gandola, M., Pia, L., Smania, N., Stracciari, A., et al. (2005). Shared cortical anatomy for motor awareness and motor control. *Science*, 309(5733), 488–491. https://doi.org/10.1126/science.1110625

Boes, A. D., Prasad, S., Liu, H., Liu, Q., Pascual-Leone, A., Caviness, V. J., et al. (2015). Network localization of neurological symptoms from focal brain lesions. *Brain*, 138, 3061–3075. https://doi.org/10.1093/brain/awv228

Borghesani, V., Monti, A., Fortis, P., & Miceli, G. (2019). Reduplicative paramnesia for places: A comprehensive review of the literature and a new case report. *Clinical Neurology and Neurosurgery*, 181(March), 7–20. https://doi.org/10.1016/j.clineuro.2019.03.022

Budson, A., Roth, H., Rentz, D., & Ronthal, M. (2000). Disruption of the ventral visual stream in a case of reduplicative paramnesia. *Annals of the New York Academy of Sciences*, 911, 447–452. https://doi.org/10.1111/j.1749-6632.2000.tb06742.x

Chawla, N. V. (2005). *Data mining for imbalanced datasets: An overview*. Springer US.

Chawla, N. V., Bowyer, K. W., Hall, L. O., & Kegelmeyer, W. P. (2002). SMOTE: Synthetic minority over-sampling technique. *Journal of Artificial Intelligence Research*, 16, 321–357. https://doi.org/10.1613/jair.953

Cohen, A. L., Soussand, L., Corrow, S. L., Martinaud, O., Barton, J. J. S., & Fox, M. D. (2019). Looking beyond the face area: Lesion network mapping of prosopagnosia. *Brain*, 142(12), 3975–3990. https://doi.org/10.1093/brain/awz332

Coltheart, M. (2010). The neuropsychology of delusions. *Annals of the New York Academy of Sciences*, 1191, 16–26. https://doi.org/10.1111/j.1749-6632.2010.05496.x

Coltheart, M., Langdon, R., & Mckay, R. (2011). Delusional belief. *Annual Review of Psychology*, 62, 271–298. https://doi.org/10.1146/annurev.psych.121208.131622

Darby, R. R., Joutsa, J., & Fox, M. D. (2019). Network localization of heterogeneous neuroimaging findings. *Brain*, 142(1), 70–79. https://doi.org/10.1093/brain/awy292

Darby, R. R., Laganiere, S., Pascual-Leone, A., Prasad, S., & Fox, M. D. (2017). Finding the imposter: Brain connectivity of lesions causing delusional misidentifications. *Brain*, 140(2), 497–507. https://doi.org/10.1093/brain/aww288

Devinsky, O. (2009). Delusional misidentifications and duplications: Right brain lesions, left brain delusions. *Neurology*, 72(1), 80–87. https://doi.org/10.1212/01.wnl.0000338625.47892.74

de Haan, B., & Karnath, H. O. (2018). A hitchhiker's guide to lesion-behaviour mapping. *Neuropsychologia*, 115, 5–16. https://doi.org/10.1016/j.neuropsychologia.2017.10.021

Ekstrom, A. D., Arnold, A. E. G. F., & Iaria, G. (2014). A critical review of the allocentric spatial representation and its neural underpinnings: Toward a network-based perspective. *Frontiers in Human Neuroscience*, 8(October), 803.

Ellis, H. D., & Young, A. W. (1990). Accounting for delusional misidentifications. *British Journal of Psychiatry, 157*, 239–248. https://doi.org/10.1192/bjp.157.2.239

Feinberg, T. E. (2013). Neuropathologies of the self and the right hemisphere: A window into productive personal pathologies. *Frontiers in Human Neuroscience, 7*. https://doi.org/10.3389/fnhum.2013.00472

Fotopoulou, A. (2014). Time to get rid of the "modular" in neuropsychology: A unified theory of anosognosia as aberrant predictive coding. *Journal of Neuropsychology, 8*(1), 1–19. https://doi.org/10.1111/jnp.12010

Foulon, C., Cerliani, L., Kinkingnéhun, S., Levy, R., Rosso, C., Urbanski, M., et al. (2018). Advanced lesion symptom mapping analyses and implementation as BCBtoolkit. *GigaScience, 7*(3), 1–17. https://doi.org/10.1093/gigascience/giy004

Griffis, J. C., Metcalf, N. V., Corbetta, M., & Shulman, G. L. (2019). Structural disconnections explain brain network dysfunction after stroke. *Cell Reports, 28*(10), 2527–2540. https://doi.org/10.1016/j.celrep.2019.07.100

Hartwright, C. E., Apperly, I. A., & Hansen, P. C. (2012). Multiple roles for executive control in belief-desire reasoning: Distinct neural networks are recruited for self perspective inhibition and complexity of reasoning. *NeuroImage, 61*(4), 921–930. https://doi.org/10.1016/j.neuroimage.2012.03.012

He, H., & Garcia, E. A. (2019). Learning from imbalanced data. *IEEE Transactions on Knowledge and Data Engineering, 21*(9), 1263–1284. https://doi.org/10.1109/tkde.2008.239

Herbet, G., & Duffau, H. (2020). Revisiting the functional anatomy of the human brain: Toward a meta-networking theory of cerebral functions. *Physiological Reviews, 100*(3), 1181–1228. https://doi.org/10.1152/physrev.00033.2019

Jenkinson, M., Beckmann, C. F., Behrens, T. E. J., Woolrich, M. W., & Smith, S. M. (2012). FSL. *NeuroImage, 62*(2), 782–790. https://doi.org/10.1016/j.neuroimage.2011.09.015

Kandylaki, K. D., Nagels, A., Tune, S., Wiese, R., Bornkessel-Schlesewsky, I., & Kircher, T. (2015). Processing of false belief passages during natural story comprehension: An fMRI study. *Human Brain Mapping, 36*(11), 4231–4246. https://doi.org/10.1002/hbm.22907

Karolis, V. R., Corbetta, M., & Thiebaut de Schotten, M. (2019). The architecture of functional lateralisation and its relationship to callosal connectivity in the human brain. *Nature Communications, 10*(1), 1417–1424. https://doi.org/10.1038/s41467-019-09344-1

Liew, S. L., Anglin, J. M., Banks, N. W., Sondag, M., Ito, K. L., Kim, H., et al. (2018). A large, open source dataset of stroke anatomical brain images and manual lesion segmentations. *Scientific Data, 5*, 1–11. https://doi.org/10.1038/sdata.2018.11

Luque, A., Carrasco, A., Martín, A., & de las Heras, A. (2019). The impact of class imbalance in classification performance metrics based on the binary confusion matrix. *Pattern Recognition, 91*, 216–231. https://doi.org/10.1016/j.patcog.2019.02.023

Murai, T., Toichi, M., Sengoku, A., Miyoshi, K., & Morimune, S. (1997). Reduplicative paramnesia in patients with focal brain damage. *Neuropsychology, Neuropsychiatry, and Behavioral Neurology, 10*(3), 190–196.

Nagahama, Y., Okina, T., Suzuki, N., Matsuda, M., Fukao, K., & Murai, T. (2007). Classification of psychotic symptoms in dementia with Lewy bodies. *American Journal of Geriatric Psychiatry, 15*(11), 961–967. https://doi.org/10.1097/JGP.0b013e3180cc1fdf

Nozais, V., Forkel, S. J., Foulon, C., Schotten, M. T. De, & Petit, L. (2021). Functionnectome as a framework to analyse the contribution of brain circuits to fMRI. *Communications Biology*, 1–12. https://doi.org/10.1038/s42003-021-02530-2

Pacella, V., Foulon, C., Jenkinson, P. M., Scandola, M., Bertagnoli, S., Avesani, R., et al. (2019). Anosognosia for hemiplegia as a tripartite disconnection syndrome. *ELife, 8*, 1–13. https://doi.org/10.7554/elife.46075

Pedregosa, F., Varoquaux, G., Gramfort, A., Michel, V., Thirion, B., Grisel, O., et al. (2011). Scikit-learn: Machine learning in Python. *Journal of Machine Learning Research, 12*, 2825–2830. https://doi.org/10.1145/2786984.2786995

Perini, G., Carlini, A., Pomati, S., Alberoni, M., Mariani, C., Nemni, R., et al. (2016). Misidentification delusions: Prevalence in different types of dementia and validation of a structured questionnaire. *Alzheimer Disease and Associated Disorders, 30*(4), 331–337. https://doi.org/10.1097/WAD.0000000000000141

Petrides, M. (2005). Lateral prefrontal cortex: Architectonic and functional organization. *Philosophical Transactions of the Royal Society B: Biological Sciences, 360*(1456), 781–795. https://doi.org/10.1098/rstb.2005.1631

Petrides, M., Alivisatos, B., & Frey, S. (2002). Differential activation of the human orbital, mid-ventrolateral, and mid-dorsolateral prefrontal cortex during the processing of visual stimuli. *Proceedings of the National Academy of Sciences of the United States of America, 99*(8), 5649–5654. https://doi.org/10.1073/pnas.072092299

Pick, A. (1903). Clinical studies III. On reduplicative paramnesia. *Brain, 26*, 260–267.

Politis, M., & Loane, C. (2012). Reduplicative paramnesia: A review. *Psychopathology, 45*(6), 337–343. https://doi.org/10.1159/000337748

Prigatano, G. (2010). *The study of anosognosia*. New York: Oxford University Press.

Rojkova, K., Volle, E., Urbanski, M., Humbert, F., Dell'Acqua, F., & Thiebaut de Schotten, M. (2016). Atlasing the frontal lobe connections and their variability due to age and education: A spherical deconvolution tractography study. *Brain Structure & Function, 221*(3), 1751–1766. https://doi.org/10.1007/s00429-015-1001-3

Sharp, D. J., Bonnelle, V., De Boissezon, X., Beckmann, C. F., James, S. G., Patel, M. C., et al. (2010). Distinct frontal systems for response inhibition, attentional capture, and error processing. *Proceedings of the National Academy of Sciences of the United States of America, 107*(13), 6106–6111. https://doi.org/10.1073/pnas.1000175107

Thiebaut de Schotten, M., Foulon, C., & Nachev, P. (2020). Brain disconnections link structural connectivity with function and behaviour. *Nature Communications, 11*(1). https://doi.org/10.1038/s41467-020-18920-9

Thiebaut de Schotten, M., Tomaiuolo, F., Aiello, M., Merola, S., Silvetti, M., Lecce, F., et al. (2014). Damage to white matter pathways in subacute and chronic spatial neglect: A group study and 2 single-case studies with complete virtual "in vivo" tractography dissection. *Cerebral Cortex, 24*(3), 691–706.

Tournier, J. D., Smith, R., Raffelt, D., Tabbara, R., Dhollander, T., Pietsch, M., et al. (2019). MRtrix3: A fast, flexible and open software framework for medical image processing and visualisation. *NeuroImage*, 202. https://doi.org/10.1016/j.neuroimage.2019.116137

Umarova, R. M., Schumacher, L. V., Schmidt, C. S. M., Martin, M., Egger, K., Urbach, H., et al. (2021). Interaction between cognitive reserve and age moderates effect of lesion load on stroke outcome. *Scientific Reports, 11*(1), 1–10. https://doi.org/10.1038/s41598-021-83927-1

Vocat, R., Saj, A., & Vuilleumier, P. (2013). The riddle of anosognosia: Does unawareness of hemiplegia involve a failure to update beliefs? *Cortex, 49*(7), 1771–1781. https://doi.org/10.1016/j.cortex.2012.10.009

Vu, A. T., Auerbach, E., Lenglet, C., Moeller, S., Sotiropoulos, S. N., Jbabdi, S., et al. (2015). High resolution whole brain diffusion imaging at 7T for the human connectome project. *NeuroImage, 122*, 318–331. https://doi.org/10.1016/j.neuroimage.2015.08.004

Winkler, A. M., Ridgway, G. R., Webster, M. A., Smith, S. M., & Nichols, T. E. (2014). Permutation inference for the general linear model. *NeuroImage, 92*, 381–397. https://doi.org/10.1016/j.neuroimage.2014.01.060

Witwer, B. P., Moftakhar, R., Hasan, K. M., Deshmukh, P., Haughton, V., Field, A., et al. (2002). Diffusion-tensor imaging of white matter tracts in patients with cerebral neoplasm. *Journal of Neurosurgery, 97*(3), 568–575. https://doi.org/10.3171/jns.2002.97.3.0568

Yarkoni, T., Poldrack, R. A., Nichols, T. E., Essen, D. C. Van, & Wager, T. D. (2011). Large-scale automated synthesis of human functional neuroimaging data. *Nature Methods, 8*(8), 665–670. https://doi.org/10.1038/nmeth.1635

Young, A. W., Hellawell, D. J., Wright, S., & Ellis, H. D. (1994). Reduplication of visual stimuli. *Behavioural Neurology, 7*(3–4), 135–142. https://doi.org/10.3233/BEN-1994-73-405

Received: 1 August 2022 | Accepted: 31 August 2022

DOI: 10.1111/ene.15557

european journal of neurology
the official journal of the european academy of neurology

ORIGINAL ARTICLE

Clinical presentation and neural correlates of stroke-associated spatial delusions

Pedro N. Alves[1,2,3] | Ana C. Fonseca[2,3,4] | Teresa Pinho-e-Melo[2,3,4] | Isabel P. Martins[1,2,3]

[1]Laboratório de Estudos de Linguagem, Centro de Estudos Egas Moniz, Faculdade de Medicina, Universidade de Lisboa, Lisbon, Portugal

[2]Serviço de Neurologia, Departamento de Neurociências e Saúde Mental, Hospital de Santa Maria, CHULN, Lisbon, Portugal

[3]Instituto de Medicina Molecular João Lobo Antunes, Faculdade de Medicina, Universidade de Lisboa, Lisbon, Portugal

[4]Centro de Estudos Egas Moniz, Faculdade de Medicina, Universidade de Lisboa, Lisbon, Portugal

Correspondence
Pedro Nascimento Alves, Laboratório de Estudos de Linguagem, Centro de Estudos Egas Moniz, Hospital de Santa Maria, Avenida Professor Egas Moniz, Lisboa 1649-028, Portugal.
Email: pedronascimentoalves@gmail.com

Funding information
Bolsa de investigacao em Doencas Vasculares Cerebrais 2017 - SPAVC; Premio Joao Lobo Antunes 2018 - SCML

Abstract

Background and purpose: Incongruent beliefs about self-localization in space markedly disturb patients' behavior. Spatial delusions, or reduplicative paramnesias, are characterized by a firm conviction of place reduplication, transformation, or mislocation. Evidence suggests they are frequent after right hemisphere lesions, but comprehensive information about their clinical features is lacking.

Methods: We prospectively screened 504 acute right-hemisphere stroke patients for the presence of spatial delusions. Their behavioral and clinical features were systematically assessed. Then, we analyzed the correlation of their duration with the magnitude of structural disruption of belief-associated functional networks. Finally, we described the syndrome subtypes and evaluated whether the clinical categorization would be predicted by the structural disruption of familiarity-associated functional networks using an unsupervised *k*-means clustering algorithm.

Results: Sixty patients with spatial delusions were identified and fully characterized. Most (93%) localized the misidentified places closer to home than the hospital. The median time duration was 3 days (interquartile range = 1–7 days), and it was moderately correlated with the magnitude of structural–functional decoupling of belief-associated functional networks ($r = 0.39$, $p = 0.02$; beta coefficient regressing for lesion volume = 3.18, $p = 0.04$). Each clinical subtype had characteristic response patterns, which were reported, and representative examples were provided. Clustering based on structural disruption of familiarity- and unfamiliarity-associated functional networks poorly matched the clinical categorization (lesion: Rand index = 0.47; structural disconnection: Rand index = 0.51).

Conclusions: The systematic characterization of the peculiar clinical features of stroke-associated spatial delusions may improve the syndrome diagnosis and clinical approaches. The novel evidence about their neural correlates fosters the clarification of the pathophysiology of delusional misidentifications.

KEYWORDS
reduplicative paramnesia, spatial delusions, stroke

INTRODUCTION

In 1788, Charles Bonnet reported a peculiar form of spatial disorientation characterized by an incoherent belief of space mislocation [1]. Later, in 1903, Arnold Pick further characterized the syndrome and denominated it "reduplicative paramnesia" [2]. Pick described a 67-year-old woman who had been admitted to a clinic in Prague due to the subacute onset of cognitive and behavioral changes. Five months after her admission, she started to believe that she was not in Prague anymore, but in a replica of the original clinic that was located in her birthplace, "the suburb clinic." She could not be convinced otherwise and insistently tried to find explanations to justify her belief [2]. Since Pick's description, reduplicative paramnesias (also called spatial delusions or delusional misidentifications of space) were defined as a firm conviction of being in a different place from the real one, which does not change when the patient is confronted with clear counterfactual evidence [3, 4].

Different forms of spatial delusions have been described [5], representing different poles of pathological familiarity [6]. Place reduplication typifies hypofamiliarity for places and corresponds to the original description made by Pick, that is, the patients are convinced that they are in a replica of the original place. Chimeric assimilation is characterized by the fusion or combination of two different places (e.g., the hospital is inside the patient's home). In confabulatory mislocation, patients believe that they are in a place that is substantially different from the real one (e.g., believing to be at home instead of being at the hospital). Both embody place hyperfamiliarity [7].

At the structural and functional levels, spatial delusions are associated with a dual pattern of structural disconnection involving right frontothalamic and right occipitotemporal circuits [8], which prompts structural–functional decoupling of belief, familiarity, and place-associated functional networks [9]. At the clinical level, the striking incongruence between the patient's conviction and the surrounding environment may markedly disturb the patient's behavior [3, 10]. Although traditionally seen as a rare syndrome, evidence suggests that spatial delusions can be a frequent manifestation of right hemisphere lesions [11–13], particularly in the acute phase of right hemisphere strokes [8]. So far, the available knowledge about spatial delusions' clinical features is mainly based on case reports and small case series [3, 5]. Misdiagnosis of spatial delusions as delirium or psychomotor agitation may lead to erroneous approaches in terms of pharmacological treatment, behavioral interventions, and support of family members and caregivers.

Here, we systematically studied a large sample of patients with spatial delusions after right hemisphere acute stroke to shed light on their clinical presentation and pathophysiology. First, we aimed to characterize the clinical phenotype of spatial delusions and their subtypes. Second, we studied the neural correlates of these clinical features. Specifically, we hypothesized that there was a correlation between the duration of the reduplicative paramnesia and the magnitude of structural disruption of belief-associated functional networks and that the disturbances of familiarity-associated networks would predict the syndrome subtypes.

METHODS

Study design and patient selection

This research work is a subanalysis of a prospective, cumulative, case–control study that we performed from December 2016 to February 2020 in a stroke unit of a tertiary university hospital in Lisbon, Portugal [8]. The study aimed to investigate the neural basis of spatial delusions after stroke. Spatial delusions are right hemisphere syndromes [4]. Four hundred patients admitted within the acute phase (≤72 h) of right hemisphere stroke (ischemic or hemorrhagic) were screened for the presence of spatial delusions. An additional 104 cases were recruited from March 2020 to June 2021. Patients with dementia, acute confusional state (delirium), and decreased level of consciousness were excluded (the full description of exclusion criteria is detailed in Table S1).

The screening was performed in the first 72 h of admission and then at regular intervals of 48 h until the patients' discharge, using the systematic approach detailed in the following section. Patients with the syndrome whose phenomenological presentation was fully registered were selected for this study.

The study was approved by the Joint Ethics Committee of the Lisbon Academic Medical Centre.

Screening and phenotypic characterization of reduplicative paramnesia

Patients were asked if they knew where they were, specifically the type of building (hospital), the city (Lisbon), and the city district. If the patients did not know or gave a wrong answer, their correct location was explained, namely that they were in a hospital, which was called “Hospital de Santa Maria” and was located in Lisbon, more specifically in “Campo Grande/Cidade Universitária” (city district). When the patients disagreed, counterevidence was systemically shown to convince them otherwise. The questions and confrontations were tailored to the subtype of reduplicative paramnesia. When the patients believed they were in a place other than a hospital (i.e., confabulatory mislocation), they were asked: Question 1) why health care professionals would be in the referred place; Question 2) why medical equipment (oxygen masks, infusion tubes, vital signs monitor) would be there; Question 3) why the patients' clothes and bed sheets were labeled “Hospital de Santa Maria”; Question 4) why other patients would be in the referred place; Question 5) in which home division they would be (in the case they believed they were at home/living house); and Question 6) why it would be possible to see from the window distinct landmarks, such as Alvalade Stadium (the stadium of a leading football club in Portugal), the Lisbon airport, or Lisbon University (for those whose clinical condition allowed them to stand and to show them the window view).

For patients presenting chimeric assimilation, in addition to the questions referred to above, they were asked: Question 7) whether they had noticed or heard about any construction work in the referred place; and Question 8) why a hospital would be constructed inside that place.

For patients presenting with place reduplication, Questions 3 and 6 were posed. In addition, they were asked: Question 9) why "Lisbon" would be written next to the hospital logo; and Question 10, how many "Hospital de Santa Maria" they thought there were.

The diagnosis of reduplicative paramnesia was made when the patients maintained the belief of mislocation after exposure to the abovementioned counterevidence.

Clinical characterization

Demographic, clinical, and reduplicative paramnesia-related variables were collected (detailed in Table S2).

The geodesic distances between the misidentified place, the patients' home, and "Hospital de Santa Maria" were calculated and the relative distance of the misidentified place to the patient's home and to "Hospital de Santa Maria" ($r\Delta$) was determined:

$$r\Delta = \frac{\Delta place\_hospital}{\Delta place\_hospital + \Delta place\_home}$$

where $\Delta place\_hospital$ = the distance between the misidentified place and the "Hospital de Santa Maria" and $\Delta place\_home$ = the distance between the misidentified place and the patient's home (values closer to 1 represent mislocation closer to the hospital; values closer to 0 represent mislocation closer to the patient's home).

Neuroimaging correlations

Stroke lesions were defined based on brain magnetic resonance imaging (MRI; preferentially) or on computed tomography (CT) performed 24–72 h after stroke onset (MRI, $n = 22$; CT, $n = 38$). Magnetic resonance images were acquired with a Philips Achieva 3-T or Philips Intera 1.5-T scanner. CT images were acquired with a Philips Brilliance 64-channel scanner. The delineation was done manually on axial slices with a thickness of 3 mm in the patient's native space by a researcher with clinical experience in acute stroke lesion analysis. The researcher was blind to clinical variables. Lesions were normalized to a common space, MNI152 [14]. For MRI, the diffusion-weighted imaging was the sequence of reference for delineation [15]. T1 images were registered to MNI152 space through linear (affine transformation, 12 degrees of freedom) and nonlinear transformations, using the FMRIB Software Library functions "flirt" and "fnirt" [14]. For CT images, the registration was made to the CT-derived MNI152 template using a linear transformation [16]. Finally, the registration deformation fields were applied to the lesion masks.

To compute the structural disconnection pattern of each lesion, we used a tractwise approach [17]. Using the tool "Disconnectome" from the software package BCBtoolkit (www.bcblab.com), each lesion was overlapped with a group of 178 healthy subjects' tractography from the Human Connectome Project 7-T dataset [18]. Tractographies were obtained using a whole-brain deterministic approach in StarTrack software (https://mr-startrack.com), applying a spherical deconvolution methodology, specifically a damped Richardson–Lucy algorithm. They were made available with the BCBtoolkit (http://www.bcblab.com). The full details of preprocessing are described in Karolis et al. [19]. A voxelwise probability of disconnection was calculated [20]. The voxels were included in the disconnectome map if they were disconnected in >50% of healthy subjects' tractographies [20].

It has been demonstrated that delusional misidentifications are associated with structural–functional decoupling of belief and familiarity-associated functional networks [9, 21]. Neurosynth is a validated brain-mapping platform that performs large-scale automated extraction of meta-analytic functional maps of terms of interest [22]. We used Neurosynth to obtain the meta-analytic maps of the terms "belief," "familiar," and "unfamiliar." Association test maps were extracted [22]. The maps are corrected for multiple comparisons applying a false discovery rate of 0.01. Then, we computed the volumetric spatial overlap of these meta-analytic maps with the individual stroke lesion and with the structural disconnectome maps.

The Spearman correlation between the duration of spatial delusions and the structural disruption (either lesion or structural disconnection) of belief-associated networks was calculated. Lesion volume is an important confounder in the establishment of lesion–behavior associations [23, 24]. A regression analysis was performed to investigate whether the putative correlations were independent of lesion volume. In addition, we computed a voxelwise beta-coefficient map using the linear regression function of scikit-learn [25], to analyze which voxels' lesion or disconnection best predicted the duration of the phenomenon.

To evaluate the classification performance of cases based on the structural disruption of familiarity-associated networks, we performed an unsupervised machine learning partition using the *k*-means clustering algorithm from scikit-learn [25]. The number of clusters to form was defined as three (the number of clinical subtypes of reduplicative paramnesia). The variables included in the model were the structural disruption (either lesion or structural disconnection) of "familiar" specific regions and the structural disruption of "unfamiliar" specific regions. Then, we calculated the Rand index to determine the similarity between the familiarity-derived clustering and the clinical subtype classification (1 meaning perfect agreement and 0 meaning no agreement). An alternative analysis was computed in which we defined the number of clusters to form as two, considering confabulatory mislocation and chimeric assimilation to be a unique category of hyperfamiliarity syndromes and place reduplication to be a hypofamiliarity syndrome [7]. The first presentation was considered for patients with more than one subtype of reduplicative paramnesia.

Statistical analysis

The Spearman correlation, linear regression, and *k*-means clustering were applied as explained above. When the residuals of the linear model were not normally distributed, a quantile regression was performed.

Alpha levels were set at 0.05 for statistical significance. The statistical software packages scipy.stats 1.7.1, Stata 14, and scikit-learn 0.24 [25] were used.

RESULTS

Clinical and demographic features

Sixty patients with spatial delusions were identified and fully characterized (the flowchart of patients' inclusion is available in Figures S1 and S2). Fifty-seven had an ischemic stroke (95%), and three had a hemorrhagic stroke (5%). Their median age was 81 years (interquartile range [IQR] = 73–85, range = 55–93), and the female/male ratio was 31/29. The median National Institutes of Health Stroke Scale at admission was 14 (IQR = 12–18) and at discharge was 8 (IQR = 3–12). The median admission time was 8 days (IQR = 6–12, range = 2–46). The affected territories are reported in Table S3.

The median time of diagnosis of reduplicative paramnesia was 1 day after stroke (IQR = 1–3 days, range = 0–7 days). Nineteen patients (32%) had at least one observation in which they were oriented in space before the manifestation of reduplicative paramnesia. Twenty-eight patients (47%) spontaneously expressed that they had previously been in the (original) "Hospital de Santa Maria" before being brought to the place where they believed they were.

Subtypes of reduplicative paramnesia and places of mislocation

Confabulatory mislocation was the most frequent presentation subtype (n = 36, 60%), followed by place reduplication (n = 16, 27%) and chimeric assimilation (n = 8, 13%). Most patients maintained the same subtype during the period of spatial delusion (n = 48, 80%). Most places of mislocation were closer to the patient's home than to the hospital (n = 56, 93%; Figure 1).

Patients with confabulatory mislocation most frequently believed that they were at home (n = 27, 75%), followed by believing they were in their relative's home or vacation home (n = 4, 11%) or in another hospital or clinic (n = 2, 6%). The remaining three were mislocated in extravagant places: an ambulance, a former bus garage, and a social security office. Of these, 14 patients (39%) changed the place of delusional mislocation during their presentation; five (14%) changed to a chimeric assimilation subtype, five (14%) changed to a place reduplication subtype, and four (11%) changed the place of confabulatory mislocation.

All patients with place reduplication were convinced they were in a branch of "Hospital de Santa Maria" (n = 9, 56%) or in a replica of the hospital (n = 7, 44%) located in another place. During the period of spatial delusion, three (19%) changed the location of the reduplicated building and one (6%) changed to a confabulatory mislocation form.

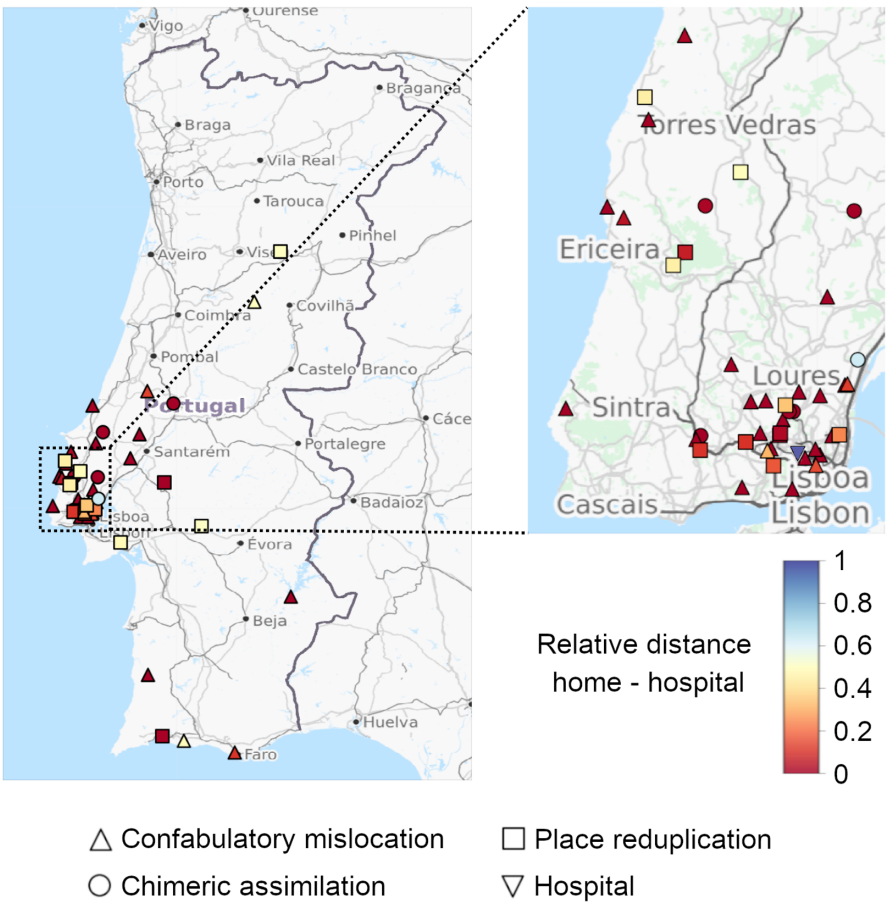

FIGURE 1 Map representation of the mislocation places' geographical location (https://www.openstreetmap.org). The color gradient represents the relative position of the mislocation place. Values closer to 1 represent mislocation closer to the hospital; closer to 0 means closer to the patient's home. Only the first is shown in patients presenting more than one place of mislocation

Regarding the patients presenting chimeric assimilation, three (38%) believed their home had been transformed into a hospital, three (38%) that a relative's home had been transformed into a hospital, and two (25%) that the hospital was inside their home. One patient (13%) changed his delusional belief to a place reduplication form.

Overall, 19 patients changed the place of mislocation during the period of reduplicative paramnesia (32%). The second place of mislocation was significantly closer to the hospital in the majority of patients ($n = 11$, 58%; distance difference: median = 28.86 km, range = 0.39–201.26 km) and farther in four patients (21%; distance difference: 0.08 km, range 0.01–2.03 km; $p < 0.01$). The remaining four changed the misidentification belief, but the geographical position of the misidentified place remained the same (21%).

Name of the misidentified place

Eighteen patients (30%) named the place that was misidentified as "Hospital de Santa Maria". In these cases, reduplicative paramnesia was uncovered when they were asked about their location (i.e., the city or town in which they were). The majority ($n = 15$) expressed that it was because they were in a replica or in a branch of the original hospital (i.e., place reduplication). The remaining three patients believed that there was a hospital ward inside their homes (i.e., chimeric assimilation), also named "Hospital de Santa Maria".

Duration of spatial delusions and disruption of belief-associated networks

The median duration of reduplicative paramnesia was 3 days (IQR = 1–7 days, range = 1–29 days; Figure 2a). In 23 cases, the patients were discharged still presenting reduplicative paramnesia.

The duration of reduplicative paramnesia was moderately correlated with the volume of structural disconnection overlapping the belief-associated functional network (Spearman correlation = 0.39, $p = 0.02$; Figure 2b), and this association was independent of lesion volume (beta coefficient = 3.18, 95% confidence interval = 0.12–6.24, $p = 0.04$). The voxelwise linear regression revealed that higher beta-coefficients mostly overlapped inferior temporal white matter fibers of the left hemisphere (Figure 2c), that is, the disconnection of these fibers had a stronger association with the duration of reduplicative paramnesia. No independent association was found with lesion overlap ($p = 0.53$).

The lesion and the structural disconnection overlap maps are available in Figure S3. The belief-associated meta-analytic functional map, derived from 83 studies, is available in Figure S4.

Semantic knowledge about the location of places and spatial routes

All patients were able to say their own address, and the majority knew the location of the (original) "Hospital de Santa Maria" ($n = 52$, 87%).

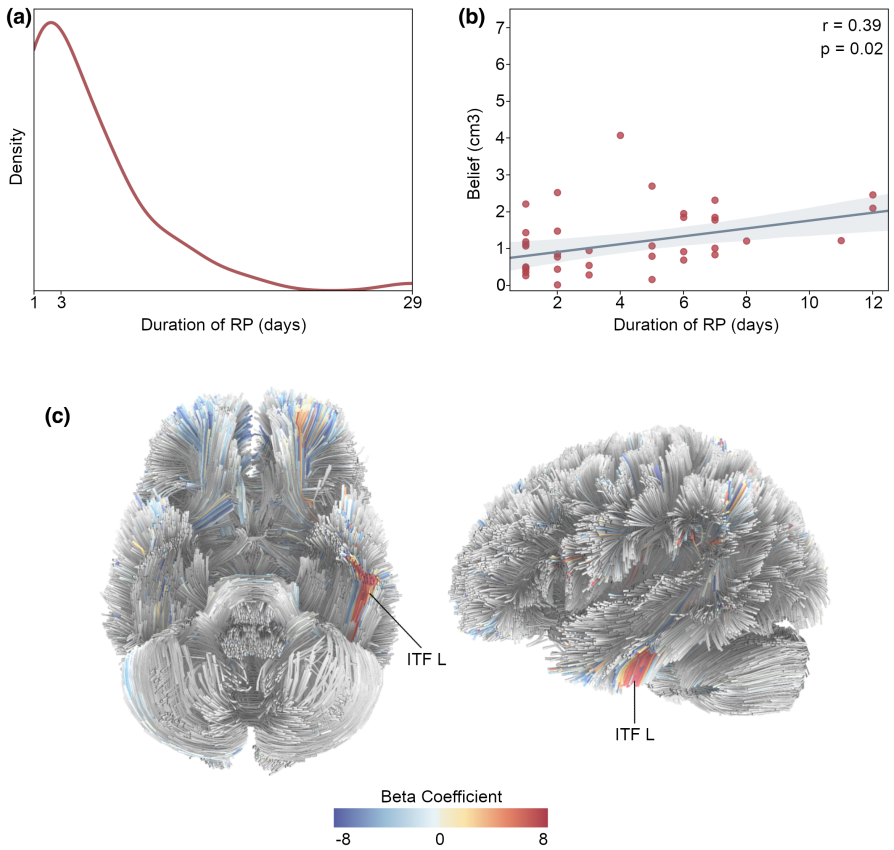

FIGURE 2 Reduplicative paramnesia duration. (a) Density distribution of the duration of reduplicative paramnesia. (b) Relationship between the duration of reduplicative paramnesia and the structural disconnection of the belief network expressed in the volume of overlap. The blue line represents the robust regression line, and the blue shadow, the 95% confidence interval. (c) Tract representation of the beta-coefficient values obtained in the voxelwise linear regression between the duration of reduplicative paramnesia and the structural disconnection of the belief network. The colormap represents the projection of the beta-coefficient map on a white matter tract template, using DSI Studio (https://dsi-studio.labsolver.org). ITF, inferior temporal fibers; L, left; *r*, Spearman correlation; RP, reduplicative paramnesia

TABLE 1 Representative descriptions of patients with confabulatory mislocation

Why are health care professionals here?
"You are the doctor from Hospital de Santa Maria. You came here to take care of me. I was there before. How did you know the address of my home? Did you find it well?"
Why is medical equipment here?
"Usually, this equipment exists in the hospitals. It is similar to the one I had in Hospital de Santa Maria. The hospital should have put it here. Nowadays, technology can be anywhere. This building is my home, but many things should have been brought from Hospital de Santa Maria."
Why does it say "Hospital de Santa Maria" on your bed sheets and hospital clothes?
"These clothes should have come in the ambulance. When the ambulance was called, the clothes should have been put inside."
Why are other patients in this room?
"These patients shoul have come with me in the ambulance, with the permission of the doctors and the nurses. It would be rude to send them away from my home."
What do you think about this window view? The building, the stadium…
"I had never noticed that I could see the sports stadium from home. But if I were in Hospital de Santa Maria, I would also see Benfica's stadium."

TABLE 2 Representative descriptions of patients with place reduplication

Why does it say "Hospital de Santa Maria" on your bed sheets and hospital clothes?
"This shall be a duplication of the service provided by Hospital de Santa Maria. The name is the same, but it covers other geographical areas."
Why does it say "Lisbon" next to the hospital logo?
"I had not read it. They made a mistake. They should have put the name of this town."
How many "Hospital de Santa Maria" do you think there are?
"There is only one. The original one. This is a dependency, not the main one. They might have built this one for the periods when the main one is full. Hospital de Santa Maria is much bigger than this one."
What do you think about this window view? The building, the stadium…
"These buildings are not typical of this district. I had never seen them. The architecture is similar the original Hospital de Santa Maria. I am going to put on my glasses, so that you do not say I am confused or disoriented. I might have lost some cognitive abilities after the stroke, but my spatial orientation is intact. The proof that it is possible to see Sporting's Stadium from this district is that I am seeing it."

Twenty-eight patients (47%) were able to correctly describe the spatial route between two or more points of interest (home–"Hospital de Santa Maria", place of mislocation–home, place of mislocation–"Hospital de Santa Maria").

Orientation in time

Most patients correctly knew the current year (n = 48, 80%) and month (n = 49, 82%).

Specific phenomenology of confabulatory mislocation

Representative descriptions of patients with confabulatory mislocation are presented in Table 1.

The most frequent answers are presented in Table S4.

Specific phenomenology of place reduplication

Representative descriptions of patients with place reduplication are presented in Table 2.

The most frequent answers are presented in Table S5.

Specific phenomenology of chimeric assimilation

Representative descriptions of patients with chimeric assimilation are presented in Table 3.

The most frequent answers are presented in Table S6.

Clustering based on familiarity-associated functional networks

The k-means clustering results based on the volume of lesion and volume of structural disconnection overlapping familiarity- and unfamiliarity-associated functional networks are presented in Figure 3. The familiarity- and unfamiliarity-associated meta-analytic functional maps, derived from 275 and 183 studies, respectively, are available in Figure S4.

The Rand index was 0.47 for lesion maps and 0.51 for structural disconnection maps (poor similarity). The classification similarity remained low when the number of clusters was reduced to two: lesions maps, Rand index = 0.64; structural disconnection maps, Rand index = 0.56.

DISCUSSION

In this work, we analyzed the clinical phenomenology and neural correlates of stroke-associated spatial delusions. First, we characterized the

TABLE 3 Representative descriptions of patients with chimeric assimilation

Why does it say "Hospital de Santa Maria" in your bed sheets and hospital clothes?
"That's because Hospita is here and my home is here too. Please open the door because my maid should be arriving. The house is mine. The hospital is not mine."
Why are other patients in this room?
"I do not know these patients. I do not know what they are doing here. They should have been brought here when I was sleeping. Probably, there were not enough beds at the hospital and they were sent here."
Have you noticed or heard about any construction work?
"It's strange how they have done it so quickly. They transformed my home into a hospital. In the future, I might make some profit from this."
Why would a hospital be built inside your home (or in your relatives' home)?
"Maybe the hospital was full and they used this space. The other patients were brought here too. You are asking me all these questions to see if my mind is fine, but I assure you that it is."
What do you think about this window view? The building, the stadium…
"My building is very similar to Hospital de Santa Maria. It should have been designed by the same architect. Everything with public funds, maybe…"

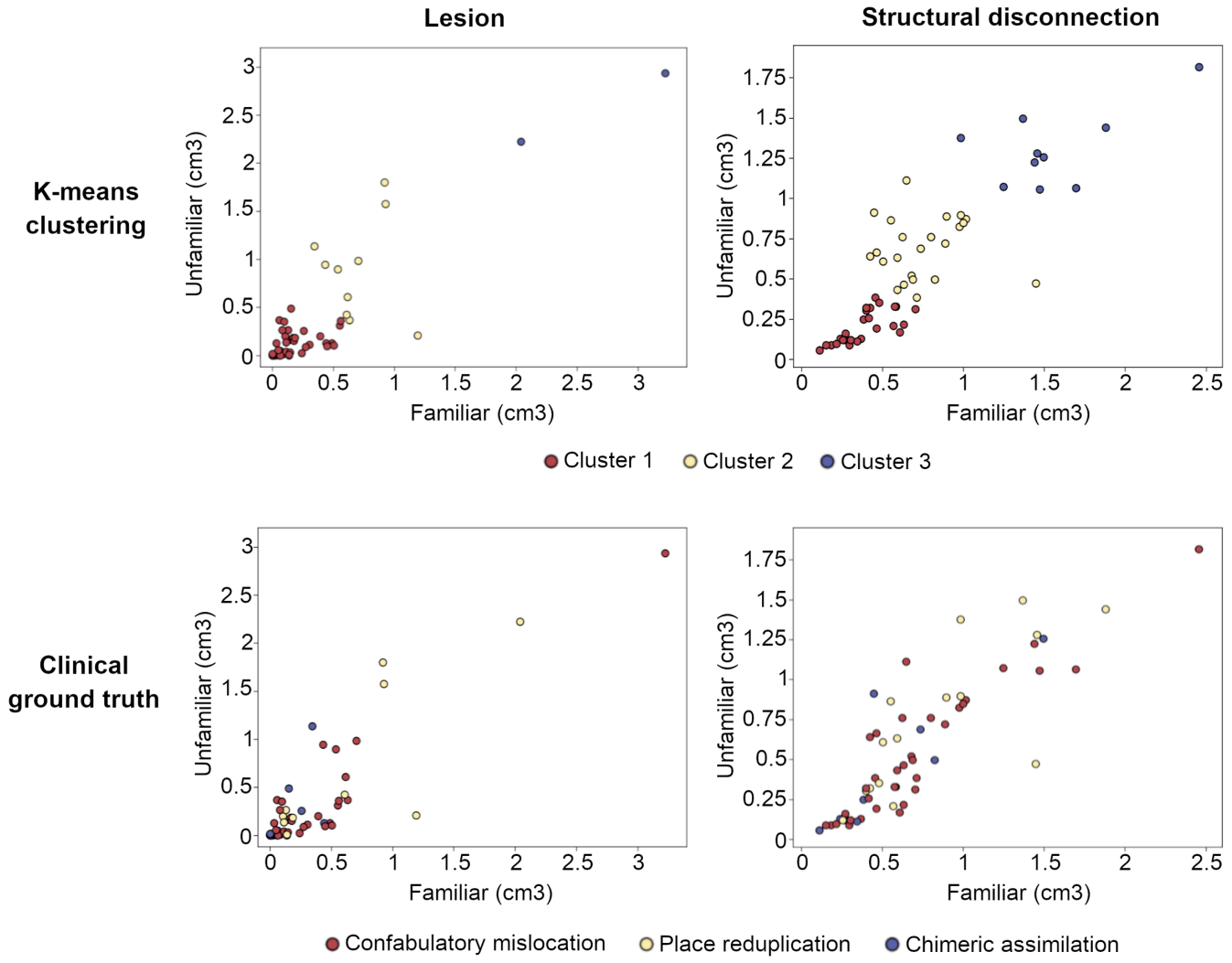

FIGURE 3 Reduplicative paramnesia subtypes and familiarity-associated functional networks. Clustering of reduplicative paramnesia cases based on the volume of the lesion (top left) and of structural disconnection (top right) overlapping familiarity- and unfamiliarity-associated functional networks are compared with the ground truth classification based on clinical presentation (bottom)

location of misidentified places and described the general phenotypic features of the syndrome. We demonstrated that the duration of spatial delusions is moderately correlated with the structural decoupling of belief-associated functional networks. Second, we reported associated clinical features, such as the patients' knowledge about the location of the misidentified places and their orientation in time. Third, we

described the most common patterns of patients' response according to spatial delusion subtypes and provided representative examples to facilitate recognition and diagnosis. Finally, we showed that case clustering based on structural disruption of familiarity/unfamiliarity-associated functional regions poorly matches the clinical classification.

The large majority of patients localized the misidentified place closer to their homes than to the hospital. Limbic-related models of delusional misidentifications support that misidentified stimuli tend to be emotionally relevant for patients [26], and an association between spatial delusions and structural disconnection of limbic structures has been established [8].

Belief, as a neural process, can be defined as the integration of perceived information with internal representations of personal significance and emotional value [27]. Distinct neural systems in the prefrontal cortex and the limbic system mediate the states of assent, dissent, and uncertainty [28, 29]. Deregulations of belief processes seem to be a cardinal condition for delusional misidentifications [27, 30]. As our phenomenological analysis showed, patients recognize that the surrounding environment looks like "Hospital de Santa Maria" but still do not believe they are there. For the first time, we showed that the magnitude of structural disconnection of belief-associated functional networks is correlated with the duration of reduplicative paramnesia. Interhemispheric unbalance models propose that delusional misidentifications result from right hemisphere damage and left hemisphere unleashing [6]. Whereas previous evidence shows that the emergence of spatial delusions is predicted by disconnection of right temporal regions [8, 9], here we showed that the disconnection of left temporal regions best predicts the syndrome's duration. This result may provide structural–functional support to the role of left hemisphere dysfunction in the pathophysiology of reduplicative paramnesia [6, 31]. This effect might be mediated by contralateral hemisphere diaschisis [32].

The erroneous beliefs and the disturbed mechanisms of implicit memory and recognition overwhelm the patient's semantic knowledge about the spatial localization of misidentified places [26, 33, 34]. In our sample, all patients were able to say their own address and the large majority knew the location of (the original) "Hospital de Santa Maria". The maintenance of correct orientation of time in most patients evidences the spatial specificity of the syndrome.

The strong emotional valence associated with reduplicative paramnesia, evident in the pioneer and in subsequent descriptions [2, 11, 35], manifests at opposite poles of pathological familiarity [6]. However, the clustering classification based on structural disruption of familiarity/unfamiliarity-associated functional networks had a poor capacity to predict clinical subtype classification. Finer functional interactions between familiarity-associated brain regions and psychological factors might be crucial to determine this phenomenological divergence [36].

Knowledge about the phenomenological features of the syndrome is important to make an appropriate diagnosis and to avoid misinterpretations of patients' general cognitive status. Nearly one third of the patients called "Hospital de Santa Maria" to the misidentified place, which may contribute to the underdiagnosis of the syndrome. Simple questions, such as asking in which town/district patients are, might be crucial for the diagnosis and should be performed during the neurological examination, especially in patients with right hemisphere lesions. In addition, in at least one third of the patients, the syndrome was not hyperacute, that is, the patients were oriented in space for at least 1 day before the emergence of reduplicative paramnesia, and nearly half spontaneously said that they had previously been in the (original) "Hospital de Santa Maria" before being brought to the place where they were at that moment. The physiopathological reason for this deferred onset remains to be clarified but may be due to delayed diaschisis [32].

As a limitation of our study, we were not able to conduct a prospective follow-up of patients after their hospital discharge. In addition, the study was performed in a tertiary stroke unit and may not represent the entire stroke population. Finally, in a considerable proportion of patients, MRI was not performed. However, modern CT scanners also provide high-resolution images suitable for stroke lesion analysis studies [15].

In conclusion, our work reports a systematic description of the peculiar clinical features of stroke-associated spatial delusions, which may boost the awareness and the proper diagnosis of the syndrome. It also contributes to a better understanding of the neural background of delusional misidentifications by providing novel evidence about the neural correlates of the syndrome.

AUTHOR CONTRIBUTIONS

Pedro N. Alves: Conceptualization (equal), data curation (lead), formal analysis (lead), funding acquisition (lead), investigation (lead), methodology (equal), visualization (lead), writing–original draft preparation (lead). Ana C. Fonseca: Conceptualization (equal), methodology (equal), writing–review and editing (equal). Teresa Pinho-e-Melo: Conceptualization (equal), writing–review and editing. Isabel P. Martins: Conceptualization (equal), methodology (equal), project administration (lead), supervision (lead), writing–review and editing (equal).

ACKNOWLEDGMENTS

We acknowledge our colleagues from the Department of Neurology and from the Language Research Laboratory for their contribution to patient screening, particularly the contribution of Dr Daniela Pimenta Silva.

FUNDING INFORMATION

This work was supported by the following grants: PRÉMIO JOÃO LOBO ANTUNES 2018–SCML and Bolsa de InvestigaçÃo em Doenças Vasculares Cerebrais 2017–SPAVC.

CONFLICT OF INTEREST

None

DATA AVAILABILITY STATEMENT

The anonymized data supporting this study's findings are available on request from the corresponding author. The data are not publicly available due to ethical approval restrictions and because their containing information could compromise the privacy of research participants.

ORCID

Pedro N. Alves https://orcid.org/0000-0001-5740-5904
Ana C. Fonseca https://orcid.org/0000-0001-6913-5526
Isabel P. Martins https://orcid.org/0000-0002-9611-7400

REFERENCES

1. Förstl H, Beats B. Charles Bonnet's description of Cotard's delusion and reduplicative paramnesia in an elderly patient (1788). *Br J Psychiatry*. 1992;160:416-418. doi:10.1192/bjp.160.3.416
2. Pick A, Clinical studies III. On reduplicative paramnesia. *Brain*. 1903;26:260-267.
3. Borghesani V, Monti A, Fortis P, Miceli G. Reduplicative paramnesia for places: a comprehensive review of the literature and a new case report. *Clin Neurol Neurosurg*. 2019;181(March):7-20. doi:10.1016/j.clineuro.2019.03.022
4. Bartolomeo P, De VS, Seidel T. Space-related confabulations after right hemisphere damage. *Cortex*. 2016;87:166-173. doi:10.1016/j.cortex.2016.07.007
5. Politis M, Loane C. Reduplicative paramnesia: A review. *Psychopathology*. 2012;45(6):337-343. doi:10.1159/000337748
6. Devinsky O. Delusional misidentifications and duplications: right brain lesions, left brain delusions. *Neurology*. 2009;72(1):80-87. doi:10.1212/01.wnl.0000338625.47892.74
7. Darby R, Prasad S. Lesion-related delusional misidentification syndromes: a comprehensive review of reported cases. *J Neuropsychiatry Clin Neurosci*. 2016;28(3):217-222. doi:10.1176/appi.neuropsych.15100376
8. Alves PN, Fonseca AC, Silva DP, et al. Unravelling the neural basis of spatial delusions after stroke. *Ann Neurol*. 2021;89(6):1181-1194. doi:10.1002/ana.26079
9. Alves PN, Silva DP, Fonseca AC, Martins IP. Mapping delusions of space onto a structural disconnectome that decouples familiarity and place networks. *Cortex*. 2021;146:250-260. doi:10.1016/j.cortex.2021.11.008
10. Moser DJ, Cohen RA, Malloy P, Stone WM, Rogg JM. Reduplicative paramnesia: longitudinal neurobehavioral and neuroimaging analysis. *J Geriatr Psychiatry Neurol*. 1998;11(4):174-180. doi:10.1177/089198879901100402
11. Murai T, Toichi M, Sengoku A, Miyoshi K, Morimune S. Reduplicative paramnesia in patients with focal brain damage. *Neuropsychiatry Neuropsychol Behav Neurol*. 1997;10(3):190-196.
12. Hoffmann M. Isolated right temporal lobe stroke patients present with geschwind gastaut syndrome, frontal network syndrome and delusional misidentification syndromes. *Behav Neurol*. 2008;20(3–4):83-89. doi:10.3233/BEN-2008-0218
13. Stangeland H, Orgeta V, Bell V. Poststroke psychosis: a systematic review. *J Neurol Neurosurg Psychiatry*. 2018;89(8):879-885. doi:10.1136/jnnp-2017-317327
14. Jenkinson M, Beckmann CF, Behrens TEJ, Woolrich MW, Smith SM. FSL. *Neuroimage*. 2012;62(2):782-790. doi:10.1016/j.neuroimage.2011.09.015
15. de Haan B, Karnath HO. A hitchhiker's guide to lesion-behaviour mapping. *Neuropsychologia*. 2018;115:5-16. doi:10.1016/j.neuropsychologia.2017.10.021
16. Rorden C, Bonilha L, Fridriksson J, Bender B, Karnath HO. Age-specific CT and MRI templates for spatial normalization. *Neuroimage*. 2012;61(4):957-965. doi:10.1038/mp.2011.182.doi
17. Thiebaut de Schotten M, Acqua FD, Forkel SJ, et al. A lateralized brain network for visuospatial attention. *Nat Neurosci*. 2011;14(10):1245-1247. doi:10.1038/nn.2905
18. Vu AT, Auerbach E, Lenglet C, et al. High resolution whole brain diffusion imaging at 7T for the Human Connectome Project. *Neuroimage*. 2015;122:318-331. doi:10.1016/j.neuroimage.2015.08.004
19. Karolis VR, Corbetta M, Thiebaut de Schotten M. The architecture of functional lateralisation and its relationship to callosal connectivity in the human brain. *Nat Commun*. 2019;10(1):1417-1424. doi:10.1038/s41467-019-09344-1
20. Foulon C, Cerliani L, Kinkingnéhun S, et al. Advanced lesion symptom mapping analyses and implementation as BCBtoolkit. *Gigascience*. 2018;7(3):1-17. doi:10.1093/gigascience/giy004
21. Darby RR, Laganiere S, Pascual-Leone A, Prasad S, Fox MD. Finding the imposter: brain connectivity of lesions causing delusional misidentifications. *Brain*. 2017;140(2):497-507. doi:10.1093/brain/aww288
22. Yarkoni T, Poldrack RA, Nichols TE, Van EDC, Wager TD. Large-scale automated synthesis of human functional neuroimaging data. *Nat Methods*. 2011;8(8):665-670. doi:10.1038/nmeth.1635
23. Sperber C, Karnath HO. Impact of correction factors in human brain lesion-behavior inference. *Hum Brain Mapp*. 2017;38(3):1692-1701. doi:10.1002/hbm.23490
24. DeMarco AT, Turkeltaub PE. A multivariate lesion symptom mapping toolbox and examination of lesion-volume biases and correction methods in lesion-symptom mapping. *Hum Brain Mapp*. 2018;39(11):4169-4182. doi:10.1002/hbm.24289
25. Pedregosa F, Varoquaux G, Gramfort A, et al. Scikit-learn: machine learning in Python. *J Mach Learn Res*. 2011;12:2825-2830. doi:10.1145/2786984.2786995
26. Ellis HD, Young AW. Accounting for delusional misidentifications. *Br J Psychiatry*. 1990;157:239-248. doi:10.1192/bjp.157.2.239
27. Seitz RJ. Beliefs: A challenge in neuropsychological disorders. *J Neuropsychol*. 2021;16:21-37. doi:10.1111/jnp.12249
28. Sacks O, Hirsch J. A neurology of belief. *Ann Neurol*. 2008;63(2):129-130. doi:10.1002/ana.21378
29. Harris S, Sheth SA, Cohen MS. Functional neuroimaging of belief, disbelief, and uncertainty. *Ann Neurol*. 2008;63(2):141-147. doi:10.1002/ana.21301
30. Pacella V, Foulon C, Jenkinson PM, et al. Anosognosia for hemiplegia as a tripartite disconnection syndrome. *Elife*. 2019;8:1-13. doi:10.7554/elife.46075
31. Gazzaniga MS. Cerebral specialization and interhemispheric communication. Does the corpus callosum enable the human condition? *Brain*. 2000;123(7):1293-1326. doi:10.1093/brain/123.7.1293
32. Carrera E, Tononi G. Diaschisis: Past, present, future. *Brain*. 2014;137(9):2408-2422. doi:10.1093/brain/awu101
33. Ellis HD, Young AW, Quayle AH, De Pauw KW. Reduced autonomic responses to faces in Capgras delusion. *Proc Biol Sci*. 1997;264(1384):1085-1092. doi:10.1098/rspb.1997.0150
34. Coltheart M, Langdon R, Mckay R. Delusional Belief. *Annu Rev Psychol*. 2011;62:271-298. doi:10.1146/annurev.psych.121208.131622
35. Benson DF, Gardner H, Meadows JC. Reduplicative paramnesia. *Neurology*. 1976;26(2):147-151.
36. Ovelacg E, Gallois P, Berteloot E, Catrysse C, Steinling M, Dereux JF. Le delire des lieux: apport de la bebitmetrie cerebrale. *Cortex*. 1988;24(2):329-337. doi:10.1016/S0010-9452(88)80041-8

SUPPORTING INFORMATION

Additional supporting information can be found online in the Supporting Information section at the end of this article.

How to cite this article: Alves PN, Fonseca AC, Pinho-e-Melo T, Martins IP. Clinical presentation and neural correlates of stroke-associated spatial delusions. *Eur J Neurol*. 2023;30:125-133. doi: 10.1111/ene.15557

Unravelling the Neural Basis of Spatial Delusions After Stroke

Pedro N. Alves, MD,[1,2,3] Ana C. Fonseca, MD, MPH, PhD,[2,3] Daniela P. Silva, MD,[2] Matilde R. Andrade, MSc,[4] Teresa Pinho-e-Melo, MD,[2,3] Michel Thiebaut de Schotten, PhD,[5,6] and Isabel P. Martins, MD, PhD[1,2,3]

Objective: Knowing explicitly where we are is an interpretation of our spatial representations. Reduplicative paramnesia is a disrupting syndrome in which patients present a firm belief of spatial mislocation. Here, we studied the largest sample of patients with delusional misidentifications of space (ie, reduplicative paramnesia) after stroke to shed light on their neurobiology.

Methods: In a prospective, cumulative, case-control study, we screened 400 patients with acute right-hemispheric stroke. We included 64 cases and 233 controls. First, lesions were delimited and normalized. Then, we computed structural and functional disconnection maps using methods of lesion-track and network-mapping. The maps were compared, controlling for confounders. Second, we built a multivariate logistic model, including clinical, behavioral, and neuroimaging data. Finally, we performed a nested cross-validation of the model with a support-vector machine analysis.

Results: The most frequent misidentification subtype was confabulatory mislocation (56%), followed by place reduplication (19%), and chimeric assimilation (13%). Our results indicate that structural disconnection is the strongest predictor of the syndrome and included 2 distinct streams, connecting right fronto-thalamic and right occipitotemporal structures. In the multivariate model, the independent predictors of reduplicative paramnesia were the structural disconnection map, lesion sparing of right dorsal fronto-parietal regions, age, and anosognosia. Good discrimination accuracy was demonstrated (area under the curve = 0.80 [0.75–0.85]).

Interpretation: Our results localize the anatomic circuits that may have a role in the abnormal spatial-emotional binding and in the defective updating of spatial representations underlying reduplicative paramnesia. This novel data may contribute to better understand the pathophysiology of delusional syndromes after stroke.

ANN NEUROL 2021;89:1181–1194

Interpretation of space is a continuous process that allows us to explicitly know where we are.[1] Perceived sensorial information from the environment is integrated in spatial orientation networks that mediate the recognition of known spatial landmarks and navigation with regard to allocentric and egocentric references.[2] Although comprehensive cognitive models have been proposed for spatial representation,[3] the anatomic systems supporting explicit spatial interpretation remain poorly documented.

Stroke lesions may strikingly disrupt spatial interpretation. Reduplicative paramnesia is a rare spatial misidentification syndrome in which patients firmly believe that they are in a different place from the real one.[4] Despite recognizing surrounding landmarks, they believe that a certain place is mislocated (ie, confabulatory mislocation), reduplicated (ie, place reduplication), or fused with other space (ie, chimeric assimilation).[5] Notably, they are rather insensitive to surrounding incongruences, and

View this article online at wileyonlinelibrary.com. DOI: 10.1002/ana.26079

Received Oct 24, 2020, and in revised form Mar 30, 2021. Accepted for publication Mar 31, 2021.

Address correspondence to Dr Alves, Laboratório de Estudos de Linguagem, Faculdade de Medicina, Avenida Professor Egas Moniz, 1649-028 Lisbon, Portugal. E-mail: pedronascimentoalves@gmail.com

From the [1]Language Research Laboratory, Faculty of Medicine, Universidade de Lisboa, Lisbon, Portugal; [2]Department of Neurosciences and Mental Health, Neurology, Hospital de Santa Maria, CHULN, Lisbon, Portugal; [3]Instituto de Medicina Molecular João Lobo Antunes, Faculty of Medicine, Universidade de Lisboa, Lisbon, Portugal; [4]Institute of Psychiatry, Psychology and Neuroscience, King's College of London, University of London, London, UK; [5]Brain Connectivity and Behaviour Laboratory, Sorbonne Universities, Paris, France; and [6]Groupe d'Imagerie Neurofonctionnelle, CEA, Univ. Bordeaux, CNRS, IMN, UMR 5293, Bordeaux, France

Additional supporting information can be found in the online version of this article.

their convictions do not change when confronted with clear counter-evidence. Even with an otherwise coherent behavior, this may increase patients' disability and complicate medical care.

The intriguing nature of reduplicative paramnesia has fostered the development of different models to explain its pathophysiology. Memory-related theories have proposed an abnormal integration of new visual information with past memories, leading to a defective update of patients' spatial representations.[6] Ellis and Young emphasized that patients with delusional misidentification have a deficit in the attribution of appropriate emotional valences to visual stimuli.[7] They demonstrated that the expected autonomic responses are not generated in these patients when confronted with familiar stimuli.[8] In addition, it has been proposed that reduplicative paramnesia and other delusional misidentification syndromes result from a combination of right hemisphere injury and left hemisphere overactivity.[9] Different neuroanatomic hypotheses have emerged from these cognitive models; however, solid empirical evidence is lacking.[5]

Here, we explored the anatomy of lesions leading to reduplicative paramnesia in a large dataset of patients to shed light on the brain mechanisms supporting the explicit interpretation of space.

Methods

Study Design and Patient Selection

We performed a prospective, cumulative, case-control study that included patients from the stroke unit of a tertiary university hospital in Lisbon, Portugal. Recruitment lasted from December 2016 to February 2020. Reduplicative paramnesia is a right-hemisphere stroke syndrome.[10] We consecutively included adult patients with right hemisphere stroke who were admitted in the acute phase (72 hours or less) of stroke. Patients with either ischemic or hemorrhagic strokes were considered. The exclusion criteria were as follows: acute confusional state, according to the criteria defined in the fifth edition of the Diagnostic and Statistical Manual of Mental Disorders; decreased level of consciousness, somnolence, stupor, or coma; subarachnoid hemorrhage; epileptic seizures during admission, either symptomatic or in patients with a previous diagnosis of epilepsy; aphasia or severe dysarthria, precluding screening for reduplicative paramnesia; severe visual deficit, precluding confrontation with counter-evidence stimuli; history of dementia, defined as a cognitive decline that interfered with the instrumental activities of daily living (according to the clinical history provided by the patient's relatives and/or to the patient's medical records in the national electronic health platform), as referred in the criteria of major neurocognitive disorder in the fifth edition of the Diagnostic and Statistical Manual of Mental Disorders; absence of a stroke lesion in brain imaging, or unavailable brain images.

A history of stroke was not an exclusion criterion, because some pathophysiological models of delusional misidentification syndromes propose a "2-hit" process[11] and there are reports hypothesizing that prior brain lesions may contribute to the occurrence of reduplicative paramnesia.[12]

This study was approved by the Joint Ethics Committee of the Lisbon Academic Medical Centre, and patient informed consent was obtained for acquisition and publication of individuals' data.

Clinical Screening

Of 400 patients screened, 297 fulfilled our study criteria. The reasons for patient exclusion are presented in the Supplementary Table S1. Sixty-four of the 297 patients presented with reduplicative paramnesia. Patients were screened for reduplicative paramnesia within the first 72 hours of admission and then at regular intervals of 48 hours. Spatial orientation was evaluated through a structured interview asking patients if they knew where they were, namely, the kind of building (hospital), the city (Lisbon), and the city district they were in. The patients who did not know or who gave a wrong answer were given the correct location. If patients disagreed with the given answer, they were then confronted with clear evidence proving otherwise. Whenever they thought they were in a place other than a medical facility, they were shown and asked to identify medical equipment (vital signs monitor, venous infusion tubes, and oxygen masks), and other patients in the same room or medical staff (physicians, nurses, and physiotherapist). Whenever they believed they were in another hospital or in another place/city, they were shown either (a) the hospital logotype in the medical coats and bed sheets and asked to read the corresponding inscription, which included the hospital and the city names, or/and (b) the view from a window and asked to identify unique nearby landmarks, such as Lisbon airport and the stadium of an emblematic Portuguese football team. The patients who maintained a false conviction of spatial mislocation after being effectively exposed to these counterfactual stimuli (confabulatory mislocation, place reduplication, or chimeric assimilation) were considered cases of reduplicative paramnesia. The patients who were oriented in space or patients who were disoriented but accepted the evaluator's explanation or changed their belief after being exposed to the referred counter-evidence were considered controls.

An illustrative case of reduplicative paramnesia is described in the Supplementary Table S2 and in the Supplementary Video S1.

Clinical and demographic data were collected. The descriptions of the patients with reduplicative paramnesia were classified according to the subtypes defined in the literature (ie, place reduplication, confabulatory mislocation, and chimeric assimilation).[5] We also screened for other delusional misidentification syndromes, namely, Capgras syndrome, Fregoli syndrome, asomatognosia, and somatoparaphrenia.

Regarding neuroimaging parameters, the grades of cerebral atrophy and small-vessel disease burden were visually rated (either on computed tomography [CT] or magnetic resonance imaging [MRI], as specified in the following section). The Global Cortical Atrophy scale was used to assess cortical atrophy.[13] This scale was originally designed to grade cortical atrophy in patients who had a stroke and consists of an ordinal scale, ranging from 0 (no atrophy) to 3 ("knife blade" atrophy), that includes a discrete assessment of the frontal, the parieto-occipital, and the temporal regions. The Medial Temporal Lobe Atrophy score was also evaluated.[14] It is a widely used ordinal scale to assess medial temporal lobe atrophy that ranges from 0 (no atrophy) to 4 (marked widening of the choroid fissure and of the temporal horn, marked atrophy, and internal structure loss of the hippocampus). The Age-Related White Matter Changes was used to grade small-vessel disease burden.[15] It evaluates both white matter disease and basal ganglia small-vessel lesions in 2 ordinal scales ranging from 0 (no lesions) to 3 (diffuse or confluent lesions).[15] These 3 scales were chosen because they have good intra and interobserver reliability[15,16] and they have been recommended for the routine clinical assessment of CT and MRI images.[17] The rater was blind to patients' outcome during the assessment.

Lesion Topography Analysis

Brain MRI or CT images were used to define stroke lesions. Delimitation was manually performed on axial slices with a thickness of 3 mm. The researchers were blind to the status of the patient (ie, case or control). MRI images were acquired in a Philips Achieva 3.0 T or Philips Intera 1.5 T scanner. The sequence of reference in MRI was the diffusion-weighted imaging.[18] When MRI was not available, CT was performed 24 to 72 hours after stroke onset was used. CT images were acquired in a Philips Brilliance 64-channel scanner. The proportion of MRI/CT scans in the groups of cases and controls were 23/41 and 118/115, respectively ($p = 0.06$).

Brain MRI and CT images were normalized to MNI152 space. For an MRI, T1 images were used as the reference for normalization. We performed a first step of linear registration, applying an affine transformation (12 degrees of freedom), using the FSL software FLIRT tool. A second step of nonlinear registration was performed using FSL's FNIRT tool.[19] For a CT, a linear registration was performed applying the same parameters as before and using the CT-derived MNI152 template.[18] In both cases, the calculated deformation field was applied to the lesions.

Randomise is an FSL tool that allows nonparametric comparisons of brain images.[20] A 2-sample unpaired analysis was performed using this tool to compare lesion maps of the 2 groups. Five thousand permutations were computed, a threshold-free cluster enhancement was applied, and the obtained p values were family-wise error (FWE) corrected. Possible confounders were included in the model as covariates, namely, lesion volume, stroke clinical severity (measured by the National Institutes of Health Stroke Scale), imaging modality (MRI or CT), and stroke vascular territory. The analysis was whole-brain based.

A brain map of the areas where the lesion or sparing was significantly associated with reduplicative paramnesia was created.

A less conservative follow-up analysis was also performed, applying a false discovery rate (FDR) correction for multiple comparisons. FDR-corrected maps were computed using FSL's fdr tool.

To investigate neuroimaging differences among the 3 subtypes of reduplicative paramnesia, we also computed an F-test with *Randomise*, contrasting patients with place reduplication, confabulatory mislocation, and chimeric assimilation.[20] If the F-test revealed statistically significant intergroup differences, individual 2 sample tests were calculated to determine the direction of the effect.

We included prior brain lesions in the lesion mask. Because the neurobiological processes underlying acute and chronic stroke lesions differ, a sensitivity analysis including only patients with first-ever strokes was performed.

Structural Disconnection Analysis

Some neurobehavioral syndromes are better explained by the pattern of white matter disconnection rather than by a specific lesion localization.[21,22] With this in mind, we also compared the pattern of structural disconnection between the cases and controls.

The tool Disconnectome from the software package BCBtoolkit (http://toolkit.bcblab.com) indirectly calculates the probability of structural disconnection caused by focal lesions.[23] The probability of disconnection is derived from healthy subjects' tractography from the Human Connectome Project 7 T dataset (n = 178).[24] Tractography was processed as described by Karolis and colleagues.[25] This analysis produces a Disconnectome map revealing disconnection patterns

only when more than 50% of the tractographies of healthy subjects were disconnected.

A *Randomise* 2-sample test was computed to compare the Disconnectome maps of the 2 groups using the same parameters and the same confounding covariates considered in the lesion topography analysis.[20] A brain map of areas whose disconnection was significantly associated with reduplicative paramnesia was created.

Similar to the approach taken in the previous section, an F-test was calculated to investigate structural disconnection differences between the subtypes of reduplicative paramnesia.

We also computed a structural disconnection matrix. The Automated Anatomical Labeling atlas 3 (AAL3)[26] was the chosen parcellation because it includes cortical and subcortical structures. We used MRtrix's tool *tckedit* to select the tracts of each of 178 tractographies of reference that crossed the individual stroke lesions.[27] Then, MRtrix's tool *tck2connectome* was run to create a connectivity matrix. To calculate the proportion of disruption, we divided the number of disrupted streamlines by the total number of streamlines connecting each pair of regions. The mean of the 178 individual matrices was computed, in order to obtain single individual connectivity matrices. The difference in the proportion of disruption between the cases and controls and 2-sample unpaired statistics were calculated, applying a multiple comparisons Bonferroni-corrected p value (p value < 3.5E-6).

Functional Connectivity Analysis

There is a considerable relationship between structural and functional disconnection, but the overlap is far from absolute.[28] Lesion network mapping of some neuropsychiatric syndromes, such as peduncular hallucinosis, has been achieved through functional connectivity analysis.[29] Therefore, we complemented the connectivity characterization of reduplicative paramnesia with a functional connectivity study.

Stroke lesions were used as seeds. We calculated the correlation between the average time course of every lesion and the time course of the other brain voxels using the Funcon connectivity tool from BCBtoolkit (http://toolkit.bcblab.com).[23] We used 175 preprocessed 7 T resting state functional MRIs from the Human Connectome Project S1200 dataset.[30] Preprocessing was performed according to the Human Connectome Project pipelines.[30] To create the functional Disconnectome map of each patient, we followed the protocol developed by the Laboratory for Brain Network Imaging and Modulation.[31] Correlation values were converted to a normal distribution using Fisher's r to z transform. FSL's tool *Randomise* 1-sample test was used to compute statistically significant correlations, applying a threshold-free cluster enhancement. Statistical maps were thresholded and binarized at $t > \pm 4.25$ to create positive and negative functional Disconnectome maps.[32,33] We chose the same threshold as Darby and colleagues in their work about delusional misidentifications syndromes, to allow a more direct comparison between studies.[32] A *Randomise* 2-sample test was used to compare the maps of the 2 groups using the same parameters and the same confounding covariates applied in the lesion topography and in the structural connectivity analyses. We run additional analyses without a t-value threshold and with alternative t-value thresholds of 4.16 ($p < 0.00005$) and of 4.71 ($p < 0.000005$) to evaluate the consistency of the results.[34] An F-test to investigate intergroup functional connectivity differences between the subtypes of reduplicative paramnesia was computed as well.

It has been demonstrated that cognitive processing is enhanced when there is functional-structural coupling.[35] In addition, it is expected that white matter disruption induces functional changes at the cortical level.[36] Therefore, we performed a complementary analysis aimed to integrate functional and structural maps. We defined significant functional regions and adjacent white matter voxels as seeds for tractography in the seed tracking algorithm provided by DSI Studio (http://dsi-studio.labsolver.org). Then, we identified the areas of overlap between the obtained structural connectivity map and the map of significant structural disconnection.

Statistical Analysis

Continuous variables were reported as the mean (SD) or median (interquartile range) and compared using 2-sample unpaired t tests or Mann–Whitney tests, according to their distribution. Categorical variables were reported as frequencies and compared using chi-square or Fisher's tests, as appropriate.

A multivariate logistic regression model was built using Stata14. Variables with a statistically significant association in the bivariate analysis or those that were considered clinically or biologically relevant were included using a step-up approach. Competing models were evaluated by their goodness-of-fit and complexity using Akaike information criterion.

Finally, the obtained model was cross-validated. We computed a support vector machine k-fold nested cross-validation using sklearn. We used *RepeatedStratifiedKFold* as a randomized cross-validation splitter, and 50 splits were performed, leaving 20% of the data out.[37] A structural disconnection map and a lesion spared map were computed in each cross-validation fold (ie, 50 different structural disconnection and lesion spared maps were

calculated). The maps derived solely from the training sample that was randomly selected at each iteration, so that the predictive capacity of the model was tested in a group of subjects (test sample) that did not contribute to the computation of these maps. We applied GridSearchCV for parameter hyperoptimization and C-Support Vector Classification as a classifier. A receiver operating characteristic (ROC) curve was plotted to evaluate the classifier's output, and the median and interquartile range of the area under the curve (AUC) scores were computed. The positive and negative predictive values of the model were also calculated.

Due to the hypothesis that psychiatric comorbidities might increase the likelihood of delusional misidentifications of space, a subgroup analysis was performed comparing demographic, clinical, and neuroimaging parameters between reduplicative paramnesia patients with and without prior psychiatric disease.

Alpha levels were set at 0.05 for statistical significance, and the p value was corrected for multiple comparisons whenever appropriate, as specified in the previous section.

Results

Clinical Features

The demographic, clinical, and neuroimaging features of the cases and controls are presented in Table 1 and in the Supplementary Table S3.

The patients with reduplicative paramnesia were older, had more severe neurological deficits, and had worse functional outcomes at discharge than controls. Anosognosia, neglect, and other delusional misidentification syndromes were more frequent in patients with reduplicative paramnesia. There was no difference in terms of history of psychiatric disease. The patients with reduplicative paramnesia had higher lesion volumes and higher grades of cortical atrophy. There was no difference in terms of small vessel disease burden, both at the white matter and basal ganglia levels.

The median duration of reduplicative paramnesia was 2 days (interquartile range = 1–5 days) and ranged from 1 to at least 17 days. Nineteen patients maintained reduplicative paramnesia at the time of discharge (or transference to another hospital).

The most frequent subtype of reduplicative paramnesia was confabulatory mislocation (56%), followed by place reduplication (19%), and chimeric assimilation (13%). The most frequent places of mislocation were: believing to be at home, in confabulatory mislocation; believing to be at a replica of the original hospital, in place reduplication; or believing that home was inside the hospital or transformed into a hospital, in chimeric assimilation. In 8 patients (12%), there was a change of the subtype of reduplicative paramnesia during the period of hospitalization. A detailed description of the subtypes of reduplicative paramnesia and of the places of mislocation is presented in Table 2.

In the subgroup of patients with prior psychiatric disease, none had a history of delusions. There was no statistically significant difference between patients with reduplicative paramnesia with and without prior psychiatric disease in terms of age, frequency of anosognosia, clinical severity, lesion volume, and small vessel disease burden. There was a tendency, not statistically significant, for lower grades of parieto-occipital and temporal atrophy in patients with prior psychiatric disease (Supplementary Table S4).

Lesion Topography

Lesion overlap maps of cases and controls are presented in Figure 1A. The comparison between the 2 groups, regressing for confounders, did not reveal any voxels significantly more often lesioned in the cases than controls (both in the primary FWE adjusted and in the follow-up FDR adjusted analyses). Conversely, there were voxels topographically located in the dorsal regions of the parietal and frontal lobes that were significantly more often lesioned in controls than in cases (FWE-corrected p value < 0.05; Fig 1B).

The sensitivity analysis including only patients with a first-ever stroke (n = 276, 60 cases, 216 controls) revealed similar results.

There was no statistically significant intergroup difference among the 3 subtypes of reduplicative paramnesia or between reduplicative paramnesia patients with and without prior psychiatric disease.

Structural Disconnection

The comparison of the structural disconnection maps between cases and controls, regressing for confounders, revealed a map of voxels significantly more often disconnected in cases than controls (FWE-corrected p value < 0.05; Fig 2A). There were no voxels significantly more often disconnected in the controls than in cases. Two main segments of disconnection were evident: right thalamo-frontal and right occipitotemporal (Fig 2B). The right thalamo-frontal segment overlapped the anterior thalamic radiations and the fronto-striatal projections (Fig 2C, left). The right occipitotemporal segment overlapped the inferior fronto-occipital fasciculus and the inferior longitudinal fasciculus (see Fig 2C, right).

The sensitivity analysis, including only patients with a first-ever stroke (n = 276, 60 cases, 216 controls) revealed similar results.

TABLE 1. Demographic, Clinical, and Neuroimaging Features

		Cases (n = 64)	Controls (n = 233)	*p* value
Demographic features	Age (years)	78 [71–83]	68 [58–78]	<0.01
	Gender (F/M), n	31/33	99/134	0.40
Clinical features	Type of stroke (Isch/ICH), n	62/2	212/21	0.18
	Screening start (days)	2 [1–2]	2 [1–2]	0.18
	Length of admission (days)	8 [5–12]	7 [5–11]	0.44
	NIHSS admission	15 [12–18]	11 [6–15]	<0.01
	NIHSS discharge	10 [5–15]	3 [1–8]	<0.01
	mRankin discharge	4 [3–4]	2 [1–4]	<0.01
	Anosognosia, n (%)	44 (69%)	73 (31%)	<0.01
	Neglect, n (%)	41 (64%)	109 (47%)	0.01
	Other DMS, n (%)	12 (21%)	6 (3%)	<0.01
	Fregoli syndrome	8 (14%)	1 (0.4%)	
	Asomatognosia	1 (1.7%)	2 (0.9%)	
	Somatoparaphrenia	2 (3%)	3 (1.3%)	
	Fregoli + asomatognosia	1 (1.7%)	0 (0%)	
Comorbidities	Prior psychiatric disease, n	9 (14%)	26 (11%)	0.52
	Depression	8 (13%)	19 (8%)	
	Anxiety	0	6 (3%)	
	Bipolar disorder	1 (2%)	0	
	PTSD	0	1 (0.4%)	
Neuroimaging features	Lesion volume (cm3)	54 [25–136]	17 [4–61]	<0.01
	ARWMC			
	White matter	1 [1–2]	1 [0–2]	0.19
	Basal ganglia	1 [0–2]	1 [0–2]	0.46
	Global cortical atrophy			
	Frontal	1 [0–2]	0 [0–1]	0.02
	Parieto-occipital	1 [1–2]	1 [0–2]	<0.01
	Temporal	1 [0–2]	0 [0–1]	0.04

Values are presented as the median [interquartile range], unless otherwise specified.
ARWMC = age-related white matter changes; DMS = delusional misidentification syndromes; F = female; Isch/ICH = ischemic; M = male; NIHSS = National Institutes of Health stroke scale; mRankin = modified Rankin scale; PTSD = post-traumatic stress disorder.

All the lesions associated with reduplicative paramnesia hit at least one of these segments (Fig 3B). Most intersected both the right thalamo-frontal and the right occipitotemporal segments (81%, n = 52). The remaining intersected the right occipitotemporal segment only (19%, n = 12).

The structural disconnection matrix is presented in Figure 2D. The pairs of AAL3 nodes with the highest differences in terms of proportion of disconnection between the 2 groups were: (1) the right fusiform gyrus with the right anterior orbitofrontal cortex; (2) the right cuneus and superior occipital gyrus with the right superior

TABLE 2. Subtypes of Reduplicative Paramnesia and Places of Mislocation

Subtype			Place of mislocation	
Place reduplication		19% (n = 12)	Hospital replica	13% (n = 8)
			Hospital dependency	6% (n = 4)
Chimeric assimilation		13% (n = 8)	Home inside hospital	5% (n = 3)
			Home transformed into a hospital	5% (n = 3)
			Relative's house transformed into a hospital	3% (n = 2)
Confabulatory mislocation		56% (n = 36)	Home	41% (n = 26)
			New clinic	3% (n = 2)
			Other clinic	3% (n = 2)
			Relative's house	2% (n = 1)
			Ambulance	2% (n = 1)
			Farm	2% (n = 1)
			Garage	2% (n = 1)
			Kindergarten	2% (n = 1)
			Military base	2% (n = 1)
More than one subtype	Confabulatory mislocation and place reduplication	6% (n = 4)	Home and hospital dependency	5% (n = 3)
			Relative's house and hospital dependency	2% (n = 1)
	Confabulatory mislocation and chimeric assimilation	6% (n = 4)	Home and home inside hospital	5% (n = 3)
			Home and home transformed into a hospital	2% (n = 1)

temporal gyrus; (3) the right thalamic ventral anterior nucleus with the right frontal middle gyrus; and (4) the right midbrain with the right medial superior frontal gyrus (Fig 2E). The difference between the 2 groups was statistically significant (Bonferroni's corrected p value < 3.5E-6), with higher proportions of disconnection in patients with reduplicative paramnesia than in controls.

In the analysis of intergroup differences between the different subtypes of reduplicative paramnesia, we found a statistically significant effect in a right frontal region that overlaps the thalamo-frontal circuit (see Fig 3A). The individual 2-sample analyses showed that the effect was driven by higher probabilities of disconnection of this circuit in patients with place reduplication or with confabulatory mislocation than in patients with chimeric assimilation.

There was no statistically significant difference between patients with reduplicative paramnesia with and without prior psychiatric disease.

Functional Disconnection

The statistical comparison of the positive correlation maps, regressing for confounders, revealed one area significantly associated with reduplicative paramnesia that was located in the right precuneus (FWE-corrected p value < 0.05; Fig 4A). There was no significant association when the negative correlation maps were compared. White matter tracts seeded from the significant functional area in the right precuneus included: (a) a right lateral temporal bundle (Fig 4B, top) that partially overlapped the temporal region with significant structural disconnection (Fig 4C); and (b) a right medial bundle (see Fig 4B, bottom), that partially overlapped the frontal region with significant structural disconnection (see Fig 4C).

The sensitivity analysis, including only patients with a first-ever stroke (n = 276, 60 cases, 216 controls) revealed similar results.

The additional analyses applying t-value thresholds of 4.16 and 4.71 showed similar results. The unthresholded analysis did not reveal statistically significant differences between cases and controls.

There was no statistically significant intergroup difference among the 3 subtypes of reduplicative paramnesia.

Multivariate Model

The multivariate model with the best classification performance included the following independent variables:

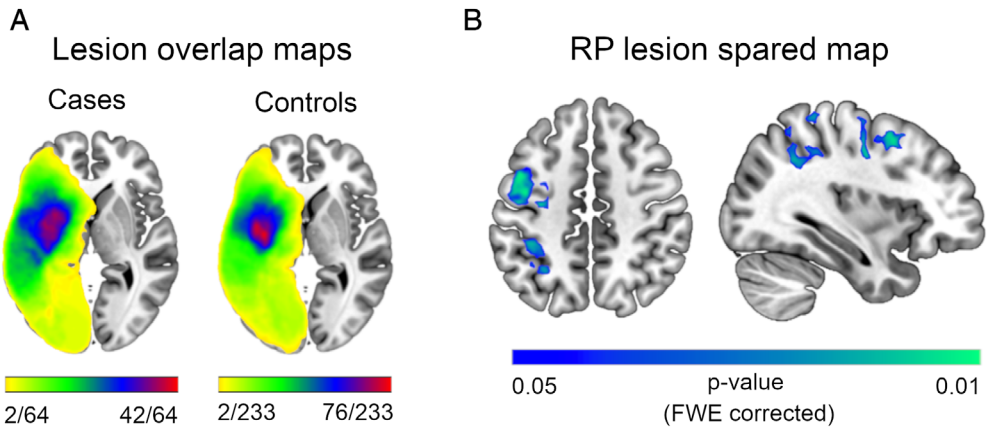

FIGURE 1: Lesion topography analysis. (A) Lesion overlap maps of cases (*left*) and controls (*right*). (B) Statistical mapping of areas significantly more often spared in cases of reduplicative paramnesia than in controls, regressing for confounders. FWE = family-wise error family-wise error; RP = reduplicative paramnesia.

volume of an individual's structural disconnection map intersecting the reduplicative paramnesia structural disconnection map, volume of an individual's lesion intersecting the reduplicative paramnesia lesion spared map, age, and anosognosia (Table 3). The total volume of the lesion, the total volume of the individual Disconnectome map and the grade of cortical atrophy were not independent predictors of reduplicative paramnesia.

The validation of this model, namely, performing a support vector machine 50-fold nested cross-validation, revealed good discrimination accuracy with a median AUC of 0.80 (interquartile range = 0.75–0.85; Fig 5).

The model correctly classified 85% of the patients, presenting a positive predictive value of 70% and a negative predictive value of 87%. The variable with best discriminability per se was the volume of an individual's structural disconnection map intersecting the reduplicative paramnesia structural disconnection map (AUC = 0.80).

Discussion

In this study, we investigated the anatomic basis of delusional misidentifications of space. We analyzed lesion topography and structural and functional connectivity patterns, addressing the pathophysiological hypotheses that had been proposed to date. Three main findings emerged from this research. First, the structural disconnection map was the most important predictor of reduplicative paramnesia and was composed of 2 main streams, connecting the right anterior thalamus with the right prefrontal cortex and the right occipital cortex with the right temporal cortex. Second, reduplicative paramnesia was associated with functional disconnection with the right precuneus, and a functional-structural link was demonstrated at this level. Finally, we found that the independent predictors of reduplicative paramnesia were structural disconnection of the above-mentioned regions, lesion sparing of the right dorsal frontoparietal areas, age, and anosognosia.

At a neurobehavioral level, delusional misidentifications have been associated with defective binding of a proper emotional value to perceived visual information.[7] In reduplicative paramnesia, misidentified spaces are mostly reduplicated or mislocated to emotionally relevant places.[38] The limbic system is a key circuit for emotional integration, particularly the limbic temporo-amygdala-orbitofrontal division.[39] It has been shown that visual scenes that are affectively significant induce stronger amygdaline responses[40] and that lesions of the right inferior longitudinal fasciculus disturb visual-emotional integration.[41,42] The amygdala and the orbitofrontal cortex are densely connected by bidirectional pathways and synergistically regulate the cognitive control of emotion.[43] The anterior nuclei of the thalamus belong to the limbic system.[44] They seem to modulate amygdala-orbitofrontal activity and participate in emotional-cognitive interactions.[45] The connection of the anterior thalamic nuclei with the limbic regions of the prefrontal cortex is through the anterior thalamic projections that run in the anterior limb of the internal capsule.[39] This pattern matches the thalamo-frontal stream identified in our study.

Translating these findings to the functional network organization of the brain, we have recently demonstrated that the anterior thalamus integrates the default mode network.[46] The default mode network works as a multimodal integrator of domain-specific networks. The disruption of multimodal integration is phenomenologically evident in reduplicative paramnesia. For instance, patients recognize environmental landmarks and know where these landmarks are located but still misjudge their own position in space. Furthermore, they understand the

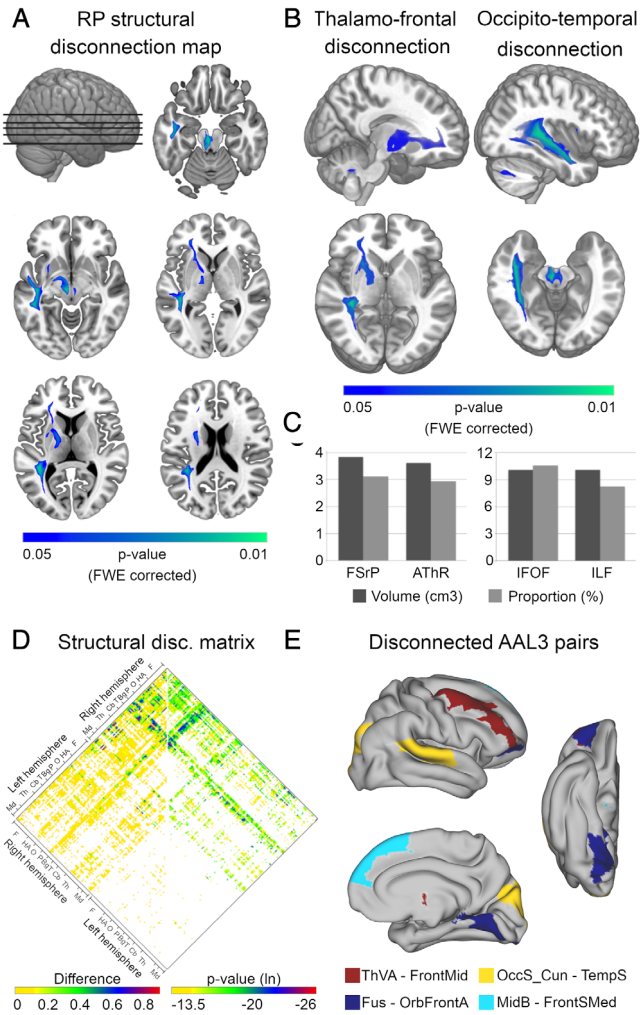

FIGURE 2: Structural disconnection analysis. (A) Statistical mapping of areas more often disconnected in patients with reduplicative paramnesia than controls, regressing for confounders. (B) Three-dimensional representation of statistical mapping, evidencing the segments of the right thalamo-frontal and right occipitotemporal disconnection. (C) Volume and proportion of the right fronto-striatal projections (FSrP), right anterior thalamic radiations (AThR), right inferior fronto-occipital fasciculus (IFOF) and right inferior longitudinal fasciculus (ILF) that are intersected by the statistical map of disconnection. (D) Structural disconnection matrix. The left half represents the difference between the proportions of disconnection in cases and controls (cases minus controls). The right half represents the corresponding *p* values (in a natural logarithmic scale). Each line represents an AAL3 node. Nodes were grouped into regions according to the corresponding labels (Bg = basal ganglia; Cb = cerebellum; F = frontal; HA = hipoccampal-amygdaline complex; Mid = midbrain; O = occipital; P = parietal; T = temporal; Th = thalamus). A complete indexing of AAL3 nodes is available in the Supplementary Table S5. (E) Surface representation of the pairs with the highest difference of disconnection between the cases and controls. Each color represents a pair of nodes. AAL3 = Automated Anatomical Labeling atlas 3; FrontMid = medial frontal gyrus; FrontSMed = medial surface of the superior frontal gyrus; Fus = fusiform gyrus; FWE = family-wise error; MidB = midbrain; OccS_Cun = superior occipital gyrus and cuneus; OrbFrontA = anterior orbitofrontal cortex; RP = reduplicative paramnesia; TempS = superior temporal gyrus; ThVA = thalamic ventral anterior nucleus.

counter-evidence that is shown but still do not update their belief.

The processes of identifying incongruent information and reality monitoring are mediated by the anterior prefrontal cortex.[47] The anterior prefrontal cortex also has a determinant role in the self-referential processing of external stimuli through the activation of a network composed of the anterior right middle frontal gyrus, the medial superior frontal gyrus, and the anterior orbitofrontal cortex.[48] Early reports identified frontal lesions as an important risk factor for reduplicative paramnesia,[49] but several cases were described missing this feature.[5] Our results revealed that the significant determinant for the emergence of reduplicative paramnesia is the disconnection of distinct areas of the prefrontal cortex, rather than frontal lesion per se.

In addition to right fronto-thalamic disruption, the structural disconnection map associated with reduplicative paramnesia included a right occipitotemporal stream. Ventral visual pathways constitute a core system for visual categorization and mediate the connection of the occipital

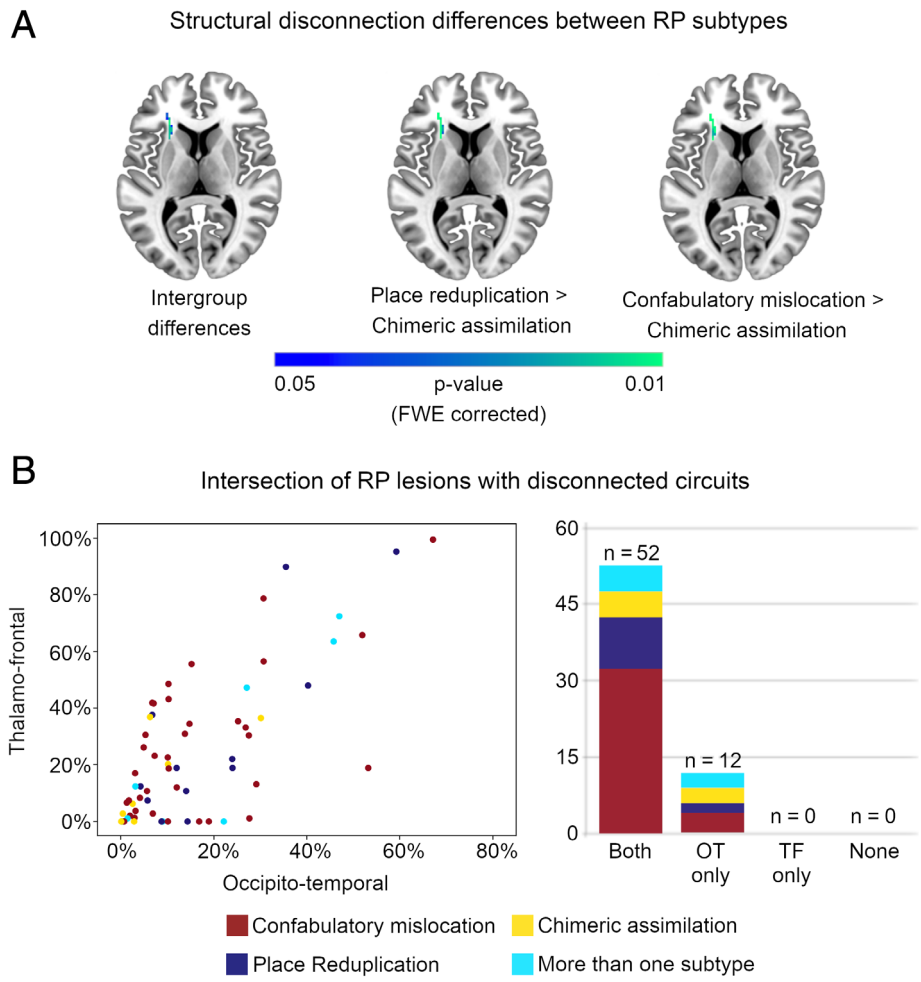

FIGURE 3: (A) Structural disconnection differences between the different subtypes of reduplicative paramnesia; left: intergroup differences; center: structural disconnection more frequent in place reduplication than in chimeric assimilation; and right: structural disconnection more frequent in confabulatory mislocation than in chimeric assimilation. (B) Intersection of reduplicative paramnesia lesions with the disconnected circuits of interest; left: percentage of the right occipitotemporal circuit and of the right thalamo-frontal circuit that are intersected by each lesion; right: number of patients in whom the stroke lesion hit both circuits, the right occipitotemporal circuit only, the right thalamo-frontal circuit only or none of the circuits. FWE = family-wise error; OT = occipitotemporal circuit; RP = reduplicative paramnesia; TF = thalamo-frontal circuit.

cortex with medial temporal structures involved in object-context memory, such as the hippocampus.[50] Furthermore, ventral visual pathways include longer fibers connecting the occipitotemporal cortex with the ventrolateral prefrontal cortex and with the orbitofrontal cortex.[51] We showed that the occipitotemporal stream associated with reduplicative paramnesia overlaps both the right inferior longitudinal fasciculus and the inferior fronto-occipital fasciculus and that the right fusiform gyrus and the right anterior orbitofrontal cortex were among the pairs of regions with the highest difference in structural disconnection between the cases and controls. This anatomic relationship between posterior and anterior regions has important functional implications because perceptual integration is strictly linked with reality monitoring.[52] Such a relationship has been demonstrated in other delusional disorders, namely in schizophrenia.[53]

The ventral visual system is also the main mediator of allocentric spatial representations. Hippocampal cells are well known to fire in specific spatial locations,[54] whereas the parahippocampal cells are activated by objects that are implicitly or explicitly retrieved in decisive points during navigation.[55] The precuneus interacts with this system and seems to be important for updating the representation of objects in space.[56] Defective allocentric positioning is manifested in patients with reduplicative paramnesia by their inability to properly localize themselves and the place where they are in the environment. Conversely, egocentric references seem to be intact in reduplicative paramnesia. Patients are able to correctly describe routes between different places, including routes starting from the place that they are misinterpreting.[49] Egocentric spatial references are processed in the dorsal visual stream,[57] and our data showed that lesion sparing of the right dorsal frontal and parietal regions is an

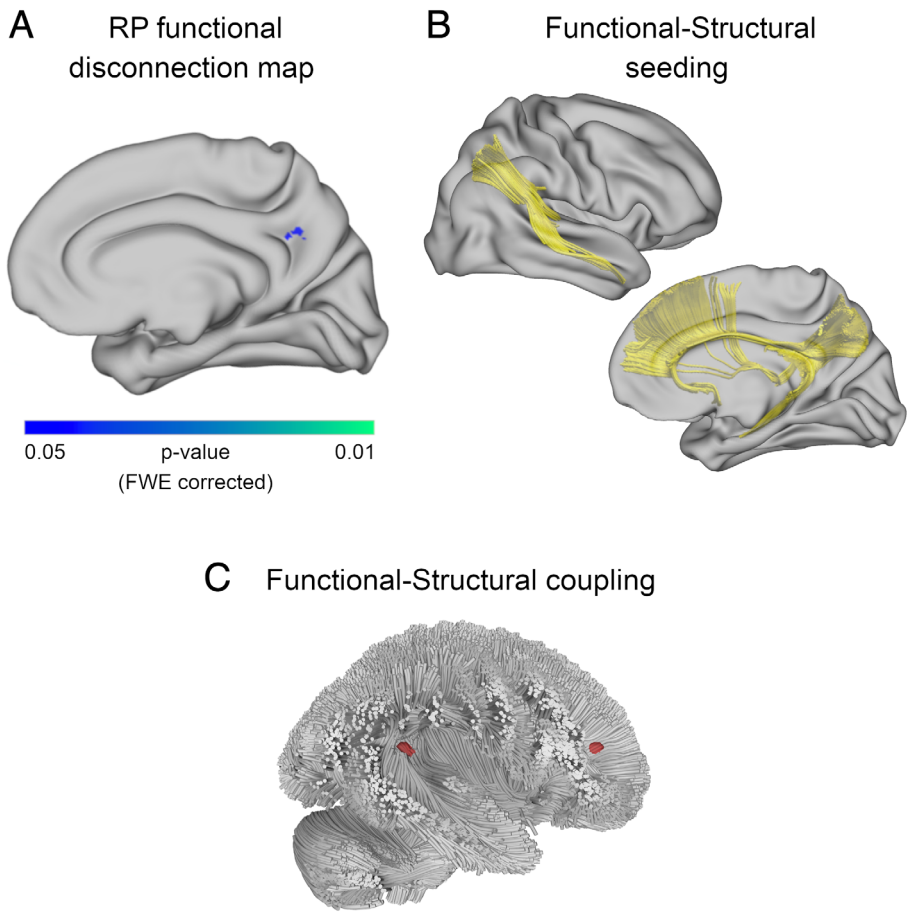

FIGURE 4: Functional disconnection analysis. (A) Statistical map corresponding to the comparison of the positive correlation maps between patients and controls, regressing for confounders, projected on a cortical surface. The mapped area is significantly associated with reduplicative paramnesia. (B) White matter tracts seeding from the significant functional area. (C) Areas of intersection (in red) of the structural connectivity map seeded from areas of significant functional disconnection with the map of significant structural disconnection. FWE = family-wise error; RP = reduplicative paramnesia.

independent predictor of reduplicative paramnesia. The right dorsal frontoparietal network also contributes to the attentional shifts between external stimuli and internal representations, favoring the processing of internally generated mnemonic constructions.[58,59] We hypothesize that injury of this network may preclude the creation of the resilient internal spatial representations that could support the emergence of reduplicative paramnesia.

The pattern of structural disconnection differed between the subtypes of reduplicative paramnesia. We speculate that the stronger association of place reduplication and of confabulatory mislocation with disconnection

TABLE 3. Logistic Model with the Best Classification Performance

Variable	Odds ratio	95% CI	*p* value
Structural disconnection intersecting reduplicative paramnesia structural disconnection map (cm3)	1.26	1.17–1.36	<0.01
Lesion intersecting reduplicative paramnesia lesion spared map (cm3)	0.79	0.68–0.92	<0.01
Age (years)	1.08	1.05–1.12	<0.01
Anosognosia (yes/no)	2.54	1.24–5.19	0.01

CI = confidence interval.

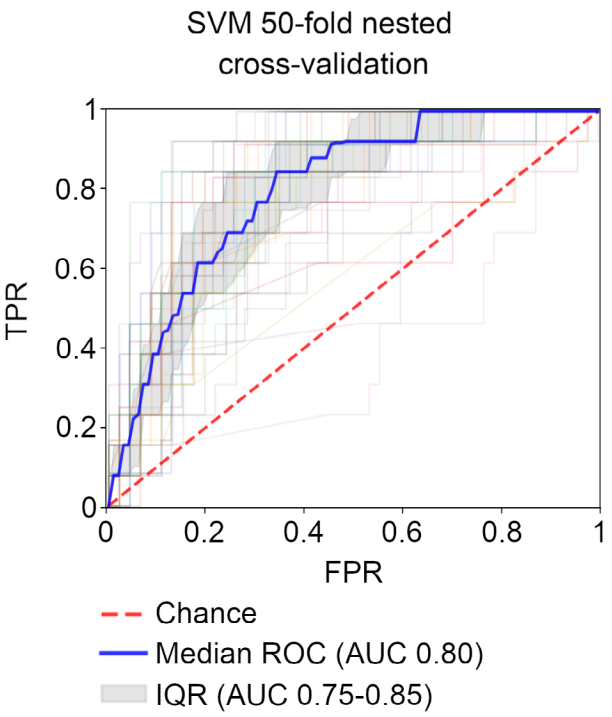

FIGURE 5: Multivariate model ROC curves from the 50-fold nested SVM cross-validation. ROC curves for individual folds are represented by different colors. AUC = area under the curve; FPR = false positive ratio; IQR = interquartile range; ROC = receiver operating characteristic; SVM = support vector machine; TPR = true positive ratio.

of the thalamo-frontal stream might be due to higher limbic dysregulation in these subtypes. In place reduplication, there is a notable loss of familiarity for place, because patients typically believe that they are in a replica rather than in the original place.[9] Conversely, in confabulatory mislocation, there is a resilient increase of familiarity for place, as patients usually misidentify a strange environment as a familiar one.[9] Chimeric assimilation might be more heavily related with a defective interpretation of allocentric spatial references and with dysfunction of the occipitotemporal stream.

In this imbalance of familiarity regulation, patients who undergo a stroke tend to be particularly prone to hyperfamiliarity phenomena. The most frequent place of mislocation in our sample was patients' homes. In addition, hyperfamiliarity misidentifications in other modalities, namely Fregoli syndrome, were more frequent than hypofamiliar delusions, such as Capgras syndrome or somatoparaphrenia. The inverse pattern is observed in other diseases, namely in schizophrenia spectrum disorders.[60]

In addition to neuroimaging variables, age and anosognosia were independent predictors of reduplicative paramnesia. A systematic review of how aging affects spatial navigation showed that allocentric strategies are particularly prone to deterioration.[61] Aging may also increase the risk of deficits in neuropsychological domains associated with reduplicative paramnesia, namely, executive dysfunction, visual memory impairment, and visuospatial deficits. In anosognosia, patients are resistant to demonstrations of their deficits. This shared behavioral feature with reduplicative paramnesia, as well as a common neuroanatomic limbic dysfunction,[62] may justify its predictive significance.

As limitations of our study, brain imaging does not reflect the full extent of brain dysfunction after stroke, and the delimitation of the visible lesion varies according to the modality used.[63] In addition, the results obtained in the thresholded functional connectivity analyses were not corroborated in the unthresholded analysis. The presence of large lesions may have affected the performance of lesion network mapping methodology in our sample.[64] Finally, this study was performed in a tertiary stroke unit and may not be representative of the entire stroke population.

In conclusion, on the basis of a large sample of patients with reduplicative paramnesia, we demonstrated that delusional misidentifications of space occur due to a pattern of disconnection involving fronto-thalamic limbic regions and occipitotemporal ventral visual structures of the right hemisphere. We propose that disruption of this network might explain the abnormal spatial-emotional binding and the defective updating of spatial representations that characterize delusional misidentifications of space.

Acknowledgments

The authors acknowledge our colleagues from the Department of Neurology and from the Language Research Laboratory for their contribution to patient screening. This work received funding from "PRÉMIO JOÃO LOBO ANTUNES" – SCML (grant to P.N.A.), from "Bolsa de InvestigaÇÃo em Doenças Vasculares Cerebrais 2017" – SPAVC (grant to P.N.A.) and from the European Research Council (ERC) under the European Union's Horizon 2020 research and innovation program (grant agreement No. 818521 to M.T.S.). "Data were provided in part by the Human Connectome Project, WU-Minn Consortium (Principal Investigators: David Van Essen and Kamil Ugurbil; 1U54 MH091657) funded by the 16 NIH Institutes and Centers that support the NIH Blueprint for Neuroscience Research; and by the McDonnell Center for Systems Neuroscience at Washington University."

Author Contributions

P.N.A., A.C.F., and I.P.M. contributed to the conception and design of the study. P.N.A., D.P.S., and M.R.A. contributed to the acquisition and analysis

of data. P.N.A., A.C.F., T.P.M., M.T.S., and I.P.M. contributed to drafting a significant portion of the manuscript and figures.

Potential Conflicts of Interest

The authors declared no conflict of interest.

Data availability

The data are not publicly available because the conditions of our ethical approval do not permit the public archiving. The anonymized data necessary for reproducing the results in this article can be requested from the corresponding authors on reasonable request.

References

1. Gooddy W, Reinhold M. Some aspects of human orientation in space I - sensation and movement. Brain 1952;75:472–509.
2. Aguirre GK, D'Esposito M. Topographical disorientation: a synthesis and taxonomy. Brain 1999;122:1613–1628.
3. Burgess N. The 2014 nobel prize in physiology or medicine: a spatial model for cognitive neuroscience. Neuron 2014;84:1120–1125.
4. Pick A. Clinical studies III. On reduplicative paramnesia. Brain 1903; 26:260–267.
5. Politis M, Loane C. Reduplicative paramnesia: a review. Psychopathology 2012;45:337–343.
6. Staton RD, Brumback RA, Wilson H. Reduplicative paramnesia: a disconnection syndrome of memory. Cortex 1982;18:23–35.
7. Ellis HD, Young AW. Accounting for delusional misidentifications. Br J Psychiatry 1990;157:239–248.
8. Ellis HD, Young AW, Quayle AH, De Pauw KW. Reduced autonomic responses to faces in Capgras delusion. Proc R Soc B Biol Sci 1997; 264:1085–1092.
9. Devinsky O. Delusional misidentifications and duplications: right brain lesions, left brain delusions. Neurology 2009;72:80–87.
10. Bartolomeo P, De Vito S, Seidel T. Space-related confabulations after right hemisphere damage. Cortex 2016;87:166–173.
11. Coltheart M. The neuropsychology of delusions. Ann N Y Acad Sci 2010;1191:16–26.
12. Moser DJ, Cohen RA, Malloy P, et al. Reduplicative paramnesia: longitudinal neurobehavioral and neuroimaging analysis. J Geriatr Psychiatry Neurol 1998;11:174–180.
13. Pasquier F, Leys D, Weerts J, et al. Inter and intraobserver reproducibility of cerebral atrophy assessment on MRI scans with hemispheric infarcts. Eur Neurol 1996;36:268–272.
14. Scheltens P, Kuiper M, Ch Wolters E, et al. Atrophy of medial temporal lobes on MRI in "probable" Alzheimer's disease and normal ageing: diagnostic value and neuropsychological correlates. J Neurol Neurosurg Psychiatry 1992;55:967–972.
15. Wahlund LO, Barkhof F, Fazekas F, et al. A new rating scale for age-related white matter changes applicable to MRI and CT. Stroke 2001;32:1318–1322.
16. Harper L, Barkhof F, Fox NC, Schott JM. Using visual rating to diagnose dementia: a critical evaluation of MRI atrophy scales. J Neurol Neurosurg Psychiatry 2015;86:1225–1233.
17. Wahlund LO, Westman E, van Westen D, et al. Imaging biomarkers of dementia: recommended visual rating scales with teaching cases. Insights Imaging 2017;8:79–90.
18. de Haan B, Karnath HO. A hitchhiker's guide to lesion-behaviour mapping. Neuropsychologia 2018;115:5–16.
19. Jenkinson M, Beckmann CF, TEJ B, et al. FSL. Neuroimage 2012;62: 782–790.
20. Winkler AM, Ridgway GR, Webster MA, et al. Permutation inference for the general linear model. Neuroimage 2014;92:381–397.
21. Thiebaut de Schotten M, Foulon C, Nachev P. Brain disconnections link structural connectivity with function and behaviour. Nature Communications. 2020;11(1):5094. http://dx.doi.org/10.1038/s41467-020-18920-9.
22. Herbet G, Duffau H. Revisiting the functional anatomy of the human brain: toward a meta-networking theory of cerebral functions. Physiol Rev 2020;100:1181–1228.
23. Foulon C, Cerliani L, Kinkingnéhun S, et al. Advanced lesion symptom mapping analyses and implementation as BCBtoolkit. Gigascience 2018;7:1–17.
24. Vu AT, Auerbach E, Lenglet C, et al. High resolution whole brain diffusion imaging at 7T for the human connectome project. Neuroimage 2015;122:318–331.
25. Karolis VR, Corbetta M, Thiebaut de Schotten M. The architecture of functional lateralisation and its relationship to callosal connectivity in the human brain. Nat Commun 2019;10:1417–1424.
26. Rolls ET, Huang CC, Lin CP, et al. Automated anatomical labelling atlas 3. Neuroimage 2020;206:116189.
27. Tournier JD, Smith R, Raffelt D, et al. MRtrix3: a fast, flexible and open software framework for medical image processing and visualisation. Neuroimage 2019;202:116137.
28. Suárez L, Markello R, Betzel R, Misic B. Linking structure and function in macroscale brain. Trends Cogn Sci 2020;24:302–315.
29. Boes AD, Prasad S, Liu H, et al. Network localization of neurological symptoms from focal brain lesions. Brain 2015;138:3061–3075.
30. Glasser MF, Sotiropoulos SN, Wilson JA, et al. The minimal preprocessing pipelines for the human connectome project. Neuroimage 2013;80:105–124.
31. Fox MD. Mapping symptoms to brain networks with the human connectome. N Engl J Med 2018;379:2237–2245.
32. Darby RR, Laganiere S, Pascual-Leone A, et al. Finding the imposter: brain connectivity of lesions causing delusional misidentifications. Brain 2017;140:497–507.
33. Fox MD, Buckner RL, White MP, et al. Efficacy of transcranial magnetic stimulation targets for depression is related to intrinsic functional connectivity with the subgenual cingulate. Biol Psychiatry 2012;72:595–603.
34. Cohen AL, Fox MD. Reply: the influence of sample size and arbitrary statistical thresholds in lesion- network mapping. Brain 2020;143: 1–6.
35. Medaglia JD, Huang W, Karuza EA, et al. Functional alignment with anatomical networks is associated with cognitive flexibility. Nat Hum Behav 2018;2:156–164.
36. Wu D, Fan L, Song M, et al. Hierarchy of connectivity-function relationship of the human cortex revealed through predicting activity across functional domains. Cereb Cortex 2020;30:4607–4616.
37. Varoquaux G, Raamana PR, Engemann DA, et al. Assessing and tuning brain decoders: cross-validation, caveats, and guidelines. Neuroimage 2017;145:166–179.
38. Murai T, Toichi M, Sengoku A, et al. Reduplicative paramnesia in patients with focal brain damage. Neuropsychiatry Neuropsychol Behav Neurol 1997;10:190–196.
39. Catani M, Dell'Acqua F, Thiebaut de Schotten M. A revised limbic system model for memory, emotion and behaviour. Neurosci Biobehav Rev 2013;37:1724–1737.

40. Lim SL, Padmala S, Pessoa L. Segregating the significant from the mundane on a moment-to-moment basis via direct and indirect amygdala contributions. Proc Natl Acad Sci U S A 2009;106:16841–16846.

41. Fischer DB, Perez DL, Prasad S, et al. Right inferior longitudinal fasciculus lesions disrupt visual-emotional integration. Soc Cogn Affect Neurosci 2016;11:945–951.

42. Bauer RM. Visual hypoemotionality as a symptom of visual-limbic disconnection in man. Arch Neurol 1982;39:702–708.

43. Ochsner KN, Silvers JA, Buhle JT. Functional imaging studies of emotion regulation: a synthetic review and evolving model of the cognitive control of emotion. Ann N Y Acad Sci 2012;1251:E1–E24.

44. Papez J. A proposed mechanism of emotion. Arch Neurol Psychiatry 1937;258:725–743.

45. Child ND, Benarroch EE. Anterior nucleus of the thalamus: functional organization and clinical implications. Neurology 2013;81:1869–1876.

46. Alves PN, Foulon C, Karolis V, et al. An improved neuroanatomical model of the default-mode network reconciles previous neuroimaging and neuropathological findings. Commun Biol 2019;2:370.

47. Simons JS, Garrison JR, Johnson MK. Brain mechanisms of reality monitoring. Trends Cogn Sci 2017;21:462–473.

48. Vinogradov S, Luks TL, Simpson GV, et al. Brain activation patterns during memory of cognitive agency. Neuroimage 2006;31:896–905.

49. Benson DF, Gardner H, Meadows JC. Reduplicative paramnesia. Neurology 1976;26:147–151.

50. Smith DM, Bulkin DA. The form and function of hippocampal context representations. Neurosci Biobehav Rev 2014;40:52–61.

51. Borra E, Gerbella M, Rozzi S, Luppino G. Anatomical evidence for the involvement of the macaque ventrolateral prefrontal area 12r in controlling goal-directed actions. J Neurosci 2011;31:12351–12363.

52. Mesulam M. Representation, inference, and transcendent encoding in neurocognitive networks of the human brain. Ann Neurol 2008;64:367–378.

53. Fletcher PC, Frith CD. Perceiving is believing: a Bayesian approach to explaining the positive symptoms of schizophrenia. Nat Rev Neurosci 2009;10:48–58.

54. Ekstrom AD, Kahana MJ, Caplan JB, et al. Cellular networks underlying human spatial navigation. Nature 2003;425:184–188.

55. Janzen G, Van Turennout M. Selective neural representation of objects rellevant for navigation. Nat Neurosci 2004;7:673–677.

56. Wolbers T, Hegarty M, Büchel C, Loomis JM. Spatial updating: how the brain keeps track of changing object locations during observer motion. Nat Neurosci 2008;11:1223–1230.

57. Kravitz DJ, Saleem KS, Baker CI, Mishkin M. A new neural framework for visuospatial processing. Nat Rev Neurosci 2011;12:217–230.

58. Wagner AD, Shannon BJ, Kahn I, Buckner RL. Parietal lobe contributions to episodic memory retrieval. Trends Cogn Sci 2005;9:445–453.

59. Lückmann HC, Jacobs HIL, Sack AT. The cross-functional role of frontoparietal regions in cognition: internal attention as the overarching mechanism. Prog Neurobiol 2014;116:66–86.

60. Kirov G, Jones P, Lewis SW. Prevalence of delusional misidentification syndromes. Psychopathology 1994;27:148–149.

61. Colombo D, Serino S, Tuena C, et al. Egocentric and allocentric spatial reference frames in aging: a systematic review. Neurosci Biobehav Rev 2017;80:605–621.

62. Pacella V, Foulon C, Jenkinson PM, et al. Anosognosia for hemiplegia as a tripartite disconnection syndrome. Elife 2019;8:1–13.

63. Hillis AE, Barker PB, Beauchamp NJ, et al. MR perfusion imaging reveals regions of hypoperfusion associated with aphasia and neglect. Neurology 2000;55:782–788.

64. Boes AD. Lesion network mapping: where do we go from here? Brain 2020;144:1–4.

COMMUNICATIONS BIOLOGY

ARTICLE

https://doi.org/10.1038/s42003-019-0611-3 OPEN

An improved neuroanatomical model of the default-mode network reconciles previous neuroimaging and neuropathological findings

Pedro Nascimento Alves[1,2,3,4*], Chris Foulon[1,2,5], Vyacheslav Karolis[1,2,6], Danilo Bzdok[7,8,9,10], Daniel S. Margulies[1,2], Emmanuelle Volle[1,2] & Michel Thiebaut de Schotten[1,2,11,12*]

The brain is constituted of multiple networks of functionally correlated brain areas, out of which the default-mode network (DMN) is the largest. Most existing research into the DMN has taken a corticocentric approach. Despite its resemblance with the unitary model of the limbic system, the contribution of subcortical structures to the DMN may be under-appreciated. Here, we propose a more comprehensive neuroanatomical model of the DMN including subcortical structures such as the basal forebrain, cholinergic nuclei, anterior and mediodorsal thalamic nuclei. Additionally, tractography of diffusion-weighted imaging was employed to explore the structural connectivity, which revealed that the thalamus and basal forebrain are of central importance for the functioning of the DMN. The contribution of these neurochemically diverse brain nuclei reconciles previous neuroimaging with neuropathological findings in diseased brains and offers the potential for identifying a conserved homologue of the DMN in other mammalian species.

[1] Brain Connectivity and Behaviour Laboratory, BCBlab, Sorbonne Universities, Paris, France. [2] Frontlab, Institut du Cerveau et de la Moelle épinière (ICM), UPMC UMRS 1127, Inserm U 1127, CNRS UMR 7225 Paris, France. [3] Department of Neurosciences and Mental Health, Neurology, Hospital de Santa Maria, CHULN, Lisbon, Portugal. [4] Language Research Laboratory, Faculty of Medicine, Universidade de Lisboa, Lisbon, Portugal. [5] Computational Neuroimaging Laboratory, Department of Diagnostic Medicine, The University of Texas at Austin Dell Medical School, Austin, TX, USA. [6] FMRIB centre, John Radcliffe Hospital, University of Oxford, Oxford, UK. [7] INRIA, Parietal Team, Saclay, France. [8] Neurospin, CEA, Gif-sur-Yvette, France. [9] Department of Psychiatry, Psychotherapy and Psychosomatics, RWTH Aachen University, Aachen, Germany. [10] JARA-BRAIN, Jülich-Aachen Research Alliance, Jülich, Germany. [11] Centre de Neuroimagerie de Recherche CENIR, Groupe Hospitalier Pitié-Salpêtrière, Paris, France. [12] Groupe d'Imagerie Neurofonctionnelle, Institut des Maladies Neurodégénératives-UMR 5293, CNRS, CEA University of Bordeaux, Bordeaux, France. *email: pedronascimentoalves@gmail.com; michel.thiebaut@gmail.com

In 1979, for the first time to our knowledge, David Ingvar used Xenon clearance to investigate resting wakefulness[1]. When aligned by scalp and skull markers, the 11 brains examined indicated an evident increase of the blood flow levels in the frontal lobe interpreted as a surrogate for undirected, spontaneous, conscious mental activity. Later, positron emission tomography (PET) was used to map more systematically task-related activation in the brain, often with resting wakefulness as a control task. The contrast between task-related and resting wakefulness led to the description of deactivation (i.e., active at rest more than during the task) in a set of regions, including retrosplenial cortex, inferior parietal cortex, dorsolateral frontal cortex inferior frontal cortex, left inferior temporal gyrus, medial frontal regions and amygdala[2,3] that quickly bore the name of default-mode network (DMN)[4]. In these studies, skull landmarks or structural magnetic resonance imaging (MRI) were used to align PET images in Talairach stereotaxic or in Montreal Neurological Institute (MNI) templates[2,3]. The advent of functional magnetic resonance imaging (fMRI), particularly of methods for analysing functional connectivity, led to the allocation of new structures to this network, such as the hippocampal formation[5–7].

Today, the DMN has largely been a cortically defined set of network nodes. Consisting of distinct regions/nodes distributed across the ventromedial and lateral prefrontal, posteromedial and inferior parietal, as well as the lateral and medial temporal cortex, the DMN is considered a backbone of cortical integration[8–11]. Its subcortical components are, however, less well characterised. Studies of whole-brain network organisation reveal subregions of the cerebellum[12,13] and striatum[14] that are functionally connected with the cortical regions of the DMN. Seed-based functional connectivity studies further demonstrate additional DMN-specific connectivity to several subcortical structures, including the amygdala[15,16] and striatum[17]. The thalamus has also been shown to be structurally and functionally connected to DMN regions[18,19]. These studies are important, as a cleaner characterisation of the anatomy of the DMN is an essential step towards understanding its functional role and its involvement in brain diseases. Particularly, an increased activity characterises the regions that compose DMN during tasks involving autobiographical, episodic and semantic memory, mind wandering, perspective-taking or future thinking[20,21]; Bendetowicz et al.[22]. Conversely, DMN regions show a decreased neural activity during attention-demanding and externally oriented tasks[21,23]. Finally, altered connectivity in the DMN has been observed in a large variety of brain diseases, including Alzheimer's disease, Parkinson's disease, schizophrenia, depression, temporal lobe epilepsy, attention deficit and hyperactivity disorder, drug addiction, among others[24–29]. Hence, while prior research provides first hints towards a broader definition of the DMN system, further research is necessary to articulate the anatomical extent of specific subcortical contributions, and to understand the independent contribution of these structures in DMN function and pathologies.

Yet, since the DMN has repeatedly been characterised as a cohesive functional network[5], an average of brain images relying exclusively on anatomical references and landmarks may be suboptimal[30,31] whether the method employed is a surface-based or volume-based registration[30,32]. Small structures of the brain may be particularly susceptible to this misalignment, especially when MRI lacks contrast. Besides morphology, cytoarchitecture and function are poorly overlapping, especially in the DMN[33,34]. Consequently, functional areas present in every subject may not overlap after averaging all structurally aligned brain images in a group analysis[30,35]. This biological misalignment can be particularly problematic for revealing significant small regions of the DMN (Fig. 1). A better alignment is also essential for the subcortical structures of the brain, as their variability is still considerable[36–39]. Specifically, cytoarchitectonic studies have shown that only one-quarter of the volume of cholinergic nuclei overlaps in at least half of the individuals studied[39]. Similarly, structures such as mammillary bodies, nucleus basalis of Meynert, or anterior thalamic nuclei can vary in size, morphology and locations, and are particularly prone to misalignment with the current methods of structural registration[32,40–42]. Functional alignment methods have already been used to overcome the high interindividual variability of the morphology of some areas of the heteromodal association cortex and led to a more accurate mapping of resting-state functional connectivity[43–45]. They also have led to better predictions of task activation patterns in group analysis when compared with morphological alignment methods and have recently enabled much improved models of cortical parcellation[43,46].

To address several of these challenges that may impede proper group analysis if relying exclusively on MRI structural landmarks, we propose to revisit the anatomical scaffold of the DMN using a coregistration based on functional alignment. We hypothesised that using a functional alignment will reveal structures of basal forebrain and the Papez's circuits, namely anterior and mediodorsal thalamic nuclei and mammillary bodies, as constituent nodes of the DMN for several reasons. First, all these regions are highly interconnected which suggest they belong to the same functional system[47,48]. Second, the current conceptualisation of DMN anatomy resembles the unitary model of the limbic system which, through the coordination of its subregions, subserves the elaboration of emotion, memories and behaviour[49–52]. Third, the basal forebrain comprises a group of neurochemically diverse nuclei, involved in dopaminergic, cholinergic and serotoninergic pathways, that are crucial in the pathophysiology of the aforementioned diseases that affect the DMN connectivity. Finally, recent electrophysiological evidence has shown that in rats the basal forebrain exhibits the same pattern of gamma oscillations than DMN and that it influences the activity of the anterior cingulate cortex[53].

Therefore, in this study, we used a functional alignment of resting-state functional MRI (rs-*f*MRI)-based individual DMN maps to build a more comprehensive DMN model that includes the contribution of subcortical structures. To provide a complete window into the anatomy of the DMN, we explored the structural connectivity of our new model of the DMN using tractography imaging techniques and revealed that the thalamus and basal forebrain had high importance in term of values of node degree and centrality for the DMN.

Results

Comparison between structural and functional alignment. DMN connectivity maps obtained from structural and functional alignmentsare displayed in Fig. 2a–c. In both maps, classical areas of the DMN were observed, namely: posterior cingulate cortex and retrosplenial cortex; ventromedial, anteromedial and dorsal prefrontal cortex; temporal pole; middle temporal gyrus; hippocampus and parahippocampal cortex; amygdala and the posterior parietal cortex.

Figure 2d illustrates the simple voxel-based subtraction between the DMN connectivity maps obtained from structural and functional alignments. Higher average connectivity was achieved in the functionally aligned DMN map in large areas, such as the medial prefrontal cortex and posterior cingulate cortex, mostly in the border zones. In fact, the highest differences in connectivity between structural and functional aligned DMN were at the level of the basal forebrain and thalamus. These areas were poorly or even not represented with alignment in the

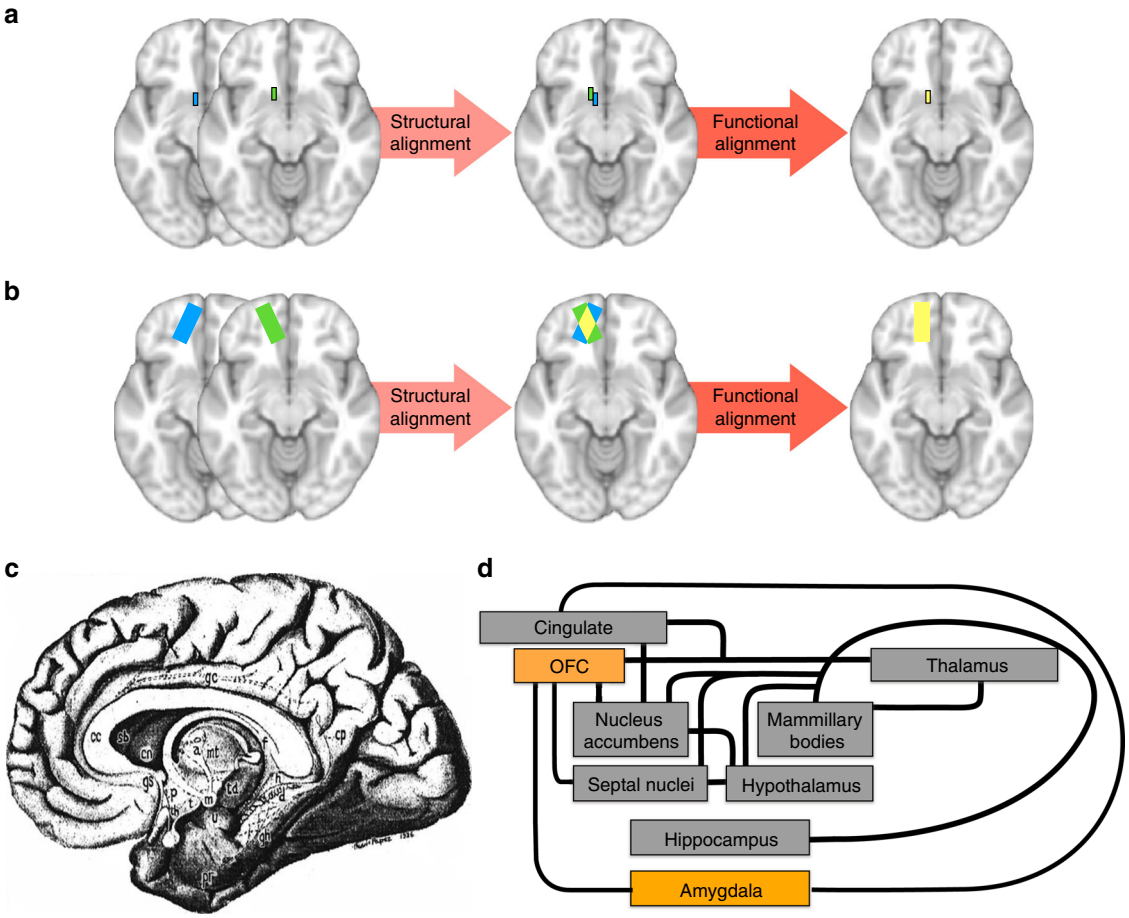

Fig. 1 Illustration of intersubject alignment of brain images and unitary model of the limbic system. Blue and green rectangles represent the same functional area in two subjects, while yellow rectangles illustrate the overlap of the two individual areas after alignment. With structural alignment, there can be a complete misalignment of small functional areas (**a**) or partial misalignment of large functional areas (**b**) due to functional–anatomical variability or poor anatomical contrasts in MRI imaging. If an additional step of functional alignment is performed, an optimised overlap of functional areas is obtained. **c** The limbic system as originally depicted by Papez[52] and (**d**) diagram of the unitary model of the limbic system[49–51,165–168]

MNI152 space, but were visible after the functional alignment. DMN connectivity was also visible in the medial mesencephalic region, as well in inferior regions in the caudate nuclei, ventrolateral prefrontal cortex, cerebellar tonsils and cerebellar hemispheres. As expected, a difference was found between the two maps bilaterally in the thalamus and in the basal forebrain, and in a peripheral zone of the left mammillary body (Fig. 2e, Table 1). Unthresholded statistical maps of the comparison between the two methods of alignment—structurally and functionally aligned DMN—are available at neurovault.org (https://neurovault.org/collections/OCAMCQFK/). Two representative cases of individual maps in the MNI152 space and in the functional space are presented in the Supplementary Fig. 1.

Functional connectivity of the DMN in the functional space. Twenty-four regions of interest were defined based on the DMN we obtained in the functional space and concordant with the previous anatomical models of the DMN[5,8]. Nine additional regions were defined as being solely revealed after the functional alignment. These regions included the left and right thalamus, the left and right basal forebrain, the midbrain, the left and right ventral lateral prefrontal cortex (VLPFC) and the left and right caudate nucleus (inferior regions of the nuclei), resulting in a total of 33 regions of interest (Supplementary Fig. 2). The association strength determined by Pearson's correlation between the rs-*f*MRI time series of the regions of interest (i.e., functional connectivity) were higher with alignment in the functional space, compared with structural space, in all pairs of regions (Fig. 3a). The difference was statistically significant in 18% of pairs after Bonferroni correction for multiple comparisons (p-value < 0.0001). Table 2 represents the MNI coordinates of the centres of gravity of all the regions of interest in the DMN map. The alternative correlation matrices using cortical DMN areas according to Gordon et al.[54] are presented in the Supplementary Fig. 3.

Regarding the hypothesised areas, the left basal forebrain demonstrated higher correlations with the right antero-median prefrontal cortex, the right posterior parietal cortex and the midbrain area, while the right basal forebrain had higher correlations with the right temporal pole and with the left cerebellar hemisphere (Supplementary Data 1). The left thalamus had higher correlations with the left parahippocampal region, the left temporal pole, the right and the left antero-median prefrontal cortex, the left and the right ventrolateral prefrontal cortex and the right posterior parietal cortex, while the right thalamus had higher correlations with the right and the left antero-median prefrontal cortex, with the left temporal pole and with the left cerebellar tonsil (Supplementary Data 1). No significant difference was found for partial correlations. Tables presenting the median, range and interquartile range of partial correlations between all regions of interests, the statistical comparison of

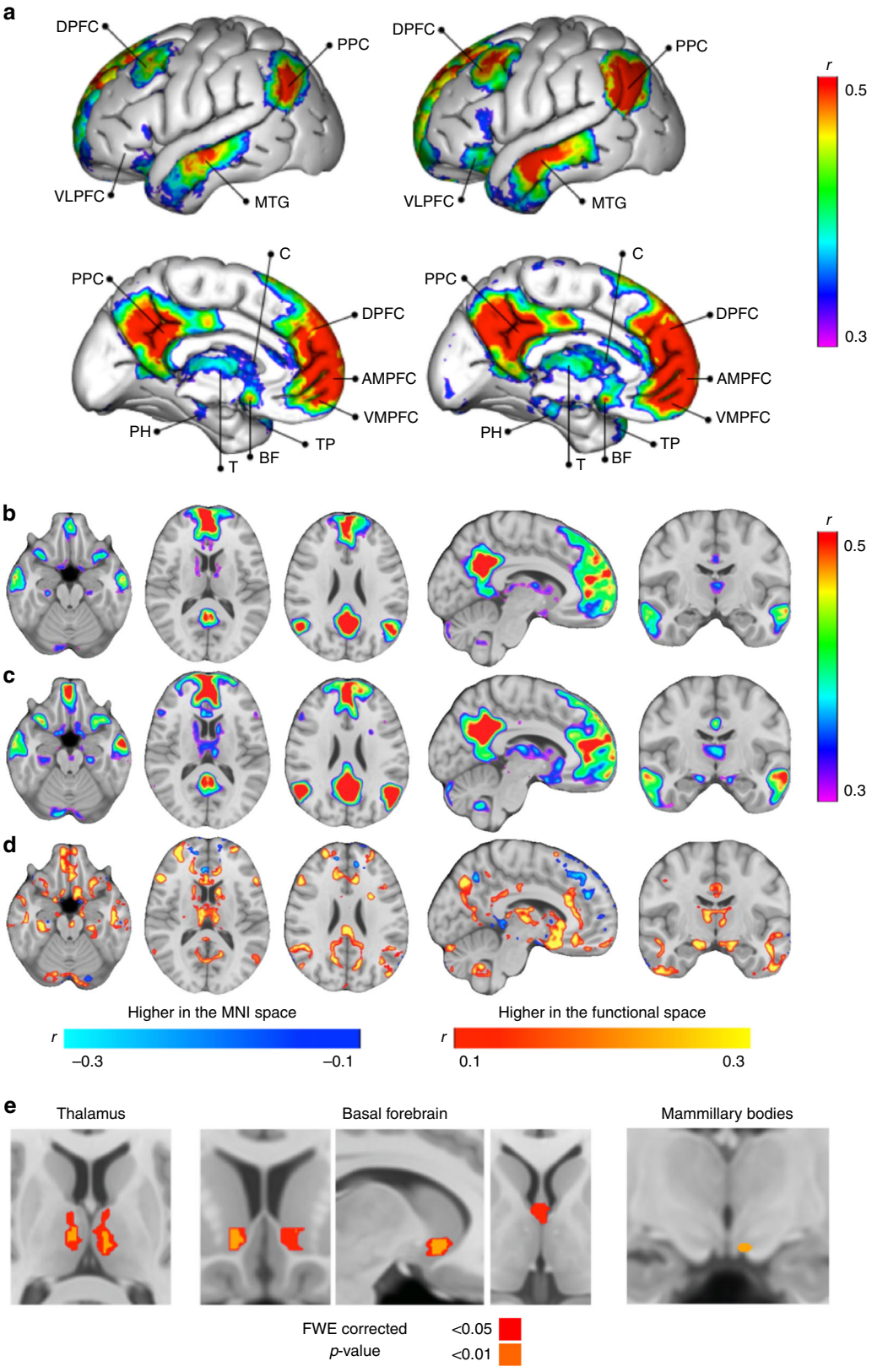

partial correlations between the two methods of alignment and the partial correlations of two representative cases are also shown in the Supplementary Data 2, 3, 4 and 5, respectively.

Anatomical validation in thalamic, basal forebrain and mesencephalic areas. Figure 4 illustrates the intersection of the new DMN map after its translation to the MNI group space using individual inverse transformation matrices specific for each individual. All subjects' DMN spatially overlapped with the templates of the left anterior thalamic nucleus, mediodorsal thalamic nuclei, medial septal nuclei and left nucleus accumbens (Table 3)[39,55–58]. The number of subjects with an intersection

Fig. 2 Maps of the DMN structurally or functionally aligned. **a** 3D view of the two DMN left panel corresponds to the structural space alignment, right panel to the functional space alignment, **b** brain sections of the structurally aligned DMN, **c** brain sections of the functionally aligned DMN, **d** subtraction of the structurally and the functionally aligned DMN maps, **e** statistical comparison (paired *t* test) between the two methods of alignment —structurally and functionally aligned DMN—in the three hypothesised regions, with colours indicating statistically significant differences at two levels of significance: <0.05 and <0.01, family-wise error (FWE) corrected *p*-values (higher in the functional space). DPFC dorsal prefrontal cortex, PPC posterior parietal cortex, VLPFC ventrolateral prefrontal cortex, MTG middle temporal gyrus, PCC posterior cingulate cortex, C caudate, DPFC dorsal prefrontal cortex, AMPFC antero-median prefrontal cortex, VMPFC ventro-median prefrontal cortex, TP temporal pole, BF basal forebrain, T thalamus, PH parahippocampal. $n = 20$ participants

Table 1 Clusters of the statistical maps obtained when comparing the two methods of alignment (*t* test)

Cluster index	Voxels	*p*-value	Effect size	MNI (*X*)	MNI (*Y*)	MNI (*Z*)
Right nucleus accumbens	43	0.001	0.839	9	13	−7
Left nucleus accumbens	21	0.007	0.721	−9	16	−6
Medial septal nuclei	38	0.007	0.721	0	−1	1
Right limbic thalamus	72	0.001	0.839	8	−12	9
Left limbic thalamus	146	<0.001	0.879	−7	−14	8
Left mammillary bodies	3	0.001	0.839	−5	−11	−14

Coordinates represent the centre of gravity and '*p*-value' of the lowest value found in the cluster

with the right anterior thalamic nucleus, right nucleus accumbens and ventral tegmental area was also very high (95, 95 and 90%, respectively), while the intersection with the other basal forebrain nuclei occurred in approximately half of the subjects, possibly due to their very small size. Maps of the mean and standard deviation Pearson's correlation of the new DMN map after registration to the MNI space are available in the Supplementary Figs. 4 and 5, respectively.

Tractography. We explored the structural connectivity of our new model of the DMN using tractography imaging techniques. The regions of interest were the same used for functional connectivity analysis (Supplementary Fig. 2). Figure 5 represents the structural connectivity of the network.

The results indicated that both anterior and posterior portions of the cingulum, as well as inferior longitudinal fasciculus, the second branch of the superior longitudinal fasciculus, the posterior segment of arcuate fasciculus, the uncinate fasciculus and some fibres of the frontal orbito-polar tract (Fig. 5, upper panel) connected the different nodes of the DMN. In addition, the anatomical connectivity of the basal forebrain and the thalamus with other regions of interest included: the anterior thalamic projections, connecting thalamus with medial prefrontal cortex; the cingulum, connecting basal forebrain with medial prefrontal cortex and posterior cingulate cortex; the fornix, connecting basal forebrain (specifically the region correspondent to the medial septal nuclei) to the hippocampus and fibres connecting basal forebrain and thalamus, some of the most medial possibly corresponding to the bundle of Vicq D'Azyr (Fig. 5, lower panel). Statistical maps of the tractography analysis are presented in the Supplementary Fig. 6.

Graph theory analysis. Figure 6 represents the analysis of the DMN structural network with a graph theory approach using the 33 regions of interest defined from the DMN in the functional space.

The results indicate that high degrees and high betweenness centrality in the network were obtained for the basal forebrain and thalamic regions, alongside the medial prefrontal cortex and the posterior cingulate–retrosplenial cortex, as well as in regions which were previously considered as hubs in the DMN.

More precisely, the [maximum–minimum] range of distribution of node degrees was [12–1] and the median [interquartile range] was 5 [8–2]. The node degrees of the left and right thalamus were 9 and 7, and of the left and right basal forebrain were 8 and 7, respectively (Supplementary Table 1). Therefore, thalamus and basal forebrain are among the structures in the network that have connections with a high number of nodes. For betweenness centrality, the [maximum–minimum] range of distribution was [0.104–0] and the median [interquartile range] was 0.004 [0.03–0.001]. The betweenness centrality of the left and right thalamus was 0.03, and of the left and right basal forebrain were 0.03 and 0.02, respectively (Supplementary Table 1). Hence, thalamus and basal forebrain make part of a high fraction of shortest paths in the network, that is, the shortest connections between two nodes.

A table showing the values for node degree and betweenness centrality at the individual level in two representative cases is shown in the Supplementary Table 2.

Discussion

In this study, we revisited the constituent elements of the DMN using an optimised method of coregistration in a functional space, besides the conventional structural alignment. Three main findings emerge from this research in healthy humans. First, higher functional connectivity correlation and sharper anatomical details were achieved when registering the DMN maps in a functional space. Second, we confirmed the hypothesis that structures of basal forebrain and anterior and mediodorsal thalamic nuclei belong to the DMN. Lastly, we characterised in detail the structural connectivity underlying functional connectivity. Based on these findings, we provided a more comprehensive neurobiological model of the DMN that bridges the gap between local differences in subcortical structures and global differences in the DMN reported in clinical studies.

The difference between alignment in the functional space and the structural space was characterised by an increase in the connectivity strength across the brain, as well as in many subcortical areas, classically not considered to be constituent nodes of the DMN. As previously reported, this confirmed that registration in the functional space provides a more accurate interindividual anatomical description and is recommended when doing functional connectivity analyses[43,44].

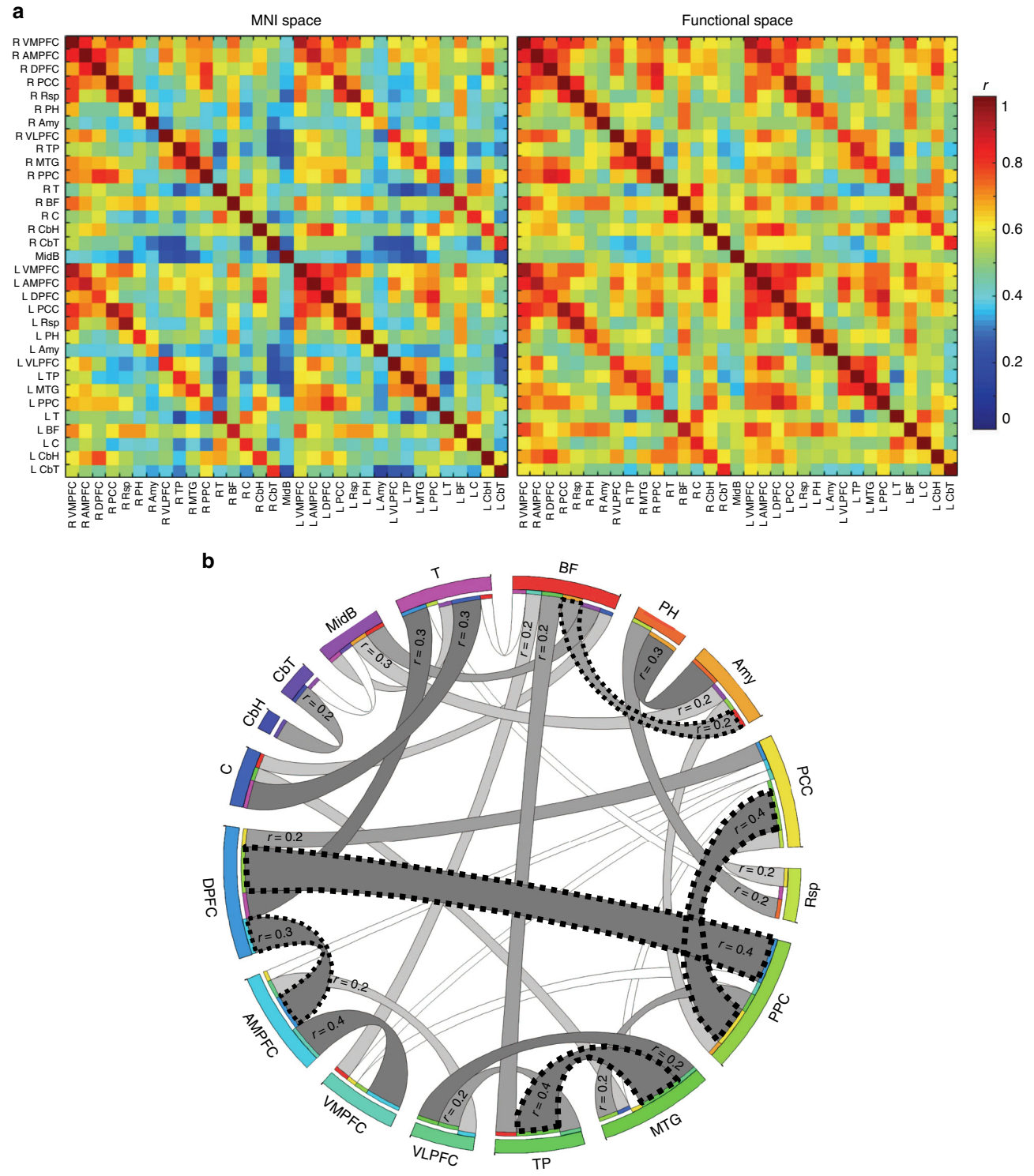

Fig. 3 Functional connectivity. **a** Matrices of the Pearson's correlations between rs-*f*MRI time series of the regions of interest in the structural and in the functional space. **b** Graph representation of the partial correlations between regions of interest in the functional space (connections with partial correlation above 0.2 are depicted; darker grey tones represent stronger connections). Statistically significant partial correlations have a dashed borderline (one-sample *t* test; $p < 0.0001$, which corresponds to the Bonferroni corrected level of significance). The left side structures are not represented, for a clearer visualisation. DPFC dorsal prefrontal cortex, PPC posterior parietal cortex, VLPFC ventrolateral prefrontal cortex, Rsp retrosplenial cortex, MTG middle temporal gyrus, PCC posterior cingulate cortex, C caudate, DPFC dorsal prefrontal cortex, AMPFC antero-median prefrontal cortex, VMPFC ventro-median prefrontal cortex, TP temporal pole, BF basal forebrain, T thalamus, PH parahippocampal region, CbH cerebellar hemisphere, CbT cerebellar tonsil, Amy amygdala, MidB midbrain. $n = 20$ participants

Table 2 Regions of interest

Region of interest	Voxels	MNI (*X*)	MNI (*Y*)	MNI (*Z*)
Left ventro-median prefrontal cortex	2267	−11	55	−5
Right ventro-median prefrontal cortex	2673	11	53	−6
Left antero-median prefrontal cortex	2243	−10	50	20
Right antero-median prefrontal cortex	2144	10	50	19
Left dorsal prefrontal cortex	3818	−20	31	46
Right dorsal prefrontal cortex	3084	23	32	46
Left posterior cingulate cortex	2484	−5	−50	35
Right posterior cingulate cortex	2224	7	−51	34
Left retrosplenial cortex	845	−6	−55	12
Right retrosplenial cortex	638	6	−54	13
Left posterior parietal cortex	2448	−46	−64	33
Right posterior parietal cortex	1733	50	−59	34
Left middle temporal gyrus	2406	−58	−21	−15
Right middle temporal gyrus	2170	59	−17	−18
Left temporal pole	348	−38	17	−34
Right temporal pole	318	43	15	−35
Left ventrolateral cortex	706	−36	23	−16
Right ventrolateral cortex	487	37	25	−16
Left parahippocampal region	355	−24	−30	−16
Right parahippocampal region	287	26	−26	−18
Left amygdala	66	−15	−9	−18
Right amygdala	58	17	−8	−16
Left caudate	303	−11	12	7
Right caudate	266	13	11	9
Left cerebellar hemisphere	906	−26	−82	−33
Right cerebellar hemisphere	1500	29	−79	−34
Left cerebellar tonsil	184	−6	−57	−45
Right cerebellar tonsil	278	8	−53	−48
Left thalamus	382	−7	−14	8
Right thalamus	305	7	−11	8
Left basal forebrain	456	−7	12	−12
Right basal forebrain	351	7	9	−12
Midbrain	65	−1	−22	−21

MNI coordinates represent the centre of gravity of each region

The maps of the DMN registered in the functional space revealed previously underappreciated parts of this network, such as basal forebrain and anterior and mediodorsal thalamic nuclei. Tractography analysis yielded structural connectivity of these new DMN regions to the other regions of the network. Mainly, the cingulum connected the basal forebrain with the medial prefrontal cortex, posterior cingulate region, retrosplenial cortex and hippocampus and parahippocampal regions[59,60]. The fornix linked basal forebrain, specifically the medial septal nuclei, with the hippocampus and parahippocampal regions[49,61,62]. The anterior thalamic projections connected the thalamus with medial and ventrolateral prefrontal regions[63] and finally some of the most medial fibres connecting the basal forebrain with the thalamus, probably corresponded to the mammillothalamic tract of Vicq D'Azyr[64,65]. The graph theory approach[66] applied to the measures of structural connectivity revealed a high node degree of the basal forebrain and the thalamus in the network, as well as high betweenness centrality[67]. These results indicate that basal forebrain and thalamus have high centrality within the network, and therefore can have an important role for network integration and resilience[66–68], along with the classically defined hubs, such as the medial prefrontal region as well as posterior cingulate and retrosplenial region[69].

The involvement of basal forebrain and anterior and mediodorsal thalamus in the DMN has theoretical and functional repercussions beyond the purely anatomical level. The involvement of the anterior and mediodorsal thalamic nuclei as well as the basal forebrain are concordant with the role of the DMN in memory processes[8,70], as all these regions are relays of the unitary model of the limbic system[49–51]. Previous reports of engagement of the mediodorsal thalamic nucleus and the DMN during memory tasks and the memory deficits provoked by lesions of the anterior and the mediodorsal thalamic nuclei also support this claim[71–74]. At a neurochemical level, the basal forebrain is also a principal actor in the production of acetylcholine[75]. Acetylcholine has a physiological and a neuropharmacological effect on memory processes. For instance, cholinergic system mediates rhythmic oscillation in the hippocampus that facilitates encoding[39,76]. The basal forebrain also contains GABAergic and glutamatergic neurons that mediate hippocampal theta synchronisation through an indirect septo-hippocampal pathway[77]. By providing evidence of the involvement of medial septal cholinergic nucleus and its structural connection to the hippocampus in our DMN model, the present work indicates a match between connectivity, neurochemistry and cognition.

The same correspondence between connectivity, neurochemistry and cognition applies to the relation between DMN and emotional modulation[78–83]. The nucleus accumbens is a central output for the dopaminergic projections and is involved in emotion regulation and affect integration[84,85]. The nucleus accumbens also receives glutamatergic inputs from the hippocampus and the prefrontal cortex[86] belonging to the DMN. Surprisingly, our analysis also revealed the ventral tegmental area, which is also a dopaminergic nucleus with projections to the nucleus accumbens and the medial prefrontal cortex[87]. This association with the mesolimbic dopaminergic pathway is reinforced by our results of functional connectivity, since ventromedial prefrontal cortex and midbrain were among the structures with highest partial correlations with basal forebrain. Hence, combining present and previous findings, we speculate that the DMN, as defined by functional connectivity, might have a putative role in the integration of cholinergic and dopaminergic systems dedicated to memory and emotion.

The new DMN's subcortical structures identified in the current work have cognitive and neurochemical roles that open a new window to the understanding of distinct brain pathologies affecting DMN connectivity (Table 4). Indeed, functional connectivity in each area of the DMN is an estimate of the global coherence of the DMN. Since we demonstrated that limbic thalamus and basal forebrain are nodes with high degree and high centrality in the DMN, damage in these structures should lead to a drastic decrease of functional connectivity in the whole DMN[88]. For instance, Alzheimer's disease is associated with degeneration of the cholinergic system, including the medial septal nuclei, even in the earliest clinical stages of Mild Cognitive Impairment[89] and apparently related to decreased functional coherence and deactivation in hub regions of DMN[90,91]. The high centrality of the basal forebrain in the DMN network may explain this early link between DMN and Alzheimer's disease. In schizophrenia, also associated with decreased DMN connectivity and activation[92,93], neuropathological evidence suggests an abnormal glutamatergic–dopaminergic interaction at the level of nucleus accumbens[94]. In addition, the ventral tegmental area is connected to the nucleus accumbens through the mesolimbic system, the classical dopaminergic pathway associated with schizophrenia, and functional data show a decrease of connectivity between VTA and several brain regions, including the thalamus, in unmedicated schizophrenic patients[95]. The pathophysiology of others diseases, such as drug addiction, depression, temporal lobe epilepsy and

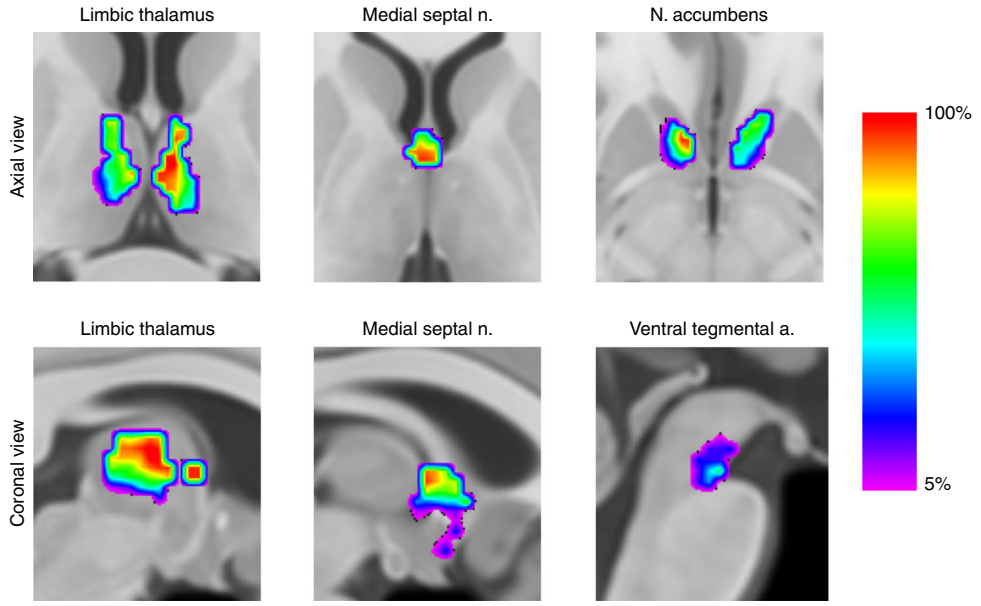

Fig. 4 Density maps of the functionally aligned individual DMN networks superimposed in the MNI152 space. Colour bar represents the percentage of individuals with a significant correlation in each voxel. This map is freely available at https://neurovault.org/collections/CTTXXAYJ/. $n = 20$ participants

Table 3 Proportion of individual DMN maps intersecting, average proportion of the intersection and average volume of the intersection for each nucleus

Nuclei	Percentage of individual DMN maps intersecting the nuclei	Percentage of nuclei volume intersected—median [IQR]	Absolute volume of intersection—median [IQR]
L middle septal nuclei	100%	22% [15–29]	248 mm^3 [169–327]
R middle septal nuclei	100%	26% [21–30]	291 mm^3 [235–336]
L mediodorsal thalamic	100%	64% [53–77]	696 mm^3 [577–838]
R mediodorsal thalamic	100%	33% [11–42]	401 mm^3 [134–511]
L anterior thalamic	100%	80% [75–88]	160 mm^3 [150–176]
R anterior thalamic	95%	62% [28–60]	193 mm^3 [87–187]
L nucleus accumbens	100%	51% [15–84]	367 mm^3 [108–605]
R nucleus accumbens	95%	49% [33–58]	333 mm^3 [224–394]
Ventral Tegmental Area	90%	17% [6–24]	48 mm^3 [17–67]
L mammillary body	50%	2% [0–9]	4 mm^3 [0–17]
L Meynert nucleus	40%	0% [0–1]	0 mm^3[0–22]
R Meynert nucleus	45%	0% [0–4]	0 mm^3 [0–97]

IQR interquartile range, *L* left, *R* right

attention-deficit and hyperactivity disorder involve modifications in the nucleus accumbens, medial septal nuclei or the thalamic nuclei that connect limbic regions as well as dysfunctional connectivity of the DMN (specified in Table 4[27,96–103]). Hence, the involvement of the basal forebrain and the thalamic nuclei in the DMN appears to bridge the gap between the subcortical anatomical differences and the global differences in the DMN previously reported.

Our results is also concordant with recent findings. For instance, Kernbach et al. recently demonstrated that grey matter variability across the DMN can well predict population variation in the microstructural properties of core white matter tracts of the limbic system—the anterior thalamic radiation and the fornix in 10,000 people[9]. As another example, Margulies et al. studied functional gradients along cortical surface and found that DMN areas were at the opposite end of primary motor/sensory areas in a spectrum of connectivity differentiation and that DMN areas exhibit the most considerable geodesic distance at the cortical level, being equidistant to the unimodal cortical areas[11]. These investigators suggested that the DMN acts as a neural relay for transmodal information. We speculate that the thalamus and basal forebrain may follow the same model at a subcortical level, integrating functional networks related to primary functions and brainstem inputs to the associative areas[104,105].

Interestingly, the thalamus and the basal forebrain are phylogenetically older than many cortical structures, and especially those that compose the DMN[106–108]. The inclusion of these structures in the anatomical model of the DMN can open a window to the exploration of DMN in other mammalian species as well[109–112]. The medial thalamus has already been shown to be part of the mouse's DMN[113], as found in rs-*f*MRI studies[114–116]. Our results are also concordant with recent neurophysiological evidence in rats about the influence of basal forebrain in the regulation of the DMN[53]. Namely, it has been shown that gamma-band local field potentials in the basal forebrain exerts influence on one of the hub regions of rat's DMN, the anterior cingulate cortex[53]. The cellular basis for the association of these two areas has been characterised with retrograde tracing studies[117,118]. In humans, it has been demonstrated that basal forebrain has a major functional coupling with the anterior cingulate cortex and with ventromedial prefrontal cortex[119]. We speculate that the putative differences in the basal forebrain

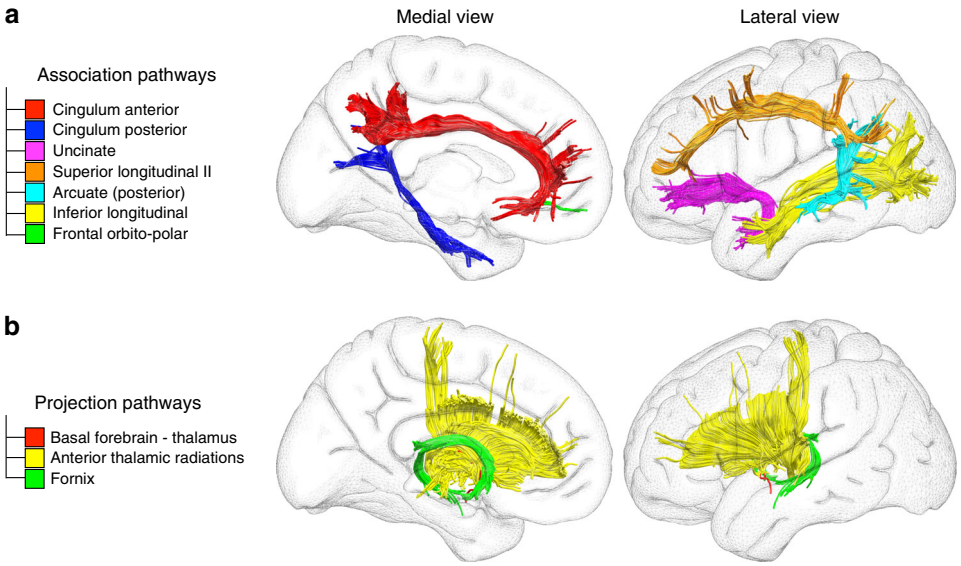

Fig. 5 Structural connections supporting the DMN. **a** corresponds to the association pathways connecting the cortical regions of the DMN. **b** illustrates the projection pathways mediating the connections between subcortical and cortical regions of the DMN

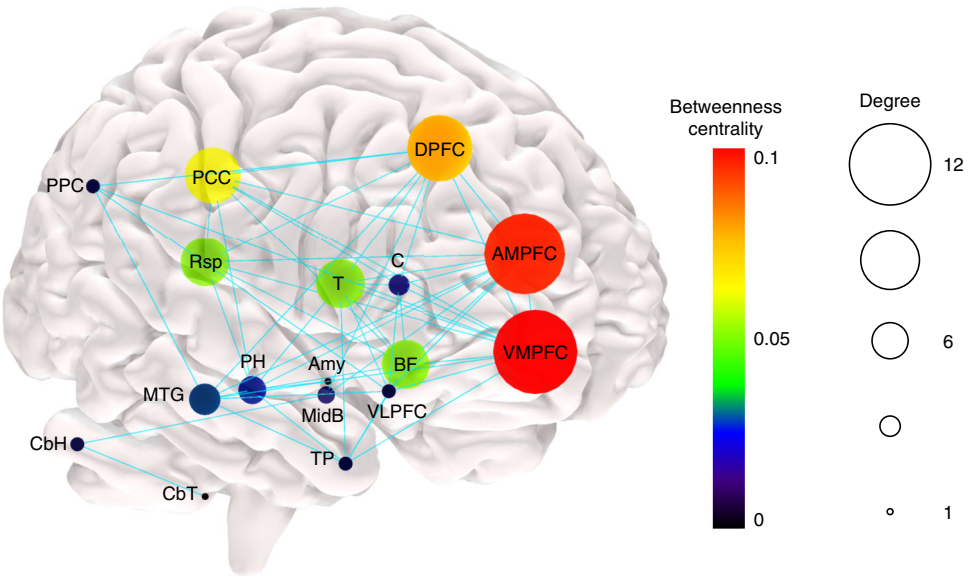

Fig. 6 Graph theory analysis of structural connectivity. The node size represents node degree and the node colour illustrates node betweenness centrality. The edges denote presence of structural connection. DPFC dorsal prefrontal cortex, PPC posterior parietal cortex, VLPFC ventrolateral prefrontal cortex, Rsp retrosplenial cortex, MTG middle temporal gyrus, PCC posterior cingulate cortex, C caudate, DPFC dorsal prefrontal cortex, AMPFC antero-median prefrontal cortex, VMPFC ventro-median prefrontal cortex, TP temporal pole, BF basal forebrain, T thalamus, PH parahippocampal region, CbH cerebellar hemisphere, CbT cerebellar tonsil, Amy amygdala, MidB midbrain. $n = 20$ participants

projections may be one explanation for the more diffuse DMN activation at the midline level in rats when compared with humans[112].

One limitation of this work is that the overlap between the DMN map and the nuclei studied is based on comparison with templates or variability maps, and not with the individual location of the nucleus in the explored subjects. The limited capacity of structural MRI to differentiate these small nuclei does not allow such comparison. Besides, the reverse transformation of the DMN from the functional space to the MNI space may not be exact, due to inherent limitations of inverse transformations. Although these limitations may decrease the accuracy of the intersection quantification with discrete nuclei, they did not alter the apparent overlap with basal forebrain and with the thalamus. Furthermore, demonstrating that the additional step of functional alignment results in higher correlation values is somewhat circular. However, our purpose was to demonstrate that this increase in correlation revealed subcortical structures that were previously neglected in the literature. The intra-individual functional connectivity variation across time may also be a source of bias[35]. However, this factor and the lack of uniformity regarding the optimal functional alignment method have not precluded the achievement of higher accurate results in previous studies[43–46]. Finally, tractography analyses can produce inaccurate results[120,121]. In order to avoid these caveats, we employed methods that have previously demonstrated high anatomical reliability when compared with axonal tracing and with post-mortem dissections[59,122–124].

Table 4 Pathophysiological associations of the subcortical structures of DMN

Disease associated with DMN dysfunction	Pathophysiological associations with subcortical DMN	References
Alzheimer's disease	Degeneration of cholinergic system (including medial septal nuclei), even in MCI stage	89
	Dysfunction of limbic thalamus in early stages of the disease	169
	Decreased functional coherence and deactivation in hub regions of DMN	90,91
Schizophrenia	Abnormalities in glutamatergic–dopaminergic interaction in the nucleus accumbens	94
	Decreased functional connectivity between the ventral tegmental area and thalamus	95
	Decreased connectivity and activation of hub regions of DMN	92,93
TLE	Dysfunctional increase in the hippocampus-mediodorsal thalamus connectivity	97
	Stimulation of anterior thalamic nucleus is efficacious in treatment of TLE	170,171
	Enlargement of medial septal nuclei in TLE	96
	Decreased functional connectivity between the hippocampus and DMN	27
Depression	Resting activity of the thalamus predicts response to anti-depressant medication	102
	Nucleus accumbens mediates response to stress and to anti-depressant medication	100

MCI mild cognitive impairment, *TLE* temporal lobe epilepsy

In conclusion, this work demonstrates that the registration of individual DMN maps in a functional space improves the definition of the anatomy of DMN by including additional structures, such as the thalamus and basal forebrain. Future research should focus on the cascade of neurochemical and pathophysiological events that follow small subcortical lesions of the DMN.

Methods

The local ethics committee (Comité de Protection des Personnes "CPP Ile de France V") approved the experiment, and all participants provided written informed consent.

Subjects and MRI acquisition. MRI images of subjects without neurological or psychiatric disease were obtained (age mean ± SD 29 ± 6 years, range 22–42 years; 11 females, 9 males) with a Siemens 3 Tesla Prisma system equipped with a 64-channel head coil.

An axial 3D T1-weighted imaging data set covering the whole head was acquired for each participant (286 slices, voxel resolution = 0.7 mm^3, echo time (TE) = 2.17 ms, repetition time (TR) = 2400 ms, flip angle = 9°).

rs-*f*MRI images were obtained using T2*-weighted echo-planar imaging (EPI) with blood oxygenation level-dependent (BOLD) contrast. EPIs (TR/TE = 2050/25 ms) comprised 42 axial slices acquired with a multiband pulse[125–128] covering the entire cerebrum (voxel size = 3 mm^3) including 290 brain scan volumes in one run of 10 min.

A diffusion-weighted imaging (DWI) acquisition sequence, fully optimised for tractography, provided isotropic (1.7 × 1.7 × 1.7 mm) resolution and coverage of the whole head with a posterior–anterior phase of acquisition, with an echo time (TE) = 75 ms. A repetition time (TR) equivalent to 3500 ms was used. At each slice location, six images were acquired with no diffusion gradient applied (*b*-value of 0 s mm^{-2}). In addition, 60 diffusion-weighted images were acquired, in which gradient directions were uniformly distributed on the hemisphere with electrostatic repulsion. The diffusion weighting was equal to a *b*-value of 2000 s mm^{-2}. This sequence was fully repeated with reversed phase-encode blips. This provides us with two data sets with distortions going in opposite directions. From these pairs, the susceptibility-induced off-resonance field was estimated using a method similar to that described in ref. [129] and corrected on the whole diffusion-weighted data set using the tool TOPUP and EDDY as implemented in FSL[130].

rs-*f*MRI analysis—overview. rs-*f*MRI images were corrected for artefacts in the Funcon-Preprocessing tool of the Brain Connectivity and Behaviour toolkit (http://toolkit.bcblab.com[131–133]). Then, they were registered to T1 high-resolution individual structural images and normalised to MNI152 standard space using Advanced Normalization Tools (ANTS; http://stnava.github.io/ANTs;[134,135]). Preprocessing steps in details:

a. *f*MRI images were first motion corrected using MCFLIRT[132], then corrected for slice timing, smoothed with a full half-width maximum equal to 1.5 times the largest voxel dimension and finally filtered for low temporal frequencies using a Gaussian-weighted local fit to a straight line. These steps are available in FEAT, as part of FSL package[133].
b. *f*MRI images were linearly registered to the T1 images, and subsequently to the MNI152 template (2 mm) using affine and diffeomorphic transformations[136,137]. Confounding signals were discarded from *f*MRI by regressing out a confound matrix from the functional data. The confound matrix included the estimated motion parameters obtained from the previously performed motion correction, the first eigenvariate of the white matter and cerebrospinal fluid, as well as their first derivative. Eigenvariates were extracted using fslmeants combined with the–eig option. White matter and cerebrospinal fluid eigenvariates were extracted using masks based on the T1-derived 3-classes segmentation thresholded to a probability value of 0.9, registered to the rs-*f*MRI images and binarised. Finally, the first derivative of the motion parameters, white matter and cerebrospinal fluid signal were calculated by linear convolution between their time course and a [−1 0 1] vector.
c. Since the rs-*f*MRI signal can be heavily affected by motion, even following motion correction between temporally adjacent volumes[138], we estimated the signal fluctuation associated with motion and regressed it out from the *f*MRI. To this aim, we employed a recently developed and validated procedure based on data-driven Independent Component Analysis (ICA), termed ICA-Aroma[139]. This method performs an ICA decomposition of the data and estimates which components reflect motion-related noise in the *f*MRI signal on the basis of a robust set of spatial and temporal features. This is made possible due the distinctiveness of the motion-related components isolated by ICA on the fMRI signal[140]. This approach outperforms other methods such as the regression of the motion parameter estimates, while limiting in the same time the loss in degrees of freedom[139]. Compared with spike removal methods such as scrubbing[141], ICA-Aroma has the advantage of preserving the temporal structure of the fMRI signal.

Individual DMN maps in the structural space. Individual subject-tailored/fitted DMN maps were obtained by correlation with seed regions of interest of a functional parcellated brain template. The regions used for the seed-based functional connectivity analysis were those defined as DMN regions in the resting-state parcellation map by Gordon et al.[54,142,143]. Gordon et al. created these parcellations according to abrupt changes in resting-state's time course profile, each parcel having a homogenous time course profile. This general-purpose atlas provides a total of 40 DMN nodes (20 in each hemisphere). The DMN nodes as defined by Gordon et al. are available in the Supplementary Fig. 7 and Supplementary Table 3, respectively). These 40 regions were used as seeds. The correlation map for each seed was obtained using the Funcon-Connectivity tool of the Brain Connectivity and Behaviour toolkit (http://toolkit.bcblab.com;[131]). This tool calculates the Pearson's correlation between the mean rs-*f*MRI time course of the seed with the rest of the brain to generate the functional connectivity map for every seed[131].

The DMN map of each participant was obtained by calculating the median of the 40 seed-based correlation maps of each individual using FSL[144]. We then calculated the median across the DMN maps of the 20 participants to obtain the median DMN map in the MNI152 space. The median was used, instead of the mean, because it is less sensitive to outliers, being a better centrality measure for small sample sizes[145].

Individual DMN maps in the functional space. To achieve the proposed optimised map of the DMN, the same 20 individual maps were functionally aligned with each other in a new functional space using the following steps:

Individual DMN maps were aligned with each other using ANTs' script buildtemplateparallel.sh, defining cross-correlation as the similarity measure and greedy SyN as the transformation model[136,137,146]. This approach consists in an iterative ($n = 4$) diffeomorphic transformation to a common space. The group map was obtained by calculating the median of all DMN maps after functional alignment.

The resulting maps correspond to alignment of the 20 individual DMN maps in a functional space (Fig. 2).

Functional connectivity comparison of the two DMN. We applied a 0.3 threshold on the functional connectivity strength for both the functional and structural-based DMN maps. This value was chosen because it corresponds to a medium effect size[147]. Time series of rs-*f*MRI of each individual in the different regions of interest identified in the DMN maps were extracted and the mean value of the voxels of each region was obtained, using the command fslstats (with the options –k and –M)[144]. Cortical regions of interest were defined according to the previous anatomical models of the DMN[5,8]. Subcortical regions of interest were defined manually based on the experienced judgement of the neuroanatomists among the authors combined with the careful comparison with previously published atlases[148,149]. Correlation and partial correlation coefficients were determined as measures of functional connectivity.

Two matrices, representing the median correlation values in the MNI152 space and in the functional space, were created using BrainNet Viewer[150]. A paired *t* test was calculated for each cell of the two connectivity matrices using Python's Scipy package, version 0.19.1 (https://www.scipy.org; scipy.stats.ttest_rel). A *p*-value corrected for multiple comparisons at a threshold of <0.0001 (Bonferroni correction) was used. Circos software was used to illustrate functional connections in the functional space (http://circos.ca;[151]).

Two alternative correlation matrices using cortical DMN areas according to Gordon et al.[54], instead of the ones defined in classical anatomical models of Andrews-Hanna et al.[8] and Buckner et al.[5], were calculated.

Anatomical validation in thalamic, basal forebrain and mesencephalic areas. Meynert nuclei, medial septal nuclei and diagonal band of Broca probabilistic maps were derived from the work of Zaborszky et al., the Harvard-Oxford probabilistic atlas was employed for the nucleus accumbens, Talairach atlas registered to the MNI152 space for mammillary bodies and thalamic nuclei, and Harvard Ascending Arousal Network Atlas for ventral tegmental area[39,55–58]. A percentage of volume overlap between the DMN map and each nucleus of interest was subsequently calculated for each subject. The same Pearson's correlation threshold of 0.3 was applied for this analysis, as specified in 2.2.3.

Tractography analysis. Diffusion-Weighted Images were corrected for signal drift[152], motion and eddy current artefacts using ExploreDTI (http://www.exploredti.com;[153]).

Whole-brain tractography was performed on the software StarTrack using a deterministic approach (https://www.mr-startrack.com). A damped Richardson–Lucy algorithm was applied for spherical deconvolutions[154]. A fixed fibre response corresponding to a shape factor of $\alpha = 1.5 \times 10.3\ mm^2/s$ was adopted. The defined number of iterations was 150, and the geometric damping parameter was 8. The absolute threshold was defined as three times the spherical fibre orientation distribution (FOD) of a grey matter isotropic voxel and the relative threshold as 8% of the maximum amplitude of the FOD[155]. A modified Euler algorithm was used[123]. An angle threshold of 35°, a step size of 0.85 mm and a minimum length of 20 mm were chosen.

Diffusion tensor images were registered to the MNI152 standard space and, then, into the functional space applying the affine and diffeomorphic deformation generated in the previous sections, using the tool tractmath as part of the software package Tract Querier[156].

The same regions of interest used for functional connectivity calculation (section 2.2.3) were also used for the tractography analysis.

The command tckedit of MRtrix toolbox (http://www.mrtrix.org/[157]) was used to extract the tracts of interest. The –include arguments were composed by combinations of DMN regions of interest to guarantee that the selected streamlines crossed at least two DMN regions of interest.

In order to have a group-representative map for each tract, individual tracts were converted into maps using tckmap command of MRtrix toolbox (http://www.mrtrix.org;[158]). Each voxel was binarised in 1 or 0 according to being or not being intersected by a streamline[159]. Lastly, a one-sample *t* test was calculated using FSL randomise, with variance smoothing of 4 mm[159]. The resulting group-representative tract maps using this method were shown to have a good anatomical correspondence with histological atlas of white matter tracts[159,160]. BrainVisa was used to create the corresponding illustration of the tracts that reached significance[161].

Graph theory analysis of structural connectivity. To explore whether the new putative regions of the DMN are essential structures and potential areas of vulnerability in the network, we investigated the hub properties of the network nodes using graph theory measures, namely node degree and betweenness centrality[66]. Node degree refers to the number of connections between a given node and the other nodes of the network. Betweenness centrality is the fraction of all shortest paths in the network that pass through a given node[66].

For each participant, an anatomical connectome matrix of the DMN was built using the tck2connectome command of MRtrix (http://www.mrtrix.org;[157]). Each region of interest was defined as a node. Only the streamlines that ended in both regions of interest were considered[162,163]. The matrices were binarised depending on the existence or absence of streamlines connecting two regions of interest[162,163]. The defined threshold for the binarisation was 1 because the number of streamlines does not reflect the connectivity strength or the true number of axonal projections between two brain regions[163,164], and previous evidence has shown that changing the streamline count threshold for binarisation (between 1 and 5) does not change the overall results of the network analysis. Brain Connectivity Toolbox for Python (https://pypi.python.org/pypi/bctpy) was used to obtain the network measures. The functions degrees_und and betweenness_bin were run, respectively, for each individual matrix[67]. The median values for each measure were obtained. The illustration of the network was made using Surf Ice (https://www.nitrc.org/projects/surfice/).

Statistics and reproducibility. In order to assess reproducibility, the effects of interest were also measured at the individual level (i.e., replicated for every subject).

Reporting summary. Further information on research design is available in the Nature Research Reporting Summary linked to this article.

Data availability

The raw data used for this research are available on demand from the corresponding authors pedroascimentoalves@gmail.com and michel.thiebaut@gmail.com. The data for the statistical comparisons presented in the paper are available in Supplementary Data 1–5. Unthresholded statistical maps of the comparison between the two methods of alignment—structurally and functionally aligned DMN—are available at neurovault.org (https://neurovault.org/collections/OCAMCQFK/).

Received: 24 January 2019; Accepted: 16 September 2019;
Published online: 10 October 2019

References

1. Ingvar, D. H. "Hyperfrontal" distribution of the cerebral grey matter flow in resting wakefulness; on the functional anatomy of the conscious state. *Acta Neurol. Scand.* **60**, 12–25 (1979).
2. Mazoyer, B. et al. Cortical networks for working memory and executive functions sustain the conscious resting state in man. *Brain Res Bull.* **54**, 287–298 (2001).
3. Shulman, G. et al. Top-down modulation of early sensory cortex. *Cereb. cortex* **7**, 193–206 (1997a).
4. Raichle, M. E. et al. A default mode of brain function. *Proc. Natl Acad. Sci. USA* **98**, 676–682 (2001).
5. Buckner, R. L., Andrews-Hanna, J. R. & Schacter, D. L. The brain's default network: anatomy, function, and relevance to disease. *Ann. N. Y. Acad. Sci.* **1124**, 1–38 (2008).
6. Greicius, M. D., Srivastava, G., Reiss, A. L. & Menon, V. Default-mode network activity distinguishes Alzheimer' s disease from healthy aging: evidence from functional MRI. *Proc. Natl Acad. Sci. USA* **101**, 4637–4642 (2004).
7. Vincent, J. L. et al. Coherent spontaneous activity identifies a hippocampal-parietal memory network. *J. Neurophysiol.* **96**, 3517–3531 (2006).
8. Andrews-Hanna, J. R., Reidler, J. S., Sepulcre, J., Poulin, R. & Buckner, R. L. Functional-anatomic fractionation of the brain's default network. *Neuron* **65**, 550–562 (2010).
9. Kernbach, J. M. et al. Subspecialization within default mode nodes characterized in 10, 000 UK Biobank participants. *Proc. Natl Acad. Sci. USA* **115**, 12295–12300 (2018).
10. Lopez-Persem, A., Verhagen, L., Amiez, C., Petrides, M. & Sallet, J. The human ventro medial prefrontal cortex sulcal morphology and its influence on its functional organization. *bioRxiv* 1–36, https://doi.org/10.1101/417824 (2018).
11. Margulies, D. S. et al. Situating the default-mode network along a principal gradient of macroscale cortical organization. *Proc. Natl Acad. Sci. USA* **113**, 12574–12579 (2016).
12. Buckner, R. L., Krienen, F. M., Castellanos, A., Diaz, J. C. & Yeo, B. T. T. The organization of the human cerebellum estimated by intrinsic functional connectivity. *J. Neurophysiol.* **106**, 2322–2345 (2011).
13. Stoodley, C. J. & Schmahmann, J. D. NeuroImage Functional topography in the human cerebellum: a meta-analysis of neuroimaging studies. *Neuroimage* **44**, 489–501 (2009).
14. Choi, E. Y., Yeo, B. T. T. & Buckner, R. L. The organization of the human striatum estimated by intrinsic functional connectivity. *J. Neurophysiol.* **108**, 2242–2263 (2012).
15. Bzdok, D., Laird, A. R., Zilles, K. & Fox, P. T. An investigation of the structural, connectional, and functional subspecialization in the human amygdala. *Hum. Brain Mapp.* **34**, 3247–3266 (2012).
16. Roy, A. K. et al. Functional connectivity of the human amygdala using resting state fMRI. *Neuroimage* **45**, 614–626 (2009).

17. Di Martino, A. et al. Functional connectivity of human striatum: a resting state fMRI study. *Cereb. Cortex* **18**, 2735–2747 (2008).
18. Cunningham, S. I., Tomasi, D. & Volkow, N. D. Structural and functional connectivity of the precuneus and thalamus to the default mode network. *Hum. Brain Mapp.* **38**, 938–956 (2016).
19. Fransson, P. Spontaneous low-frequency BOLD signal fluctuations: an fMRI investigation of the resting-state default mode of brain function hypothesis. *Hum. Brain Mapp.* **26**, 15–29 (2005).
20. Shapira-Lichter, I., Oren, N., Jacob, Y., Gruberger, M. & Hendler, T. Portraying the unique contribution of the default mode network to internally driven mnemonic processes. *Proc. Natl Acad. Sci. USA* **110**, 4950–4955 (2013).
21. Shulman, G. et al. Common blood flow changes across visual tasks: II. Decreases in cerebral cortex. *J. Cogn. Neurosci.* **9**, 648–663 (1997b).
22. Bendetowicz, D. et al. Two critical brain networks for generation and combination of remote associations. *Brain* **141**, 217–233 (2018).
23. Spreng, R. N., Mar, R. A. & Kim, A. S. N. The Common neural basis of autobiographical memory, prospection, navigation, theory of mind, and the default mode: a quantitative meta-analysis. *J. Cogn. Neurosci.* **21**, 489–510 (2009).
24. Broyd, S. J. et al. Default-mode brain dysfunction in mental disorders: a systematic review. *Neurosci. Biobehav. Rev.* **33**, 279–296 (2009).
25. Geng, X. et al. Salience and default mode network dysregulation in chronic cocaine users predict treatment outcome. *Brain* **140**, 1513–1524 (2017).
26. Tessitore, A. et al. Default-mode network connectivity in cognitively unimpaired patients with Parkinson disease. *Neurology* **79**, 2226–2232 (2012).
27. Voets, N. L. et al. Structural substrates for resting network disruption in temporal lobe epilepsy. *Brain* **135**, 2350–2357 (2012).
28. Whitfield-Gabrieli, S. & Ford, J. M. Default mode network activity and connectivity in psychopathology. *Annu Rev. Clin. Psychol.* **8**, 49–76 (2012).
29. Zhu, X., Zhu, Q., Shen, H., Liao, W. & Yuan, F. Rumination and default mode network subsystems connectivity in first-episode, drug-naive young patients with major depressive disorder. *Sci. Rep.* **7**, 43105 (2017).
30. Brett, M., Johnsrude, I. S. & Owen, A. M. The problem of functional localization in the human brain. *Nat. Rev. Neurosci.* **3**, 243–249 (2002).
31. Thiebaut de Schotten, M. & Shallice, T. Identical, similar or different? Is a single brain model sufficient? *Cortex* **86**, 172–175 (2017).
32. Despotovic, I., Goossens, B. & Philips, W. MRI segmentation of the human brain: challenges, methods, and applications. *Comput Math. Methods Med.* **2015**, 1–23 (2015).
33. Bzdok, D. et al. Subspecialization in the human posterior medial cortex. *Neuroimage* **106**, 55–71 (2015).
34. Eickhoff, S. B., Laird, A. R., Fox, P. T., Bzdok, D. & Hensel, L. Functional segregation of the human dorsomedial prefrontal cortex. *Cereb. Cortex* **26**, 304–321 (2016).
35. Braga, R. M. & Buckner, R. L. Parallel interdigitated distributed networks within the individual estimated by intrinsic functional connectivity. *Neuron* **95**, 457–471.e5 (2017).
36. Amunts, K. et al. Cytoarchitectonic mapping of the human amygdala, hippocampal region and entorhinal cortex: Intersubject variability and probability maps. *Anat. Embryol. (Berl.).* **210**, 343–352 (2005).
37. Amunts, K. et al. Broca's region revisited: cytoarchitecture and intersubject variability. *J. Comp. Neurol.* **412**, 319–341 (1999).
38. Croxson, P.L., Forkel, S.J., Cerliani, L. & Thiebaut de Schotten, M. Structural variability across the primate brain: a cross-species comparison. *Cereb. Cortex* 1–13. https://doi.org/10.1093/cercor/bhx244 (2017).
39. Zaborszky, L. et al. Stereotaxic probabilistic maps of the magnocellular cell groups in human basal forebrain. *Neuroimage* **42**, 1127–1141 (2008).
40. Liu, A. K. L., Chang, R. C. C., Pearce, R. K. B. & Gentleman, S. M. Nucleus basalis of Meynert revisited: anatomy, history and differential involvement in Alzheimer's and Parkinson's disease. *Acta Neuropathol.* **129**, 527–540 (2015).
41. Möttönen, T. et al. Defining the anterior nucleus of the thalamus (ANT) as a deep brain stimulation target in refractory epilepsy: delineation using 3 T MRI and intraoperative microelectrode recording. *NeuroImage Clin.* **7**, 823–829 (2015).
42. Tagliamonte, M., Sestieri, C., Romani, G. L., Gallucci, M. & Caulo, M. MRI anatomical variants of mammillary bodies. *Brain Struct. Funct.* **220**, 85–90 (2013).
43. Langs, G., Golland, P. & Ghosh, S. Predicting activation across individuals with resting-state functional connectivity based multi-atlas label fusion. *Med. Image Comput. Comput. Assist. Inter.* **9350**, 313–320 (2015).
44. Mueller, S. et al. Individual variability in functional connectivity architecture of the human brain. *Neuron* **77**, 586–595 (2013).
45. Robinson, E. C. et al. MSM: a new flexible framework for multimodal surface matching. *Neuroimage* **100**, 414–426 (2014).
46. Glasser, M. F. et al. A multi-modal parcellation of human cerebral cortex. *Nature* **536**, 171–178 (2016).
47. Yakovlev, P. I. Motility, behaviour and the brain: stereodynamic organization and neural correlates of behaviour. *J. Nerve Men. Dis.* **107**, 313–335 (1948).
48. Yakovlev, P. I. & Locke, S. Limbic nuclei of thalamus and connections of limbic cortex III. Corticocortical connections of the anterior cingulate gyrus, the cingulum, and the subcallosal bundle in monkey. *Arch. Neurol.* **5**, 364–400 (1961).
49. Catani, M., Dell'Acqua, F. & Thiebaut de Schotten, M. A revised limbic system model for memory, emotion and behaviour. *Neurosci. Biobehav. Rev.* **37**, 1724–1737 (2013).
50. MacLean, P. Some psychiatric implications of physiological studies on frontotemporal portion of limbic system (Visceral brain). *Electroencephalogr. Clin. Neurophysiol.* **4**, 407–418 (1952).
51. MacLean, P. Psychosomatic disease and the "visceral brain." Recent developments bearing on the Papez theory of emotion. *Psychosom. Med.* **11**, 338–353 (1949).
52. Papez, J. A proposed mechanism of emotion. *Arch. Neurol. Psychiatry* **258**, 725–743 (1937).
53. Nair, J. et al. Basal forebrain contributes to default mode network regulation. *Proc. Natl Acad. Sci. USA* **2018**, 201712431 (2018).
54. Gordon, E. M. et al. Generation and evaluation of a cortical area parcellation from resting-state correlations. *Cereb. Cortex* **26**, 288–303 (2016).
55. Desikan, R. S. et al. An automated labeling system for subdividing the human cerebral cortex on MRI scans into gyral based regions of interest. *Neuroimage* **31**, 968–980 (2006).
56. Edlow, B. L. et al. Neuroanatomic connectivity of the human ascending arousal system critical to consciousness and its disorders. *J. Neuropathol. Exp. Neurol.* **71**, 531–546 (2012).
57. Lancaster, J. L. et al. Bias between MNI and talairach coordinates analyzed using the ICBM-152 brain template. *Hum. Brain Mapp.* **28**, 1194–1205 (2007).
58. Talairach, J. & Tournoux, P. *Co-planar Stereotaxic Atlas of the Human Brain.* (Thieme, New York, 1988).
59. Catani, M. et al. Short frontal lobe connections of the human brain. *Cortex* **48**, 273–291 (2012).
60. Catani, M., Howard, R. J., Pajevic, S. & Jones, D. K. Virtual in vivo interactive dissection of white matter fasciculi in the human brain. *Neuroimage* **17**, 77–94 (2002).
61. Aggleton, J. *The Amygdala: A Functional Analysis*. 2nd edn (Oxford University Press, New York, 2000).
62. Saunders, R. & Aggleton, J. Origin and topography of fibers contributing to the fornix in macaque monkeys. *Hippocampus* **17**, 396–411 (2007).
63. Behrens, T. E. J. et al. Non-invasive mapping of connections between human thalamus and cortex using diffusion imaging. *Nat. Neurosci.* **6**, 750–757 (2003).
64. Balak, N. et al. Mammillothalamic and mammillotegmental tracts as new targets for dementia and epilepsy treatment. *World Neurosurg.* **110**, 133–144 (2018).
65. Vicq D'Azyr, F. *Traité d'anatomie et de physiologie, avec des planches coloriées représentant au naturel les divers organes de l'Homme et des Animaux.* (François-Ambroise Didot, Paris, 1786).
66. Bullmore, E. & Sporns, O. Complex brain networks: graph theoretical analysis of structural and functional systems. *Nat. Rev. Neurosci.* **10**, 186–198 (2009).
67. Rubinov, M. & Sporns, O. Complex network measures of brain connectivity: uses and interpretations. *Neuroimage* **52**, 1059–1069 (2010).
68. Hagmann, P. et al. Mapping the structural core of human cerebral cortex. *PLoS Biol.* **6**, 1479–1493 (2008).
69. van Oort, E. S. B., van Cappellen van Walsum, A. M. & Norris, D. G. An investigation into the functional and structural connectivity of the Default Mode Network. *Neuroimage* **90**, 381–389 (2014).
70. Schacter, D. L., Addis, D. R. & Buckner, R. L. Remembering the past to imagine the future: the prospective brain. *Nat. Rev. Neurosci.* **8**, 657–661 (2007).
71. Rabin, J. S., Gilboa, A., Stuss, D. T., Mar, R. A. & Rosenbaum, R. S. Common and unique neural correlates of autobiographical memory and theory of mind. *J. Cogn. Neurosci.* **22**, 1095–1111 (2010).
72. Spreng, R. N. & Grady, C. L. Patterns of brain activity supporting autobiographical memory, prospection, and theory of mind, and their relationship to the default mode network. *J. Cogn. Neurosci.* **22**, 1112–1123 (2010).
73. Child, N. D. & Benarroch, E. E. Anterior nucleus of the thalamus: functional organization and clinical implications. *Neurology* **81**, 1869–1876 (2013).
74. Danet, L. et al. Thalamic amnesia after infarct: the role of the mammillothalamic tract and mediodorsal nucleus. *Neurology* **85**, 2107–2115 (2015).
75. Zaborszky, L. et al. Neurons in the basal forebrain project to the cortex in a complex topographic organization that reflects corticocortical connectivity patterns: an experimental study based on retrograde tracing and 3D reconstruction. *Cereb. Cortex* **25**, 118–137 (2015).
76. Hasselmo, M. E. The role of acetylcholine in learning and memory. *Curr. Opin. Neurobiol.* **16**, 710–715 (2006).

77. Dannenberg, X. H. et al. Synergy of direct and indirect cholinergic septo-hippocampal pathways coordinates firing in hippocampal networks. *J. Neurosci.* **35**, 8394–8410 (2015).
78. Raichle, M. E. The brain's default mode network. *Annu. Rev. Neurosci.* **38**, 433–447 (2015).
79. Spies, M. et al. Default mode network deactivation during emotion processing predicts early antidepressant response. *Transl. Psychiatry* **7**, e1008 (2017).
80. Zhao, J., Tomasi, D., Wiers, C.E., Shokri-kojori, E. & Şükrü, B. Correlation between traits of emotion-based impulsivity and intrinsic default-mode network activity. *Neural Plast.*, https://doi.org/10.1155/2017/9297621 (2017).
81. Bzdok, D. et al. Segregation of the human medial prefrontal cortex in social cognition. *Front. Hum. Neurosci.* **7**, 1–17 (2013).
82. Alcalá-López, D. et al. Computing the social brain connectome across systems and states. *Cereb. Cortex* 1–26. https://doi.org/10.1093/cercor/bhx121 (2017).
83. Mars, R. B. et al. On the relationship between the "default mode network" and the "social brain. *Front. Hum. Neurosci.* **6**, 1–9 (2012).
84. Floresco, S. B. The nucleus accumbens: an interface between cognition, emotion, and action. *Annu. Rev. Psychol.* **66**, 25–52 (2015).
85. Laviolette, S. R. Dopamine modulation of emotional processing in cortical and subcortical neural circuits: Evidence for a final common pathway in schizophrenia? *Schizophr. Bull.* **33**, 971–981 (2007).
86. Britt, J. P. et al. Synaptic and behavioral profile of multiple glutamatergic inputs to the nucleus accumbens. *Neuron* **76**, 790–803 (2012).
87. Morales, M. & Margolis, E. B. Ventral tegmental area: cellular heterogeneity, connectivity and behaviour. *Nat. Rev. Neurosci.* **18**, 73–85 (2017).
88. van den Heuvel, M. P. & Sporns, O. Network hubs in the human brain. *Trends Cogn. Sci.* **17**, 683–696 (2013).
89. Grothe, M. et al. Reduction of basal forebrain cholinergic system parallels cognitive impairment in patients at high risk of developing alzheimer's disease. *Cereb. Cortex* **20**, 1685–1695 (2010).
90. Persson, J. et al. Altered deactivation in individuals with genetic risk for Alzheimer's disease. *Neuropsychologia* **46**, 1679–1687 (2008).
91. He, Y. et al. Regional coherence changes in the early stages of Alzheimer's disease: a combined structural and resting-state functional MRI study. *Neuroimage* **35**, 488–500 (2007).
92. Pomarol-Clotet, E. et al. Failure to deactivate in the prefrontal cortex in schizophrenia: dysfunction of the default mode network? *Psychol. Med.* **38**, 1185–1193 (2008).
93. Bluhm, R. L. et al. Spontaneous low-frequency fluctuations in the BOLD signal in schizophrenic patients: Anomalies in the default network. *Schizophr. Bull.* **33**, 1004–1012 (2007).
94. McCollum, L. A. & Roberts, R. C. Uncovering the role of the nucleus accumbens in schizophrenia: a postmortem analysis of tyrosine hydroxylase and vesicular glutamate transporters. *Schizophr. Res.* **169**, 369–373 (2015).
95. Hadley, J. A. et al. Ventral tegmental area/midbrain functional connectivity and response to antipsychotic medication in schizophrenia. *Neuropsychopharmacology* **39**, 1020–1030 (2014).
96. Butler, T. et al. Septal nuclei enlargement in human temporal lobe epilepsy without mesial temporal sclerosis. *Neurology* **80**, 487–491 (2013).
97. Dinkelacker, V. et al. Hippocampal-thalamic wiring in medial temporal lobe epilepsy: enhanced connectivity per hippocampal voxel. *Epilepsia* **56**, 1217–1226 (2015).
98. Ivanov, I. et al. Morphological abnormalities of the thalamus in youths with attention deficit hyperactivity disorder. *Image Process.* 397–408, https://doi.org/10.1176/appi.ajp.2009.09030398 (2010).
99. Scofield, M. D. et al. The nucleus accumbens: mechanisms of addiction across drug classes reflect the importance of glutamate homeostasis. *Pharmacol. Rev.* **68**, 816–871 (2016).
100. Vialou, V. et al. DeltaFosB in brain reward circuits mediates resilience to stress and antidepressant responses. *Nat. Neurosci.* **13**, 745–752 (2010).
101. Volkow, N. D. et al. Motivation deficit in ADHD is associated with dysfunction of the dopamine reward pathway. *Mol. Psychiatry* **16**, 1147–1154 (2011).
102. Yamamura, T. et al. Association of thalamic hyperactivity with treatment-resistant depression and poor response in early treatment for major depression: a resting-state fMRI study using fractional amplitude of low-frequency fluctuations. *Transl. Psychiatry* **6**, e754 (2016).
103. Zhu, Y., Wienecke, C. F. R., Nachtrab, G. & Chen, X. A thalamic input to the nucleus accumbens mediates opiate dependence. *Nature* **530**, 219–222 (2016).
104. Mease, R. A., Metz, M. & Groh, A. Cortical sensory responses are enhanced by the higher-order thalamus. *Cell Rep.* **14**, 208–215 (2016).
105. Dringenberg, H. C. & Olmstead, M. C. Integrated contributions of basal forebrain and thalamus to neocortical activation elicited by pedunculopontine tegmental stimulation in urethane-anesthetized rats. *Neuroscience* **119**, 839–853 (2003).
106. Yamamoto, K., Solal, B. & Philippe, V. New perspective on the regionalization of the anterior forebrain in Osteichthyes. *Dev. Growth Regen.* **59**, 175–187 (2017).
107. Butler, A. B. Evolution of the thalamus: a morphological and functional review. *Thalamus Relat. Syst.* **4**, 35–58 (2008).
108. Karten, H. J. Vertebrate brains and evolutionary connectomics: on the origins of the mammalian "neocortex." *Phil. Trans. R. Soc. B* **370**, 20150060 (2015).
109. Rilling, J. K. et al. A comparison of resting-state brain activity in humans and chimpanzees. *Proc. Natl Acad. Sci. USA* **104**, 17146–17151 (2007).
110. Vincent, J. L. et al. Intrinsic functional architecture in the anaesthetized monkey brain. *Nature* **447**, 83–88 (2007).
111. Buckner, R. L. & Margulies, D. S. Macroscale cortical organization and a default-like transmodal apex network in the marmoset monkey. *bioRxiv*. https://doi.org/10.1101/415141 (2018).
112. Lu, H. et al. Rat brains also have a default mode network. *Proc. Natl Acad. Sci. USA* **109**, 3979–3984 (2012).
113. Gozzi, A. & Schwarz, A. J. Large-scale functional connectivity networks in the rodent brain. *Neuroimage* **15**, 496–509 (2016).
114. Sforazzini, F., Schwarz, A. J., Galbusera, A., Bifone, A. & Gozzi, A. Distributed BOLD and CBV-weighted resting-state networks in the mouse brain. *Neuroimage* **87**, 403–415 (2014).
115. Bertero, A. et al. Autism-associated 16p11.2 microdeletion impairs prefrontal functional connectivity in mouse and human. *Brain* **141**, 2055–2065 (2018).
116. Liska, A., Galbusera, A., Schwarz, A. J. & Gozzi, A. Functional connectivity hubs of the mouse brain. *Neuroimage* **115**, 281–291 (2015).
117. Chandler, D. & Waterhouse, B. D. Evidence for broad versus segregated projections from cholinergic and noradrenergic nuclei to functionally and anatomically discrete subregions of prefrontal cortex. *Front Behav. Neurosci.* **6**, 1–9 (2012).
118. Chandler, D. J., Lamperski, C. S. & Waterhouse, B. D. Identification and distribution of projections from monoaminergic and cholinergic nuclei to functionally differentiated subregions of prefrontal cortex. *Brain Res.* **1522**, 38–58 (2013).
119. Markello, R. D., Spreng, R. N., Luh, W., Anderson, A. K. & Rosa, E. De Segregation of the human basal forebrain using resting state functional MRI. *Neuroimage* **173**, 287–297 (2018).
120. Jones, D. K. & Cercignani, M. Twenty-five pitfalls in the analysis of diffusion MRI Data. *NMR Biomed.* **23**, 803–820 (2010).
121. Maier-Hein, K. H., Neher, P. F. & Descoteaux, M. The challenge of mapping the human connectome based on diffusion tractography. *Nat. Commun.* **8**, 1349–1361 (2017).
122. Thiebaut de Schotten, M. et al. A lateralized brain network for visuospatial attention. *Nat. Neurosci.* **14**, 1245–1247 (2011a).
123. Dell'Acqua, F., Simmons, A., Williams, S. C. R. & Catani, M. Can spherical deconvolution provide more information than fiber orientations? Hindrance modulated orientational anisotropy, a true-tract specific index to characterize white matter diffusion. *Hum. Brain Mapp.* **34**, 2464–2483 (2013).
124. Karolis, V. R., Corbetta, M. & Thiebaut de Schotten, M. The architecture of functional lateralisation and its relationship to callosal connectivity in the human brain. *Nat. Commun.* **10**, 1417–1424 (2019).
125. Moeller, S. et al. Multiband multislice GE-EPI at 7 tesla, with 16-fold acceleration using partial parallel imaging with application to high spatial and temporal whole-brain FMRI. *Magn. Reson. Med.* **63**, 1144–1153 (2010).
126. Setsompop, K. et al. Blipped-controlled aliasing in parallel imaging for simultaneous multislice echo planar imaging with reduced g-factor penalty. *Magn. Reson. Med.* **67**, 1210–1224 (2012).
127. Xu, J. et al. Evaluation of slice accelerations using multiband echo planar imaging at 3T. *Neuroimage* **83**, 991–1001 (2013).
128. Feinberg, D. A. et al. Multiplexed echo planar imaging for sub-second whole brain fmri and fast diffusion imaging. *PLoS One* 5, https://doi.org/10.1371/journal.pone.0015710 (2010).
129. Andersson, J. L. R., Skare, S. & Ashburner, J. How to correct susceptibility distortions in spin-echo echo-planar images: application to diffusion tensor imaging. *Neuroimage* **20**, 870–888 (2003).
130. Smith, S. M. et al. Advances in functional and structural MR image analysis and implementation as FSL. *Neuroimage* **23**, 208–219 (2004).
131. Foulon, C. et al. Advanced lesion symptom mapping analyses and implementation as BCBtoolkit. *Gigascience* **7**, 1–17 (2018).
132. Jenkinson, M., Bannister, P., Brady, M. & Smith, S. Improved optimization for the robust and accurate linear registration and motion correction of brain images. *Neuroimage* **17**, 825–841 (2002).
133. Woolrich, M. W. et al. Bayesian analysis of neuroimaging data in FSL. *Neuroimage* **45**, S173–S186 (2009).
134. Avants, B. & Gee, J. C. Geodesic estimation for large deformation anatomical shape averaging and interpolation. *Neuroimage* **23**, 139–150 (2004).
135. Avants, B. B. et al. The optimal template effect in hippocampus studies of diseased populations. *Neuroimage* **49**, 2457–2466 (2010).
136. Avants, B. B. et al. A reproducible evaluation of ANTs similarity metric performance in brain image registration. *Neuroimage* **54**, 2033–2044 (2011).
137. Klein, A. et al. Evaluation of 14 nonlinear deformation algorithms applied to human brain MRI registration. *Neuroimage* **46**, 786–802 (2009).

138. van Dijk, K. R. A., Sabuncu, M. R. & Buckner, R. L. The influence of head motion on intrinsic functional connectivity MRI. *Neuroimage* **59**, 431–438 (2012).
139. Pruim, R. H. R., Mennes, M., Buitelaar, J. K. & Beckmann, C. F. Evaluation of ICA-AROMA and alternative strategies for motion artifact removal in resting state fMRI. *Neuroimage* **112**, 278–287 (2015).
140. Salimi-khorshidi, G. et al. Automatic denoising of functional MRI data: combining independent component analysis and hierarchical fusion of classifiers. *Neuroimage* **90**, 449–468 (2014).
141. Power, J. D., Barnes, K. A., Snyder, A. Z., Schlaggar, B. L. & Petersen, S. E. Spurious but systematic correlations in functional connectivity MRI networks arise from subject motion. *Neuroimage* **59**, 2142–2154 (2012).
142. Shine, J. M. et al. The dynamics of functional brain networks: integrated network states during cognitive task performance. *Neuron* **92**, 544–554 (2016).
143. Tomasi, D. & Volkow, N. D. Association between brain activation and functional connectivity. *Cereb Cortex* 1–13, https://doi.org/10.1093/cercor/bhy077 (2018).
144. Jenkinson, M., Beckmann, C. F., Behrens, T. E. J., Woolrich, M. W. & Smith, S. M. Fsl. *Neuroimage* **62**, 782–790 (2012).
145. Kenney, J. *Mathematics of Statistics.* (Chapman & Hall, London, 1939).
146. Avants, B. B., Epstein, C. L., Grossman, M. & Gee, J. C. Symmetric diffeomorphic image registration with cross-correlation: evaluating automated labeling of elderly and neurodegenerative brain. *Med. Image Anal.* **12**, 26–41 (2008).
147. Cohen, J. A power prime. *Psychol. Bull.* **112**, 155–159 (1992).
148. Nieuwenhuys, R., Voogd, J. & van Huijzen, C. *The Human Central Nervous System: A Synopsis and Atlas*, 4th edn. (Steinkopff, 2008).
149. Catani, M. & Thiebaut de Schotten, M. *Atlas of Human Brain Connections*, 1st edn. (Oxford University Press, 2012).
150. Xia, M., Wang, J. & He, Y. BrainNet Viewer: a network visualization tool for human brain connectomics. *PLoS One* **8**. https://doi.org/10.1371/journal.pone.0068910 (2013).
151. Krzywinski, M. et al. Circos: an information aesthetic for comparative genomics. *Genome Res.* **19**, 1639–1645 (2009).
152. Vos, S. B. et al. The importance of correcting for signal drift in diffusion MRI. *Magn. Reson. Med.* **77**, 285–299 (2017).
153. Leemans, A., Jeurissen, B., Sijbers, J. & Jones, D. ExploreDTI: a graphical toolbox for processing, analyzing, and visualizing diffusion MR data. In *17th Scientific Meeting, International Society for Magnetic Resonance in Medicine*. 3537 (Hawaii, 2009).
154. Dell'Acqua, F. et al. A modified damped Richardson-Lucy algorithm to reduce isotropic background effects in spherical deconvolution. *Neuroimage* **49**, 1446–1458 (2010).
155. Thiebaut de Schotten, M. et al. Damage to white matter pathways in subacute and chronic spatial neglect: a group study and 2 single-case studies with complete virtual "in vivo" tractography dissection. *Cereb. Cortex* **24**, 691–706 (2014).
156. Wassermann, D. et al. The white matter query language: a novel approach for describing human white matter anatomy. *Brain Struct. Funct.* **221**, 4705–4721 (2016).
157. Tournier, J. D., Calamante, F. & Connelly, A. MRtrix: diffusion tractography in crossing fiber regions. *Int. J. Imaging Syst. Technol.* **22**, 53–66 (2012).
158. Calamante, F., Tournier, J. D., Jackson, G. D. & Connelly, A. Track-density imaging (TDI): super-resolution white matter imaging using whole-brain track-density mapping. *Neuroimage* **53**, 1233–1243 (2010).
159. Thiebaut de Schotten, M. et al. Atlasing location, asymmetry and inter-subject variability of white matter tracts in the human brain with MR diffusion tractography. *Neuroimage* **54**, 49–59 (2011b).
160. Bürgel, U. et al. White matter fiber tracts of the human brain: three-dimensional mapping at microscopic resolution, topography and intersubject variability. *Neuroimage* **29**, 1092–1105 (2006).
161. Rivière, D., Geffroy, D., Denghien, I., Souedet, N. & Cointepas, Y. Anatomist: a python framework for interactive 3D visualization of neuroimaging data. In *Python in Neuroscience Workshop* (2011).
162. Shu, N. et al. Diffusion tensor tractography reveals disrupted topological efficiency in white matter structural networks in multiple sclerosis. *Cereb. Cortex* **21**, 2565–2577 (2011).
163. Gong, G. et al. Mapping anatomical connectivity patterns of human cerebral cortex using in vivo diffusion tensor imaging tractography. *Cereb. Cortex* **19**, 524–536 (2009).
164. Jones, D. K., Knösche, T. R. & Turner, R. White matter integrity, fiber count, and other fallacies: the do's and don'ts of diffusion MRI. *Neuroimage* **73**, 239–254 (2013).
165. Aggleton, J. P. Understanding anterograde amnesia: disconnections and hidden lesions. *Q. J. Exp. Psychol.* **61**, 1441–1471 (2008).
166. Haber, S. N., Kunishio, K. & Mizobuchi, M. The orbital and medial prefrontal basal ganglia circuit through the primate. *Neuroscience* **39**, 323–338 (1995).
167. Haber, S. N., Wolfe, D. P. & Groenewegen, H. J. The relationship between ventral striatal efferent fibers and the distribution of peptide-positive woolly fibers in the forebrain of the rhesus monkey. *Neuroscience* **39**, 323–338 (1990).
168. Kunishio, K. & Haber, S. N. Primate cingulostriatal projection: limbic striatal versus sensorimotor striatal input. *J. Comp. Neurol.* **350**, 337–356 (1994).
169. Aggleton, J. P., Pralus, A., Nelson, A. J. D. & Hornberger, M. Thalamic pathology and memory loss in early Alzheimer's disease: moving the focus from the medial temporal lobe to Papez circuit. *Brain* **139**, 1877–1890 (2016).
170. Osorio, I., Overman, J., Giftakis, J. & Wilkinson, S. B. High frequency thalamic stimulation for inoperable mesial temporal epilepsy. *Epilepsia* **48**, 1561–1571 (2007).
171. Salanova, V. et al. Long-term efficacy and safety of thalamic stimulation for drug-resistant partial epilepsy. *Neurology* **84**, 1017–1025 (2015).

Acknowledgements

P.N.A. work was financially supported by the Research Experience Fellowship grant of the European Academy of Neurology and by "PRÉMIO JOÃO LOBO ANTUNES" - SCML. The research leading to these results received funding from the "Agence Nationale de la Recherche" [grant number ANR-13- JSV4-0001-01]. This project has received funding from the European Research Council (ERC) under the European Union's Horizon 2020 research and innovation programme (grant agreement No. 818521) and from the Fondation pour la Recherche Médicale (FRM DEQ20150331725).

Author contributions

P.N.A. implemented part of the methods, performed the analyses and wrote the manuscript. C.F. implemented part of the methods and edited the paper, Vyacheslav Karolis contributed to the methods and edited the paper, D.B., D.S.M. and E.V. helped conceptually and edited the paper, M.T.S. conceived and coordinated the study, reviewed the neuroimaging data, wrote the paper and provided funding.

Competing interests

Michel Thiebaut de Schotten is an Editorial Board Member for *Communications Biology*, but was neither involved in the editorial review of nor the decision to publish this article. The authors declare no other competing financial or non-financial interests.

Additional information

Supplementary information is available for this paper at https://doi.org/10.1038/s42003-019-0611-3.

Correspondence and requests for materials should be addressed to P.N.A. or M.T.d.S.

Reprints and permission information is available at http://www.nature.com/reprints

Publisher's note Springer Nature remains neutral with regard to jurisdictional claims in published maps and institutional affiliations.

communications biology

ARTICLE

https://doi.org/10.1038/s42003-022-04281-0 OPEN

The subcortical and neurochemical organization of the ventral and dorsal attention networks

Pedro Nascimento Alves[1,2]✉, Stephanie J. Forkel[3,4,5,6], Maurizio Corbetta[7,8,9,10] & Michel Thiebaut de Schotten[3,11]✉

Attention is a core cognitive function that filters and selects behaviourally relevant information in the environment. The cortical mapping of attentional systems identified two segregated networks that mediate stimulus-driven and goal-driven processes, the Ventral and the Dorsal Attention Networks (VAN, DAN). Deep brain electrophysiological recordings, behavioral data from phylogenetic distant species, and observations from human brain pathologies challenge purely corticocentric models. Here, we used advanced methods of functional alignment applied to resting-state functional connectivity analyses to map the subcortical architecture of the Ventral and Dorsal Attention Networks. Our investigations revealed the involvement of the pulvinar, the superior colliculi, the head of caudate nuclei, and a cluster of brainstem nuclei relevant to both networks. These nuclei are densely connected structural network hubs, as revealed by diffusion-weighted imaging tractography. Their projections establish interrelations with the acetylcholine nicotinic receptor as well as dopamine and serotonin transporters, as demonstrated in a spatial correlation analysis with a normative atlas of neurotransmitter systems. This convergence of functional, structural, and neurochemical evidence provides a comprehensive framework to understand the neural basis of attention across different species and brain diseases.

[1] Laboratório de Estudos de Linguagem, Centro de Estudos Egas Moniz, Faculdade de Medicina, Universidade de Lisboa, Lisboa, Portugal. [2] Serviço de Neurologia, Departmento de Neurociências e Saúde Mental, Hospital de Santa Maria, CHULN, Lisboa, Portugal. [3] Brain Connectivity and Behaviour Laboratory, Sorbonne University, Paris, France. [4] Donders Institute for Brain Cognition Behaviour, Radboud University, Thomas van Aquinostraat 4, 6525GD Nijmegen, the Netherlands. [5] Centre for Neuroimaging Sciences, Department of Neuroimaging, Institute of Psychiatry, Psychology and Neuroscience, King's College London, London, UK. [6] Departments of Neurosurgery, Technical University of Munich School of Medicine, Munich, Germany. [7] Clinica Neurologica, Department of Neuroscience, University of Padova, Padova, Italy. [8] Padova Neuroscience Center (PNC), University of Padova, Padova, Italy. [9] Venetian Institute of Molecular Medicine, VIMM, Padova, Italy. [10] Department of Neurology, Radiology, Neuroscience Washington University School of Medicine, St.Louis, MO, USA. [11] Groupe d'Imagerie Neurofonctionnelle, Institut des Maladies Neurodégénératives-UMR 5293, CNRS, CEA, University of Bordeaux, Bordeaux, France. ✉email: pedronascimentoalves@gmail.com; michel.thiebaut@gmail.com

"Everyone knows what attention is. It is the taking possession by the mind, in clear and vivid form, of one out of what seem several simultaneously possible objects or trains of thought."[1].

Everything we see, feel, or smell is an illusion elaborated by our brain circuits. However, the brain's capacity is limited. This requires mechanisms for the selection of the most relevant information. The ensemble of cognitive and neural processes involved in capacity limitation and selection underlies 'attention' as defined by James[1]. Behavioral studies have distinguished orienting of attention into a slow, strategic, goal-directed, and voluntary component versus a swift, unexpected, bottom-up, and automatic component[2,3]. Task-related functional neuroimaging (*f*MRI) studies segregated these two attentional processes anatomically into a dorsal and ventral attentional network[4]. The dorsal attention network (DAN) encodes and maintains preparatory signals and modulates top-down sensory (visual, auditory, olfactory and somatosensory) regions.

In contrast, the ventral attention network (VAN) is recruited when attention is re-oriented to novel behaviorally relevant events. Classical core regions of the DAN are the intraparietal sulcus, the superior parietal lobe, and the frontal eye fields. The DAN is considered to have no hemispheric lateralization[5–9]. In contrast, the temporoparietal junction and the ventrolateral prefrontal cortex constitute the central regions of the VAN. Evidence demonstrates that the VAN is right-lateralized[7,8,10]. Within their respective networks, DAN and VAN regions have synchronous *f*MRI signal oscillations at rest[8,11–18]. Thanks to this synchronization, the two networks have consistently been identified and segregated in resting-state *f*MRI cortical parcellations[14,16–18], although their taxonomy has not always been homogenous in the literature[19,20]. Hence, the DAN and VAN are organized as independent networks even in the absence of task signals. However, their synchronization can change according to task demands, and they can be acting jointly or separately[21,22]. Furthermore, DAN and VAN task activations and synchronization levels are modified by focal lesions and correlate with behavioral deficits[23–30].

Yet, electrical recording, pathological observations, and phylogenetic comparisons demonstrate that the neuroanatomical framework of attentional mechanisms should extend well beyond a corticocentric model. Electrical recordings in primates showed that subcortical structures have a crucial role in the neural mechanisms of attention. For instance, inactivation of the superior colliculus during motion-change detection markedly disturbs visual attention without affecting the neuronal activity in the visual cortex[31]. Attentional states also modulate the thalamic pulvinar nuclei[32,33] and neuronal discharge patterns in the locus coeruleus[34,35]. Pathophysiological data from human brain disease supports the critical relevance of deep brain nuclei. Neglect is a clinical syndrome characterized by pathological hemispatial inattention[36] and can arise from subcortical lesions in the pulvinar, striatum, or superior colliculus[37–40]. Patients with attention deficit hyperactivity disorder also present alterations beyond the cortex[28], such as in the pulvinar, which is influenced by the severity of the disease and the use of stimulants[41].

Additionally, distant phylogenetic species, such as pigeons, have markedly different cortical morphologies but exhibit attention errors and reaction times similar to humans[42]. With close mammals, such as macaques, relevant functional attention dissimilarities have been described at the cortical level, including the complete absence of a VAN[43]. Hence, a core phylogenetically relevant subcortical network of areas appears to support the orientation of attention that has been mostly disregarded in the functional neuroimaging literature because of limited field strength or issues arising from average group alignments. Average group alignments of functional neuroimaging maps exclusively based on structural landmarks might typically fail to represent an accurate functional network due to interindividual differences[44,45]. Specifically, subcortical nuclei are prone to structural misalignment due to their small size, poor contrast in structural MRI, and intersubject cytoarchitectonic variability[46–49]. In contrast, advanced methods of functional alignment improve structural-functional correspondence across participants[50–53]. Further, surface interindividual alignment based on morphological features, such as cortical folding, fairly aligns unimodal cortical areas, such as the primary visual and motor cortices, but poorly overlaps higher-order cortical areas[50,54]. Methods of functional alignment based on *f*MRI signals during cognitive activation paradigms[55,56] and resting-state *f*MRI connectivity patterns[52,57] provided better function matching and have also been used for cross-species functional comparisons[58]. Functional alignment is different from hyperalignment techniques that project shared neural information beyond the three-dimensional anatomical space, i.e., in high-dimensional spaces[59–61]. At the subcortical level, our team also demonstrated that functional alignment methods can optimize the group-level mapping of functional networks, improving functional correlations and uncovering a network's deep brain nuclei components[62]. However, this method has never been applied to explore the subcortical anatomy of the VAN and the DAN.

Delineating the subcortical components of the DAN and the VAN would allow us to revisit their underlying circuitry through diffusion-weighted imaging tractography that enables in vivo reconstruction of associative, commissural, and projection white-matter tracts[63–65]. A clearer characterization of the DAN and VAN circuitry will help to better understand brain interactions in healthy and pathological brains[66,67].

Subcortical structures also play a critical role within the neurotransmitter systems. Brainstem nuclei are the primary sources of neurotransmitter synthesis and send axonal projections to the cortex and the basal ganglia. The basal ganglia are central targets of the neurotransmitter axonal projections and mediate their physiological effects. Yet the neurochemistry of the DAN and the VAN is limited to primate studies. These studies reported a noradrenergic innervation of regions of the primate attention networks, including the temporoparietal junction and the frontal lobe[68–70]. Noradrenaline has been proposed as a critical trigger for the reorientation of attention[8,70]. However, despite its essential neuroscientific and medical importance[28], the neurochemical signatures of the VAN and the DAN have never been contrasted in humans. Such an endeavor is now possible thanks to the macroscale mapping of the neurotransmitter receptors and transporters in humans by means of positron emission tomography (PET) and single-photon emission computerized tomography (SPECT) scans[71]. Accordingly, a normative atlas of nine neurotransmitter systems aligned in the MNI space is now openly available and allows the investigation of the neurochemical signature of brain circuits[72–76].

Therefore, we explored the subcortical anatomy of attention networks by aligning the individual resting-state functional maps of the VAN and the DAN in a common functional space. Based on previous electrical recordings, pathological observations, and phylogenetic reports, we hypothesized that basal ganglia and brainstem nuclei, namely the pulvinar, the striatum, the superior colliculi, and the locus coeruleus, are core phylogenetically relevant and functional constituents of the attention networks. Finally, an optimized model of the VAN and the DAN was proposed together with their structural, functional, graph centrality, and neurochemical signature.

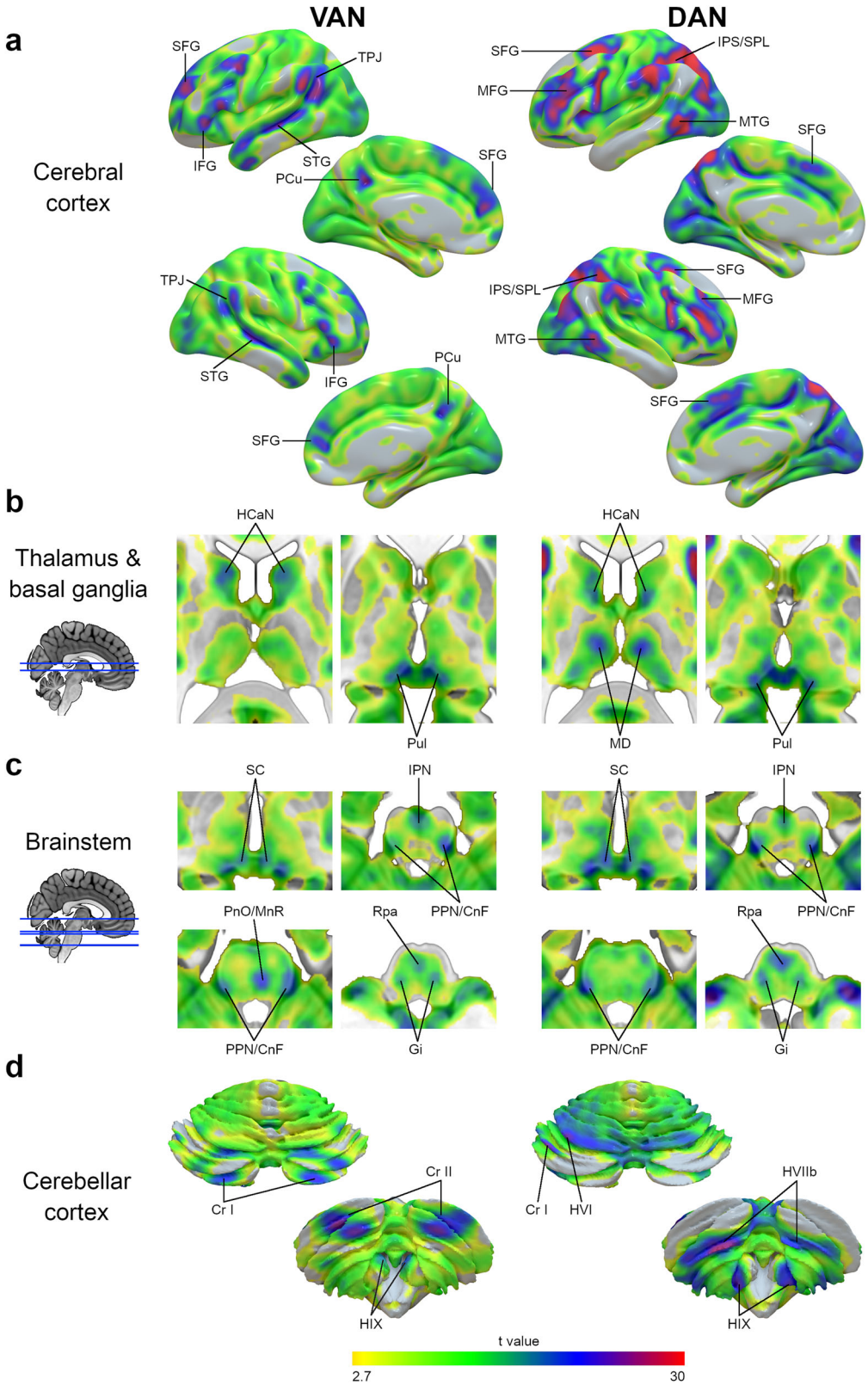

Results

VAN anatomical map. The statistical map of the VAN, after functional alignment, is represented in Fig. 1 (left column).

At the cerebral cortical level, the peaks of statistical association were observed in the temporoparietal junction, the inferior frontal gyrus, the anterior part of the superior frontal gyrus, and the superior temporal gyrus (Fig. 1a). Additionally, peaks of statistical association were also present in the crus I, crus II and superior IX cerebellar cortex (Fig. 1d).

A high statistical association was present at the thalamus and basal ganglia level in the head of caudate nuclei and the pulvinar (Fig. 1b). In the brainstem, a high statistical association was observed in voxels overlapping with the superior colliculi, the interpeduncular nucleus, and the pedunculopontine-cuneiform

Fig. 1 VAN and DAN maps after functional alignment. VAN (left) and DAN (right) maps after functional alignment at different anatomical levels, namely the cerebral cortical surface (**a**), subcortical thalamus and basal ganglia (**b**), brainstem (**c**), and cerebellar cortical surface (**d**). The color gradient represents the t-value distribution ($n = 110$). CnF cuneiform nucleus, Cr I cerebellar crus I lobule, Cr II cerebellar crus II lobule, DAN dorsal attention network, Gi gigantocellular nucleus, HCaN head of caudate nucleus, HIIb cerebellar lobule IIb, HVI cerebellar lobule VI, HIX cerebellar lobule IX (cerebellar tonsils), IFG inferior frontal gyrus, IPN interpeduncular nucleus, IPS intraparietal sulcus, MnR median raphe nucleus, MD mediodorsal nucleus of the thalamus, MTG middle temporal gyrus, PCu precuneus, PnO nucleus pontis oralis, PPN pedunculopontine nucleus, Pul pulvinar, Rpa raphe pallidus nucleus, SC superior colliculus, SFG superior frontal gyrus, SPL superior parietal lobule, STG superior temporal gyrus, TPJ temporoparietal junction, VAN ventral attention network.

Table 1 MNI coordinates of the VAN subcortical regions' centers of gravity.

Regions of interest	MNI (X)	MNI (Y)	MNI (Z)
HCaN L	−11	8	13
Pul L	−4	−30	1
SC L	−9	−31	−3
PPN/CnF L	−14	−29	−25
Gi L	−10	−25	−36
Cr I L	−31	−73	−31
Cr II L	−21	−79	−42
IPN	1	−19	−21
MnR	−3	−29	−28
Rpa	1	−28	−43
HCaN R	13	11	12
Pul R	6	−29	1
SC R	13	−30	−3
PPN/CnF R	13	−31	−25
Gi R	11	−24	−35
Cr I R	30	−74	−30
Cr II R	24	−79	−41

CnF cuneiform nucleus, *Cr I* cerebellar crus I lobule, *Cr II* cerebellar crus II lobule, *Gi* gigantocellular nucleus, *HCaN* head of caudate nucleus, *IPN* interpeduncular nucleus, *L* left, *MnR* median raphe nucleus, *PnO* nucleus pontis oralis, *PPN* pedunculopontine nucleus, *Pul* pulvinar, *R* right, *Rpa* raphe pallidus nucleus, *SC* superior colliculus.

Table 2 MNI coordinates of the DAN subcortical regions' centers of gravity.

Regions of interest	MNI (X)	MNI (Y)	MNI (Z)
HCaN L	−10	4	10
MD L	−9	−18	8
Pul L	−4	−30	1
SC L	−8	−31	−3
PPN/CnF L	−14	−30	−25
Gi L	−10	−24	−35
Cr I L	−39	−64	−29
HVI L	−25	−62	−24
HVIIb L	−24	−66	−49
HIX L	−11	−51	−50
IPN	1	−19	−21
Rpa	1	−28	−42
HCaN R	12	7	10
MD R	9	−16	8
Pul R	6	−29	1
SC R	11	−30	−3
PPN/CnF R	14	−30	−25
Gi R	11	−25	−34
HVIIb R	25	−68	−49
HIX R	11	−53	−51

CnF cuneiform nucleus, *Cr I* cerebellar crus I lobule, *Gi* gigantocellular nucleus, *HCaN* head of caudate nucleus, *HVI* cerebellar lobule VI, *HIX* cerebellar lobule IX (cerebellar tonsils), *IPN* interpeduncular nucleus, *L* left, *MD* mediodorsal nucleus of the thalamus, *PPN* pedunculopontine nucleus, *Pul* pulvinar, *R* right, *Rpa* raphe pallidus nucleus, *SC* superior colliculus.

nuclei complex pontis oralis, the gigantocellular nuclei, the raphe pallidus, and median nuclei (Fig. 1c). Table 1 represents the centers of gravity coordinates of the subcortical regions of interest. The VAN statistical and correlation maps are available at https://neurovault.org/collections/XONZLGPJ/.

DAN anatomical map. The statistical map of the DAN, after functional alignment, is represented in Fig. 1 (right column).

The peaks of the statistical association at the cerebral cortical level were in the intraparietal sulcus and superior parietal lobule, in the middle and superior frontal gyrus, and in the posterior part of the middle temporal gyrus (Fig. 1a). Peaks of statistical association were also present in the cerebellar cortex's areas VIIb, inferior IX, left VI, and left I (Fig. 1d).

At the thalamus and basal ganglia level, areas with a high statistical association were located in the head of caudate nuclei and the thalamic pulvinar and mediodorsal nuclei (Fig. 1b). High statistical associations also included voxels overlapping the superior colliculi, the interpeduncular nucleus, the pedunculopontine-cuneiform nuclei complex, the gigantocellular nuclei, and the raphe pallidus nuclei in the brainstem (Fig. 1c). Table 2 represents the centers of gravity of the subcortical regions of interest. The DAN statistical and correlation maps are available at https://neurovault.org/collections/XONZLGPJ/.

The conjunction analysis showed that most of the subcortical peaks of statistical association were shared by both networks (Fig. 2), explicitly overlapping the pulvinar, the superior colliculi, the interpeduncular nuclei, the pedunculopontine-cuneiform nuclei complex, the gigantocellular nuclei, and the raphe pallidus nuclei.

Structural and functional connectivity of the VAN nodes. The structural connectivity map of the VAN is represented in Fig. 3a.

The cortical regions of the VAN were connected by the third branch of the Superior Longitudinal Fasciculus (SLF III) and the uncinate fasciculus (Fig. 3a). Fronto-pulvinar and tecto-pulvinar projections established the connections with or between subcortical structures (Fig. 3a). The node-to-node structural and functional connectivity patterns are represented in Fig. 3b.

The maps of the VAN ROIs and the structural connectivity analysis are available at https://neurovault.org/collections/XONZLGPJ/.

Structural and functional connectivity of DAN nodes. The structural connectivity map of the DAN is represented in Fig. 3c.

The cortical regions of the DAN established connections through the first branch of the Superior Longitudinal Fasciculus (SLF I, Fig. 3c). Fronto-pulvinar, parieto-pulvinar, and tecto-pulvinar projections mediated the links with or between subcortical structures (Fig. 3c).

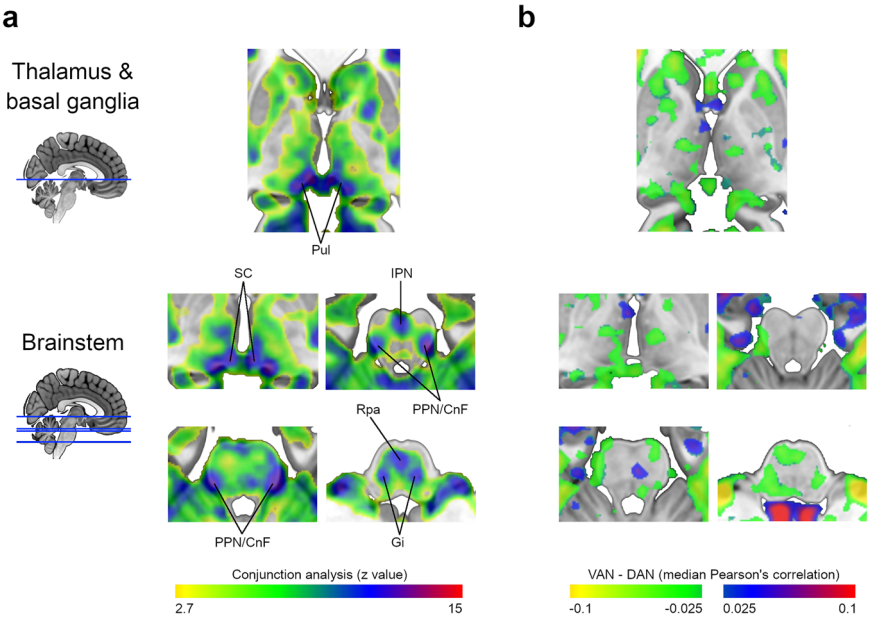

Fig. 2 VAN and DAN maps similarity. a Conjunction analysis of the VAN and DAN statistical maps at the thalamus, basal ganglia, and brainstem levels ($n = 110$). **b** Difference map resulting from the subtraction of the median DAN Pearson's correlation map from the VAN. CnF cuneiform nucleus, DAN dorsal attention network, Gi gigantocellular nucleus, IPN interpeduncular nucleus, PPN pedunculopontine nucleus, Pul pulvinar, Rpa raphe pallidus nucleus, SC superior colliculus, VAN ventral attention network. (see maps at https://neurovault.org/collections/XONZLGPJ/).

The node-to-node structural and functional connectivity patterns are shown in Fig. 3d.

The maps of the DAN ROIs and the structural connectivity analysis are available at https://neurovault.org/collections/XONZLGPJ/.

Lateralization assessment. Figure 4 illustrates the hemispheric distribution of the structural and functional connectivity measures of the VAN and the DAN.

The structural connectivity connecting the VAN was significantly larger in the right hemisphere than in the left (right hemisphere 18.7[16.5,21.1]cm^3, left hemisphere 17.0[15.3,19.7]cm^3; p value <0.001). Pearson's correlations were not different between the right and left VANs (right hemisphere 0.185[0.162,0.218], left hemisphere 0.188[0.160,0.222]; p value = 0.125).

The DAN's structural connectivity was also significantly larger in the right hemisphere (right hemisphere 33.6[30.0,36.6]cm^3, left hemisphere 30.2[28.0,32.9]cm^3; p value <0.001). Pearson's correlations were significantly higher in the left hemisphere than in the right (right hemisphere 0.240(0.049), left hemisphere 0.246(0.050); p value <0.001).

Graph theory analysis. Figure 5a illustrates the graph theory representation of the VAN and DAN structural connectivity.

The subcortical structures with the highest median betweenness centrality in the VAN were in the right pulvinar and the left caudate nucleus head (the second and the third highest of all nodes, respectively). The highest median degree of centrality was in the interpeduncular nucleus and the left pedunculopontine-cuneiform nuclei complex (the first and the second highest of all nodes, respectively).

In the DAN, the subcortical structures with the highest median betweenness centrality were the raphe pallidus nucleus and the right mediodorsal nucleus of the thalamus (the first and the seventh highest of all nodes, respectively). The highest median degree of centrality was the raphe pallidus nucleus and the left superior colliculus (the first and the second highest of all nodes, respectively).

Overall, the subcortical structures had high centrality values in both networks. The betweenness centrality and degree centrality values of all nodes in the VAN and the DAN are detailed in Supplementary Tables 3, 4. The anatomical models of the VAN and DAN are illustrated in Fig. 5b.

Correlation with the neurotransmitter system. The brainstem nuclei identified in the VAN anatomical map that synthesize neurotransmitters are the pedunculopontine nuclei (cholinergic, glutamatergic, and GABAergic; Benarroch[72]), the cuneiform nuclei (glutamatergic and GABAergic; Chang et al.[73]), the gigantocellular nucleus (glutamatergic and GABAergic; Martin et al.[74]), the raphe nucleus (serotonergic; Van De Kar and Lorens[75]), and the raphe pallidus nucleus (serotonergic; Heym et al.[76]). The brainstem nuclei identified in the DAN anatomical map synthesizing neurotransmitters are the pedunculopontine, the cuneiform, the gigantocellular nuclei, and the raphe pallidus nucleus.

The spatial correlations of these brainstem nuclei structural projections with the neurotransmitter systems are represented in Fig. 6. The distributions of acetylcholine α4β2 nicotinic receptors, dopamine transporters, and serotonin transporters were positively correlated with the distribution of VAN and DAN brainstem projections ($p < 0.001$; Fig. 6a). The scatterplots representing the distributions of the significantly correlated systems are presented in Fig. 6b. Acetylcholine α4β2 nicotinic receptors and serotonin transporters had a higher spatial correlation with the VAN than with the DAN, whereas dopamine transporters had a higher spatial correlation with the DAN ($p < 0.001$).

The supplemental pairwise correlation analyses between the average VAN and DAN structural projection maps and the neurotransmitter maps revealed similar results: the VAN had a significant positive spatial correlation with acetylcholine α4β2 nicotinic receptors and acetylcholine, dopamine, noradrenaline, and serotonin transporters (Supplementary Table 5); the DAN had a significant positive spatial correlation with acetylcholine α4β2 nicotinic receptors and acetylcholine, dopamine and noradrenaline transporters (Supplementary Table 6).

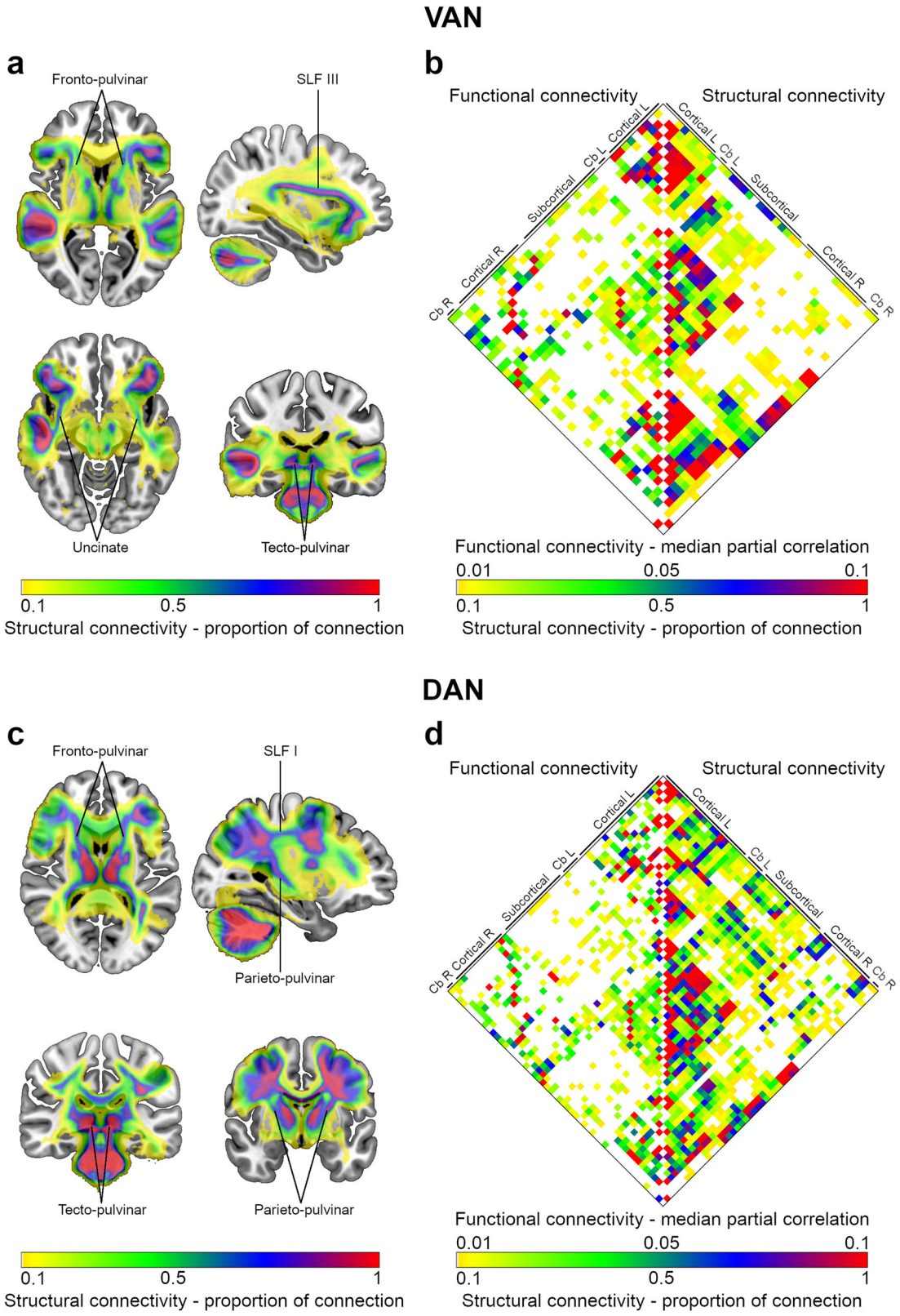

Fig. 3 Structural and functional connectivity of VAN and DAN nodes. a Structural connectivity map of the VAN. **b** Matrix with the node-to-node functional and structural connectivity of the VAN, represented on the left and right halves, respectively. **c** Structural connectivity map of the DAN. **d** Matrix with the node-to-node functional and structural connectivity of the DAN, represented on the left and right halves, respectively. Nodes of the matrices were labeled in groups according to their anatomical location. A complete list with node labels is available in Supplementary Tables 1, 2. As indicated, color gradients represent the structural connectivity (expressed as the proportion of connection) or the functional connectivity (defined as the median partial correlation). Cb cerebellum, L left, R right, SLF superior longitudinal fasciculus.

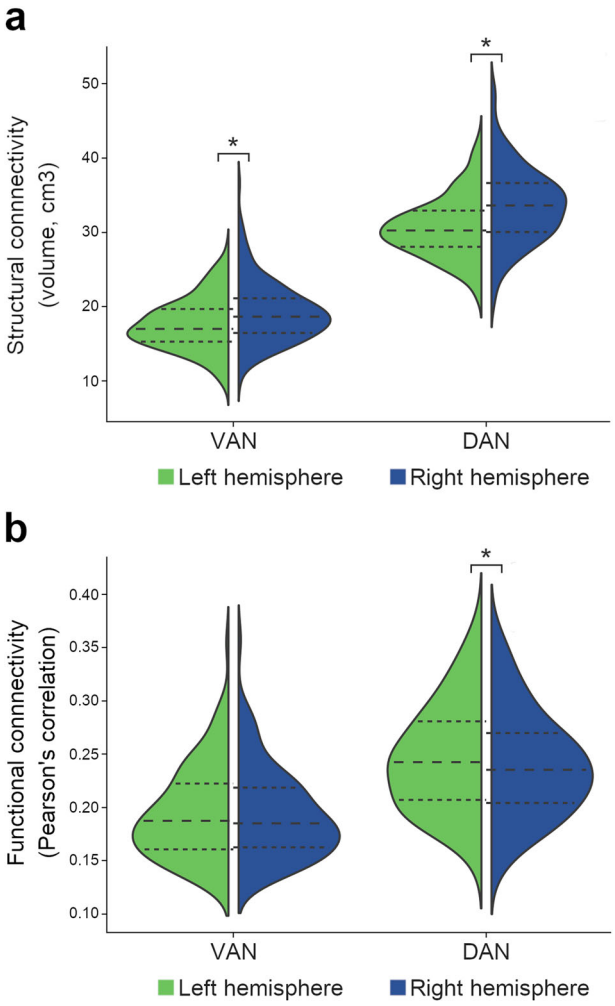

Fig. 4 VAN and DAN lateralization. Structural connectivity is expressed in volumes of the structural connection maps (**a**) and functional connectivity in average Pearson's correlations (**b**) across hemispheric nodes. Dashed lines represent the median and the interquartile range; the minimum and maximum correspond to the violin limits. DAN dorsal attention network, VAN ventral attention network. Asterisk (*), significant differences between the right and the left hemispheres ($p < 0.05$; paired analysis; structural connectivity, $n = 177$; functional connectivity, $n = 110$).

The correlation of VAN and DAN brainstem projections with the acetylcholine α4β2 nicotinic receptors was significantly higher in the left hemisphere. In contrast, the correlations with the dopamine and serotonin transporters were higher in the right hemisphere (Fig. 6c).

Discussion

This study re-examined the VAN and the DAN neuroanatomy by co-registering individual network maps in a common functional space. We propose a comprehensive model of these networks based on the convergence of functional, structural, and neurochemical findings. First, we confirmed the initial hypothesis that subcortical structures, namely the pulvinar, the superior colliculi, the head of caudate nuclei, and a group of brainstem nuclei, are constituent elements of the attentional networks. Second, we characterized the structural connections underlying functional connectivity. Deep brain nuclei are densely connected and structural network hubs. Third, we showed that the identified brainstem nuclei projections are spatially correlated with the acetylcholine α4β2 nicotinic receptors and serotonin and dopamine transporters.

Pulvinar is a high-order thalamic relay nucleus participating in cortical-thalamocortical circuits that modulate information processing[77]. Cytoarchitectonically, the pulvinar is divided into four regions: the anterior pulvinar, the inferior pulvinar, the medial pulvinar, and the lateral pulvinar[78]. The medial pulvinar is particularly important in establishing connections with heteromodal association areas, such as the superior and inferior temporal, the inferior parietal, the dorsolateral prefrontal, and the orbitofrontal cortices[79]. In our model, the pulvinar regions with the highest statistical level were medial, and we demonstrated that they were structurally connected with VAN cortical areas, through fronto-pulvinar projections, and with DAN cortical areas, by fronto-pulvinar and parieto-pulvinar projections[80–82]. Pulvinar lesions may induce hemispatial neglect[39]. Decades ago, Sprague impressively found that hemispherectomy prompted symptoms of hemispatial neglect in cats which were attenuated by removing the contralesional superior colliculus[83,84]. This effect was later observed in humans[85]. In our model, the pulvinar connects with the superior colliculi through the tecto-pulvinar fibers[86], demonstrating the importance of pulvinar—superior colliculi interactions in attention processes. Therefore, in the context of the so-called Sprague effect, removing the contralesional superior colliculus in cats with hemispatial neglect would damage the spared attentional network and might partially compensate for the imbalance in the attentional processing[87,88]. Recently, hemispatial neglect was linked to lesions of the human superior colliculus[40]. The Sprague effect is also mediated by the pedunculopontine nuclei[89,90], which is one of the brainstem nuclei included in our model. The pedunculopontine nuclei possess a population of cholinergic neurons in their caudal portion, giving rise to a distinct network that regulates attentional states and enhances the processing of salient stimuli[91]. The descending projections from these cholinergic neurons innervate the nucleus pontis oralis[92] and the gigantocellular nuclei[93], while their dorsal ascending projections innervate the colliculi[94,95] and several nuclei of the thalamus, including the pulvinar and the mediodorsal nuclei[96]. The pattern of the pedunculopontine projections closely matches the brainstem and thalamic map evidenced in our analysis. Hence, lesion analyses and axonal tracings studies confirm the validity of our subcortical model of the VAN and the DAN.

The graph theory analysis results are consistent with the subcortical nuclei hub role in the VAN and the DAN organization. Centrality measures indicate how connected a node is with other nodes. These measures are considered surrogates of the node's relevance for the flow of information and communication within a network[97,98]. The DAN and the VAN subcortical nuclei had a high degree and betweenness centrality scores, positioning them as networks' core regions as previously suggested[99–101].

The neurotransmitter system correlation analysis reinforced the proposed relationship between the subcortical nuclei of the attention networks. The highest spatial correlation of both networks was with the acetylcholine α4β2 nicotinic receptors. The acetylcholine α4β2 nicotinic receptors have a well-established relationship with sustained attention. Acetylcholine α4β2 nicotinic receptors agonists reduce adult monkey distractibility during matching-to-sample tasks with distractors[102] and increase the firing rate of dorsolateral prefrontal neurons during sustained attention tasks, an effect that is reversed by the co-administration of receptor antagonists[103]. In humans, transdermal nicotine administration improves attentiveness[104,105]. All these observations in animals and humans support the critical role of the subcortical acetylcholinergic system in attentional processes.

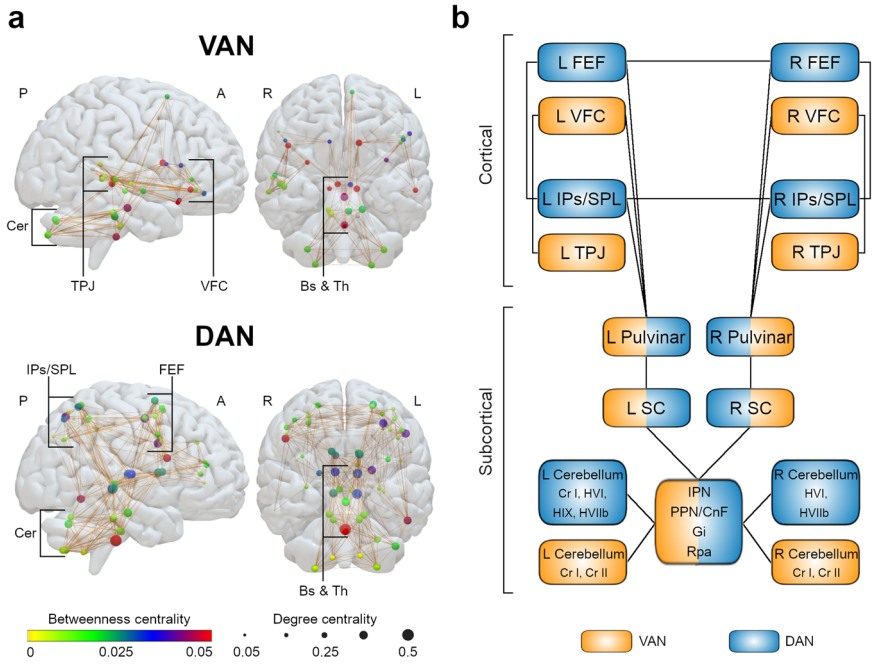

Fig. 5 Graph theory analysis and anatomical model of the VAN and DAN. a Graph theory analysis of the VAN and DAN structural connectivity. Circles illustrate nodes. Circle colors represent the median betweenness centrality of each node (according to the color gradient), while circle dimensions represent the median degree centrality. Brown lines represent node-to-node structural connections present in at least half of the subjects. **b** Anatomical model of the VAN and DAN. A anterior, CnF cuneiform nucleus, DAN dorsal attention network, Gi gigantocellular nucleus, IPN interpeduncular nucleus, L left, P posterior, PPN pedunculopontine nucleus, Pul pulvinar, R right, Rpa raphe pallidus nucleus, SC superior colliculus, VAN ventral attention network.

The VAN and DAN brainstem nuclei projections were also spatially correlated with the distribution of dopamine and serotonin transporters. This finding is consistent with the psychopharmacological knowledge about attention. Methylphenidate is the first-line treatment for attention deficit hyperactivity disorder[106]. Pharmacologically, it is a noradrenaline-dopamine reuptake inhibitor with higher potency for dopamine transporters[107,108]. Modafinil is a selective inhibitor of dopamine transporters[109] and produces attention enhancement effects[110,111]. Further studies are needed to understand how the interplay between the nicotinic acetylcholine and the dopamine systems occurs in attention networks, but it might be mediated by their interaction at the levels of the striatum[112,113] and midbrain[114,115]. Serotonin reuptake inhibitors also modulate attentional processes[116]. They increase the perceptual bias towards emotional stimuli[117,118] by regulating the activity of visual processing circuits[116]. Therefore, our improved model of the DAN and VAN functional neuroanatomy appears to reconcile previous neuroimaging and pharmacological findings. As previously suggested[8], additional pharmacological studies will be required to understand the preferential association of VAN with acetylcholine α4β2 nicotinic receptors. Similarly, pharmacological studies are required to shed light on the effect of serotonin transporter on the VAN and to reveal the relationship between dopamine transporters and the DAN. Finally, understanding the relationship between the neurochemical signature and hemispheric functional dominance still requires more research in animals and humans[8].

Characterizing the human brain's subcortical anatomy of attention networks fosters the exploration of a common structural-functional attentional framework across species. Attention is far from being a specific cognitive ability of human beings[119]. Species with either close or distant common ancestors in the phylogenetic tree, such as monkeys, rats, and pigeons, can scan, select and maintain attention to surrounding environmental stimuli[42,119–121]. A common subcortical attention framework may surpass the challenge of finding the cortical homologs of the human VAN and DAN in other species[43]. Accordingly, future studies might use the subcortical areas we highlighted to explore comparatively the organization of the VAN and the DAN in non-human species.

In our analysis, VAN and DAN structural connectivity maps were right-lateralized. The right lateralization of the VAN is established in the literature. Evidence demonstrates that the SLF III has a larger volume in the right hemisphere and that its anatomical lateralization correlates with visuomotor processing abilities and the asymmetries of visuospatial task performance[7,9,122–125]. The SLF I, the main tract connecting DAN cortical regions, does not show a preferential lateralization[7,9]. However, some DAN areas might be right-lateralized[126]. The right intraparietal sulcus[127] and frontal eye field[128] increase their activity for both visual fields, while the left preferentially reacts to contralateral stimulations. The processing of both visual fields in the right hemisphere is corroborated by right hemisphere stroke patients with hemispatial neglect who also present with deficits in goal-driven selective attention for ipsilateral stimuli[129]. Hence, while the cortical extent of the DAN was not asymmetrical, our structural connectivity analysis, including the cortico-subcortical projection tracts, might have the function-specific dimension of the right lateralization of the DAN.

Regarding functional connectivity, the distribution of VAN was not different between hemispheres, and the DAN was slightly left-lateralized. Task-based *f*MRI studies indicate right lateralization of the VAN[10,11], but the asymmetry might vary according to the nature of the task[130]. Accordingly, while functional asymmetry is expected for some task-related activations[131], resting-state functional connectivity may not capture function-specific asymmetries due to its global nature.

A limitation of our study is the inability to untangle the different roles and dynamic interactions between the proposed subcortical structures. While the cortical regions of the DAN and

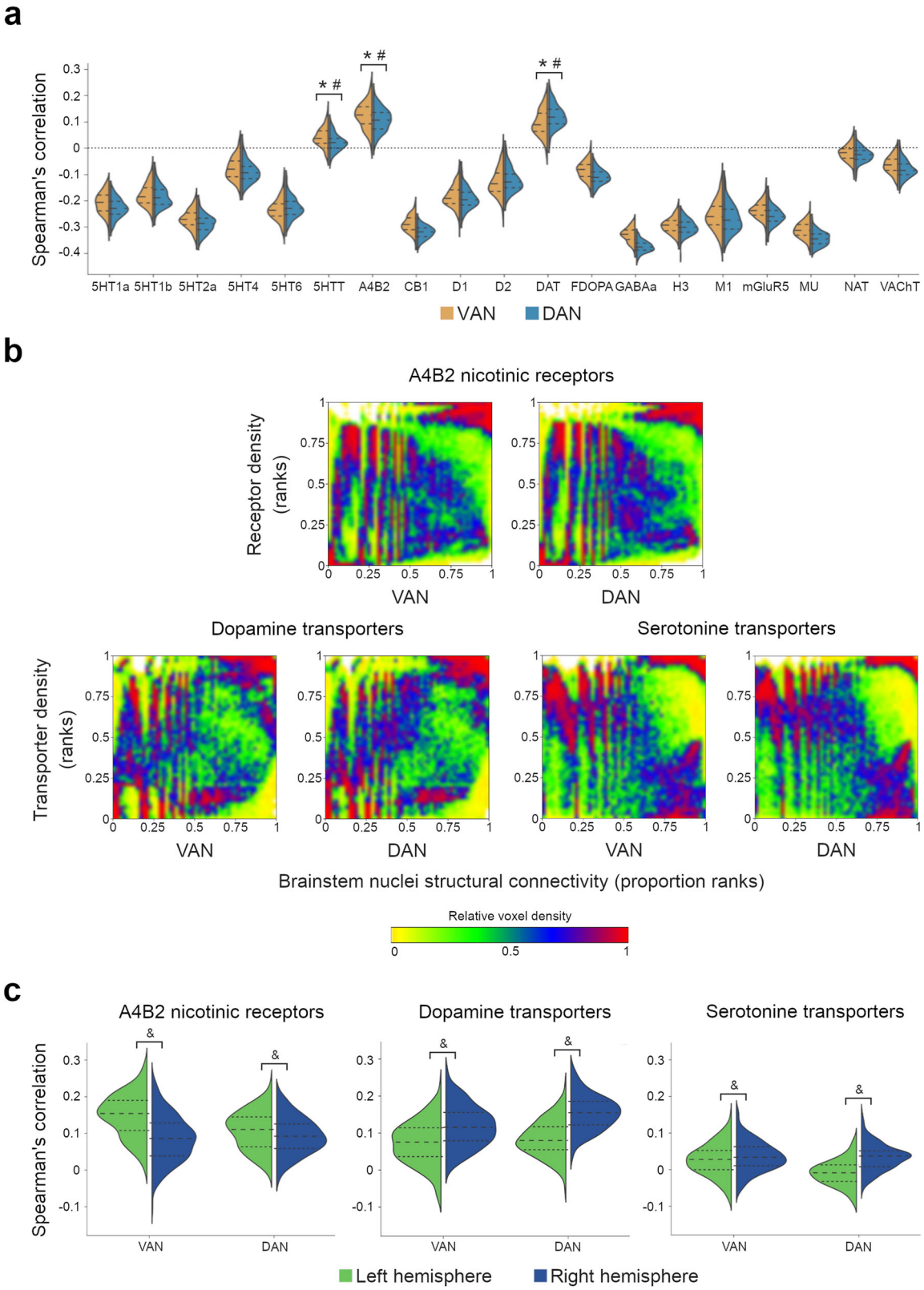

the VAN are quite neatly segregated[132], the subcortical nuclei described in our model probably contributed to both the VAN and the DAN. Future investigations using our model to explore the BOLD signal during task-related *f*MRI in humans or direct electrical recordings in animals might better dissociate the hierarchical organization and functional role of subcortical regions than resting-state *f*MRI. In addition, the neurotransmitter systems normative atlas is derived from different samples[71]. As PET and SPECT tracers are radioactive, it is not possible to map several neurotransmitter systems in the same participants. Although the atlas was replicated in an independent autoradiography dataset and all scans were acquired in healthy volunteers[71], the heterogeneity of the data sources may represent a limitation for its interpretation.

Fig. 6 Correlation between the structural projections of the brainstem nuclei and the neurotransmitter systems. a Distributions of the Spearman's correlations for the available maps of neurotransmitter receptors and transporters; for the receptors or transporters with two or more maps available, the mean correlation was calculated. Dashed lines represent the median and the interquartile range; the minimum and maximum correspond to the violin limits. **b** Graphical representation of the statistically significant positive correlations, i.e., the acetylcholine α4β2 nicotinic receptor, dopamine, and serotonin transporter maps. The color map represents the relative voxel density at each graph point. **c** Spearman's correlation of the statistically significant positive correlations with the left and right hemispheres. Dashed lines represent the median and the interquartile range; the minimum and maximum correspond to the violin limits. 5HT1a serotonin 1a receptors, 5HT1b serotonin 1b receptors, 5HT2a serotonin 2a receptors, 5HTT serotonin transporters, A4B2 acetylcholine α4β2 nicotinic receptors, CB1 cannabinoid receptors 1, D1 dopamine receptors 1, D2 dopamine receptors 2, DAT dopamine transporters, FDOPA fluorodopa, GABAa GABAa receptors, H3 histamine receptors 3, M1 muscarinic receptors 1, mGluR5 metabotropic glutamate receptors 5, MU mu-opioid receptors, NAT noradrenaline transporters, VAchT vesicular acetylcholine transporters. * Statistically significant positive correlation, corrected for multiple comparisons ($p < 0.003$); # Statistically significant difference between the VAN and the DAN, corrected for multiple comparisons ($p < 0.017$); & Statistically significant difference between right and left hemispheres, corrected for multiple comparisons ($p < 0.017$); $n = 177$.

In conclusion, this work proposes an improved neuroanatomical model of the VAN and the DAN that includes the pulvinar, the superior colliculi, the head of caudate nuclei, and a group of brainstem nuclei interrelated with the acetylcholine nicotinic and the dopamine and serotonin transporter systems. This comprehensive framework reconciles behavioral, electrophysiological, and psychopharmacological data and provides a shared foundation to explore the neural basis of attention across different species and brain pathologies.

Methods

Resting-state functional imaging (rs-*f*MRI). We used 110 7 T resting-state functional MRI datasets from the Human Connectome Project S1200[133]. Images were preprocessed and registered to the MNI152 space as specified in the Human Connectome Project protocol (http://www.humanconnectome.org/storage/app/media/documentation/s1200/HCP_S1200_Release_Reference_Manual.pdf; Glasser et al. 2013). The Human Connectome Project open access data use terms were followed.

VAN and DAN maps in the structural space. VAN and DAN maps were computed using seed regions of interest defined in the functional cortical parcellation map[14]. This template includes 23 VAN parcels (11 in the left and 12 in the right hemisphere) and 32 DAN parcels (19 in the left and 13 in the right hemisphere). This parcellation was performed according to resting-state functional connectivity patterns. Each parcel has a homogeneous resting-state functional connectivity signature and is separated from neighboring parcels by abrupt changes in their connectivity profile[14].

We calculated functional correlation maps seeded from each VAN cortical parcel using the Funcon-Connectivity tool implemented in the Brain Connectivity and Behavior toolkit (http://toolkit.bcblab.com)[134]. This tool computes Pearson's correlation between a seed region's mean resting-state activity and the brain's other voxels. Then, the median of the 23 functional connectivity maps (generated from the 23 VAN seeds) was computed to obtain the VAN's most representative map for each participant. We chose a median because it is less affected by outliers than the mean[135]. 110 individual VAN maps in the MNI152 were obtained (i.e., one per subject). The same steps were performed to obtain 32 DAN maps.

VAN and DAN maps in the functional space. The 110 individual VAN Pearson's correlation maps in the MNI152 space were aligned in a functional space to optimize their interindividual alignment of functional areas[50–53]. We used the Advanced Normalization Tools (ANTs) script "buildtemplateparallel.sh" to perform an iterative ($n = 4$) diffeomorphic transformation to a common space[62,136]. Cross-correlation was set as the similarity measure and greedy SyN as the transformation model[137,138]. The resulting transformation warps were applied to the MNI152 aligned VAN maps, using the ANTs' script "WarpImageMultiTransform" to represent the 110 individual VAN maps in the functional space. The same steps were performed with the 110 DAN Pearson's correlations maps. A schematic representation of the functional alignment steps is available in Supplementary Fig. 1.

To calculate group statistical VAN and DAN maps, we performed a permutation inference analysis using FSL's "randomise" one-sample (5000 permutations) and applied a threshold-free cluster enhancement[139]. To evaluate the similarity between the VAN and DAN statistical maps, the t-maps were z-transformed, and a conjunction analysis was computed[140]. A difference map was also calculated by subtracting the median DAN Pearson's correlation map from the VAN. Illustrations were produced in SurfIce (https://www.nitrc.org/projects/surfice/) and MRIcroGL (https://www.nitrc.org/projects/mricrogl/).

Anatomical validation of the subcortical structures. To identify thalamic nuclei, we visually compared our results with the DISTAL (Deep brain stimulation Intrinsic Template Atlas; Ewert et al. 2018) and the THOMAS (Thalamus Optimized Multi Atlas Segmentation; Su et al. 2019) atlases. The DISTAL atlas is a high-resolution template of subcortical structures in the MNI space used as a reference to localize targets for deep brain stimulation[141]. The DISTAL atlas segmentation was performed manually, based on histology, structural imaging, and diffusion-weighted imaging[141,143]. The THOMAS atlas is a template of thalamic nuclei derived from the manual segmentation of 20 White-Matter-Nulled Magnetization Prepared Rapid Gradient Echo (MP-RAGE) 7 T datasets warped to the MNI space[142]. We used the WIKIBrainStem atlas to identify the brainstem nuclei[144]. This template is based on mesoscopic T2-weighted and diffusion-weighted images obtained from the ultra-high-field scanning (11.7 T) of an ex vivo human specimen. It provides detailed segmentations of 99 brainstem structures[144].

Tractography analysis. We analyzed the structural connectivity of the VAN and DAN, including the new subcortical structures identified in our resting-state functional connectivity analysis. Tractography was computed using 177 diffusion-weighted images from the 7 T dataset of the Human Connectome Project[145]. The scanning parameters are detailed in Vu et al.[145]. Preprocessing was performed according to the default Human Connectome Project pipeline (v3.19.0)[133]. The Human Connectome Project open access data use terms were followed. Tractography processing was prepared as described in Thiebaut de Schotten et al.[67] (available at http://opendata.bcblab.com). Briefly, a whole-brain deterministic algorithm was employed using StarTrack (https://mr-startrack.com), applying a damped Richardson-Lucy algorithm optimized for spherical deconvolution[146]. Then, the individual whole-brain streamline tractograms were registered to the MNI152 space. First, they were converted into density maps, in which the voxel densities corresponded to the number of streamlines crossing each voxel[67]. Second, individual density maps were aligned to a standard template using the Greedy symmetric diffeomorphic normalization of the Advanced Normalization Tools pipeline[136]. Third, the resulting template was co-registered to the MNI152 2 mm template using the FSL's tool "flirt"[147]. Finally, the resulting transformation warps were applied to the individual whole-brain streamline tractography using Tract Querier[148].

Then, we computed the structural connectome of the VAN and DAN models. The cortical nodes were defined according to Gordon et al.[14]. To determine the subcortical regions of interest, we selected the statistically significant voxels of the subcortical structures identified in the previous sections with a median Pearson's correlation above $r = 0.1$. This correlation threshold was applied to avoid including voxels significantly associated with the network but with weak correlations[149]. The streamlines that crossed at least two ROIs (cortico-cortical, cortico-subcortical, or subcortical-subcortical) were selected using the MRtrix3's tool "tckedit"[150]. Afterward, the selected streamlines were converted into streamline density maps using the MRtrix3's tool 'tckmap'[150]. The streamline density maps were binarized, and a group-level overlap map was computed.

ROI-to-ROI structural and functional connectivity analysis. We used MRtrix3's tool "tck2connectome" to analyze ROI-to-ROI structural connectivity. The cortical and subcortical ROIs were defined as stated in the previous section. Regarding ROI-to-ROI functional connectivity, we computed the partial correlation between the network nodes using the nilearn's function "ConnectivityMeasure"[151]. The illustrations of the connectivity matrices were created with Matplotlib 3.4.2[152].

Networks lateralization. We assessed the lateralization of the VAN and DAN networks. For functional connectivity, the average Pearson's correlation across each hemisphere's VAN and DAN nodes was calculated using the FSL's function "fslmeants". The obtained values were compared between the right and left hemispheres. For structural connectivity, we extracted the fiber tracts that crossed two nodes of the same hemisphere. Then, the fiber tracts were converted into volume maps using the MRtrix3's tool "tckmap", and the individual volumes were

compared between the two hemispheres[150]. Data were presented as mean (with standard deviations) or median (with interquartile ranges), and paired analyses were performed with paired *t*-test or Wilcoxon test, according to their distribution.

Graph theory analysis of structural connectivity. To analyze if the newly identified subcortical nuclei would be core regions in the networks, we performed a graph theory analysis of the hub properties of the VAN and DAN nodes. Two measures were used, the degree centrality and the betweenness centrality[97]. Degree centrality denotes the fraction of nodes connected to the node of interest. Betweenness centrality is the fraction of all-pairs shortest paths that pass through the node of interest[97]. In graph theory, nodes with high centrality are considered network hubs, i.e., they play a crucial role in the global network function[153].

The 177 individual binarized structural connectivity matrices were converted into undirected connectivity graphs, and both measures were calculated using the NetworkX package (https://networkx.org/). ROIs, as defined in the previous sections, constituted the network nodes. The streamlines that crossed at least two ROIs defined network vertices. Considering the conservative parameters of our tractography adjusted over the years to match post-mortem Klingler dissections[154–157], there was no threshold for the streamline considered for binarization. Additionally, the streamline count does not accurately reflect the number of axonal projections between regions or the strength of connectivity[99,158], and previous work showed that the overall results of the network analysis do not change with modifications in the streamline count binarization threshold[159]. Then, we calculated the median value of both measures across the 177 network graphs for each node. The illustrations of the network graphs were created with SurfIce (https://www.nitrc.org/projects/surfice/).

Structural correlations with the neurotransmitter system. We studied the relationship between the proposed neuroanatomical models' subcortical structural projections and the neurotransmitter systems' spatial distribution. First, we selected the newly identified brainstem nuclei that synthesize neurotransmitters, according to the cytochemical evidence in the literature. Second, we computed the structural projections of these nuclei to the remaining nodes of the VAN and DAN, i.e., we selected the streamlines that crossed the brainstem nuclei of interest and every other node of the network, using the MRtrix3 tool "tckedit"[150]. Then, we used the MRtrix3 tool "tckmap" to map those streamlines into the MNI space[150] and computed the individual Spearman's correlation between the spatial distribution of the created structural projection map and the neurotransmitter maps provided by Hansen and colleagues using the neuromaps' tool "compare_images"[71,160]; https://netneurolab.github.io/neuromaps/). We obtained the correlation values distribution between the 110 individual VAN and DAN maps and each neurotransmitter map. To analyze if the obtained distributions (each composed of 110 correlation values) were significantly higher than zero, a non-parametric statistical test was performed (one-sided Wilcoxon test). The obtained *p* values were corrected for multiple comparisons using the Bonferroni correction. Finally, we analyzed whether the correlation distributions were different between VAN and DAN, and if they were different between hemispheres (paired *t*-test or Wilcoxon test, according to data distribution; the Bonferroni correction was also applied). A supplemental pairwise analysis was performed. The average map of the 110 individual VAN and DAN structural projection maps was correlated with the neurotransmitter maps (Spearman's correlation; neuromaps' tool "compare_images"; https://netneurolab.github.io/neuromaps/)[160]. To control for spatial autocorrelations and reduce the risk of false positive results, statistical significance was inferred based on null models generation[161–163]. Volumetric data were parcellated according to the Automated Anatomical Labeling atlas 3 (AAL3; Rolls et al.[164]), using the neuromaps' utility "Parcellater" (https://netneurolab.github.io/neuromaps/)[160]. AAL3 was chosen because it includes cortical and subcortical parcels. The null parcellations were generated from the average VAN and DAN structural projection maps using the neuromaps' function "nulls.burt2020" (5000 permutations, generating 5000 null parcellations; https://netneurolab.github.io/neuromaps/)[160,162]. The graphical representations were created with Matplotlib 3.4.2 and Datashader 0.13.0 (Hunter[152]; https://datashader.org).

Reporting summary. Further information on research design is available in the Nature Portfolio Reporting Summary linked to this article.

Data availability

The presented brain maps are openly available at https://neurovault.org/collections/XONZLGPJ/, the resting-state functional 7 T MRI datasets in the Human Connectome Project S1200 dataset, and the processed tractographies at http://opendata.bcblab.com. Data were provided by the McDonnell Center for Systems Neuroscience at Washington University. All other data were available from the corresponding author on reasonable request.

Code availability

Analyses were conducted using open software and toolboxes, as specified in the methods. The Funcon-Connectivity code is openly available at https://github.com/chrisfoulon/BCBToolKit; the ANTs scripts "buildtemplateparallel.sh" and "WarpImageMultiTransform" at https://github.com/ANTsX/ANTs; the code where these scripts were applied for the functional alignment performed in this work at https://github.com/Pedro-N-Alves/VAN_DAN_functional_alignment (doi: 10.5281/zenodo.7307027); the "easythresh_conj.sh" code (used for the conjunction analysis) at https://warwick.ac.uk/fac/sci/statistics/staff/academic-research/nichols/; the "tckedit", "tckmap", and "tck2connectome" commands' codes at https://github.com/MRtrix3/mrtrix3; the "ConnectivityMeasure" script at https://github.com/nilearn/nilearn/; the "betweenness_centrality" and "degree_centrality" scripts at https://github.com/networkx/networkx; and the "compare_images", "Parcellater", and "nulls.burt202" scripts at https://github.com/netneurolab/neuromaps.

Received: 28 June 2022; Accepted: 18 November 2022;
Published online: 07 December 2022

References

1. James, W. *The Principles of Psychology* (Henry Holt and Company, 1890).
2. Posner, M. I. Orienting of attention. *Q. J. Exp. Psychol.* **32**, 3–25 (1980).
3. Petersen, S. E. & Posner, M. I. The attention system of the human brain: 20 years after. *Annu. Rev. Neurosci.* **35**, 73–89 (2012).
4. Corbetta, M. & Shulman, G. L. Control of goal-directed and stimulus-driven attention in the brain. *Nat. Rev. Neurosci.* **3**, 201–215 (2002).
5. Corbetta, M., Kincade, J. M., Ollinger, J. M., Mcavoy, M. P. & Gordon, L. Voluntary orienting is dissociated from target detection in human posterior parietal cortex. *Nat. Neurosci.* **3**, 292–297 (2000).
6. Buschman, T. J. & Miller, E. K. Top-down versus bottom-up control of attention in the prefrontal and posterior parietal cortices. *Science* **315**, 1860–1864 (2007).
7. Thiebaut de Schotten, M. et al. A lateralized brain network for visuospatial attention. *Nat. Neurosci.* **14**, 1245–1247 (2011).
8. Corbetta, M., Patel, G. & Shulman, G. L. The reorienting system of the human brain: from environment to theory of mind. *Neuron* **58**, 306–324 (2008).
9. Amemiya, K., Naito, E. & Takemura, H. Age dependency and lateralization in the three branches of the human superior longitudinal fasciculus. *Cortex* **139**, 116–133 (2021).
10. Downar, J., Crawley, A. P., Mikulis, D. J. & Davis, K. D. A multimodal cortical network for the detection of changes in the sensory environment. *Nat. Neurosci.* **3**, 277–283 (2000).
11. Fox, M. D., Corbetta, M., Snyder, A. Z., Vincent, J. L. & Raichle, M. E. Spontaneous neuronal activity distinguishes human dorsal and ventral attention systems. *Proc. Natl Acad. Sci. USA* **103**, 10046–10051 (2006).
12. Vossel, S., Weidner, R., Driver, J., Friston, K. J. & Fink, G. R. Deconstructing the architecture of dorsal and ventral attention systems with dynamic causal modeling. *J. Neurosci.* **32**, 10637–10648 (2012).
13. Szczepanski, S. M., Pinsk, M. A., Douglas, M. M., Kastner, S. & Saalmann, Y. B. Functional and structural architecture of the human dorsal frontoparietal attention network. *Proc. Natl Acad. Sci. USA* **110**, 15806–15811 (2013).
14. Gordon, E. M. et al. Generation and evaluation of a cortical area parcellation from resting-state correlations. *Cereb. Cortex* **26**, 288–303 (2016).
15. Sani, I. et al. The human endogenous attentional control network includes a ventro-temporal cortical node. *Nat. Commun.* **12**, 1–16 (2021).
16. Power, J. D. et al. Functional network organization of the human brain. *Neuron* **72**, 665–678 (2011).
17. Yeo, B. T. T. et al. The organization of the human cerebral cortex estimated by intrinsic functional connectivity. *J. Neurophysiol.* **106**, 1125–1165 (2011).
18. Schaefer, A. et al. Local-global parcellation of the human cerebral cortex from intrinsic functional connectivity MRI. *Cereb. Cortex* **28**, 3095–3114 (2018).
19. Uddin, L. Q., Yeo, B. T. T. & Spreng, R. N. Towards a universal taxonomy of macro-scale functional human brain networks. *Brain Topogr.* **32**, 926–942 (2019).
20. Eickhoff, S. B., Yeo, B. T. T. & Genon, S. Imaging-based parcellations of the human brain. *Nat. Rev. Neurosci.* **19**, 672–686 (2018).
21. Corbetta, M. & Shulman, G. L. Spatial neglect and attention networks. *Ann. Rev. Neurosci.* **34**, 569–599 (2011).
22. Luo, L. et al. Ten years of nature reviews neuroscience: insights from the highly cited. *Nat. Rev. Neurosci.* **11**, 718–726 (2010).
23. Corbetta, M., Kincade, M. J., Lewis, C., Snyder, A. Z. & Sapir, A. Neural basis and recovery of spatial attention deficits in spatial neglect. *Nat. Neurosci.* **8**, 1603–1610 (2005).
24. He, B. J. et al. Breakdown of functional connectivity in frontoparietal networks underlies behavioral deficits in spatial neglect. *Neuron* **53**, 905–918 (2007).
25. Ptak, R. & Schnider, A. The dorsal attention network mediates orienting toward behaviorally relevant stimuli in spatial neglect. *J. Neurosci.* **30**, 12557–12565 (2010).
26. Li, R. et al. Attention-related networks in Alzheimer's disease: a resting functional MRI study. *Hum. Brain Mapp.* **33**, 1076–1088 (2012).

27. McCarthy, H. et al. Attention network hypoconnectivity with default and affective network hyperconnectivity in adults diagnosed with attention-deficit/hyperactivity disorder in childhood. *JAMA Psychiatry* **70**, 1329–1337 (2013).
28. Sanefuji, M. et al. Double-dissociation between the mechanism leading to impulsivity and inattention in attention deficit hyperactivity disorder: a resting-state functional connectivity study. *Cortex* **86**, 290–302 (2017).
29. Baldassarre, A. et al. Large-scale changes in network interactions as a physiological signature of spatial neglect. *Brain* **137**, 3267–3283 (2014).
30. Ramsey, L. E. et al. Normalization of network connectivity in hemispatial neglect recovery. *Ann. Neurol.* **80**, 127–141 (2016).
31. Zénon, A. & Krauzlis, R. J. Attention deficits without cortical neuronal deficits. *Nature* **489**, 434–437 (2012).
32. Saalmann, Y. B. & Kastner, S. Cognitive and perceptual functions of the visual thalamus. *Neuron* **71**, 209–223 (2011).
33. Bender, D. B. & Youakim, M. Effect of attentive fixation in macaque thalamus and cortex. *J. Neurophysiol.* **85**, 219–234 (2001).
34. Aston-Jones, G., Rajkowski, J. & Cohen, J. Role of locus coeruleus in attention and behavioral flexibility. *Biol. Psychiatry* **46**, 1309–1320 (1999).
35. Vazey, E. M., Moorman, D. E. & Aston-Jones, G. Phasic locus coeruleus activity regulates cortical encoding of salience information. *Proc. Natl Acad. Sci. U. S. A.* **115**, E9439–E9448 (2018).
36. Bartolomeo, P. *Attention Disorders After Right Brain Damage: Living in Halved Worlds* (Springer, 2013).
37. Healton, E. B., Navarro, C., Bressman, S. & Brust, J. C. M. Subcortical neglect. *Neurology* **32**, 776–778 (1982).
38. Ferro, J. M., Martins, I. P. & Távora, L. Neglect in children. *Ann. Neurol.* **15**, 281–284 (1984).
39. Karnath, H. O., Himmelbach, M. & Rorden, C. The subcortical anatomy of human spatial neglect: putamen, caudate nucleus and pulvinar. *Brain* **125**, 350–360 (2002).
40. Nyffeler, T., Kaufmann, B. C. & Cazzoli, D. Visual neglect after an isolated lesion of the superior colliculus. *JAMA Neurol.* **78**, 1531–1533 (2021).
41. Ivanov, I. et al. Morphological abnormalities of the thalamus in youths with attention deficit hyperactivity disorder. *Am. J. Psychiatry* **167**, 397–408 (2010).
42. Blough, D. S. Visual search in the pigeon: Hunt and peck method. *Science* **196**, 1013–1014 (1977).
43. Patel, G. H. et al. Functional evolution of new and expanded attention networks in humans. *Proc. Natl Acad. Sci. USA* **112**, E5377–E5377 (2015).
44. Brett, M., Johnsrude, I. S. & Owen, A. M. The problem of functional localization in the human brain. *Nat. Rev. Neurosci.* **3**, 243–249 (2002).
45. Thiebaut de Schotten, M. & Shallice, T. Identical, similar or different? Is a single brain model sufficient? *Cortex* **86**, 172–175 (2017).
46. Carmack, P. S. et al. Improved agreement between Talairach and MNI coordinate spaces in deep brain regions. *Neuroimage* **22**, 367–371 (2004).
47. Amunts, K. et al. Cytoarchitectonic mapping of the human amygdala, hippocampal region and entorhinal cortex: Intersubject variability and probability maps. *Anat. Embryol.* **210**, 343–352 (2005).
48. Zaborszky, L. et al. Stereotaxic probabilistic maps of the magnocellular cell groups in human basal forebrain. *Neuroimage* **42**, 1127–1141 (2008).
49. Amunts, K. et al. BigBrain: an ultrahigh-resolution 3D human brain model. *Science* **340**, 1472–1475 (2013).
50. Mueller, S. et al. Individual variability in functional connectivity architecture of the human brain. *Neuron* **77**, 586–595 (2013).
51. Robinson, E. C. et al. MSM: a new flexible framework for multimodal surface matching. *Neuroimage* **100**, 414–426 (2014).
52. Langs, G., Golland, P. & Ghosh, S. Predicting activation across individuals with resting-state functional connectivity based multi-atlas label fusion. *Med. Image. Comput. Comput. Assist. Interv.* **9350**, 313–320 (2015).
53. Glasser, M. F. et al. A multi-modal parcellation of human cerebral cortex. *Nature* **536**, 171–178 (2016).
54. Fischl, B. et al. Cortical folding patterns and predicting cytoarchitecture. *Cereb. Cortex* **18**, 1973–1980 (2008).
55. Sabuncu, M. R. et al. Function-based intersubject alignment of human cortical anatomy. *Cereb. Cortex* **20**, 130–140 (2010).
56. Conroy, B. R., Singer, B. D., Guntupalli, J. S., Ramadge, P. J. & Haxby, J. V. Inter-subject alignment of human cortical anatomy using functional connectivity. *Neuroimage* **81**, 400–411 (2013).
57. Nenning, K. H. et al. Joint embedding: a scalable alignment to compare individuals in a connectivity space. *Neuroimage* **222**, 117232 (2020).
58. Xu, T. et al. Cross-species functional alignment reveals evolutionary hierarchy within the connectome. *Neuroimage* **223**, 117346 (2020).
59. Haxby, J. V., Guntupalli, J. S., Nastase, S. A. & Feilong, M. Hyperalignment: modeling shared information encoded in idiosyncratic cortical topographies. *Elife* **9**, 1–26 (2020).
60. Haxby, J. V. et al. A common, high-dimensional model of the representational space in human ventral temporal cortex. *Neuron* **72**, 404–416 (2011).
61. Guntupalli, J. S. et al. A model of representational spaces in human cortex. *Cereb. Cortex* **26**, 2919–2934 (2016).
62. Alves, P. N. et al. An improved neuroanatomical model of the default-mode network reconciles previous neuroimaging and neuropathological findings. *Commun. Biol.* **2**, 370 (2019).
63. Catani, M. & Thiebaut de Schotten, M. *Atlas of Human Brain Connections* (Oxford Univ. Press, 2012).
64. Zhang, F. et al. Quantitative mapping of the brain's structural connectivity using diffusion MRI tractography: a review. *Neuroimage* **249**, 118870 (2022).
65. Behrens, T. E. J. et al. Non-invasive mapping of connections between human thalamus and cortex using diffusion imaging. *Nat. Neurosci.* **6**, 750–757 (2003).
66. Suárez, L., Markello, R., Betzel, R. & Misic, B. Linking structure and function in macroscale brain. *Trends Cogn. Sci.* **24**, 302–315 (2020).
67. Thiebaut de Schotten, M., Foulon, C. & Nachev, P. Brain disconnections link structural connectivity with function and behaviour. *Nat. Commun.* **11**, 5094 (2020).
68. Morrison, J. H. & Foote, S. L. Noradrenergic and serotoninergic innervation of cortical, thalamic, and tectal visual structures in old and new world monkeys. *J. Comp. Neurol.* **243**, 117–138 (1986).
69. Foote, S. L. & Morrison, J. H. Extrathalamic modulation of cortical function. *Annu. Rev. Neurosci.* **10**, 67–95 (1987).
70. Bouret, S. & Sara, S. J. Network reset: a simplified overarching theory of locus coeruleus noradrenaline function. *Trends Neurosci.* **28**, 574–582 (2005).
71. Hansen, J. Y. et al. Mapping neurotransmitter systems to the structural and functional organization of the human neocortex. *Nat. Neurosci.* **25**, 1569–1581 (2022).
72. Benarroch, E. E. Pedunculopontine nucleus: functional organization and clinical implications. *Neurology* **80**, 1148–1155 (2013).
73. Chang, S. J., Cajigas, I., Opris, I., Guest, J. D. & Noga, B. R. Dissecting brainstem locomotor circuits: converging evidence for cuneiform nucleus stimulation. *Front. Syst. Neurosci.* **14**, 1–8 (2020).
74. Martin, E. M. et al. Molecular and neuroanatomical characterization of single neurons in the mouse medullary gigantocellular reticular nucleus. *J. Comp. Neurol.* **519**, 2574–2593 (2011).
75. Van De Kar, L. D. & Lorens, S. A. Differential serotonergic innervation of individual hypothalamic nuclei and other forebrain regions by the dorsal and median midbrain raphe nuclei. *Brain Res.* **162**, 45–54 (1979).
76. Heym, J., Steinfels, G. F. & Jacobs, B. L. Activity of serotonin-containing neurons in the nucleus raphe pallidus of freely moving cats. *Brain Res.* **251**, 259–276 (1982).
77. Sherman, S. M. The thalamus is more than just a relay. *Curr. Opin. Neurobiol.* **17**, 417–422 (2007).
78. Stepniewska, I. & Kaas, J. H. Architectonic subdivisions of the inferior pulvinar in New World and Old World monkeys. *Vis. Neurosci.* **14**, 1043–1060 (1997).
79. Bridge, H., Leopold, D. A. & Bourne, J. A. Adaptive pulvinar circuitry supports visual cognition. *Trends Cogn. Sci.* **20**, 146–157 (2016).
80. Bos, J. & Benevento, L. A. Projections of the medial pulvinar to orbital cortex and frontal eye fields in the rhesus monkey (Macaca mulatta). *Exp. Neurol.* **49**, 487–496 (1975).
81. DeVito, J. L. A horseradish peroxidase-autoradiographic study of parietopulvinar connections in saimiri sciureus. *Exp. Brain Res.* **32**, 581–590 (1978).
82. Lemaire, J. J. et al. White matter anatomy of the human deep brain revisited with high resolution DTI fibre tracking. *Neurochirurgie* **57**, 52–67 (2011).
83. Sprague, J. M. Interaction of cortex and superior colliculus in mediation of visually guided behavior in the cat. *Science* **153**, 1544–1547 (1966).
84. Krauzlis, R. J., Lovejoy, L. P. & Zénon, A. Superior colliculus and visual spatial attention. *Annu. Rev. Neurosci.* **36**, 165–182 (2013).
85. Weddell, R. A. Subcortical modulation of spatial attention including evidence that the Sprague effect extends to man. *Brain Cogn.* **55**, 497–506 (2004).
86. Luppino, G., Matelli, M., Carey, R. G., Fitzpatrick, D. & Diamond, I. T. New view of the organization of the pulvinar nucleus in Tupaia as revealed by tectopulvinar and pulvinar-cortical projections. *J. Comp. Neurol.* **273**, 67–86 (1988).
87. Vuilleumier, P., Hester, D., Assal, G. & Regli, F. Unilateral spatial neglect recovery after sequential strokes. *Neurology* **46**, 184–189 (1996).
88. Bartolomeo, P., Thiebaut De Schotten, M. & Doricchi, F. Left unilateral neglect as a disconnection syndrome. *Cereb. Cortex* **17**, 2479–2490 (2007).
89. Durmer, J. S. & Rosenquist, A. C. Ibotenic acid lesions in the pedunculopontine region result in recovery of visual orienting in the hemianopic cat. *Neuroscience* **106**, 765–781 (2001).
90. Valero-Cabré, A., Toba, M. N., Hilgetag, C. C. & Rushmore, R. J. Perturbation-driven paradoxical facilitation of visuo-spatial function: revisiting the 'Sprague effect'. *Cortex* **122**, 10–39 (2020).
91. Mena-Segovia, J. & Bolam, J. P. Rethinking the pedunculopontine nucleus: from cellular organization to function. *Neuron* **94**, 7–18 (2017).

92. Mena-Segovia, J., Sims, H. M., Magill, P. J. & Bolam, J. P. Cholinergic brainstem neurons modulate cortical gamma activity during slow oscillations. *J. Physiol.* **586**, 2947–2960 (2008).
93. Martinez-Gonzalez, C., Van Andel, J., Bolam, J. P. & Mena-Segovia, J. Divergent motor projections from the pedunculopontine nucleus are differentially regulated in Parkinsonism. *Brain Struct. Funct.* **219**, 1451–1462 (2014).
94. Jeon, C. -J., Spencer, R. F. & Mize, R. R. Organization and synaptic connections of cholinergic fibers in the cat superior colliculus. *J. Comp. Neurol.* **333**, 360–374 (1993).
95. Motts, S. D. & Schofield, B. R. Sources of cholinergic input to the inferior colliculus. *Neuroscience* **160**, 103–114 (2009).
96. Steriade, M., Paré, D., Parent, A. & Smith, Y. Projections of cholinergic and non-cholinergic neurons of the brainstem core to relay and associational thalamic nuclei in the cat and macaque monkey. *Neuroscience* **25**, 47–67 (1988).
97. Bullmore, E. & Sporns, O. Complex brain networks: graph theoretical analysis of structural and functional systems. *Nat. Rev. Neurosci.* **10**, 186–198 (2009).
98. Girvan, M. & Newman, M. E. J. Community structure in social and biological networks. *Proc. Natl Acad. Sci. USA* **99**, 7821–7826 (2002).
99. Gong, G. et al. Mapping anatomical connectivity patterns of human cerebral cortex using in vivo diffusion tensor imaging tractography. *Cereb. Cortex* **19**, 524–536 (2009).
100. Hagmann, P. et al. Mapping the structural core of human cerebral cortex. *PLoS Biol.* **6**, 1479–1493 (2008).
101. Barabási, A.-L. & Albert, R. Emergence of scaling in random networks. *Science* **286**, 509–512 (1999).
102. Prendergast, M. A. et al. Central nicotinic receptor agonists ABT-418, ABT-089, and (–)-nicotine reduce distractibility in adult monkeys. *Psychopharmacology* **136**, 50–58 (1998).
103. Sun, Y. et al. Nicotinic α4β2 cholinergic receptor influences on dorsolateral prefrontal cortical neuronal firing during a working memory task. *J. Neurosci.* **37**, 5366–5377 (2017).
104. Levin, E. D. et al. Transdermal nicotine effects on attention. *Psychopharmacology* **140**, 135–141 (1998).
105. Valentine, G. & Sofuoglu, M. Cognitive effects of nicotine: recent progress. *Curr. Neuropharmacol.* **16**, 403–414 (2017).
106. Cortese, S. et al. Comparative efficacy and tolerability of medications for attention-deficit hyperactivity disorder in children, adolescents, and adults: a systematic review and network meta-analysis. *Lancet Psychiatry* **5**, 727–738 (2018).
107. Gatley, S. J., Pan, D., Chen, R., Chaturvedi, G. & Ding, Y.-S. Affinities of methylphenidate derivatives for dopamine, norepinephrine and serotonin transporters. *Life Sci.* **58**, 231–239 (1996).
108. Faraone, S. V. The pharmacology of amphetamine and methylphenidate: relevance to the neurobiology of attention-deficit/hyperactivity disorder and other psychiatric comorbidities. *Neurosci. Biobehav. Rev.* **87**, 255–270 (2018).
109. Zolkowska, D. et al. Evidence for the involvement of dopamine transporters in behavioral stimulant effects of modafinil. *J. Pharmacol. Exp. Ther.* **329**, 738–746 (2009).
110. Turner, D. C., Clark, L., Dowson, J., Robbins, T. W. & Sahakian, B. J. Modafinil improves cognition and response inhibition in adult attention-deficit/hyperactivity disorder. *Biol. Psychiatry* **55**, 1031–1040 (2004).
111. Repantis, D., Schlattmann, P., Laisney, O. & Heuser, I. Modafinil and methylphenidate for neuroenhancement in healthy individuals: a systematic review. *Pharmacol. Res.* **62**, 187–206 (2010).
112. Zoli, M. et al. Identification of the nicotinic receptor subtypes expressed on dopaminergic terminals in the rat striatum. *J. Neurosci.* **22**, 8785–8789 (2002).
113. Exley, R. & Cragg, S. J. Presynaptic nicotinic receptors: a dynamic and diverse cholinergic filter of striatal dopamine neurotransmission. *Br. J. Pharm.* **153**, 283–297 (2008).
114. Forster, G. L. & Blaha, C. D. Pedunculopontine tegmental stimulation evokes striatal dopamine efflux by activation of acetylcholine and glutamate receptors in the midbrain and pons of the rat. *Eur. J. Neurosci.* **17**, 751–762 (2003).
115. Blaha, C. D. & Winn, P. Modulation of dopamine efflux in the striatum following cholinergic stimulation of the substantia nigra in intact and pedunculopontine tegmental nucleus-lesioned rats. *J. Neurosci.* **13**, 1035–1044 (1993).
116. Harmer, C. J. & Cowen, P. J. 'It's the way that you look at it'-a cognitive neuropsychological account of SSRI action in depression. *Philos. Trans. R. Soc. B Biol. Sci.* **368**, 20120407 (2013).
117. Browning, M., Reid, C., Cowen, P. J., Goodwin, G. M. & Harmer, C. J. A single dose of citalopram increases fear recognition in healthy subjects. *J. Psychopharmacol.* **21**, 684–690 (2007).
118. Harmer, C. J., Shelley, N. C., Cowen, P. J. & Goodwin, G. M. Increased positive versus negative affective perception and memory in healthy volunteers following selective serotonin and norepinephrine reuptake inhibition. *Am. J. Psychiatry* **161**, 1256–1263 (2004).
119. Washburn, D. A. & Taglialatela, L. A. in *Comparative cognition: Experimental explorations of animal intelligence* (eds. Wasserman, E. A. & Zentall, T. R.) Ch. 7 (Oxford Univ. Press, 2006).
120. Mackintosh, N. J. Selective attention in animal discrimination learning. *Psychol. Bull.* **64**, 124–150 (1965).
121. Wasserman, E. A. & Castro, L. Assessing attention in category learning by animals. *Curr. Dir. Psychol. Sci.* **30**, 495–502 (2021).
122. Budisavljevic, S. et al. Asymmetry and structure of the fronto-parietal networks underlie visuomotor processing in humans. *Cereb. Cortex* **27**, 1532–1544 (2017).
123. Cazzoli, D. & Chechlacz, M. A matter of hand: causal links between hand dominance, structural organization of fronto-parietal attention networks, and variability in behavioural responses to transcranial magnetic stimulation. *Cortex* **86**, 230–246 (2017).
124. Chechlacz, M., Gillebert, C. R., Vangkilde, S. A., Petersen, A. & Humphreys, G. W. Structural variability within frontoparietal networks and individual differences in attentional functions: an approach using the theory of visual attention. *J. Neurosci.* **35**, 10647–10658 (2015).
125. Howells, H. et al. Frontoparietal tracts linked to lateralized hand preference and manual specialization. *Cereb. Cortex* **28**, 1–13 (2018).
126. Bartolomeo, P. & Seidel Malkinson, T. Hemispheric lateralization of attention processes in the human brain. *Curr. Opin. Psychol.* **29**, 90–96 (2019).
127. Sheremata, S. L. & Silver, M. A. Hemisphere-dependent attentional modulation of human parietal visual field representations. *J. Neurosci.* **35**, 508–517 (2015).
128. Szczepanski, S. M., Konen, C. S. & Kastner, S. Mechanisms of spatial attention control in frontal and parietal cortex. *J. Neurosci.* **30**, 148–160 (2010).
129. Snow, J. C. & Mattingley, J. B. Goal-driven selective attention in patients with right hemisphere lesions: how intact is the ipsilesional field? *Brain* **129**, 168–181 (2006).
130. Doricchi, F., MacCi, E., Silvetti, M. & MacAluso, E. Neural correlates of the spatial and expectancy components of endogenous and stimulus-driven orienting of attention in the posner task. *Cereb. Cortex* **20**, 1574–1585 (2010).
131. Shulman, G. L. et al. Right hemisphere dominance during spatial selective attention and target detection occurs outside the dorsal frontoparietal network. *J. Neurosci.* **30**, 3640–3651 (2010).
132. Vossel, S., Geng, J. J. & Fink, G. R. Dorsal and ventral attention systems: distinct neural circuits but collaborative roles. *Neuroscientist* **20**, 150–159 (2014).
133. Glasser, M. F. et al. The minimal preprocessing pipelines for the Human Connectome Project. *Neuroimage* **80**, 105–124 (2013).
134. Foulon, C. et al. Advanced lesion symptom mapping analyses and implementation as BCBtoolkit. *Gigascience* **7**, 1–17 (2018).
135. Kenney, J. *Mathematics of Statistics* (Chapman & Hall, 1939).
136. Avants, B. B. et al. A reproducible evaluation of ANTs similarity metric performance in brain image registration. *Neuroimage* **54**, 2033–2044 (2011).
137. Avants, B. B., Epstein, C. L., Grossman, M. & Gee, J. C. Symmetric diffeomorphic image registration with cross-correlation: evaluating automated labeling of elderly and neurodegenerative brain. *Med. Image Anal.* **12**, 26–41 (2008).
138. Klein, A. et al. Evaluation of 14 nonlinear deformation algorithms applied to human brain MRI registration. *Neuroimage* **46**, 786–802 (2009).
139. Jenkinson, M., Beckmann, C. F., Behrens, T. E. J., Woolrich, M. W. & Smith, S. M. Fsl. *Neuroimage* **62**, 782–790 (2012).
140. Nichols, T., Brett, M., Andersson, J., Wager, T. & Poline, J. B. Valid conjunction inference with the minimum statistic. *Neuroimage* **25**, 653–660 (2005).
141. Ewert, S. et al. Toward defining deep brain stimulation targets in MNI space: a subcortical atlas based on multimodal MRI, histology and structural connectivity. *Neuroimage* **170**, 271–282 (2018).
142. Su, J. H. et al. Thalamus optimized multi atlas segmentation (THOMAS): fast, fully automated segmentation of thalamic nuclei from structural MRI. *Neuroimage* **194**, 272–282 (2019).
143. Chakravarty, M. M., Bertrand, G., Hodge, C. P., Sadikot, A. F. & Collins, D. L. The creation of a brain atlas for image guided neurosurgery using serial histological data. *Neuroimage* **30**, 359–376 (2006).
144. Lechanoine, F. et al. WIKIBrainStem: an online atlas to manually segment the human brainstem at the mesoscopic scale from ultrahigh field MRI. *Neuroimage* **236**, 118080 (2021).
145. Vu, A. T. et al. High resolution whole brain diffusion imaging at 7T for the Human Connectome Project. *Neuroimage* **122**, 318–331 (2015).
146. Dell'Acqua, F. et al. A modified damped Richardson-Lucy algorithm to reduce isotropic background effects in spherical deconvolution. *Neuroimage* **49**, 1446–1458 (2010).
147. Jenkinson, M., Bannister, P., Brady, M. & Smith, S. Improved optimization for the robust and accurate linear registration and motion correction of brain images. *Neuroimage* **17**, 825–841 (2002).

148. Wassermann, D. et al. The white matter query language: a novel approach for describing human white matter anatomy. *Brain Struct. Funct.* **221**, 4705–4721 (2016).
149. Cohen, J. *Statistical Power Analysis for the Behavioural Sciences* (Lawrence Erlbaum Associates, 1988).
150. Tournier, J. D. et al. MRtrix3: A fast, flexible and open software framework for medical image processing and visualisation. *Neuroimage* **202**, 116137 (2019).
151. Pedregosa, F. et al. Scikit-learn: machine learning in python. *J. Mach. Learn. Res.* **12**, 2825–2830 (2011).
152. Hunter, J. Matplotlib: a 2D graphics environment. *Comput. Sci. Eng.* **9**, 90–95 (2007).
153. van den Heuvel, M. P. & Sporns, O. Network hubs in the human brain. *Trends Cogn. Sci.* **17**, 683–696 (2013).
154. Thiebaut de Schotten, M. et al. Atlasing location, asymmetry and inter-subject variability of white matter tracts in the human brain with MR diffusion tractography. *Neuroimage* **54**, 49–59 (2011).
155. Catani, M. et al. Short frontal lobe connections of the human brain. *Cortex* **48**, 273–291 (2012).
156. Vergani, F., Mahmood, S., Morris, C. M., Mitchell, P. & Forkel, S. J. Intralobar fibres of the occipital lobe: a post mortem dissection study. *Cortex* **56**, 145–156 (2014).
157. Catani, M. The anatomy of the human frontal lobe. *Handb. Clin. Neurol.* **163**, 95–122 (2019).
158. Jones, D. K., Knösche, T. R. & Turner, R. White matter integrity, fiber count, and other fallacies: the do's and don'ts of diffusion MRI. *Neuroimage* **73**, 239–254 (2013).
159. Shu, N. et al. Diffusion tensor tractography reveals disrupted topological efficiency in white matter structural networks in multiple sclerosis. *Cereb. Cortex* **21**, 2565–2577 (2011).
160. Markello, R. D. et al. Neuromaps: structural and functional interpretation of brain maps. *Nat. Methods* **19**, 1472–1479 (2022).
161. Markello, R. D. & Misic, B. Comparing spatial null models for brain maps. *Neuroimage* **236**, 118052 (2021).
162. Burt, J. B., Helmer, M., Shinn, M., Anticevic, A. & Murray, J. D. Generative modeling of brain maps with spatial autocorrelation. *Neuroimage* **220**, 117038 (2020).
163. Alexander-Bloch, A. F. et al. On testing for spatial correspondence between maps of human brain structure and function. *Neuroimage* **178**, 540–551 (2018).
164. Rolls, E. T., Huang, C. C., Lin, C. P., Feng, J. & Joliot, M. Automated anatomical labelling atlas 3. *Neuroimage* **206**, 116189 (2020).

Acknowledgements

This project has received funding from the European Research Council (ERC) under the European Union's Horizon 2020 research and innovation program (grant agreement No. 818521; M.T.d.S.), the Marie Skłodowska-Curie program (grant agreement No. 101028551; S.J.F.), a Donders Mohrmann Fellowship (S.J.F., No. 2401512), "Prémio João Lobo Antunes 2018"—SCML (P.N.A.), and "Bolsa de Investigação em Doenças Vasculares Cerebrais 2017"—SPAVC (P.N.A.). Additional funding comes from the University of Bordeaux's IdEx "Investments for the Future" program RRI "IMPACT," which received financial support from the French government. M.C. was supported by MIUR—Departments of Excellence Italian Ministry of Research (MART_ECCELLENZA18_01); Fondazione Cassa di Risparmio di Padova e Rovigo (CARIPARO)(Grant Agreement number 55403); Ministry of Health Italy NEUROCONN (RF-2008 -12366899); Celeghin Foundation Padova (CUP C94I20000420007); BIAL foundation grant (No. 361/18); H2020 European School of Network Neuroscience-euSNN, H2020-SC5-2019-2, (Grant Agreement number 869505); H2020 VARCITIES, H2020-SC5-2019-2 (Grant Agreement number 869505); Ministry of Health Italy: EYEMOVINSTROKE (RF-2019-12369300).

Author contributions

P.N.A. implemented part of the methods, performed the analyses, contributed conceptually, and wrote the manuscript. S.J.F. and M.C. contributed conceptually and edited the paper. M.T.d.S. conceived and coordinated the study, reviewed the neuroimaging data, wrote the manuscript, and provided funding.

Competing interests

Michel Thiebaut de Schotten is an Editorial Board Member for *Communications Biology*, but was not involved in the editorial review of, nor the decision to publish this article. The authors declare no competing interests.

Additional information

Supplementary information The online version contains supplementary material available at https://doi.org/10.1038/s42003-022-04281-0.

Correspondence and requests for materials should be addressed to Pedro Nascimento Alves or Michel Thiebaut de Schotten.

Peer review information *Communications Biology* thanks Sandra Hanekamp, Boris Bernhardt and the other, anonymous, reviewer(s) for their contribution to the peer review of this work. Primary Handling Editor: George Inglis. Peer reviewer reports are available.

Reprints and permission information is available at http://www.nature.com/reprints

Publisher's note Springer Nature remains neutral with regard to jurisdictional claims in published maps and institutional affiliations.